

**This PDF was created from the British Library's microfilm copy of the original thesis. As such the images are greyscale and no colour was captured.**

**Due to the scanning process, an area greater than the page area is recorded and extraneous details can be captured.**

**This is the best available copy**

D3767781

Attention is drawn to the fact that the copyright of this thesis rests with its author.

This copy of the thesis has been supplied on condition that anyone who consults it is understood to recognise that its copyright rests with its author and that no quotation from the thesis and no information derived from it may be published without the author's prior written consent.

III

D 37677/81.

CLARKE K.M

PP

284

Double Paged Inserts

Back

COLOURS AND  
OTHER OPTICAL PROPERTIES  
OF BINARY NOBLE METAL-NOBLE METAL  
ALLOYS

by

Keith M Clarke, BSc(UMIST)

A thesis submitted to the CNAA in partial  
fulfilment of the requirements for  
the degree of PhD.

Department of Metallurgy  
and Materials  
Sir John Cass School of Science  
and Technology  
City of London Polytechnic

March 1980

In collaboration with:  
Goldsmiths Research  
Foundation

ACKNOWLEDGEMENTS

I would like to thank Dr E F I Roberts for guidance, patience and constant encouragement, and my wife and family for their tolerance. I have had many useful discussions with Dr D Ross and Mr R Hunt. I would also like to thank the Worshipful Company of Goldsmiths and Intergold Corporation for provision of materials, equipment and technical assistance.

GLOSSARY

- $L_3, L_2$  etc Points where the band 3 (or 2, etc) pass the reciprocal lattice point L.
- $X_5, X_4$  etc Similarly for the reciprocal lattice point X.
- $L_2$  (FS) The point where band 2 intersects the Fermi surface near L.
- $L_2$  (FS)  $\rightarrow$   $L_1$  A transition with the initial state at the Fermi surface near to  $L_2$ , and the final state near to  $L_1$ . Because of the 'necks' at L, the Fermi surface does not intersect the reciprocal lattice vector L.
- $L_{4-} \rightarrow L_{4+}$  Is relativistic notation for  $L_2 \rightarrow L_1$ . That is, band 2  $\equiv$  band 4<sup>-</sup> etc. Beaglehole and Erlbach (1972) imply  $L_{6-} \rightarrow L_{6+}$  is comparable with  $L_2 \rightarrow L_1$ .
- s Saturation:  
a subjective term; the most saturated colours are the monochromatic radiations. Mixing of these with 'white' or achromatic light desaturates the observed colour. When the term is used quantitatively in this thesis, it is equivalent to excitation purity (eg Bouma 1972).
- $\lambda_d$  Dominant wavelength: the wavelength of the monochromatic radiation which, when mixed with white light, yields a light having the same colour co-ordinates as the object under discussion.
- L Relative luminance: the quantity in the CIE 1931 System which correlates with subjective brightness of an object.
- x,y Colour co-ordinates in the CIE 1931 Standard System.
- u,v Colour co-ordinates in the CIE 1960 Uniform Colour System.
- A,P Ellipsometric analyser and polariser readings for the ellipsometric configuration and conventions used at the City of London Polytechnic, ie.  $A=45-\psi$ ,  $P=\Delta+2$ . Other ellipsometric notation and convention follows Muller (1969), the Nebraska Convention.

CONTENTS

Acknowledgements.	
Abstract.	
Glossary.	
1. INTRODUCTION	7
2. LITERATURE SURVEY	
2.1 Colorimetry.	10
2.2 Optical and Electronic Properties of the Noble Metals.	14
3. EXPERIMENTAL	
3.1 Instrumentation.	47
3.2 Sample Preparation.	54
3.3 Measurement Procedure.	61
4. THEORY	
4.1 Colorimetry.	67
4.2 The Application of Ellipsometry to the Determination of Reflectance and the Dielectric Function.	72
4.3 Fundamental Equations.	78
4.4 Optical Properties of Two-Phase Alloys.	84
5. COMPUTATION	
5.0 General - Program Design.	87
5.1 Calculation of the Dielectric Function.	89
5.2 The Optical Functions $R_N, R_S, R_P, \psi, \Delta, A, P$	99
5.3 Intrinsic Spectral Substrate Functions $\epsilon_2^f, \epsilon_2^b, \text{Im}^1/\epsilon, \text{Im}^1/\epsilon+1, \sigma$	101
5.4 Non-Spectral Intrinsic Substrate Functions $\omega_p, \epsilon_1^b(0), \tau$	103
5.5 Colorimetry.	103

6. RESULTS	
6.1 The Primary Metals: Silver, Gold and Copper.	106
6.2 Ag-Au Binary Alloys.	131
6.3 Au-Cu Binary Alloys.	151
6.4 Ag-Cu Binary Alloys.	177
7. DISCUSSION	
7.1 Experimental Method.	206
7.2 Performance of Computer Programs.	208
7.3 Effects of Sample Preparation.	210
7.4 Effects of Alloying on the Inter-band Absorption.	231
7.5 Effects of Alloying on the Intra-band Absorption.	247
7.6 Heterogeneous Alloys.	249
8. CONCLUSIONS AND SUGGESTIONS FOR FURTHER WORK.	258

ABSTRACT

The method of ellipsometry is applied to the study of the optical properties of Ag-Au, Ag-Cu and Au-Cu alloys and the results are interpreted in terms of alloy colour and electronic properties. Variation of colour with alloy composition is placed on a quantitative basis for the first time and discussed in terms of the most fundamental properties of the materials. Use of ellipsometry in the investigation also makes possible the assessment of the effects of tarnish and other contaminant films. The influence of sample preparation on the optical properties is discussed, and the importance of using 'real' surfaces, in order to make possible the industrial and commercial application of the work, is emphasised.

A survey is given of previous studies both theoretical and experimental that are related to the noble metals or the experimental technique used. Sample requirements are discussed and the preparation methods adopted are described. Relevant electronic, optical and colorimetric theory is presented and unified in a computational system that takes full advantage of the great power of modern computers. Ellipsometric results are given and compared with the optical results of workers using other techniques. The effect of cuprite tarnish on the properties and on the accuracy of their determination is presented in detail.

It is found that by far the most significant determinant of noble alloy colours is the width of the d- $\pi$  gap near to L. Tarnishing of copper rich alloys has a visually observable and measurable effect only when prolonged over many hours, but a rapidly formed film is probably responsible for an ellipsometrically observed increase in the saturation of these red metals that borders on the perceptible.

1. INTRODUCTION

The aim of the investigation was to examine the optical properties of a ternary alloy system of commercial significance, either Ag-Au-Cu or Al-Cu-Zn, and to relate the observations to both the electronic properties and technological problems, such as corrosion, annealing, surface de-alloying and enrichment.

The Ag-Au-Cu system was preferred for several reasons. There is interesting structure in or near to the visible spectrum of all the alloys, hence the colours; the system encompasses a range of different alloy types (for instance, the Ag-Au binary alloys are fully miscible solid solutions, silver and copper are almost totally immiscible and form two-phase alloys, whilst Au-Cu alloys form several inter-metallic compounds showing order-disorder transformations. The alloy system is used as the basis of 'gold' jewellery alloys, so that optical measurements have their own intrinsic commercial application, as they can be used to provide a physical interpretation of jewellery alloy colours. Finally, many of the alloys develop only thin surface films in air, simplifying the experimental procedure and the analysis of the results.

The commercial application of the project implied the use of what might be considered 'sub-standard' metal surfaces in the context of an investigation aimed solely at uncovering fundamental properties of the alloys. In fact, analysis of the results (in terms of electronic properties, surface

disorder and superficial tarnish formation) was hindered by the use of mechanically polished samples. These can never be truly clean, as cleaning techniques inevitably involve altering the state of the surface in several ways. Annealing in a reducing atmosphere would remove oxide or sulphide tarnish and probably also adsorbed organic layers, but would reduce the level of structural disorder introduced in polishing, and alter alloy morphology and long-range order. Cleaning by ion-bombardment would introduce additional structural imperfections. Accordingly, all samples were measured after a standard metallurgical polish and measured in air, in accordance with common industrial practice.

Ellipsometry was chosen as the method of acquiring optical data, as this technique offers many advantages. The direct measurement of the optical constants (complex refractive index) of a surface enables the reflectance to be calculated, as required for colorimetry, as well as the computation of dielectric function to aid interpretation in terms of electronic structure. Direct measurement of reflectance with the same accuracy as can be furnished by ellipsometry is difficult, but not more so than the construction of a modern ellipsometer. In the present case an excellent instrument was already available that needed only relatively minor modifications to convert it into a spectral-scanning ellipsometer. Calculation of the dielectric function from reflectance measurements can be done using the well-known

Kramers-Kronig relations, but these require data over an optical range greatly exceeding the range of interest, ie. the visible. In practice measurements in the vacuum ultra-violet would be needed. The Kramers-Kronig relations are not applicable to filmed systems, and at short wavelengths even thin adsorbed layers could seriously affect the results. Thus ellipsometry offered the most useful tool for the investigation, considering all its aims.

Three main directions of effort emerged during the research program:

- (i) development of computational analysis of optical measurements to give information on colour and electronic properties;
- (ii) preparation and measurement of three binary alloy systems, Ag-Au, Ag-Cu and Au-Cu;
- (iii) investigation of the effect of thermal and mechanical treatment of the alloys and of tarnishing.

## 2. LITERATURE SURVEY

### 2.1 Colorimetry

Coloured finishes have been used for human artefacts since prehistoric times. This is true of dyes used for textiles, pigments in paints and ceramic glazes, and of metals used in jewellery and household utensils. There was, until very recently, no possibility of synthesising colours or otherwise producing colours to order, so that choice was limited to those which occur naturally. Only when the situation was altered by the great advance of organic chemistry during the nineteenth century was there any need for a science of colorimetry. This developing science was closely co-ordinated by the International Commission on Colorimetry (the CIE or Commission Internationale D'Eclairage) so that here it is not necessary to refer to a great body of literature. An excellent introduction to the subject and a thorough account of the contemporary state of knowledge is given by Bouma (1971).

Measurements were made by various workers (references are given in Bouma, 1971) to determine the physical and psychological mechanisms of human colour vision. The most significant finding was that of the tristimulus nature of colour perception; that is, that a unique set of three numbers was both necessary and sufficient to identify any one of all possible colour sensations. The choice of the system to be used in the determination of these numbers is to a large extent arbitrary, and several systems were proposed. Perceived colours evidently depend on the nature of the illumination and the properties of the observer as much as they do on the substance being observed. Colour is a function of the spectral intensity of a light entering

the eye, and of the spectral variation of sensitivity of the eye. Thus it is necessary to know the spectral energy distribution of the illumination, the spectral reflectance of the subject, and something about the eye. The tristimulus nature of perception suggests that any three independent spectral functions could be chosen to describe the sensitivity of the eye. In 1931 the CIE adopted a system with what was considered a near-optimal set of properties. It was amenable to exact calculation; the quantities computed correlated well with visual assessments; and the colour of additive mixtures of incoherent beams of light could be described by the appropriate weighted average of the three parameters for each of the two beams. The chief disadvantages of this system (the CIE 1931 Standard System) are that (i) it was chosen to correlate well with visual data obtained using a rather small field of view, namely, that samples should subtend an angle of  $2^\circ$  at the eye of the observer, and (ii) that no attempt was made to ensure that the system was uniform. This means that equal perceived colour differences do not correspond to equal differences in the calculated parameters, except over very small regions of the 'colour space'.

It is possible to compute alternative sets of parameters from those discussed above which avoid some of the disadvantages or which have special advantages of their own. This process is merely a transformation

of Cartesian co-ordinates, for which reason the terms 'colour co-ordinates' and 'colour space' are often used. One possible transformation is to compute the dominant wavelength,  $\lambda_d$ , and saturation,  $S$ . Billmeyer and his co-workers (1961) found excellent correlation between  $\lambda_d$  and perceived hue for yellow-red colours, our present region of interest, even for saturation significantly higher than those found here.

The possibility of co-ordinate transformations is the basis for the simple type of colorimeter frequently employed in quality-control laboratories. These use three filters of known characteristics and measure the intensity of light reflected from a sample and transmitted through each filter. The three intensity readings can then be transformed into the corresponding CIE co-ordinates of the sample. The technique is not very accurate, depending as it does on the stability of the light source and on the precision of the transformation, often performed by analogue electronics. For this reason measurements of reflectance are often made for many monochromatic colours and numerical integration used to obtain the required co-ordinates (equations for this integration are given in Section 6). This method has been employed by Gardam (1966) actually in a study of metals and alloys. He used a simple spectrophotometer which required calibration against an external 'white'

standard. For this he chose electroplated silver, which aptly illustrates the unsuitability of the method for measuring very unsaturated colours. Among the metals studied were sterling silver and fine gold. Gardam was able to determine the reflectivity at only a small number of wavelengths in the visible ( $\approx 10$ ), so that accurate results could not be expected. The interval between wavelengths of about 40nm is very much larger than that conventionally employed in colour measurement. Typically, a constant wavelength interval of 5 or 10nm is used. The labour of experiment and calculation is obviously greatly reduced by increasing this interval, but at the expense of accuracy. A constant interval is preferred so that the weighted ordinate method of integration can be used. Now that the computations are invariably performed automatically, there is not particular reason to prefer this method, although Ohta and Wysecki (1975) state that it remains in use 'almost exclusively'. These authors show, not unreasonably, that a large wavelength interval can cause very large errors if the sample reflectance varies rapidly with wavelength.

The problem of adequately describing small colour differences has also received recent attention. The most obvious question relates to the perceptibility of a calculated colour difference.

The usual experimental arrangement is to match the colour of interest with a mixture of three coloured lights. Small quantifiable variations in this mixture then enable a 'just noticeable colour difference' (J.N.C.D) to be defined. This has clear disadvantages when comparing a surface colour with the coloured lights as the surface texture may have an effect quite unrelated to colour. Rich and Billmeyer (1975) have given a computational method for obtaining JNCD's by comparison of a set of coloured samples in the visual test.

A second problem relates to the non-uniformity of the 1931 colour space. This makes it difficult to relate the magnitude of small compositional changes to the magnitude of the resulting colour change. For example, a change of 5% in the composition of Ag-Au alloy may be expected to alter the colour much more in a gold-rich alloy than in a silver-rich one. Again, various 'uniform colour systems' (U.C.S) have been proposed. The CIE adopted one in 1960 which has gained a wide acceptance. More recently a new system has also been put forward, the  $L^*a^*b^*$  UCS. This, however, has not been finally settled, for example Pauli (1976) has recently proposed a modification.

## 2.2 Optical and Electronic Properties of the Noble Metals

The study of light reflected at the interfaces between media was initiated by Drude (1890). At this time it was not clear what form these interfaces might take, and Drude is responsible for the acceptance of Fresnel's theory describing the reflection at a simple, plane interface between homogeneous isotropic media. He showed the apparent failure of the theory was due to the presence of very thin surface films, whose effects were felt even when the thickness was only a few Angstroms. The equations he

derived for reflection when a homogeneous, isotropic film is present have proved of great utility in many physical systems, as has the experimental technique of ellipsometry which is also his invention.

The simplest experiment which is adequate to define the colour is, as has been said, to measure the spectral reflectance. However, interpretation of the results is made much simpler if both of the real and imaginary parts of the refractive index,  $n-ik$ , (or the dielectric function) are available. Early workers on metal optics did not have available the Kramers-Kronig relations, which relate the real and imaginary parts of the refractive index, and furthermore they did not have instrumentation which covered a large enough wavelength range to make them useful. Thus it was necessary to make two independent measurements at each wavelength in order to determine  $n$  and  $k$ . These could be the ellipsometric parameters of Drude, or the values of reflectivity  $|R_s|$   $|R_p|$ , or the reflectivity at two angles of incidence, or the values of reflectance and transmittance of a thin film. Nathanson (1938), Heavens (1955) and Givens (1958) describe all of these techniques, Heavens' book concerning those useful for thin films. For the purposes of this investigation it is the values characteristic of the bulk metals that are of interest, but this does not preclude the use of films that have a suitable structure, as the penetration of light into a metal is only of the order of  $100\text{\AA}$ . Methods which involve the reflection of polarized light from opaque samples can be regarded as optically equivalent, although they may vary considerably in complexity, suitability

for automation, useful wavelength range etc. This point has been discussed in detail by Meadows (1975). Early workers who used polarimetric methods to study the optical properties of copper include Drude (1890), Minor (1903), Tool (1910), Forsterling and Freedericksz (1913), Margenau (1929) and Lowery (1936).

The variations between the results obtained were discussed by Nathanson (1938). There was general agreement that the degree of polishing had a profound effect on the measured values of  $n$ ,  $k$  and  $R$ . Tool observed that an 'incomplete' polish led to rather low values of  $k$ ; this may have been a purely geometric effect associated with using a rough specimen. Tool, Margenau and Lowery agreed that heavier polishing caused an increase in  $n$ , while Drude had early found that  $n$  decreased when surface strain was reduced by glowing. Polishing and strain relief were held to have less effect on  $k$  and these workers disputed the magnitude and even the direction of such an effect. It can be seen from the Drude equations for free electron absorption (Section 4) that  $\epsilon_1^f = -k^2 - \omega_p^2/\omega^2$ , so that there is no direct dependence of  $k$  on the relaxation time ( $\tau$ ), for wavelength regions where  $\omega\tau \gg 1$  and  $n^2 \ll k^2$ . On the other hand,  $\epsilon_2$  and  $n$  are (roughly) inversely proportional to the relaxation time in the same wavelength region, so that these early results are consistent with polishing producing surface disorder and thus reducing  $\tau$ . Calculations based on the optical measurements showed  $\tau$  to be much less than that expected on the basis of the direct current (low frequency) conductivity, while the 'effective number of free electrons' also differed from the atomic

valence that it was expected to equal. In an attempt to produce surfaces more characteristic of the bulk material Lowery turned to electropolishing, which removed the damage caused by mechanical polishing. Beilby (1921) had proposed that this consisted of an amorphous layer some  $500\text{\AA}$  thick which could be reasonably expected to be quite unrepresentative of the bulk metal. French (1932) had objected that a truly amorphous layer was unlikely (it requires only a very small mean displacement from a random array of atoms in order to produce an f.c.c. lattice, as has been pointed out by Hunderi (1976). A microcrystalline surface, with grains  $\sim 50\text{\AA}$  in diameter, was equally unrepresentative however, and electropolishing to remove this layer became an accepted technique. It has frequently been pointed out that electropolishing produces a relatively thick solid layer on the metal surface, and that this may present greater problems than surface disorder. Novak et al (1970) report a  $60\text{\AA}$  solid layer produced on copper during polishing; this was reduced to less than  $10\text{-}20\text{\AA}$  by careful washing and drying. The remaining film is comparable in thickness to that formed in air at room-temperature (Young and Gwathmey, 1951; Young and Cathcart, 1956). After electropolishing, Lowery annealed his samples in an atmosphere of hydrogen to reduce the amount of strain, which should also have removed any remaining film. Thus these experiments were for a long time the best that had been performed.

At this stage, theory appears to have lagged some way behind experiment. Nevertheless, the next major effort was again experimental. Beattie and Conn (1955) and Hodgson (1955) took advantage of new technology to extend measurements into the

infra-red. Again the chief aim was to test the validity of the classical Drude theory of free-electron absorption, but now in a wavelength region inaccessible using the eye as detector. Schultz (1957) also carried out experiments on silver, gold and copper, using metal films evaporated onto the faces of glass prisms. By using opaque (thick) films and making the measurements at the glass/metal interface, as well as by careful annealing of the films, he was able to obtain reproducible results comparable to those on bulk samples. The mechanism of conduction electron absorption was now better understood, and theory was found to give a good account of the results when an 'optical effective mass' ( $m^*$ ) and an 'optical relaxation time' were used to replace the electron rest mass and d.c relaxation time of the Drude theory. Following Schultz' work Givens (1958) reviewed the state of knowledge with particular regard to the optical properties of the noble metals; it was now possible to expand on the reasons for the sudden departure of these materials from Drude-like behaviour as the wavelength was decreased. Mott and Jones (1936) had ascribed this property, the well-known 'absorption edge', where  $k$  and  $\epsilon_2$  increase very rapidly, to optically induced electronic transitions from the d-bands of the metal to empty states near the Fermi surface. The possibility of transitions, originating at the Fermi surface, to empty conduction bands, was also considered. These ideas now made their reappearance. Zhuraleva and Norskov (1957) detailed the various scattering processes, and their temperature dependence, that contributed to the optical relaxation time. This suggested the possibility of determining the various contributions (namely electron-phonon, electron-

electron and electron-impurity collisions), by measuring the variation of the optical constants with temperature. S Roberts (1960) used electropolished bulk samples of copper in experiments at 90K, 300K and 500K. He accepted the existence of the 'amorphous' Beilby layer, stating that this must lead to a larger electrical resistivity,  $n$  and  $\epsilon_2$  than are possessed by an undeformed copper surface. The samples were annealed in vacuum, with a residual reducing atmosphere, which, Roberts postulated, removed some  $10\text{\AA}$  of adsorbed water and  $20\text{\AA}$  of cuprous oxide. It had previously been shown (Winterbottom 1955) that annealing in hydrogen at 460K was adequate to reduce the natural oxide formed on copper.

An expression for computing the dielectric function of crystalline materials from an exact knowledge of their electronic structure was given by Cohen and Ehrenreich (1959). This provided a framework in which Ehrenreich and Phillip (1962) were able to interpret the results of optical experiments on silver and copper, using the electronic energy band structure for copper that had been derived by Ham and Segall (1961). Ehrenreich and Phillip used electropolished bulk samples, as had Roberts, but made some of the optical measurements in air. The near-normal incidence reflectance was measured for photon energies from one to twenty electron-volts, that is from  $12.4\mu$  in the infra-red to about  $500\text{\AA}$  in the vacuum ultraviolet. Although, necessarily, the high energy measurements were made in a good vacuum, at this stage an airformed film would already have been present. Nevertheless, good agreement for values of  $m^*$  and  $\tau$  was found with the results of Schultz and of Roberts. Kramers-Kronig analysis

was used to calculate the phase shift on reflection,  $\phi(\omega)$ , from the experimental  $R(\omega)$ , enabling  $\epsilon(\omega)$  to be readily computed. Extrapolations of  $R(\omega)$  were made to match the values of  $\epsilon$ , thus obtained, to those of Schultz and Roberts. By using the theoretical expression for  $\epsilon(\omega)$ , and by examining the experimental results, Ehrenreich and Philipp showed that absorption  $\epsilon_2(\omega)$  below the absorption edge was entirely due to conduction electron transitions for which the initial and final states of the excited electron lie within the same band. Thus the low energy absorption was labelled 'intraband'. In the nearly-free-electron limit, intraband absorption is described by a Drude-like expression, in which the constant  $m^*$  can be related to the shape of the conduction band and Fermi surface. In the particular case of the noble metals, intraband absorption is quite small near the absorption edge and at higher energies. Thus at high energies the absorption is almost entirely due to optically induced transitions for which the initial and final electronic states lie in different bands, or 'interband' transitions. Due to the possibility of confusion between these similar terms, 'free electron' and 'bound electron' absorption are often preferred (hence  $\epsilon = \epsilon^f + \epsilon^b$ ). It should be evident from the early suggestion of Mott and Jones, previously mentioned, that interband transitions may involve conduction electrons as their initial states, that the 'free' electrons are involved in both processes. Ehrenreich and Philipp identified the particular transitions responsible for the near-visible absorption in silver and copper as due to transitions from  $L_3 \rightarrow FS$  (a 3.9eV gap in silver), and also  $L_3 \rightarrow FS$  (2.1eV) and  $X_5 - X_4'$  (4.5 eV) in

copper. These were postulated to be momentum conserving ('direct') transitions, involving only the electron and photon. Indirect transitions have also been postulated in which a phonon interaction ensures conservation of momentum. In the latter case, transitions would not necessarily take place at a single point in the reduced Brillouin zone, such as X; and the final state in the  $L_3 \rightarrow FS$  transitions would not have to be near L. The calculation of  $m^*$  and  $\tau$  in Ehrenreich and Phillips paper did not proceed in the same way as previously used by fitting the experimental  $\epsilon$  to a Drude-like expression at low energies. If this is done, it is essential to allow a contribution to  $\epsilon_1$  from interband transitions as  $\epsilon_1^f$  and  $\epsilon_1^b$  are not separated into non-overlapping wavelength ranges as can be assumed for  $\epsilon_2^f$  and  $\epsilon_2^b$ . At long wavelengths  $\epsilon_1^b$  can be considered constant, which simplifies the analysis. It has frequently been referred to as the term due to 'polarisation of the bound electrons'. Ehrenreich and Phillip performed a Kramers-Kronig transformation on  $\epsilon_2^b(\omega)$  to give  $\epsilon_1^b(\omega)$  explicitly, including its frequency dependence near the edge. Thus  $\epsilon_1^f$  could be separated from the experimental data as well as  $\epsilon_2^f$ . That the calculated values of  $m^*$  and  $\tau$  were similar to those of Schultz and Roberts is not very significant, as  $\epsilon_1(\omega)$  and  $\epsilon_2(\omega)$  had been deliberately matched to the earlier workers' results.

Wessel (1963) performed reflectance measurements on a series of Ag-Au alloys, in response to the increasing understanding of the pure noble metals. The alloys were electropolished to remove surface damage, as before. Wessel observed that a

prolonged electropolish increased the reflectance from about 67% to 80% at 3.4eV, in the case of silver. The sharpness of the reflectance edge was also greatly increased. F Stern (1963) gave another general review of the optical properties of metals, to follow that of Givens. The important role of Kramers-Kronig treatment of reflectance data was highlighted by a comprehensive description of this technique. The question of sample preparation also received further attention. Donovan et al (1963) compared mechanically polished, electropolished and polycrystalline films of germanium. Only the electropolished surface showed any fine structure in the optical spectrum, variations of five percent in reflectivity being found using the other methods. Fromhold (1963) investigated vacuum cleaning techniques in connection with removing the polishing layer from electropolished samples and the strained layer from mechanically prepared surfaces. It was found that vacuum annealing at 600°C produced surface roughening, while argon-ion bombardment caused similar structural disorder to mechanical polishing. Some of Fromhold's mechanically polished silver samples gave an anomalous peak in the real part of the refractive index, at a wavelength of 540nm. A theory of optical reflections from rough surfaces was advanced by Porteus (1963). This was an important movement towards a complete theory of realistic surfaces, complementary to the approach of making ideal surfaces to test the more fundamental theory. This continued to attract a lot of attention; Burge and Bennett (1964) made various calculations of the effect oxide films (on silicon and aluminium) in optical measurements, and of the inaccuracy of the computed refractive index if the presence of oxide layers was ignored. In the case of silicon

at  $5461\text{\AA}$  wavelength, a  $100\text{\AA}$  film of  $\text{SiO}_2$  is enough to increase the apparent value of  $k$  from 0.028 to 0.872. The errors in the case of an aluminium substrate are not so large, but would be significant because of the large thickness of the oxide layer, either air-formed or produced during electro-polishing. These difficulties led to the re-investigation of opaque evaporated films as possible substrates. Spencer and Givens (1964) used a vacuum of better than  $10^{-8}$  Torr to prepare films of copper. As had been noted by Heavens (1955), at a pressure of  $10^{-5}$  Torr the vapour pressure of the residual gas is comparable to that of the metal during evaporation. Samples prepared at different partial pressures of oxygen ( $10^{-5}$  to  $10^{-8}$  Torr) had different properties and also aged differently. Using the best vacuum, copper films annealed spontaneously at room-temperature. The fact that, under the highest pressures used, no ageing took place was attributed to dissolved oxygen inhibiting the annealing process. Rouard (1965) prepared thin films of silver, gold and copper in vacuum and observed an anomalous absorption peak for each of these, which moved to longer wavelengths as the film thickness was increased. This is just the behaviour expected of a non-continuous metal film in the context of the Maxwell-Garnet theory, assuming the fraction of metal in the film increases with increasing thickness (see, for example, Heavens 1955).

Electroplated bulk samples were used on several new investigations. Cooper et al (1965) extended the work of Ehrenreich and Phillipp (1962) to include also gold. Similar techniques were used. The fundamental absorption edge in each of the

noble metals was attributed to  $d \rightarrow FS$  transitions, as before, originating on states near  $L_{32}$  and with final states where the  $L_2$  band cuts the Fermi surface. The sharpness of the absorption edge was attributed to the flatness of the  $d$ -band at this point. Gold and copper have additional absorption peaks near the visible, which were identified with transitions  $X_5 \rightarrow X_4'$  as before. This transition in the band diagram used corresponded to a critical point of the type  $S_2$  (described by van Hove in connection with semi-conductor absorption). A calculation of the imaginary part of the dielectric function\* for copper was presented, which included only  $d$ -band excitations. The computed absorption strength was only one-third of the experimental value. Beaglehole (1965) measured the optical properties of copper and gold over the wavelength range 460nm to 46nm (2.7 to 27eV), using electropolished samples that had been annealed in a reducing atmosphere of  $10^{-6}$  Torr at  $400^\circ\text{C}$ . The reflectance was computed at several angles of incidence, so that the dielectric function could be calculated without the use of Kramers-Kronig analysis. This analysis was used in an original way to improve the interpretation of his results. By extrapolating his results to the onset of interband absorption (only 0.7eV below where his measurements began), Beaglehole was able to check the consistency of his results and obtain values for  $m^*$  and  $\tau$  (Beaglehole, 1966). The assignments of structure in the optical spectrum by Cooper et al were strongly disputed by Beaglehole, who felt that the data were ambiguous, and that in particular silver and gold were so poorly understood as to make unambiguous identification of transitions impossible. He was willing to accept only that transitions near  $L$  and  $X$  are responsible for structure below 10eV, and

emphasised the possibility of interband transitions involving conduction electrons near L ( $L_6 \rightarrow L_7$ ).

McAlister et al (1965) presented the results of more work on Ag-Au alloys. Using measurements of the Faraday effect, they were able to show that the shape of the Fermi surface varied smoothly with concentration, implying close similarity between the electronic structures of silver and gold. Stern (1965) took up this point, and interpreted Wessel's (1963) results as showing a similar effect. He plotted the position of the absorption as a function of composition, the small departure from linearity being attributed to a transfer of d-electrons from gold to silver ions in the alloy. In a theoretical paper (Stern 1966b) the same author found that the known properties of Ag-Au alloys could be correctly described using a model in which the periodic lattice potential was some average of the pure metal potentials (Virtual Crystal Model), adjusted by transferring d-state charge density from gold to silver. Fukutani and Sueoka (1966) presented new experimental data for Ag-Au alloys, in the energy range 2.5 to 4.1 eV. Experiments were carried out using opaque films of 800-2000 Å thickness, evaporated in a vacuum of about  $10^{-6}$  Torr and annealed at 400°C for 1.5 hours. The results agreed with those of Wessel, giving a similar curve of edge position versus composition. Ehrenreich (1966) used a pseudopotential method to calculate new energy band structures for silver, gold and copper. He was unable to confirm the hypothesis that only

direct transitions are excited in optical experiments, but assigned the main absorption peaks in copper to  $L_{32} \rightarrow L_{2'}$  (ie.  $d \rightarrow FS$ , 2.1eV) and  $X_5 - X_{4'}$  (4.8eV).

Workers considering the effect of oxide films on experimental results have generally used the refractive index of the stoichiometric bulk oxide for their hypothetical film. Thus Roberts (1960), assuming the contamination to be cuprous oxide, used values of  $n$  and  $k$  appropriate to cuprite. Wieder and Czernanda (1966) produced non-stoichiometric films of copper oxide on dielectric substrates and found the optical constants to be significantly different from those of cuprite. This indicates the hazard of making unsupported assumptions about the properties of contaminating films.

Further work on alloys was reported by Köster and Stahl (1967) who studied electropolished samples of silver and gold, as well as sputtered samples of Ag-Au and Au-Cu alloys. The purpose of the investigation was to examine the effect of heat treatment. It was found that annealing of the sputtered samples reduced  $\epsilon_2^f$ , corresponding to reduced structural disorder and increased relaxation time, while  $\epsilon_2^b$  increased on annealing. The width of the absorption edge in the Ag-Au alloys was found to depend strongly on composition, reaching a maximum of  $\approx 1\text{eV}$  for the  $\text{Ag}_{50}\text{Au}_{50}$  alloy. Ordered  $\text{AuCu}_3$  was found to have an absorption peak which was absent in the disordered alloy, while ordering produced two sharp peaks at 340nm and 350nm in AuCu.

Gerhardt et al (1967) measured the piezo reflectance of copper for various strain axes, which enabled them to reduce the ambiguity, noted by Beaglehole, in interpreting the absorption

spectrum in terms of the energy bands. Kramers-Kronig analysis was used to derive the piezo- $\epsilon_2$  spectrum. The onset of interband absorption near 2eV was again attributed to  $d \rightarrow$  FS transitions while the structure near 4eV was resolved into two components,  $X_5 - X_4'$  at 3.9eV and  $FS(L_2') \rightarrow L_1$  at 4.3eV. The latter transition is very sensitive to the crystal potential and moved rapidly under the appropriate strain. Gerhardt (1968) reported similar results, this time giving the energies as 4.0eV ( $X_5 - X_4'$ ) and 4.15eV ( $FS \rightarrow L_1$ ). In order to analyse piezo reflectance data, single crystal specimens are used so that the strain axis can be aligned with a particular crystal vector such as L, ie. the [111] direction. Using polycrystalline samples Gerhardt found a change in reflectance on straining below the interband threshold, which was absent from the single crystal spectra. This immediately suggests a grain boundary effect.

Mueller and Phillips (1967) calculated the interband spectrum,  $\epsilon_2(\omega)$ , for copper using the Random Phase Approximation of Cohen and Ehrenreich (1959). The calculation gave an improved fit to experimental data ( $\sim 50\%$ ) compared with that of Cooper et al (1965). When broadening effects were not included in the calculation, structure due to critical points (such as  $X_5 \rightarrow X_4'$ ) appeared as an infinite discontinuity. Broadening reduces this to an abrupt step, suggesting the use of the point of maximum slope as the 'edge position'. The computation was compared with experimental data by Phillips (1968). The experimental peak in  $\epsilon_2(\omega)$  between 4 and 5eV was attributed to  $L_2' - L_1$  transitions, as found by Gerhardt. This corresponded to

transitions from  $4_p$  - like states to  $4_s$  - like states in the calculation.

There was still no agreement concerning the need for optically induced transitions to conserve momentum, despite the success of the RPA calculation (which assumes direct transitions). Stern (1967) considered the effect of the metal surface on the problem and concluded that, for the noble metals, the presence of the surface permitted indirect transitions to take place.

Theorists had been unable, up to this moment, to treat the electronic properties of alloys as rigorously as those of pure metals, due to the lack of periodicity in a substitutionally disordered lattice. Soven (1967) proposed a method based on finding a periodic, self-consistent pseudo-potential for the alloy which would lead to the observed properties. This has become known as the Coherent Potential Approximation (CPA). Velicky et al (1968) examined the theoretical properties of the CPA and demonstrated that in certain limited applications it reduced to previously known forms, derived from perturbation theory. There was thus some encouragement that the method would be useful for more general cases that had formerly been intractable. An important result of the theory was the prediction that for small values of the ratio (band separation + band width) for the electronic bands of the constituent metals, a single band would result in the alloy. Large values would lead to split bands.

Lewis and Lee (1968) presented a non-first-principles calculation of the energy band structure of silver, for which the d-band

energies were adjusted to fit the optical data. Even with this adjustment, the method did not accurately reproduce the 4eV peak in  $\epsilon_2^b$ ; the authors pointed out the tentative nature of the assumptions made in the computation of  $\epsilon_2^b(\omega)$  from the electronic density of states. These were, that the one-electron band structure is literally true; that structure in the experimental  $\epsilon_2^b(\omega)$  was, in fact, entirely due to direct interband transitions; and that the probability of an electronic transition depends only on the density of initial states, the density of final states and the energy gap separating them. The calculations of the band gaps was consistent with the 4eV edge as being due to transitions  $FS(L_{2'}) \rightarrow L_1$  as well as  $d \rightarrow FS(L_3 \rightarrow L_{2'})$ . Hodgson (1968) made a fresh determination of the optical properties of gold, using the method of Schultz (1957). Opaque gold films were evaporated in a vacuum of better than  $10^{-7}$  Torr onto one face of a glass prism, following which the samples were annealed for several hours at  $200^\circ\text{C}$ .  $|R_p|$  and  $|R_s|$  were measured from the glass side of the film. The form of  $\epsilon_2$  below the absorption edge -  $\epsilon_2^f$  - was not Drude-like (proportional to the cube of the wavelength) but could be described by an expression

$$\frac{\epsilon_2^f(\lambda)}{\lambda} = \alpha\lambda^2 + \beta$$

The constants  $(\alpha, \beta)$  were found to vary, but independently, with sample structure. He suggested that a variation in the magnitude of the peak in  $\epsilon_2^b(\omega)$  was due to the existence of voids in the films, the quantity of which were also a function of preparation. An absorption peak ( $\delta\epsilon_2 \approx 0.25$ ) was also found near 1.5eV at room temperature; at 445K the strength increased

to  $\delta\epsilon_2 = 0.75$ . Myers et al (1968) measured the optical properties of silver, gold and copper as part of a study of noble-transition metal alloys. They found good agreement between their own values for  $m^*$  and  $\tau$  and those of many earlier workers, although for both silver and gold it was not clear whether the correct value was slightly less than or rather more than one.

Noble metal alloys attracted increasing attention. Nilsson et al (1968) studied gold, copper and the Au-Cu alloys. It was found that, as in Ag-Au alloys, the first interband edge moved smoothly with composition. Ordered samples of intermetallic compound proportions had absorption edges approximately 0.05eV higher in energy than the disordered samples. The edge in gold near 3.8eV was not found to move on addition of copper, and addition of gold to copper did not move the structures at 3.9 and 4.8eV. Nilsson and Norris (1969) stated that the optical properties of disordered  $\text{AuCu}_3$  were a superposition of the spectra of gold and copper, while the ordered alloy has an additional peak at 3.4eV. Photoemission data indicated an increase in the electronic density of states  $\approx 3.8\text{eV}$  above the Fermi level. Thus they identified the new peak in  $\epsilon_2(\omega)$  with transitions from the Fermi surface to the conduction band. Stahl et al (1969) studied the temperature dependence of the optical properties of gold, copper and  $\text{AuCu}_3$ . The main absorption edge energy was found to be almost independent of temperature in all three materials, while the second absorption peak in each metal were found to move to lower energies as the temperature was increased. At high temperatures a new peak

to  $\delta\epsilon_2 = 0.75$ . Myers et al (1968) measured the optical properties of silver, gold and copper as part of a study of noble-transition metal alloys. They found good agreement between their own values for  $m^*$  and  $\tau$  and those of many earlier workers, although for both silver and gold it was not clear whether the correct value was slightly less than or rather more than one.

Noble metal alloys attracted increasing attention. Nilsson et al (1968) studied gold, copper and the Au-Cu alloys. It was found that, as in Ag-Au alloys, the first interband edge moved smoothly with composition. Ordered samples of inter-metallic compound proportions had absorption edges approximately 0.05eV higher in energy than the disordered samples. The edge in gold near 3.8eV was not found to move on addition of copper, and addition of gold to copper did not move the structures at 3.9 and 4.8eV. Nilsson and Norris (1969) stated that the optical properties of disordered  $\text{AuCu}_3$  were a superposition of the spectra of gold and copper, while the ordered alloy has an additional peak at 3.4eV. Photoemission data indicated an increase in the electronic density of states  $\approx 3.8\text{eV}$  above the Fermi level. Thus they identified the new peak in  $\epsilon_2(\omega)$  with transitions from the Fermi surface to the conduction band. Stahl et al (1969) studied the temperature dependence of the optical properties of gold, copper and  $\text{AuCu}_3$ . The main absorption edge energy was found to be almost independent of temperature in all three materials, while the second absorption peak in each metal were found to move to lower energies as the temperature was increased. At high temperatures a new peak

near 3.6eV was found for AuCu<sub>3</sub>, due to ordering. A small increase in absorption at about 0.7eV also took place. Pant and Joshi (1970) calculated the energy band structure of disordered AuCu<sub>3</sub>, and considered that the X<sub>5</sub> + X<sub>4</sub> band gap contributed optical absorption near 2.4eV. Rivory (1969) prepared thin, continuous films of Ag-Au alloys and measured the optical properties by reflection and transmission. She observed a similar variation of the interband threshold as had Wessel (1963) and Fukutani and Sueoka (1966). The relaxation time and optical effective mass varied parabolically with composition,  $\tau$  and  $m^*$  showing a minimum for Ag<sub>50</sub>Au<sub>50</sub>. Beaglehole and Hendrickson (1969) prepared opaque films of gold and Au-Fe alloys, annealing the samples at 600°C for 20 minutes in vacuum. This prevented further room-temperature aging of the specimens while avoiding surface roughening due to recrystallization. The absorption,  $\epsilon_2^f$ , was found to vary approximately as  $\omega^{-2}$ , which led the authors to postulate a frequency dependent relaxation time entering a typical Drude-like expression. Some absorption below 2.3eV was observed, which could not be interpreted as intraband or direct interband absorption.

Morris and Lynch (1969) studied silver and Ag-In alloys using piezo-reflectance. The interband absorption edge of silver was found to have two almost exactly superimposed peaks, one of which moved under strain and one of which did not. Noting that theoretical calculations showed a strong sensitivity of the L<sub>1</sub> energy level (an s-like state) to the crystal potential, and that the L<sub>3</sub>(d-like) and L<sub>2</sub>(p-like) levels are

insensitive, the peak was assigned to  $L_3 \rightarrow L_2'$  (FS) and  $L_2'$  (FS)  $\rightarrow L_1$ . They also found structure in the piezo-spectrum below the interband threshold (cf. Gerhardt, 1968, on copper) which was attributed to indirect transitions. Nilsson and Sandell (1970) made the same assumption regarding low energy structure which they found for  $Ag_{90}Au_{10}$  when carrying out similar experiments on silver rich Ag-Au alloys, and indicated essentially the same assignments concerning the interband transitions.

Pells and Shiga (1969) measured the temperature dependence of the optical properties of gold and copper using electro-polished samples annealed in vacuum. The fundamental edge in both metals was attributed to  $L_3 \rightarrow L_2$  (FS), with additional structure in the visible spectrum due to transitions at  $X_5 - X_4'$  (4.55eV for gold and 3.97eV for copper); and  $L_2' \rightarrow L_1$  (4.08eV for gold and 4.78eV for copper). In a theoretical calculation of the dielectric function for copper, Dresselhaus (1969) assumed the optical edge near 2.2eV to be due to transitions from the top of d-bands to the Fermi surface, i.e.  $L_3 \rightarrow L_2'$ , and adjusted the d-band energies accordingly. The gap from the bottom d-band at  $L(L_1)$  to the Fermi surface was then 4.2eV, accounting for the peak near 4eV. This procedure yielded a good fit to the experimental spectrum. Krokilowski and Spicer (1970) computed the dielectric function of gold over a wide energy range using photoemission data for the electronic density of states. The results were consistent with the  $d \rightarrow FS$  interpretation of the interband threshold, but the authors argued that indirect electronic transitions play a large part in the optical absorption spectrum of gold.

Liljenvall and Mathewson (1970) also found evidence of the composite nature of the silver absorption edge, using ellipsometric measurements at various high temperatures. The  $L_2 + L_1$  component was found to move to lower energies with increasing temperature, which effect was attributed entirely to the change in lattice constant, in accordance with theoretical expectations. Irani et al (1971) interpreted the results of their experiments on silver rich Ag-Al alloys in terms of a shift of the  $L_1$  energy level caused by the modification of the crystal potential by aluminium impurities. Splitting of the absorption edge was exactly as in Liljenvall and Mathewson's thermo-modulation experiments.

The optical properties of gold were studied by Theye (1970) who used a combination of reflection and transmission measurements on thin films, the thickness being independently determined. Continuous films were obtained by rigorous attention to cleanliness, these having a roughness similar to that of the substrates used. Absorption at long wavelengths was not Drude-like, and a small inter-band absorption 'tail' was found below the band edge (2.4eV) extending to  $\sim 1.5$ eV. Badly crystallised samples also had an absorption band  $\sim 1$ eV broad centred at the latter energy, which was absent in well annealed samples.

Dujardin and Theye (1971) investigated the effect of structural disorder, through varying the conditions of preparation, on the optical properties of semi-transparent silver films. They found no dependence of the position of the absorption

edge on grain size, suggesting that disorder does not lead to splitting of this edge. The optical mass was found to be quite insensitive to structure, increasing slightly for 'poor' films, which could be interpreted as a decreasing electron concentration due to the formation of pin-holes and other imperfections, which is borne out by the decrease in  $\epsilon_2^b(\omega)$  found in the same circumstances. The relaxation time increased drastically with structural disorder. Some samples, smooth enough for no surface plasmon absorption to be excited, showed an absorption band at about 1.5eV,  $\epsilon_2$  increasing by as much as 0.3.

Hunderi and Myers (1973) and Hunderi (1973) prepared partially disordered opaque films of silver, observing a double absorption peak at 2.4eV and 3.2eV. The peaks were very broad ( $\sim 1$ eV) and, in some cases, rather strong, increases in  $\epsilon_2$  of  $\approx 2.5$  at 2.4eV and  $\approx 0.7$  at 3.2eV being observed. These were clearly observable over the Drude background. A quantitative theory was proposed, based on a hypothetical microcrystalline structure for the samples. It was supposed that the films were composed of grains less than or about one micron in diameter, separated by grain boundary regions only a few  $\text{\AA}$  units across. The thickness of the grain boundaries was supposed independent of the grain size. The properties (optical mass and relaxation time) of the grains was considered to be equal to those of bulk silver, while the properties of the boundaries were modelled by extremely oblate ellipsoids, the unique axis normal to the plane of the boundary.  $m^*$  and  $\tau$  of the boundary were used as adjustable parameters, as were the axes of the ellipsoids (equivalent to adjusting either the volume fraction of the

boundaries or the grain size), the width of a distribution of  $m^*$  values, and the depolarisation factor for the ellipsoids. With these five adjustable quantities a good fit to the experimental data was obtained by Hunderi and Myers (1973), which was made more convincing by Hunderi (1973) who showed that any reasonable values for four of these could be used (as the results were not sensitive to the actual choices). The remaining parameter was the volume fraction of grain boundaries ( $V_f$ ) which scaled the magnitude of the absorption peak. Fitted values of  $V_f$  were reasonable but unfortunately were not directly measured. It is possible that different values of  $m^*$  and  $\tau$  for the disordered boundaries would suffice to move the absorption to 1.5eV, where it was found by Dujardin and Theye, but this has also not been investigated. Oy and Wu (1971) extended the CPA to treat structural disorder but did not discuss the implications for the optical properties.

Cristensen and Seraphin (1971) presented a relativistic band structure calculation for gold. Relativistic corrections were found to be large, leading to band splittings of the order of one electron-volt. They calculated  $\epsilon_2^b(\omega)$  from the energy band diagram, finding good agreement with the experimental work of Pells and Shiga (1969) and Theye (1970). The calculation accurately reproduced the absorption 'tail' without any new assumptions (such as electron-electron interactions or indirect transitions) being made. This edge is attributed to transitions from the top of the d-bands to the Fermi surface, around the neck at L, and over an extended region of the Brillouin zone. In non-relativistic notation, that is  $L_3 \rightarrow L_2$  (FS). In the notation of

of the above authors, this becomes transitions from band 5 to band 6. Additional absorption around 2.9eV is due to transitions from the d-bands near X to the Fermi surface; in non-relativistic notation  $X_5 \rightarrow FS$ . At 3.2eV absorption is due to transitions from band 4 to band 6, and at 3.6eV to transitions at L. These are described as  $L_4^- \rightarrow L_4^+$  and are analogous to the previously discussed  $L_2' \rightarrow L_1$ . Further absorption at 4.1eV is due to transitions near X (cf.  $X_5 \rightarrow X_4'$ ) and at 4.6eV transitions from band 3 to the Fermi surface become possible. The role of critical points was felt to be small, most of the absorption being due to transitions from flat d-bands to the Fermi surface. The success of the Random Phase Approximation in describing the results of optical experiments was partly explained by Beeferman and Ehrenreich (1970) who made a theoretical study of the effects of electron-electron interactions, which are neglected in the RPA. They showed that these effects are small when considering interband transitions, but noted that this does not rule out the possibility of a significant effect on the intraband relaxation time (due to electron-electron scattering) as discussed by Gurzhi (1959) and Theye (1970).

Velicky and Levin (1970) gave some properties of the Coherent Potential Approximation for disordered alloys in another theoretical paper. This was taken up by Brauers and Brouers (1970) who discussed the CPA in the context of Ag-Au alloys. They suggested that the non-Drude-like behaviour of  $\epsilon_2^f$ , interpreted as a frequency dependent relaxation time by Rivory (1969) and Theye (1970), was due to a type of disorder not normally included in theoretical calculations. Levin and Ehrenreich

(1971) used a simple model of Ag-Au alloys and the CPA to interpret the non-linearity of the shift of the absorption edge and composition. Rivory's (1969) results could be fitted assuming an s-electron charge transfer from gold to silver ions of 30%, neglecting charge transfer of d-electrons and assuming the absorption edge to be entirely due to transitions from  $d + FS$ . Fukutani (1971) reported new experimental results for Ag-Au alloys which agreed well with those of Rivory. He assigned the structure in his optical spectrum to the same set of transitions as had been frequently cited for copper:  $L_3 + L_2'$ ,  $X_5 + X_4'$  and  $L_2' + L_1$ . Partly on the basis of movement of structure with alloy concentration,  $L_3 + L_2'$  (FS) was assigned to the 2eV edge in gold and the 4eV edge in silver while  $X_5 + X_4'$  transitions were suggested at 3.5eV in gold and 5.2eV in silver. Structure near 4.1eV in the gold spectrum was assigned to  $L_2' - L_1$ . A relativistic band structure calculation for silver was presented by Chritensen (1972). He obtained a band gap of only 3.49eV at L for the conduction electron transition  $L_{4-} + L_{4+}$  (equivalent to  $L_2' + L_1$  in non-relativistic notation), and 3.98eV for d-electron transitions to the Fermi surface near X and L.

Wallden and Gustavsson (1972) gave a value of 4.17eV for the silver  $L_2' + L_1$  energy gap, using photo-emission experiments. Piezo-reflectance and electroreflectance measurements were made by Cheyssac et al (1972), for both silver and gold, but no interpretation of the results was offered.

Steel and Treherne (1972) measured the optical properties of Ag-Mn and Au-Mn alloys, observing that the behaviour of  $\epsilon_2(\omega)$  was not Drude-like below the absorption edge. For the purpose of extrapolating the low frequency experimental  $\epsilon_2(\omega)$  - assumed equal to  $\epsilon_2^f(\omega)$  - to higher frequencies, so that it could be subtracted from  $\epsilon_2(\omega)$  to give  $\epsilon_2^b(\omega)$ , these authors used a power law expression

$$\epsilon_2^f(\omega) = \alpha\lambda^\beta$$

The value of the coefficient  $\beta$  (3 in the Drude theory when  $\omega\tau \gg 1$ ) was not given. Mechanically polished specimens were used, which led to a 'small' variation in the magnitude of  $\epsilon_1$  and  $\epsilon_2$  but did not affect the spectral features. Steel(1972) also made polarimetric measurements on mechanically polished gold samples, finding some additional absorption around  $\hbar\omega \approx 2.4\text{eV}$  as Hodgson (1968), Pells and Shiga (1969) and Theye (1970) had also reported. The identification of the 2.4eV absorption edge with  $d \rightarrow FS$  transitions near to  $L_3 \rightarrow L_2'$  was accepted.

Dilute noble metal-noble metal alloys were studied by Beaglehole and Erlbach (1972), who directly measured the change in normal reflectance caused by alloying additions between 0.3 and 3 atomic percent. Both ends of the concentration range for each of the three binary systems were studied. Assignments of spectral structure to various transitions, as previously cited, were accepted by the authors, who used their results to compute the change in the corresponding energy gaps due to alloying. The results for Ag-Au alloys agreed with those of Rivory (1969) - addition of gold to silver moved the edge at 4eV to lower energies, and addition of silver to gold moved the 2.5eV edge

to higher energies. The shift in the silver absorption edge was resolved into two components, at 3.9 and 4.1eV. The second absorption edge in gold (3.5eV) moved to lower energies on addition of silver. Piezo reflectance data show that the rate of change of these energies with strain is such that the effects of the very small change in lattice constant can be neglected. In the Au-Cu system, alloying additions at both ends of the concentration range moved all structures in the visible to lower energies. In the case of copper-rich Au-Cu alloys, this was explained as due to the expansion of the copper lattice caused by addition of gold. In the Ag-Cu alloys, no shift of the fundamental edges was observed, although alloying reduced the strength of the host absorption. The 4.1eV structure in silver moved to higher energies on addition of copper, the 4.3eV peak in copper moved to lower energies on addition of silver. Silver-rich Ag-Cu alloys had a contribution to  $\epsilon_2^b(\omega)$  between  $\omega \approx 2$  and  $\omega \approx 4$ eV, due to copper impurity states. For this alloy, the optical effective mass increased from the pure metal value on alloying; for all other five dilute alloys  $m^*$  decreased. The use of such dilute alloys, combined with a narrow bandwidth optical system and the direct measurement of the change in reflectance on alloying, allowed very precise measurements to be made. This would not be the case with concentrated alloys as the increased disorder introduced would greatly broaden optical structures because of impurity scattering of the electrons.

Abeles (1972) reviewed contemporary understanding of the optical properties of metals, with emphasis on the properties of pure

metals. Intraband properties of gold were discussed (mainly using the results of Theye, 1970), in the context of electron-electron interactions and the shape of the Fermi surface. The first interband transition in gold was firmly identified as a 'parallel band' transition; that is, from a flat d-band to the flat Fermi surface, because of the parabolic behaviour of  $\omega^2 \epsilon_2^b(\omega)$ . The relevance and validity of the Coherent Potential and Virtual Crystal models of metallic alloy properties was also discussed. A general graduate textbook describing the optical properties of metallic and dielectric solids was contributed in the same year by Wooten (1972). Again, the emphasis was on perfect crystals, but a very useful introduction to the Drude and Lorentz theories was given, with a lucid account of the quantum mechanical, energy band approach. A comprehensive review of the CPA method for energy bands was given by Elliott et al (1974), showing the usefulness of this method for calculating many diverse properties of disordered alloys, such as the phonon and photoemission densities of states, as well as the optical functions. The CPA was used by Gelatt and Ehrenreich (1974) in an analysis of the concentration dependence of the d + FS band gap for Ag-Au alloys. The earlier work of Levin and Ehrenreich (1971) was extended to consider the effect of transfer of d-electrons in addition to that of s-electrons. A best fit to the experimental data was now obtained with a net charge transfer (Au + Ag) of only 0.07e/a compared with 0.3 for s-electrons alone. The improved theory did not offer any improvement in the description of optical data but was in accord with non-optical experiments which indicate a very small net charge transfer.

A simple theoretical model of the optical absorption of silver was used by Antonangeli et al (1974) to describe the temperature dependence of  $\epsilon_2^b(\omega)$  as measured by Liljenvall and Mathewson (1970). Since band structure calculations, piezo-reflectance and photo-emission studies had all supported the assumption that  $L_3 \rightarrow L_2'$  (FS) and  $L_2' \rightarrow L_1$  transitions are responsible for the absorption near 4eV, these identifications were assumed. Theoretical expressions for the dependence of  $\epsilon_2^b(\omega)$  on frequency for just these two transitions are quite tractable if the energy gaps and oscillator strengths are treated as adjustable parameters. Using this method,  $\epsilon_2^b$  could be fitted to within 5% of the experimental value over a wide range of temperatures. The energy gap obtained by this 'lineshape analysis' is then of more use in a theoretical model of the energy bands than that taken from some arbitrary spectral feature such as the energy where the absorption reaches half of its maximum value. Colavita et al (1975) also used lineshape analysis to fit the data of Pells and Shiga (1969) for the temperature dependence of the interband absorption of copper. Again two transitions were assumed,  $L_3 \rightarrow L_2'$  (FS) (2.095eV at r.t)  $X_5 \rightarrow X_4'$  (FS) (2.30eV at r.t). On this occasion the fit was of the order of 1%. The temperature dependence of the optical properties of copper were the subject of fresh experimental attention by Johnson and Christy (1975) who measured the reflectance and transmittance of thin evaporated films. Janak et al (1975) reported the results of a two-parameter band theory of copper, in which one parameter was used to fit the shape of the Fermi surface to the results of de Haas-van Alphen and cyclotron resonance measurements, while the other was used

to fit the optical spectrum. Agreement to within the experimental variation was found using only these parameters. The great improvement over the results of Mueller and Phillips (1967) was attributed to the use of a more accurate crystal potential and the explicit calculation of transition probabilities.

Weiss and Muldrew (1974) used Kramers-Kronig (K - K) analysis of reflectance data to obtain  $\epsilon_2(\omega)$  for gold and Au-Zn alloys. They pointed out that  $\epsilon_2$  was scaled by the high frequency extrapolation of  $R(\omega)$ . Veal and Paulikas (1974) discussed the low frequency extrapolation of reflectance data for K - K inversion, concluding that the value ultimately obtained for  $\tau$  was dominated by this choice. However, structure in the absorption spectrum is less sensitive to these somewhat arbitrary extrapolations, and Weiss and Muldrew found shoulders in  $\epsilon_2^b(\omega)$  at 3.7eV and 4.4eV as well as the edge at 2.3eV and peaks at 3.05 and 3.9eV, in their experiments on gold.

Ellipsometry was used to study the optical properties of silver and some dilute silver alloys by Flaten and Stern (1975), who used the alloy results to separate the two contributions to the band edge at 4eV, extrapolating the alloy results to zero concentration to obtain the values for pure silver. Christensen's (1972) relativistic band structure was used to interpret the results, the  $L_4^- \rightarrow L_4^+$  energy gap being estimated as 3.3eV. The silver films used in these experiments were not annealed, as no room temperature aging effects were observed. Grebennik et al (1975) have shown that self-annealing does not take place if silver films are coated with germanium, presumably due to

the suppression of diffusion of dissolved oxygen. It cannot be assumed that room temperature stability indicates a similar crystalline state to that obtained by annealing at several hundred degrees. Rivory and Theye (1975) found that a partial pressure of argon stabilised vapour quenched Ag-Cu films.

The latter work was concerned with studying Ag-Cu alloys at concentrations much greater than those employed by Beaglehole and Erlbach (1972). It was found that silver added to copper did not perturb the edge at 2.1eV, but moved the edge near 4.5eV to lower energies. This was attributed to a perturbation of the bottom copper d-band,  $L_1$ , by the upper silver d-band. Copper added to silver did not perturb the edge at 4eV despite the sensitivity of the  $L_1$  level to the potential; a new absorption band centred at 3.1eV and 0.4eV wide was observed. The magnitude of this,  $\frac{\delta\epsilon_2}{C}$ , was about 0.04 per atomic per cent copper. These results were consistent with those of Beaglehole and Erlbach at lower concentrations. Similar data were reported by Rivory (1976) with the addition of direct current resistivity measurements. Despite the microcrystalline (grain size 15 - 20Å) nature of the metastable samples, the resistivity of the samples were found to increase with increasing impurity concentration. Rivory (1977) gave new results for Ag-Cu alloys, including calculation of the effect of alloying additions on the optical mass and relaxation time. The observations were only qualitative, again agreeing with those of Beaglehole and Erlbach.

Au-Cu alloys were studied by Scott and Muldrew (1974) and Rivory (1977). The absorption edge of disordered AuCu<sub>3</sub> was

found by Scott and Muldrew to be at a slightly lower energy than that of pure copper (as found by Beaglehole and Erlbach for up to 3% gold in copper), while on ordering the edge moved 0.2eV to higher energies (this is in a region of the spectrum where the eye is very sensitive) and a new absorption peak appeared at 3.28eV. However, it was reported that ordering produced no noticeable effect on colour. Rivory(1977) found the absorption peak at 3.6eV for ordered  $\text{Au}_{19}\text{Cu}_{31}$ , in agreement with Nilsson and Norris (1969). For ordered  $\text{Au}_{46}\text{Cu}_{54}$ , the peak was at a slightly higher energy (3.75eV). The variation of the onset of interband transitions for disordered Au-Cu alloys was found to have a negative deviation from linear interpolation between the pure metal values, as for Ag-Au alloys. No significant shift was found for gold concentrations between 0 and 30 at.%, and no measurements were made between 30 and 60 at.% gold.

The term 'thermvariation' was coined by Winsemius et al (1976) to describe the measurement of optical properties at different temperatures, with sufficient accuracy to enable the difference spectrum  $\delta\epsilon_2 = \epsilon_2(T_1) - \epsilon_2(T_2)$  to be calculated. This is obviously closely related to the thermomodulation technique. Beattie's (1955) polarimetric method was used to obtain thermvariation spectra for silver, gold and copper at temperatures between 40K and 840K. It was concluded that for these metals, temperature induced changes in lattice constant dominated the results obtained, so that these could be directly compared with hydrostatic piezo-modulation data. Thermal broadening of the Fermi surface did not have a large effect. Line shape analysis of the  $\delta\epsilon_2$  spectra, similar to

that of Antonangeli et al (1974), was used to aid interpretation. In the case of silver, transitions which were held to contribute to the visible absorption were  $L_{4-}(\text{FS}) \rightarrow L_{4+}$  at 3.86eV, extended transitions  $d \rightarrow \text{FS}$  at 3.98eV and  $L_{4-} \rightarrow L_{4+}$  at 4.11eV. The importance of Fermi surface to conduction band  $L_{4-}(\text{FS}) \rightarrow L_{4+}$  and the extended  $d \rightarrow \text{FS}$  transitions was heavily emphasised. For gold, the important transitions are  $X_7^{+3} \rightarrow \text{FS}$  at 1.94eV, which is responsible for the absorption 'tail' noted by several authors,  $L_{5+} + 6+ \rightarrow L_{4-}(\text{FS})$  at 2.45eV,  $X_7^{+3} \rightarrow X_6-$  at 2.87eV,  $L_{4-}(\text{FS}) \rightarrow L_{4+}$  at 3.57eV and  $L_{4-} \rightarrow L_{4+}$  at 4.20eV. Copper has contributions from three transitions;  $L_{5+} + 6+ \rightarrow L_{4-}(\text{FS})$  at 2.13eV,  $L_{4-}(\text{FS}) \rightarrow L_{4+}$  at 4.31eV and  $L_{4-} \rightarrow L_{4+}$  at 4.81eV. Clearly an accurate representation of the spectra requires the consideration of a large number of band gaps for these particular metals. Note, however, that none of these assignments correspond to transitions from the bottom of the d-bands to the Fermi surface, as suggested by many previous authors for the second large absorption peaks in gold and copper. Rather, the onset of absorption is again attributed to transitions from the top of the d band to the Fermi surface near L (with a contribution near X for gold), and the other transitions are all between conduction bands, including initial states at the Fermi energy. Rivory (1977) accepts the assignment of transitions from the top of the d-bands to the Fermi surface as responsible for the fundamental absorption edge in each of the pure noble metals; for silver the influence of transitions  $L_{4-} \rightarrow L_{4+}$  is also cited, but there is no mention of  $L_{4-}(\text{FS}) \rightarrow L_{4+}$ . Higher energy transitions (3.5 - 5eV) in gold and copper are attributed as before to inter-conduction band transitions and those from the bottom

d-band to the Fermi surface near L. Contributions near to X are again mentioned in the case of gold, for energies near to 4eV.

Rivory also discusses the intraband absorption of the noble metals, giving the optical masses and relaxation times. A frequency dependent component of the relaxation time was found, which was interpreted as due to the effects of disorder. Structural disorder in the pure metals was held to be similar to substitutional disorder in alloys, which leads to a frequency dependent impurity scattering term in the relaxation time.

### 3. EXPERIMENTAL

#### 3.1 Instrumentation

The automatic following ellipsometer described in Roberts and Meadows (1974) and more fully in Meadows (1975) was modified to allow continuous spectral operation from the near ultra-violet to the near infra-red (250-850 nm). The modifications were carried out progressively, and caused some degradation of the instrument's performance, in terms of resolution and absolute accuracy. Measurements made early during the research program were at only a few discrete wavelengths, as a mercury arc light source was still in use, but had a resolution of the order of  $0.001^\circ$ . Later, when the Ag-Au binary alloys were first studied, a xenon arc light source was available, which permitted continuous measurements over the range 250-575 nm. The final experiments were made over a range of 250-850 nm using an additional, red-sensitive photo-multiplier.

A brief description of the ellipsometer will be given, paying particular attention to those aspects which differ from the account of Meadows (1975). A diagram showing both optical and electronic systems is given in Figure 3.1, to which the numbers in parenthesis that follow refer.

#### Optical Path.

The light source (1) originally used was a Hytek mercury vapour, 250W type ME/D arc lamp. This provided a line spectrum of sufficient intensity to enable operation on 577.1, 546.1, 435.8 and 366 nm. According to the manufacturers' data, the radiance of the 546.1 nm line is the greatest at  $1.4\text{W sr}^{-1}$ . For an arc size of  $0.5 \times 3.75$  mm (manufacturers' data), this implies an

absolute radiance of about  $23\text{W sr}^{-1}\text{ cm}^{-2}$ . In order to provide a continuous spectral source, this lamp was replaced by an AEG-Osram high pressure xenon lamp, type XBO450W/4, rated at 450W and having a 'spectrosil' window, transparent in the ultra-violet. The absolute spectral radiance of this source is stated as  $\sim 0.4\text{W sr}^{-1}\text{ cm}^{-2}\text{ nm}^{-1}$  over most of the visible, so that for a 10nm bandwidth about  $4\text{W sr}^{-1}\text{ cm}^{-2}$  can be expected, or about one-fifth of the value for the original lamp. Meadows observed that the ellipsometer operated satisfactorily, although at increased noise level, for light of intensity down to about one-tenth; it has been found during this work that resolution has been reduced to of the order of  $0.01^\circ$  in analyser and polariser values over most of the spectral range, for an operating bandwidth of 10nm.

It is frequently suggested that smaller xenon arc lamps make more suitable light sources for this type of application, as the reduced light intensity is compensated by reduced arc size. Indeed, 75W xenon lamps have a similar luminance to 450W lamps (40,000 Lumens compared with 35,000), although arcs of intermediate power (150W, 250W) are much inferior. It is difficult to judge the relative merits of these options without a trial, but it seems probable that better collimation could be achieved with a 75W arc, whilst the 450W arc may permit a larger luminous flux in the beam, should collimation be rather less good.

The lamp was operated from an 80V, 30A direct current supply, using a  $\pi$  filter to remove 100Hz ripple from the full-wave regulated d.c. Two sections of 5000 $\mu\text{F}$  capacitors were used with a 10mH inductor to achieve a total ripple of less than 25mV. It is important to reduce this figure as much as possible for

two reasons. It is the alternating component of the lamp current which is primarily responsible for erosion of the cathode, causing enlargement of the arc, arc wobble and eventually lamp failure. Secondly, modulation of the lamp's radiance at any frequency increases the possibility of overloading the detector amplifiers. An adjustable ballast resistor was used to control the lamp current and to ensure high stability, both this resistor and the lamp-housing being water-cooled to reduce fluctuations in the temperature of the laboratory. A total of about 3kW has to be dissipated. Additionally, forced air convection is used to cool the power supply and lamp. Air is drawn over the lamp, keeping the silica envelope at a uniform temperature and carrying away the large quantities of ozone produced. This is blown through a filter of activated charcoal before being released into the air. The light is collimated (2) using a single plano-convex silica lens, of focal length 75mm. This was used with both mercury and xenon light sources, allowing operation at 366nm with the mercury lamp. The beam is then stopped down to a diameter of  $\sim 2$ mm (3, 4) before entering the polarising prism. To isolate single lines from the mercury lamp, a graded interference filter was placed before the polariser; it had a U.V transparent backing plate, and a bandwidth of 25nm. The polariser (5) was a Glan-Foucault (air-gap) type, usable to 230nm wavelength and was mounted in a servo-goniometer. Next in the optic train is the polarizer Faraday-modulator (6) containing a 50mm core. Two types of core were used: with the mercury lamp, and for the 250-575nm range with the xenon lamp, a silica core was used; for the range 480-850nm with

the xenon lamp, a double-extra-dense flint glass core (Chance Pilkington DEDF) was used. Optimum modulation was about  $\pm 1^\circ$  which was achieved by the silica cores at  $\sim 300\text{nm}$  and the DEDF cores at  $\sim 600\text{nm}$ . It is instructive to consider the mechanism of the Faraday Effect, by which a longitudinal magnetic field is used to modulate the plane of polarization of the transmitted beam. Normal dispersion over the useful wavelength range of the core materials is caused by the presence of absorption bands in the ultra-violet region. The effect of the magnetic field is to produce Zeemann splitting of the absorption bands, so that at any particular wavelength there are two different effective refractive indices. One of these is appropriate for left-handed circularly polarized light while the other is appropriate for right-handed, so that these travel at different velocities through the core. If the linearly polarized light entering the modulator is decomposed into left- and right-hand circularly polarized components, it can be seen that a phase-lag between the components is introduced by the Zeemann splitting. Recombination of the components shows that the plane of polarization has been rotated. The amount of rotation depends on the phase lag, and hence on the difference between the refractive indices. Because of dispersion, this difference depends not only on the amount of splitting (and thus the magnetic field), but also on the distance from the absorption band. At long wavelengths, the refractive index is decreasing only slowly with wavelength and modulation is small. On the other hand, the short wavelength range is necessarily restricted by the presence of the absorption band. Clearly it is difficult to cover a wide spectral range using a single modulator core material.

### Mechanical Assembly

The ellipsometer was constructed on a massive cast-iron marking table, the surface of which was machined flat to one-thousandth of an inch per foot. On this the incident arm was firmly fixed; carrying the light source, polariser goniometer, Faraday modulator and compensator. A vertical plate was provided, on which samples could be fixed, which has an axis of rotation co-incident with the optic-axis along the incident arm. This back plate had kinematic controls facilitating accurate adjustment of the position of the sample and the plane of its surface. A mechanical linkage connected the back plate to a movable post-reflection section of optical bench, designed so that the plane of the sample was automatically turned through half of any angle through which the post-reflection arm was turned. This eliminated the need to re-adjust the sample when the angle of incidence was changed, and facilitated adjustment of the compensator and servo-systems, as the arm could easily be returned to the 'straight-through' position. The post-reflection arm carried a Faraday-modulator, analyser goniometer, grating-monochromator and photo-multiplier assembly. This amounted to a considerable mass, for which reason an air lubricated bearing was fitted, distributing the load over about  $5\text{cm}^2$  of the bench. This reduced wear during movement of the arm, and simply by turning off the compressed air supply, the arm could be locked rigidly in position. Vertical movement of the arm, previously caused largely by eccentricity in the wheel on which it was supported, has been effectively eliminated.

After passing through the polarizer modulator, the beam goes through a second stop (7) before entering the compensators (8). This consists of an achromatic quarter-wave rhomb (King and Downs 1969), calibrated by Dr R King of the National Physical Laboratory to be within  $0.1^\circ$  of  $90^\circ$  over the entire visible spectrum. The position of the rhomb on the fixed incident arm is preferred to the alternative position on the post-reflection arm, as the quarter-wave device is extremely sensitive to vibration. Temperature control of the rhomb as was previously employed for a mica quarter-wave plate has been found to be unnecessary. Thus elliptically polarized light falls on the reflecting surface (9), which restores linear polarization. A second stage of plane-of-polarization modulation then takes place (the analyser modulator, (11)) in a Faraday-cell similar to the polarizer modulator, but operated at 1230Hz rather than 1630Hz. The doubly modulated light then passes through a third stop before entering the analyser prism (12). The analyser prism and servo-goniometer are of identical construction to the polariser components. When the mercury-lamp was in use, the next stage was detection in a U.V-sensitive photo-multiplier, EMI type 9656QR. Subsequently, a grating-monochromator (13) was placed between analyser and photo-multiplier (14). A Spex Mini Mate monochromator was used with 10mm slits, giving an optical bandwidth of 10nm. In some earlier experiments, a bandwidth of 20nm was used. A red-sensitive photo-multiplier R.C.A type 8852 is used to supplement the E.M.I tube. Normal practice was to use the EMI tube with silica modulator cores to cover 250-540nm, and to employ the R.C.A tube with DEDF cores for the range 480-850nm.

The servo-goniometers were as described by Meadows (1975) with the exception that the subsidiary gear-box was replaced, reducing resolution to  $0.001^\circ$ , which was better than the prevailing noise figure by an order of magnitude. This provided an increase in speed to about  $1^\circ \text{ s}^{-1}$ , and made possible direct readout of analyser and polariser settings in units of  $0.001^\circ$ .

Reproducibility of angle of incidence was improved to about  $0.01^\circ$ , by the addition of a linear dial-gauge. The linkage between the sample mounting plate and post-reflection arm was via a sine arm which provided a convenient place for monitoring angle of incidence, as there was a collar sliding on a fixed bar, the relative positions of which uniquely determined the angle between incident and post-reflection optic axes. Provided the sample was accurately aligned to the optic axes, the dial-gauge reading enabled the same angle of incidence to be consistently re-used.

#### Electronic Systems

Each of the Faraday modulators was driven from a small power-amplifier, which in turn was driven from a Wien-bridge oscillator (frequency  $f_1$  or  $f_2$ ). The resulting photo-multiplier signal consists - at the null - of  $2f_1$ ,  $2f_2$  and noise. Away from the null  $f_1$  and  $f_2$  appear, the phases of which depend on the sense of the deviation from the null. Phase-sensitive detectors provided error signals which were used to derive pulse trains for operation of stepping-motors on the servo-goniometers, so that any deviation or error was continuously minimised. Reversible decade counters monitored the stepping pulses,

providing direct readouts of the differences between analyser and polariser settings and their calibrated 'zeroes'. Resolution was rather better than  $0.01^\circ$  over most of the range 350-750nm, deteriorating to  $\sim 0.1^\circ$  at the extremes (250 and 850nm).

### 3.2 Sample Preparation

Initially, a set of thirty samples was to be prepared. These were required to be 10mm by 25mm by 1mm thick, to accommodate the ellipsometer beam and for convenience in handling. Most samples were prepared by melting a billet 10mm in diameter and a few millimetres in height, and then working this by a combination of forging and rolling into the desired form. To relieve internal stresses and prevent cracking, intermediate anneals were performed after each stage of working, and finally the samples were invariably quenched. One sample, 80.1Au - 19.9Cu, was approximately the composition of the intermetallic compound AuCu and proved extremely brittle. It was impossible to work into the required form and was therefore recast as a plaquette. When homogeneity was poor, the samples were remelted. This was necessary for several of the samples melted in the vacuum and induction furnaces, which were allowed to cool by natural convection, and so the last samples prepared were quenched from the melt.

Mechanical working of the samples served both to homogenise and reduce them to the desired form. The Au-Cu alloys generally required more cycles of working and annealing due to their brittleness, but the alloy mentioned above was the only one to cause real difficulty. Subsequently, another sample of nominal 80Au-20Cu was cast into plaquette form and polished

without any mechanical treatment.

The fine gold and Ag-Au binary alloys were annealed in air, while the others required a protective atmosphere. Initially a continuous flow of argon was used at just above atmospheric pressure, and subsequently these samples were sealed into glass ampoules under vacuum. Quenching was normally performed by tipping the samples into water.

#### Melting

Several different furnace arrangements were tried, and a settled method was not achieved until all but a few of the samples had been prepared. The first melt was carried out in a Wilde-Barfield vacuum furnace, type 2904B, under a pressure of  $50\mu$  torr dry nitrogen. The metals, in the form of small granules (Ag-Au) and small pieces of copper rod, were intimately mixed in alumina crucibles and placed in the furnace. No stirring during the melt was possible, nor was it possible to observe the crucibles. Temperature was monitored using a platinum-rhodium thermo-couple. After a suitable period of time the alloys were removed from the furnace, when it was found that silver from two of the crucibles had evaporated, modifying the composition of the nominal 90Ag-10Au and contaminating the Au, Cu and 90Au-10Cu samples. The results of the analyses performed by the Assay Office, London, support this view. Accordingly, the next melt was carried out under dry nitrogen at 1.5 p.s.i above atmospheric pressure in the same furnace. The furnace was flushed by evacuation followed by refilling with dry nitrogen. Since the billets had proved hard to release from the alumina crucibles, a graphite block

was machined to accept six charges in well-separated pockets. Although this proved successful, a suspicion that the temperature gauge was working incorrectly and the operational difficulty of the procedure meant that another method was tried.

A Radyne high frequency induction furnace, Model C90, was used to heat the charges. The induction coil was wrapped around a vertical silica tube, through which a continuous flow of dry nitrogen was maintained. The graphite block then acted as susceptor as well as container. As with the vacuum furnace, no stirring was possible and the alloys were left to cool over a period of about thirty minutes. Temperature was monitored using an optical pyrometer.

Again, this technique gave adequate results, but sample homogeneity was not always good from the first melt. Segregation of the components seemed a likely possibility during the relatively slow cooling and solidification and so a quench furnace was constructed. This was made from a graphite block, with only one pocket so that only one melt could be carried out in each operation. At the bottom of the pocket a small hole was drilled, through which the molten metal could pour. This hole was blocked by a graphite slip until the appropriate temperature had been reached. A polished steel dish filled with oil was placed under the container and this arrangement ensured rapid quenching from the melt. The top of the pocket was loosely sealed by a wood-charcoal plug, to reduce oxidation, as it was not possible to provide a protective atmosphere. Support was provided by the induction coil, which was wound

directly on the graphite container. This technique gave improved homogeneity, and flatter billets which required less working to produce the one millimetre thick samples needed for the ellipsometer.

#### Thermo Mechanical Treatment

Typically, two stages of mechanical work were performed. The first stage was cold forging, using a 30-ton Amsler mechanical testing machine in compression, and the second consisted of cold rolling using a small jeweller's rolling mill.

The samples were forged between polished steel plattens to prevent contamination. Between each stage of this treatment intermediate stress-relieving annealing was performed. The billets produced by vacuum furnace, and those induction furnace melts which were not quenched from the melt, were forged under different compressive loads. In each case the load was applied to the point, in the operator's judgement, when the maximum degree of work hardening had been induced in the sample. Some idea of the brittleness of the alloys may be gauged from the number of cycles of working/annealing needed to reduce the samples to one millimetre thickness. In general the Ag-Au alloys needed about half the number of cycles found necessary for the Ag-Cu and Au-Cu alloys. The dilute alloys are softer than the concentrated ones. Subsequent stages of forging were carried out in the same manner.

Smooth, polished steel rollers were used in the rolling stages. Each stage comprised repeated reduction by small amounts until the sample appeared to have acquired its

maximum hardness or resistance to deformation without cracking. At this point the sample would again be annealed. Some anisotropy appears to have been introduced into the two-phase (Ag-Cu) alloys by rolling.

Most samples underwent forging as the final stage of mechanical treatment, but the last samples prepared, those quenched from the melt, were rolled.

The first attempt to anneal any samples was made on the nominal 10Au-90Cu and 80Au-20Cu. A horizontal tube furnace, constructed in the department, was employed. This featured an alumina tube, with a 'kanthal' heating element, and hinged at the centre so that samples could be tipped out for a rapid quench. Argon was passed through the tube throughout the procedure, to provide a protective atmosphere. Due to difficulty in sealing the ends of the tube, the protective atmosphere was not sufficient to prevent contamination and this method was not pursued.

Consequently, a vertical tube furnace of similar construction was tried. In this, the samples were suspended in a small bag of glass-fibre, arranged so that they could be dropped out into water for quenching. Again, Argon was passed up through the furnace. Although this was an improvement, some contamination again took place. The contamination film, presumably oxide, was removed using sulphuric and nitric acids.

The method adopted for the majority of samples involved the use of an air circulating furnace, which could accommodate a large number of samples at an even temperature (Heraeus type KL200). The alloys which required protection from oxidation

were sealed in small glass vacuoles, which were flushed out using dry nitrogen and evacuated using a rotary pump. The usual annealing temperature was  $600^{\circ}\text{C}$ , but the vacuoles retained their integrity even for the two cases when annealing took place at  $750^{\circ}\text{C}$ . Quenching of the sealed samples was by tipping into water. In the rare case when the glass failed to fracture on contact with the water the annealing procedure was repeated. For those alloys annealed in air (Au, Ag-Au), it was considered that a water-quench was unnecessary. In their final form the plaquettes were one millimetre thick, so that cooling would have been extremely rapid once they were removed from the furnace. Accordingly, they were simply withdrawn and allowed to cool in air. In a few cases, alloys annealed in air were water-quenched along with some vacuum annealed ones.

Quenching of the vacuum annealed samples, although appearing satisfactory, left certain of the Au-Cu alloys in a rather brittle condition. It was felt that to achieve a more rapid quench, the glass vacuoles previously used would have to be dispensed with. Accordingly, an electric salt bath furnace was used. No suitable salt for  $600^{\circ}\text{C}$  was available, ICI salt Cassel AS650 (melting point  $650^{\circ}\text{C}$ ) being used instead. Short anneal times are sufficient to produce complete disordering of Au-Cu intermetallic compounds at this temperature.

#### Mounting

Two methods of mounting the alloys (for polishing and optical measurement) were used. In both cases, cylindrical mounts were produced of about 30mm diameter and 10-15mm depth. The

mounts could be drilled and tapped for fixing on the ellipsometer back-plate, and were convenient for grinding and polishing.

The Ag, Au, Cu, Ag-Au and Ag-Cu alloys were mounted in bakelite in a 'Metalo' automatic mounting press, manufactured by M E Lowe. According to the manufacturers, the maximum temperature experienced during this operation should not exceed 140-150°C. This was felt to be too high for mounting the Au-Cu samples, as the intermetallic phases are very easily produced. These were 'cold-mounted' using Metset slow-setting mounting plastic, manufactured by Metaserv. This involves an exothermic reaction which for samples of this size should not have produced temperatures in excess of 30-40°C.

#### Grinding and Polishing

The samples were ground by hand, using wet silicon carbide papers on a flat perspex base. Care was taken not to use excessive pressure, avoiding contamination by particles of carbide. Copious quantities of water were used to keep the carbide papers free of loose grit during the grinding process.

Four grades of successively finer grinding paper were used: 320, 400, 500 and 600 lines per inch. The final paper was pre-worn using brass blanks to reduce the depth of the final scratches, removed by polishing. Between each grade of paper the samples were carefully rinsed, and rotated through 90°. This procedure makes it clear when the coarser scratches from the previous paper have been completely removed, and avoids 'smearing' the surface of the metal, which can result in a heavily worked layer overlying deep scratches.

Mechanical polishing in three stages, using diamond grit lubricated by white spirit, was used to produce the final surface. Grit sizes of 6, 1 and  $\frac{1}{2}$  micron were used for this stage. Between each grit size and following the final polish, the samples were cleaned using 'teepol' and distilled water. It was possible to rinse the teepol from the sample surface using a jet of distilled water, which then broke away from the surface leaving it clean and dry. Ellipsometric measurements were started within fifteen minutes and normally completed within three hours.

#### Analysis

The alloys were assayed, using chemical and electro-chemical methods, by the Assay Office, Goldsmiths' Hall, London. Analysis was made of only one component in each alloy, the other component being determined by difference. This is indicated in the Table 3.1 by the use of parentheses.

#### 3.3 Measurement Procedure

Basic alignment of the optical components, adjustment of the compensator to  $45^\circ$  azimuth and adjustment of the electronic systems was carried out as in Meadows (1975) Section 3. The quarter-wave device and electronics were set up at 500nm, as this is the middle of the overlap of the two detectors and modulator cores. Alignment of the reflecting surface was also carried out by much the same method. A frame was constructed to hold a small laser (0.5mW He-Ne, 632.8nm) in a vertical position immediately in front of the lamp housing. A thick aluminium plate attached to the base of this laser by two large spring-loaded screws allowed small adjustments to be made

to the laser's position and tilt. A small front-silvered mirror at  $45^\circ$  to the vertical could be placed on the optical bench beneath the laser, to reflect the beam along the optic axis. Fine adjustment of the height of the beam could be made with this mirror. Using this arrangement, with a plane mirror at the far end of the optical bench to return the beam, the optical axis could routinely be defined in a matter of minutes. However, it was found that after two passes along the axis the beam became too faint to distinguish from reflections from the many optical components, so that a somewhat shorter path length was obtained. This could be increased by removing some components from the bench, but replacement of these (either delicate or massive) components caused greater errors so that no benefit was obtained. For this reason adjustment of the reflecting surface to only  $\sim 0.01^\circ$  is claimed (cf.  $\sim 0.002^\circ$  by Meadows).

A complete experiment required less than 4 hours, from the final  $\frac{1}{2}\mu$  diamond polish of the alloy to the final ellipsometric reading. The time between final polishing and the first measurement was in the range 5-10 minutes, during which the reflecting surface was aligned, monochromator and photo-multiplier replaced, post-reflection arm moved to the chosen angle of incidence and the goniometers moved to the required position for nulling. As the main problem concerning duration of an experiment is with tarnishing and oxidation of the metal surface the short-wavelength ellipsometric parameters were measured first. The effect of contamination films increases with film thickness but decreases with wavelength, so this method should minimise the errors introduced by neglecting surface films. The interval between successive readings was of the order of one minute,

as the small wavelength change (5 or 10nm) did not normally involve large angular displacements of the prisms. The servo-mechanism was able to follow changes of this order without a very large settling time, although it was necessary to leave the monochromator at each wavelength setting for about one minute to avoid errors from the lag of the servo system.

An E.M.I photo-multiplier type 9656QR was used to cover the wavelength range 250-540nm. When the latter wavelength was reached, the instrument was returned to the 'straight-through' position and checked for drift. Assuming this was  $\sim 0.02^\circ$ , the silica modulator cores were then replaced by those of DEDF. A period of about 20 minutes was allowed for these to reach thermal equilibrium, since the modulators run several degrees above ambient despite being water-cooled. The compensator and electronic systems were then reset to eliminate error from stress in the new cores. The reflecting surface was re-aligned, and the instrument restored to the same angle of incidence. Measurements were then taken in the range 480-850nm using an R.C.A 8852 photo-multiplier. Finally the ellipsometer was again returned to the straight-through position and checked for drift.

as the small wavelength change (5 or 10nm) did not normally involve large angular displacements of the prisms. The servo-mechanism was able to follow changes of this order without a very large settling time, although it was necessary to leave the monochromator at each wavelength setting for about one minute to avoid errors from the lag of the servo system.

An E.M.I photo-multiplier type 9656QR was used to cover the wavelength range 250-540nm. When the latter wavelength was reached, the instrument was returned to the 'straight-through' position and checked for drift. Assuming this was  $\approx 0.02^\circ$ , the silica modulator cores were then replaced by those of DEDF. A period of about 20 minutes was allowed for these to reach thermal equilibrium, since the modulators run several degrees above ambient despite being water-cooled. The compensator and electronic systems were then reset to eliminate error from stress in the new cores. The reflecting surface was re-aligned, and the instrument restored to the same angle of incidence. Measurements were then taken in the range 480-850nm using an R.C.A 8852 photo-multiplier. Finally the ellipsometer was again returned to the straight-through position and checked for drift.

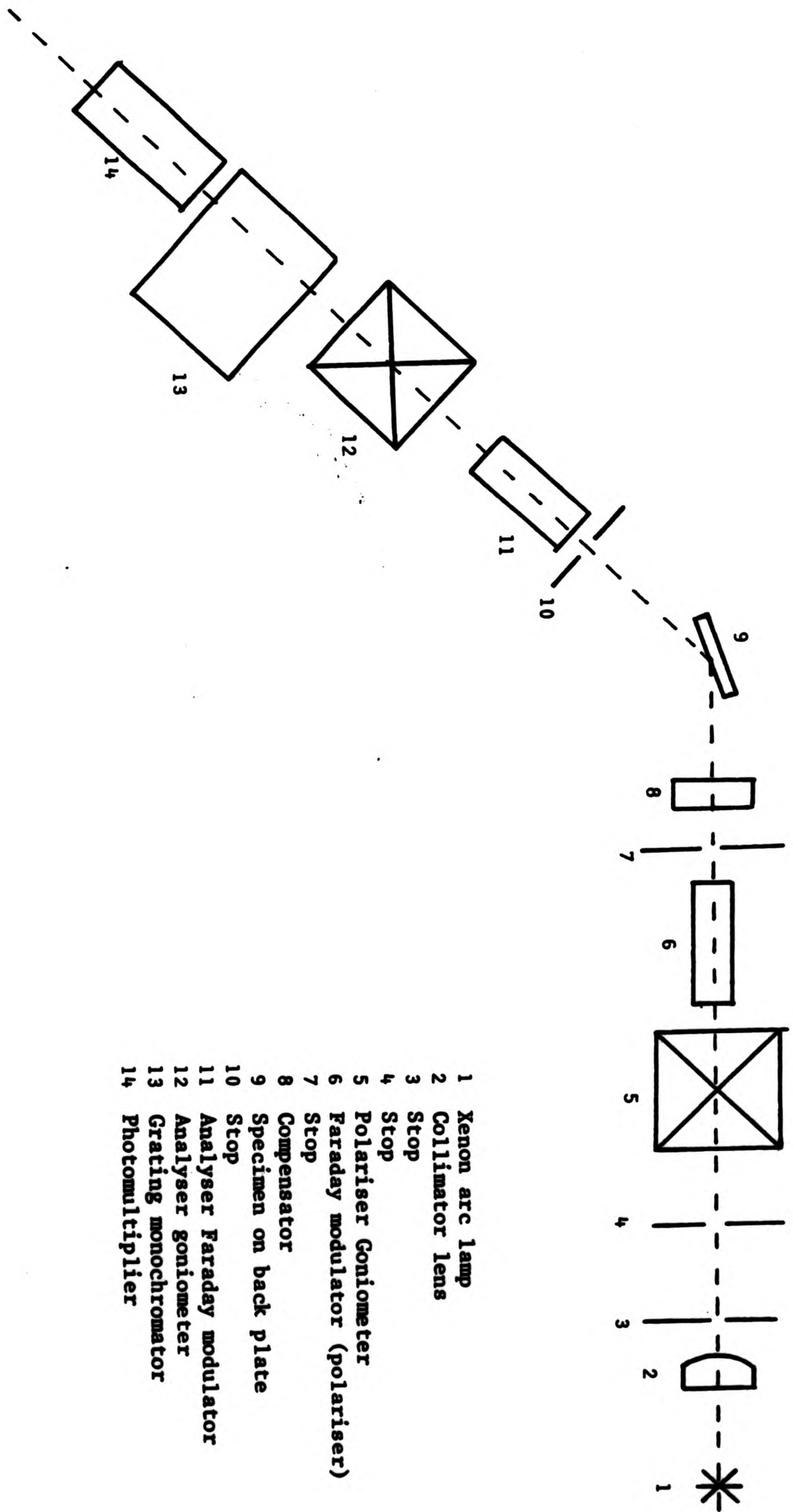


Figure 3.1. The arrangement of the optical elements.

Table 3.1. Thermomechanical Treatment

Alloy reference no.	Assayed composition (weight percent)			final melt conditions					No. of work/anneal cycles	final anneal			
				furnace	atmosphere	quench	melt time (minutes)	No. of melts		atmosphere	temperature (C°)	duration (hrs)	final quench
	Ag	Au	Cu										
1	-	-	98.3	V	V		-	1	2	V	600	2	W
1R		-	100	I	C	oil	-	1	1	V	350	1	W
2		9.9	(90.1)	I	N		20	3	2	V	600	2	W
3		18.2	(81.8)	I	N		15	2	5	V	600	2	W
4		31.2	(68.8)	I	N		20	1	4	V	600	2	W
5		34.9	(65.1)	I	N		20	1	4	V	600	2	W
6		48.5	(51.5)	I	N		15	2	5	V	600	2	W
7		63.1	(36.9)	I	N		10	1	5	V	600	2	W
8		70.0	(30.0)	I	N		10	1	5	V	600	2	W
9 <sup>(1)</sup>		80.1	(19.9)	I	N		-	3					
9R		80.3	19.8	I	N	oil	-	2	1	S	660	1	W
10 <sup>(2)</sup>		86.1	(13.9)	V	N		-	1	3	V	600	2	W
10R		89.5	(10.5)	I	C	oil	-	1	1	V	600	17	W
11 <sup>(2)</sup>		95.6		V	V		-	2	2	A	600	2	A
11R		99.98		I	C	oil	-	1	1	A	600	16	W
12	89.5	-	(10.5)	I	N		15	2	4	V	600	2	W
13	79.9	-	(20.1)	I	N		15	2	4	V	600	2	W
14	69.2	-	(30.8)	I	N		15	2	4	V	600	2	W
15	60.8	-	(39.2)	I	N		10	1	4	V	600	2	W
16	50.3	-	(49.7)	I	N		20	2	4	V	600	2	W
17	39.9	-	(60.1)	I	N		20	2	4	V	600	2	W
18	30.1	-	(69.9)	I	N		20	1	4	V	600	2	W
19	19.4	-	(80.6)	I	N		20	1	5	V	600	2	W
20	(10.6)	-	(89.4)	I	N		20	1	5	V	600	2	W

**Key:** (i) Compositions in parentheses are calculated by difference  
(ii) V - melted in Wilde Barfield vacuum furnace  
I - melted in Radyne induction furnace  
(iii) V - vacuum, C - air deoxygenated with hot charcoal,  
N - nitrogen, S - salt bath, A - air, W - water

**Notes:** (1) Sample 9 was used as cast  
(2) Samples 10 and 11 were probably contaminated by silver

Table 3.1 (contd.)

Alloy reference no.	Assayed composition (weight percent)			final melt conditions					final anneal				
				furnace	atmosphere	quench	melt time (minutes)	No. of melts	No. of work/anneal cycles	atmosphere	temperature (C)	duration (hrs)	final quench
	Ag	Au	Cu										
21	(9.8)	90.2		V	N			1	2	A	600	1	A
22	(20.0)	80.2		I	N		10	1	2	A	600	1	A
23	(29.8)	70.2		I	N		10	1	2	A	600	1	A
24	(39.8)	60.2		I	N		10	1	2	A	600	1	A
25	(50.0)	50.0		I	N		10	1	2	A	600	1	A
26	(60.1)	39.9		I	N		10	1	2	A	600	1	A
27	(70.0)	30.0		I	N		15	2	2	A	600	1	A
28	79.4	(20.6)		I	N		15	2	2	A	600	1	A
29	79.0	(21.0)		V	V			1	1	A	600	1	A
29R	39.9	(10.1)		I	C	oil		1	1	A	600	16	W
30	99.9			V	V			1	2	A	600	1	A
30R	99.97			I	C	oil		1	1	A	600	16	W
67	(0.5)	99.5											
68	98.2	1.7											
69	1.5		(98.5)										
70	99.4		0.7	I	C	oil		1	1	V	600	17	W
71		0.92	(99.08)										
72		99.7	(0.3)										
73	91.3		(8.7)										
74													
75	2.1		(97.9)	I	C	oil		1	1	V	750	17	W
76	96.0		(4.0)	I	C	oil		1	1	V	750	17	W
77		95.2	(4.8)	I	C	oil		1	1	V	600	17	W
78	(5.3)	94.7		I	C	oil		1	1	A	600	16	W

#### 4.1 Colorimetry

The objective measurement of colour is made by combining information about the spectral reflectance of the object under consideration with details about the brightness of the illumination and the responsivity of the human eye. It is necessary to consider the illumination, as it is the colour of the light entering the eye which is directly perceived and is subsequently translated by the brain into a judgement of the colour of the object. The problem is more complicated than simply noting that under blue light, say, an object appears more blue than it does in red light, as the observer's expectations influence his judgement. This is known as chromatic adaptation and cannot satisfactorily be quantified. It is of particular significance with regard to judgements of 'whiteness', which similarly cause difficulty. In this study these problems have not been fully treated, as useful results of a largely comparative nature can be very readily obtained.

##### The CIE 1931 Standard System

It is found that under restrictive experimental conditions, three quantities suffice to define any colour sensation. The restrictions are aimed at reducing the amount of information available to an observer and standardising the way in which it is presented. The CIE 1931 Standard System has been chosen, which specifies that psychological data be obtained by comparing samples for equality of sensation, with a  $2^{\circ}$  field of view against a neutral grey background. Experiments of this kind have been used to define responsivity curves

$\bar{x}(\lambda)$ ,  $\bar{y}(\lambda)$  and  $\bar{z}(\lambda)$ , describing the properties of a 'standard observer'. It is not necessary that these functions correspond directly to physiological properties, since they are used to compute only the three coefficients which define the colour sensation. Transformations may be applied to the coefficients to yield alternative and equivalent sets, which may be done to alter their individual significance. For instance, the quantities derived in the 1931 system ( $x$ ,  $y$  - the chromaticity co-ordinates,  $Y$ , the luminance), are specially significant only in the separation of the luminance (brightness) and chromaticity. In general, objects having the same luminance are judged to be equally bright, whilst those having the same chromaticity are judged to have the same hue and purity (or saturation). Objects having all three quantities in common are subjectively indistinguishable under the standard viewing conditions. The following relations are used to define  $x$ ,  $y$  and  $Y$ :

$$k = \left[ \int_{\lambda} S(\lambda) \bar{y}(\lambda) d\lambda \right]^{-1} \quad (4.1)$$

$$X = k \int_{\lambda} R(\lambda) S(\lambda) \bar{x}(\lambda) d\lambda \quad (4.2a)$$

$$Y = k \int_{\lambda} R(\lambda) S(\lambda) \bar{y}(\lambda) d\lambda \quad (4.2b)$$

$$Z = k \int_{\lambda} R(\lambda) S(\lambda) \bar{z}(\lambda) d\lambda \quad (4.2c)$$

$$x = \frac{X}{X + Y + Z} \quad y = \frac{Y}{X + Y + Z} \quad (4.3)$$

$R(\lambda)$  is the spectral reflectance of the object, which may be directly and accurately measured;  $S(\lambda)$  is the spectral brightness of the illumination;  $\bar{x}(\lambda)$ ,  $\bar{y}(\lambda)$  and  $\bar{z}(\lambda)$  represent

psychophysical data. These latter quantities are all available from tables,  $S(\lambda)$  being defined for several 'Standard Illuminants'.

#### Saturation and Dominant Wavelength

A non-analytic transformation has been applied to the  $(x,y)$  co-ordinates to obtain alternative quantities  $(s, \lambda_d)$  - saturation and dominant wavelength - which correlate with subjective assessments of purity and hue. They are derived in the following way -

- (a) Obtain the co-ordinates  $(x_0, y_0)$  corresponding to a neutral object colour, ie. one which has equal reflectance at all wavelengths in the visible. Obtain a set of pairs of co-ordinates  $(x_\lambda, y_\lambda)$  which define the locus of monochromatic radiations - these define the spectral colours which are the purest obtainable.
- (b) Extend a straight line from the point  $(x_0, y_0)$  through the point  $(x, y)$  until it intercepts the locus  $(x_\lambda, y_\lambda)$  at, say,  $(x_d, y_d)$ . The wavelength  $\lambda_d$  corresponding to the point  $(x_d, y_d)$  is called the dominant wavelength.
- (c) The saturation is the ratio of the distances  $(x_0, y_0) \rightarrow (x, y)$  and  $(x_0, y_0) \rightarrow (x_d, y_d)$ , ie.

$$s = \frac{\sqrt{(x - x_0)^2 + (y - y_0)^2}}{\sqrt{(x_d - x_0)^2 + (y_d - y_0)^2}} \quad (4.4)$$

The significance of this lies in the additive nature of colour sensations in the CIE system, which has been defined so that the chromaticity of a mixture of two colours A and B, having

co-ordinates  $(x_a, y_a)$  and  $(x_b, y_b)$  lie on a straight line joining  $(x_a, y_a)$  and  $(x_b, y_b)$ . If A and B are of equal luminance, then the distance of the mixture's co-ordinates along this line is proportional to the relative quantities of A and B. Thus the saturation is the relative proportions of white and mono-chromatic light of wavelength  $\lambda_d$ , needed to match the colour  $(x, y)$ . Should  $\lambda_d$  be undefined as it is for purple colours - then the complementary wavelength  $\lambda_c$  may be obtained by extending the line in the opposite direction.

#### Uniform Colour Spaces and the Colour Difference Formula

A useful property that the Standard system lacks is that it is not uniform; that is, colour differences which are in practice judged to be equal do not yield trichromatic co-ordinates of equal separations. This is particularly important as Just-Noticeable-Colour-Differences correspond to quite different separations in different parts of the diagram. It is thus not possible to state directly from Standard System calculations whether or not two alloys are subjectively indistinguishable. The CIE 1960 Uniform Colour System has been used in attempt to relieve this problem. The alternative co-ordinates  $(u, v)$  replace  $(x, y)$  -

$$u = \frac{4X}{X+15Y+3Z} \quad v = \frac{6Y}{X+15Y+3Z} \quad (4.5a, b)$$

where the quantities, X, Y and Z are as defined above. This system may be used to prepare colour diagrams in which equal colour differences are represented by equal lengths. However, even this system does not enable differences in

luminance to be included. For this purpose, the CIE 1964 Colour Difference Formula has been used -

$$W^* = 25Y^{1/3} - 17 \quad (4.6a)$$

$$V^* = 13W^*(v - v_0) \quad (4.6b)$$

$$U^* = 13W^*(u - u_0) \quad (4.6c)$$

where  $(u_0, v_0)$  represents the achromatic stimulus. Then

$$\Delta E = \sqrt{\{ (U_1^* - U_2^*)^2 + (V_1^* - V_2^*)^2 + (W_1^* - W_2^*)^2 \}} \quad (4.7)$$

#### Choice of Reflectance Function

The recommended methods for measuring simple reflectance involve non-specular scattering, typically by illuminating the sample at normal incidence and measuring the scattered flux at  $45^\circ$ . In the traditional applications, which may for instance concern coloured fabrics, paints or tiles, specular reflection would result in saturation being grossly underestimated due to the sheen or gloss of the materials. Colour measurement is often made at the quality control stage of manufacture, where variations due to sample finish are as important as those due to compositional or structural differences.

In this study of the noble alloys, an attempt has been made to isolate the effects of alloy composition from those of surface finish. For this reason, rather than try to produce samples that would give a strong non-specular reflection (by finishing with an abraded surface), the usual specular reflectance has been used. Normal reflectance has been calculated from the optical constants at wavelengths throughout the visible range, with 5nm intervals. In order to investigate

the effect of the angle of incidence (or reflection) on calculated colour co-ordinates, Fresnel's relations have been used to calculate the angle-of-incidence dependant reflectance.

Some consideration has also been made of the effect of surface roughness on the computed colour co-ordinates. Beaglehole and Hunderi (1970) have made an extensive investigation of the effect of micro-roughness on measured spectral reflectance, considering the effect of surface plasmon excitations as well as the effect of roughness period when this is of the order of a wavelength. They have found that short range roughness reduces the specular reflectance by an amount proportional to  $e^{-\frac{4\pi\sigma}{\lambda}}$ , which would make the reflected beam redder. However, when the roughness dimensions are much larger than a wavelength, the common observation (the "Tyndall Effect") is that scattering is independant of wavelength. In this case, one would still expect the scattered intensity to depend on the absorption of the material.

If diffraction effects are neglected, then light which enters the eye having been scattered from an (opaque) metal surface may be considered to be composed of a mixture of beams which have undergone different numbers of reflections at the surface. For example, some light will be directly reflected from the plane areas between large scratches, while some light may be reflected from each side of the scratch in turn before escaping. For samples observed under diffuse lighting conditions, the fact that these beams will be scattered in

different directions is not important. Accordingly, an attempt has been made to describe the properties of grossly rough surfaces (such as those produced by abrading with emery paper), by replacing the plane-surface reflectance  $R(\lambda)$  by a rough surface function  $R^R(\lambda)$ :

$$R^R(\lambda) = R(\lambda)^n \quad (4.8)$$

where  $n$  is an integer.

#### 4.2 The Application of Ellipsometry to the Determination of Reflectance and the Dielectric Function.

The automatic ellipsometer described by Meadows (1975) and Roberts (1974) has been used to determine the ellipsometric parameters  $\Psi$  and  $\Delta$  for light reflected from the polished surface of each of the noble alloys. The actual quantities measured are angular displacements of a pair of prisms, the Polariser and Analyser, these values being denoted  $P$  and  $A$ . They are simply related to  $\Psi$  and  $\Delta$  only if a perfect compensator is employed, that is, one which introduces a phase-shift of exactly  $90^\circ$ . Should this not be the case, then the compensator error should be determined and a set of equations given by, eg. Hunter Eaton and Sah (1970) used to correct the readings. In this investigation the achromatic quarter-wave rhomb described by Clapham, Downs and King (1969) provided a phase-shift of  $90^\circ \pm 0.1^\circ$  throughout the visible spectrum and so no correction has been applied. With the compensator on the incident arm,  $\Psi$  and  $\Delta$  are given by the following expressions.

$$\Psi = 45.0 - A \quad ; \quad P = 2\Delta \quad (4.9a,b)$$

$\Psi$  and  $\Delta$  represent, respectively, the relative amplitude change

and relative phase-shift of the p and s components of the light. The complex quantity  $\hat{\rho}$  is defined (on the Muller (1969) convention) by

$$\hat{\rho} = \tan \psi e^{i\Delta} = \hat{R}_p / \hat{R}_s \quad (4.10)$$

where  $\hat{R}_p$  and  $\hat{R}_s$  are the complex amplitude reflection coefficients for p and s polarized light.  $\hat{\rho}$  exactly defines the ellipticity of the reflected light.

The amplitude reflection coefficients for reflection of plane waves at a mathematically sharp, plane interface between two semi-infinite, homogeneous and isotropic media are given by Fresnel's relations:

$$\hat{r}_{01}^s = \frac{n_0 \cos \phi_0 - \hat{n}_1 \cos \phi_1}{n_0 \cos \phi_0 + \hat{n}_1 \cos \phi_1} = \frac{\sin(\hat{\phi}_1 - \phi_0)}{\sin(\hat{\phi}_1 + \phi_0)} \quad (4.11)$$

$$\hat{r}_{01}^p = \frac{\hat{n}_1 \cos \phi_0 - n_0 \cos \hat{\phi}_1}{\hat{n}_1 \cos \phi_0 + n_0 \cos \hat{\phi}_1} = \frac{\tan(\phi_0 - \hat{\phi}_1)}{\tan(\phi_0 + \hat{\phi}_1)} \quad (4.12)$$

$\hat{r}_{01}$  refers to the reflection of light passing from the medium of (real) refractive index  $n_0$  to a material of complex refractive index  $\hat{n}_1$ .  $\phi_0$  is the angle of incidence and  $\hat{\phi}_1$  is related to the angle of refraction. It is obtained by the use of a generalisation of Snell's Law:

$$n_0 \sin \phi_0 = \hat{n}_1 \sin \hat{\phi}_1 = n_j \sin \hat{\phi}_j \quad (4.13)$$

#### Clean substrate equations

These expressions for  $\hat{r}^s$  and  $\hat{r}^p$  are applicable directly in the case of reflection from polished, bulk metal samples provided that there is no contamination or corrosion of the surface. They may be inverted to give an equation for  $\hat{n}_1$ ,

the substrate refractive index, in terms of  $\rho$  and hence of the ellipsometric parameters:

$$\hat{n} = n_o \tan \phi_o \left[ 1 - \frac{4\hat{\rho} \sin^2 \phi_o}{(\hat{\rho} + 1)^2} \right]^{\frac{1}{2}} \quad (4.14)$$

$\Psi$  and  $\Delta$  are obtained from equation 4.10 which can be rearranged to give

$$\Psi = \tan^{-1} |\hat{\rho}| \quad ; \quad \Delta = \tan^{-1} (\text{Im } \hat{\rho} / \text{Re } \hat{\rho}) \quad (4.15a,b)$$

It is necessary to adjust the value of  $\Delta$  so obtained, according to the sign of the real part of  $\hat{\rho}$ , so as to achieve a value of  $\Delta$ ,  $0 < \Delta < 360^\circ$ , in the correct quadrant.

Equations (4.14) and (4.15) can be combined and expressed as real numbers, which can be convenient for computation, but at great expense in terms of elegance. Remembering that

$$\hat{\epsilon} = \hat{n}^2 = (n^2 - k^2) - 2nki = \epsilon_1 - i\epsilon_2 \quad (4.16)$$

One may write

$$\epsilon_1^{\text{substrate}} = n_1^2 - k_1^2 = n_o^2 \sin^2 \phi_o \left[ 1 + \frac{\tan^2 \phi_o (\cos^2 2\Psi - \sin^2 2\Psi \sin^2 \Delta)}{(1 + \sin 2\Psi \cos \Delta)^2} \right] \quad (4.17a)$$

$$\epsilon_2^{\text{substrate}} = 2n_1 k_1 = 2n_o^2 \sin^2 \phi_o \tan^2 \phi_o \left[ \frac{\sin 2\Psi \cos 2\Psi \sin \Delta}{(1 + \sin 2\Psi \cos \Delta)^2} \right] \quad (4.17b)$$

The substrate optical constants ( $n_1$ ,  $k_1$ ) are readily calculated from  $\hat{\epsilon}$  without the use of complex numbers -

$$n_1 = \left\{ \frac{1}{2} (\epsilon_1^2 + \epsilon_2^2)^{\frac{1}{2}} + \epsilon_1 \right\}^{\frac{1}{2}} \quad (4.18a)$$

$$k_1 = \epsilon_2 / 2n_1 \quad (4.18b)$$

Once the substrate refractive index is known, it is possible to compute normal reflectivity,  $R_N$ , and the reflectivities

the substrate refractive index, in terms of  $\rho$  and hence of the ellipsometric parameters:

$$\hat{n} = n_o \tan \phi_o \left[ 1 - \frac{4\hat{\rho} \sin^2 \phi_o}{(\hat{\rho} + 1)^2} \right]^{\frac{1}{2}} \quad (4.14)$$

$\Psi$  and  $\Delta$  are obtained from equation 4.10 which can be rearranged to give

$$\Psi = \tan^{-1} |\hat{\rho}| \quad ; \quad \Delta = \tan^{-1} (\text{Im } \hat{\rho} / \text{Re } \hat{\rho}) \quad (4.15a,b)$$

It is necessary to adjust the value of  $\Delta$  so obtained, according to the sign of the real part of  $\hat{\rho}$ , so as to achieve a value of  $\Delta$ ,  $0 < \Delta < 360^\circ$ , in the correct quadrant.

Equations (4.14) and (4.15) can be combined and expressed as real numbers, which can be convenient for computation, but at great expense in terms of elegance. Remembering that

$$\hat{\epsilon} = \hat{n}^2 = (n^2 - k^2) - 2nki = \epsilon_1 - i\epsilon_2 \quad (4.16)$$

One may write

$$\epsilon_1^{\text{substrate}} = n_1^2 - k_1^2 = n_o^2 \sin^2 \phi_o \left[ 1 + \frac{\tan^2 \phi_o (\cos^2 2\Psi - \sin^2 2\Psi \sin^2 \Delta)}{(1 + \sin 2\Psi \cos \Delta)^2} \right] \quad (4.17a)$$

$$\epsilon_2^{\text{substrate}} = 2n_1 k_1 = 2n_o^2 \sin^2 \phi_o \tan^2 \phi_o \left[ \frac{\sin 2\Psi \cos 2\Psi \sin \Delta}{(1 + \sin 2\Psi \cos \Delta)^2} \right] \quad (4.17b)$$

The substrate optical constants ( $n_1$ ,  $k_1$ ) are readily calculated from  $\hat{\epsilon}$  without the use of complex numbers -

$$n_1 = \left\{ \frac{1}{2} (\epsilon_1^2 + \epsilon_2^2)^{\frac{1}{2}} + \epsilon_1 \right\}^{\frac{1}{2}} \quad (4.18a)$$

$$k_1 = \epsilon_2 / 2n_1 \quad (4.18b)$$

Once the substrate refractive index is known, it is possible to compute normal reflectivity,  $R_N$ , and the reflectivities

for p- and s-polarized light at other angles -

$$R_N = \left| \frac{n_0 - \hat{n}_1}{n_0 + \hat{n}_1} \right|^2 \quad (4.19)$$

$R_p$  and  $R_s$  are calculated using equations (4.11) and (4.12)

$$R_p = |\hat{r}_p|^2 \quad R_s = |\hat{r}_s|^2 \quad (4.20)$$

The reflection coefficient for randomly polarized light is the arithmetic mean of these values, since perpendicular components of the polarization do not interfere. This quantity has been denoted  $R_\theta$  to distinguish it from  $R_N$ .

$$R_\theta = (R_p + R_s)/2 \quad (4.21)$$

#### Reflection involving a thin surface film

This case is of present interest for several reasons. Silver-Copper binary alloys are subject to tarnishing and oxidation in the normal laboratory atmosphere, as are the low carat gold binary alloys. The effect of a possible surface film had therefore to be considered for its effect on the measured values of  $\psi$  and  $\Delta$  and also for the effect on alloy colour. Making the usual assumption that any surface film is homogeneous, isotropic, plane and parallel-sided, the Fresnel relations may be used to express the amplitude reflection coefficients for reflections at each of the two interfaces in terms of the refractive indices of each of the three phases and the angle of incidence. The overall coefficients depend on these as well as the ratio of film

thickness to wavelength. Extending the notation of (4.11), we have

$$\begin{aligned} n_0 & \text{ ambient R.I} \\ \hat{n}_1 & \text{ film R.I} \\ \hat{n}_2 & \text{ substrate R.I} \end{aligned}$$

$\hat{r}_{01}^s, \hat{r}_{01}^p$  Fresnel reflection coefficients for the ambient/film interface.

$\hat{r}_{12}^s, \hat{r}_{12}^p$  Fresnel reflection coefficients for the film/substrate interface.

Additionally,  $d$  represents the geometrical thickness of the film and  $\lambda$  the wavelength of the light probe in vacuo. Thus,

$$\hat{R} = (\hat{r}_{01} + \hat{r}_{12}e^{-2i\delta}) / (1.0 + \hat{r}_{01}\hat{r}_{12}e^{-2i\delta}) \quad (4.22)$$

where  $\delta = 2\pi \frac{d}{\lambda} \hat{n}_1 \cos \theta_1$ .

The correct expressions for  $\hat{r}^s$  and  $\hat{r}^p$  must be substituted into (4.22) to obtain  $\hat{R}^p$  and  $\hat{R}^s$ .  $\psi$  and  $\Delta$  are evaluated as above.

In the general case,  $\hat{n}_2$ ,  $\hat{n}_1$  and  $d$  are all unknown, so that five real quantities must be calculated at each wavelength. This implies a minimum of three independent measurements of  $\psi$  and  $\Delta$ . Further complexity arises from the impossibility of inverting the above set of equations to yield analytic solutions for the experimental unknowns, even when sufficient information is available. Further consideration of this problem is left for the following chapter, except to note that in a method implemented by Roth et al (1968), Lorenzian

functions of the form

$$\hat{\epsilon}(\omega) = \epsilon_{\infty} + \sum_j \frac{s_j}{1 - (\omega/\omega_j)^2 + i\Gamma_j(\omega/\omega_j)} \quad (4.23)$$

were used to fit the film refractive index. The variable  $\omega$  is the circular frequency corresponding to light wavelength  $\lambda$ , ie.

$$\omega = 2\pi c/\lambda \quad (4.24)$$

where  $c$  is the velocity of light in vacuo. The variables  $s_j$ ,  $\omega_j$  and  $\Gamma_j$  are the strength, natural frequency and relative line width of the  $j^{\text{th}}$  oscillator. When spectral data is available, use of functions of this type may reduce the number of unknowns to  $\sim 17$  compared with  $\sim 250$ , if the data at each wavelength were treated separately.

#### 4.3 Fundamental Equations

The relationship between  $\hat{n}$  and  $\hat{\epsilon}$  has already been described. Since optical properties may most easily be related to fundamental electronic properties by means of the dielectric function, this will be used in what follows. It is understood that  $\hat{\epsilon}$  refers to the metal substrate alone, and in particular there should be no confusion between the use of  $\epsilon_1$  and  $\epsilon_2$  for the real and imaginary parts of  $\hat{\epsilon}$ , and the use of  $\hat{n}_1$  and  $\hat{n}_2$  for film and substrate refractive index.

#### The Lorentzian Function

The Lorentzian function expression given above is derived from a more fundamental one given, for example, by Wooten (1975).

$$\hat{\epsilon} = 1 + \frac{4\pi e^2}{m} \sum_j \frac{N_j}{(\omega_j^2 - \omega^2) + i\Gamma_j\omega} \quad (4.25)$$

where a change of sign has been made to accord with ellipsometric convention, which implies

$$\hat{\epsilon} = \epsilon_1 - i\epsilon_2$$

as distinct from the normal solid-state physics usage, which has

$$\hat{\epsilon} = \epsilon_1 + i\epsilon_2$$

$N_j$  is the number of electrons per unit volume contributing to absorption in the  $j^{\text{th}}$  absorption line,  $\omega_j$  is the centre frequency,  $\Gamma_j$  is the absolute line width, and  $m$  the electronic mass. Thus

$$S_j = \frac{4\pi e^2 N_j}{m\omega_j^2} ; \quad \Gamma_j^{\text{relative}} = \Gamma_j^{\text{absolute}} / \omega_j \quad (4.26)$$

#### Drude Equations

The long-wavelength optical absorption by noble alloys can be approximated by a 'free electron' dielectric function derived by Drude by considering only one absorption process (or oscillator) with a natural frequency of zero. Manipulation of the equation, and substitution of

$$\omega_p^2 = \frac{4\pi N e^2}{m} ; \quad \tau = \frac{1}{\Gamma} \quad (4.27)$$

$N$  is now the number of 'free' electrons per unit volume.

$$\text{gives } \epsilon_1^f = 1 - \frac{\omega_p^2 \tau^2}{(1 + \omega^2 \tau^2)} \quad (a) \quad (4.28)$$

$$\epsilon_2^f = \frac{\omega_p^2 \tau}{\omega(1 + \omega^2 \tau^2)} \quad (b)$$

$\omega_p$  is the 'bulk plasmon frequency' and  $\tau$  the conduction electron relaxation time. In practice, absorption due to quantum-mechanical transitions involving electrons not in the conduction band contribute additional absorption. In contrast to the 'free electron' behaviour of conduction electrons, these are 'bound electron' processes and so the new terms are labelled  $\epsilon_1^b$  and  $\epsilon_2^b$ .

$$\hat{\epsilon} = \hat{\epsilon}^f + \hat{\epsilon}^b \quad (4.29)$$

The term  $\epsilon_2^b$  is zero for the noble alloys for values of  $\omega$  such that  $\omega \lesssim 2\text{eV}$ , i.e. for wavelengths longer than  $\sim 650\text{nm}$ . On the other hand,  $\epsilon_1^b$  does not go to zero at low energies but rather approaches a constant value at energies a long way below the onset of interband absorption. Equation (4.28(a)) should therefore be replaced by

$$\epsilon_1 = \epsilon_1^b - \frac{\omega_p^2 \tau^2}{(1 + \omega^2 \tau^2)} \quad (4.30)$$

where this  $\epsilon_1$  is a low energy value, corresponding to the same energy range as  $\epsilon_2^b \hat{=} 0$ , i.e.  $\epsilon_2 = \epsilon_2^f$ .

Assuming  $\epsilon_1^b = \text{constant}$ , then  $\tau$  may be calculated from (4.28(b) and 4.30) without making any special assumptions.

The equation

$$\omega \epsilon_2 = \frac{-1\epsilon_1}{\tau} + \frac{\epsilon_1^b}{\tau} \quad (4.31)$$

indicates that  $\tau$  and  $\epsilon_1^b$  may be taken from a graph of  $\omega \epsilon_2$  versus  $\epsilon_1$ . In the limit  $\omega \tau \gg 1$ ,

$$\epsilon_2^f = \frac{\omega_p^2}{\omega^3 \tau} \quad (4.32)$$

So that, given  $\tau$  as above,  $\omega_p$  may be evaluated from a graph of  $\epsilon_2^f$  versus  $\omega^3$ . It is found that this expression does not very well describe  $\epsilon_2^f$  for noble metals in the near infra-red, so that for some purposes the cubic relation is relaxed and a power-law expression used instead:

$$\epsilon_2^f \propto \omega^{-n} \propto \lambda^n$$

#### Interband Absorption

The constant of proportionality and power coefficient may be found from a logarithmic plot, although they do not appear to have much physical significance. Once obtained, they can be used to extrapolate  $\epsilon_2^f$  to higher energies where  $\epsilon_2^b > 0$ , enabling the background  $\epsilon_2^f$  to be subtracted from that experimentally determined.

$$\epsilon_2^b = \epsilon_2 - \epsilon_2^f$$

This aids interpretation of the spectra.

### Plasma Oscillations

The bulk plasmon frequency  $\omega_p$ , mentioned above, corresponds to a frequency  $\omega = \omega_p$  at which  $\epsilon_1 \sim 0$ , as can be seen by substitution in (4.28(a)). In practice the existence of  $\epsilon_1^b$  tends to alter the relationship a small amount, but at this frequency it is possible to create large period oscillations (plasmons) in the conduction electrons. Unless  $\epsilon_2$  is also small, these oscillations are of low amplitude and little importance, but when they occur they are capable of absorbing energy and by altering the electric field inside the metal invalidate the use of the Fresnel relations. A function of  $\hat{\epsilon}$ , known as the bulk plasmon energy loss function

$$\text{Im } 1/\hat{\epsilon} \quad (4.33)$$

can be calculated, which shows the frequencies when this is likely to be a problem. The position of the peak in this function is found to vary with alloy concentration.

Oscillations of the conduction electrons are also possible in the surface of a metal. In this case the natural frequency is that at which  $\epsilon_1 \sim 1$ , and the 'surface plasmon energy loss function' may be computed:

$$\text{Im } 1/(\hat{\epsilon} + 1) \quad (4.34)$$

Electromagnetic radiation will not couple to <sup>surface plasmon modes in</sup> perfectly plane samples, but may set up surface plasmons in rough samples which modify the dielectric function. It will be seen from equation (4.27) that  $\omega_p$  depends on the electronic mass. In the quantum mechanical picture electron mass

is a function of band structure, so that an effective electronic mass  $m^*$ , where

$$m^* = \frac{4\pi N e^2}{\omega_p^2} \quad (4.35)$$

is applicable here. Calculation of this can yield information about Fermi surface topology.

#### Optical Conductivity

Some workers in metal optics, particularly those who study conduction electron absorption in the infra-red, express their results not in terms of a complex dielectric function but as an optical conductivity ( $\sigma$ ) or complex optical conductivity ( $\hat{\sigma} = \hat{\sigma}_1 - i\sigma_2$ ). This is a consequence of the way Maxwell's Equations are applied to the problem. If one starts by considering non-absorbing, non-conducting media having real dielectric functions, and then generalises by allowing the dielectric function to take complex values, then the system that has been used here may be derived. Alternatively, if the conduction of the medium is considered from the start, then equations analogous to those used here result, but in which the expression

$$\epsilon = \frac{i4\pi\sigma}{\omega}$$

replaces the complex dielectric function  $\hat{\epsilon}$ . Thus

$$\epsilon_1 = \epsilon \quad \text{and} \quad \epsilon_2 = \frac{4\pi\sigma}{\omega} \quad (4.36)$$

It is also possible to study optical properties by generalizing the direct current transport equation, deriving

a complex optical conductivity (which is a free electron conductivity)

$$\sigma = \sigma_0 / (1 + i\omega\tau) \quad (4.37)$$

#### 4.4 Optical Properties of 2-Phase Alloys

Most of the Ag-Cu alloys studied were not in the fairly narrow solid solution ranges of this system. For this reason, the assumption of homogeneity may not be made for these alloys.

##### The Maxwell-Garnet Theory

Previous workers on isotropic homogeneous systems have employed a theory derived by Maxwell-Garnet in 1904. He treated the case of small metallic particles embedded in a dielectric, assuming that the particles were small compared with a wavelength, that they did not interact, and that they are spherical. He derived the following relation:

$$\frac{\hat{\epsilon}_{\text{eff}} - \epsilon_{\text{matrix}}}{\hat{\epsilon}_{\text{eff}} + 2\epsilon_{\text{matrix}}} = q \frac{\hat{\epsilon}_{\text{metal}} - \epsilon_{\text{matrix}}}{\epsilon_{\text{metal}} + 2\epsilon_{\text{matrix}}} \quad (4.38)$$

where  $q$  is the volume fraction of metal. This may be readily extended to the 2-phase alloy case by allowing  $\epsilon_{\text{matrix}}$  to take complex values. The equation may then be solved for  $\hat{\epsilon}_{\text{eff}}$ , if measurements are available of the saturated solid solution dielectric functions, and  $q$  can be independently determined. It should be noted, however, that various assumptions do not seem particularly likely:

- (a) The minority phase is not in general in the form of small spheres, although spherodisation may take place on annealing;
- (b) The particle size (or grain size) is, in general, rather longer than a wavelength;
- (c) The dielectric functions of the two phases may differ from those of bulk solid solutions of the same composition due to size effects.

#### Interference between reflected beams

For the special case where the size of the crystallites is much greater than either one wavelength or the penetration depth in either phase, an alternative simplifying assumption presents itself. Provided that the light beam is coherent and large enough to sample a representative region of the sample, and is focussed down to a small spot on the detector so that interference can occur, then the weighted average of the amplitude reflection coefficients will be measured.

$$\begin{aligned}\hat{r}_p &= (1 - q)\hat{r}_p^\alpha + q\hat{r}_p^\beta \\ \hat{r}_s &= (1 - q)\hat{r}_p^\alpha + q\hat{r}_p^\beta\end{aligned}\tag{4.39}$$

The ratio of surface areas is equal to the ratio of volumes, as before. This hypothesis may be tested by comparing the quantities thus calculated with those determined by separate experiments on the two phases. As the reflection coefficients are functions of angle of incidence, the 'effective' dielectric function (which may be computed by applying the

ellipsometric relations with equation 4.39), will also depend on angle of incidence.

Linear Addition of the Dielectric Functions

A particularly simple way of forming an effective dielectric constant, applicable to the extreme microscopic case of mixed media, is simply to form a linear addition of the dielectric constants of the 2 phases:

$$\hat{\epsilon}^{\text{eff}} = (1 - q)\hat{\epsilon}^{\alpha} + q\hat{\epsilon}^{\beta}$$

When the difference between  $\hat{\epsilon}^{\alpha}$  and  $\hat{\epsilon}^{\beta}$  is small, this does not give vastly different results from either the Maxwell-Garnet Theory or the interference model.

## 5. COMPUTATION

### 5.0 General

Computer programs for the analysis of ellipsometric data have been designed by several authors. Perhaps that of McCracken (1969) of the National Bureau of Standards, Washington, is the most comprehensive and widely used, while those of Schueler (1969) and Roth et al (1975) appear to be the most powerful. Broadly, these programs can be broken down into two types; firstly, there is the large group of calculations that can be performed analytically, and secondly, the smaller group that require numerical techniques. The first group has included (i) computation of substrate refractive index from film-free ellipsometric data, (ii) computation of film thickness from ellipsometric data and a complete set of known refractive indices; and (iii) computation of ellipsometric parameters for a completely defined system, be it filmed or film-free. Until recently, ellipsometry has been performed almost exclusively at single wavelengths in the visible, typically 546.1nm, so that there has been no requirement that spectral data, obtained at a large number of wavelengths, be conveniently handled. Similarly, there has been no necessity to compute functions such as optical conductivity, reflectance or the dielectric function. The equations given in Chapter 4 enable sixteen useful functions to be calculated, depending on the choice of six independent variables. At the beginning of the investigation, it was not clear which of these would be of most interest and use in the analysis. It was decided to provide a framework in which choices could be readily made when the computer program was run, rather than design a simpler, though rigid, program which would reduce freedom of

choice at later stages. As well as a large variety of output functions, there was a large amount of data to be specified. This included analyser and polariser readings at 134 wavelengths in each experiment, angle of incidence and ambient refractive index. There was also the question of presentation of output. Rarely is it desirable merely to produce a large printed table of results, as often graphical output is more readily understood; or perhaps the spectral data may be summarised in a small number of quantities such as relaxation time or colour co-ordinates. Again, there is an area of selection even in the exact way this is done. For instance, there is a choice of illuminant to be made when performing CIE calculations, and a choice of axes when producing graphical output. In the program to be described, all these choices may be made by presenting appropriate data to the program at run-time.

Rather different considerations apply to the problem of obtaining film or substrate dielectric functions from ellipsometric measurements on filmed systems. The necessary data take longer to acquire and since the equations have to be solved numerically, the calculations are much more expensive and also take a great deal longer. It is therefore practical to spend more time preparing each calculation so that a sophisticated run-time system is not required. For this reason, unlike the McCracken programs, this aspect of analysis is performed by entirely separate programs. Once dielectric functions have been obtained which acceptably

describe the optical measurements, then further analysis can be pursued using the analytic program.

## 5.1 Calculation of the Dielectric Function

### 5.1.1 Clean substrates

The computer service at the City of London Polytechnic is based on a DEC System 10 time-sharing computer manufactured by the Digital Equipment Corporation. Terminals are provided in the laboratories for research use, and disk storage is available for programs and data. This storage takes the form of disk 'files', to which the user assigns a unique identification (the 'filename'). Data may be entered into files, and corrected, using editing programs provided as part of the system. This provides a convenient way of handling the spectral ellipsometric data, about 1,400 digits per experiment. Thus measurements on a silver-gold alloy may be stored in a file called, for example, "AGAU".

Given the experimental conditions, and the validity of the Fresnel relations, knowledge of the clean substrate analyser and polariser values is equivalent to knowledge of the refractive index or dielectric constant. Also, it is sufficient to give either the wavelength or photon energy at which each measurement was made. The program has therefore been designed to accept various permutations of data in the disk files, all of which are converted to values of  $\hat{\epsilon}(\lambda)$  whenever the data is used. The choice of  $\hat{\epsilon}(\lambda)$  is to some extent arbitrary, as for example  $\hat{n}(\omega)$  would do just as well. Mnemonics are used to identify the required output, thus "WL" indicates wavelength, "E1" the real part

of the substrate dielectric function,  $\epsilon_1$ , and "E2" the imaginary part of the dielectric function  $\epsilon_2$ . Mnemonics are also used to specify the operation or operations that are to be performed on the data, eg. "LIST" to print values on the computer terminal and "PLOT" for graphical output. A logical syntax has been devised so that it is not necessary to carefully format the mnemonics, for example into standard printing positions in the input data, as, instead, a syntax scanning algorithm can decode the data. This reduces the chances of error considerably. Finally, mnemonics are used to specify data (or data file names), as a further aid to memory. As an example, supposing the results of an experiment on fine gold to have been entered into a file called "AU", then, after some essential preliminary dialogue with the computer, a line of data such as

PLOT WL, E2/SUBSTRATE:AU

will cause a graph to be produced of  $\epsilon_2(\lambda)$ , using the data (A and P values) on gold from the file "AU". Similarly,

PLOT ENERGY, E2/SUBSTRATE:AU

would cause a graph of  $\epsilon_2(\hbar\omega)$  to be plotted.

Although the gold data may have been taken from a clean substrate experiment, this does not limit the application of the dielectric function so obtained. Measurements made on bulk oxide (for example) can be used to provide a spectrum of  $\hat{n}(\lambda)$  which can then be used as 'film' values in optical calculations

/FILM: CU20

This may specify a file of  $A(\lambda)$ ,  $P(\lambda)$  from a clean substrate

experiment on  $\text{Cu}_2\text{O}$ , although it is a gross assumption that the bulk values are applicable in the thin film case. Nevertheless, this type of calculation can be very useful. As well as computing  $\hat{\epsilon}$  at each wavelength in the data files, interpolations are made to match the data in different files. This enables data to be compared, which may have been obtained from different sources at different wavelengths. Also, it may not be necessary to provide as much data to adequately define the film dielectric function as may be needed to define the substrate dielectric function, since the latter may contain more or finer structure.

A complete 'User's Guide' to the analytic ellipsometry has been provided (Clarke 1978).

<u>Input</u>	<u>Internal Store</u>	<u>Output</u>
$A(\lambda), P(\lambda)$	<u>or</u>	$R(\lambda)$
$n(\lambda), k(\lambda)$	<u>or</u> + $\hat{\epsilon}(\lambda)$ +	$\Psi(\lambda), \Delta(\lambda)$
$\epsilon_1(\lambda), \epsilon_2(\lambda)$	<u>or</u>	colorimetric quantities
$\Psi(\lambda), \Delta(\lambda)$		electronic properties

### 5.1.2 Filmed Systems

Several approaches to the calculation of substrate or film refractive index for filmed systems have been tried. These can be separated into techniques applicable at single wavelengths, and one which takes advantage of the spectral nature of the measurements made on the automatic ellipsometer.

#### Measurements at a single wavelength

Initially, following the method of Shewchun and Rowe (1970) it was hoped to compensate for the presence of surface films

and compute accurate substrate refractive indices, while simultaneously determining film thickness and refractive index. The method involved successive guesses of substrate  $n$  and  $k$  and film  $n$  and  $k$ . At each guess, values of complex film thickness were determined using the experimental  $\Psi$  and  $\Delta$  at several angles of incidence. The guesses were generated simply by incrementing the two pairs of optical constants over a specified range. When the modulus of the imaginary part of the computed thickness was a minimum, then a new iteration was performed using smaller increments over a narrower range. Another criterion employed was that the standard deviation of the computed thickness be a minimum. This procedure was followed until, at the minimum, the real part of the thickness gave calculated  $\Psi$  and  $\Delta$  within experimental error of the measured values. The method amounts to a pattern search for the minimum of the error function

$$f(\hat{n}_2, \hat{n}_1, \Psi, \Delta) = \sum_j | \text{Im } \hat{d}_j |$$

alternated with minimising  $s(\text{Re } \hat{d}_j)$ ;  $s$  is the standard deviation. During this search no use is made of the detailed behaviour of the function  $f$ , for instance by calculating approximations to derivatives, and, although convergence is limited to a small set of solutions by the limits put on  $\hat{n}_2$  and  $\hat{n}_1$ , convergence is not guaranteed. An attempt to improve the algorithm by using a gradient following algorithm was made. This required calculation of the partial derivatives:

$$\frac{\partial f}{\partial n_1}, \frac{\partial f}{\partial k_1}, \frac{\partial f}{\partial n_2}, \frac{\partial f}{\partial k_2}$$

These were approximated by differences, and therefore were not of great accuracy. Although some improvement was made, difficulties caused by this inaccuracy prevented completely satisfactory convergence. As an additional step, minimisation of the least squares error function.

$$\sum_j (\psi_j^{\text{calc}} - \psi_j^{\text{expt}})^2 + (\Delta_j^{\text{calc}} - \Delta_j^{\text{expt}})^2$$

was included. At this stage it became clear that the computer program was evolving in the direction of those of Schueler (1969) and Oldham (1969), which seek to minimise the error function

$$f = \sum_j | \hat{\rho}_j^{\text{calc}} - \hat{\rho}_j^{\text{expt}} |^2$$

in order to solve simultaneously  $\hat{\rho}_j = \tan \psi_j \exp(i\Delta_j)$ , for  $j$  independent measurements. In Schueler's work, these involved using 3 angles of incidence, while Oldham employed pairs of similar films of different thicknesses. Both workers used traditional minimisation methods - Newton's and Gauss' - which require partial derivative calculations. Experience showed that estimation of these by differences could not be relied on to be of sufficient accuracy, while analytic solutions would be of great complexity and of small generality. In order to produce an algorithm of general usefulness and ready adaptability a minimisation method which did not require derivatives was sought. That of Powell (1964) has achieved wide acceptance as an economical and reliable technique, and was also quite readily available. Oldham's

and Schueler's ideas were combined, the new error function being

$$\sum_{ij} (\psi_{ij}^{\text{calc}} - \psi_{ij}^{\text{expt}})^2 + (\Delta_{ij}^{\text{calc}} - \Delta_{ij}^{\text{expt}})^2$$

where  $i$  labels the various angles of incidence and  $j$  various films. The resulting program was used to confirm Schueler's result that multiple angle of incidence measurements are of little use for films of gold of less than 20nm thickness. The error function given above requires slightly more computation than that of Schueler, but it is felt to be conceptually simpler and gives equal weighting to the experimental angles which are determined to similar accuracy. Johnson and Bashara (1971), who employed Schueler's program, indicated that minimisation of  $f(\underline{x})$ , where (in their case)

$$\underline{x} = \begin{pmatrix} n_1 \\ k_1 \\ d \end{pmatrix}$$

sometimes gave results with  $k < 0$ . This is not surprising, as the method will search the vector space  $R^3$  for a solution, ie. for values of  $n$ ,  $k$  and  $d$  over the entire field of real numbers. Apart from the lack of physical significance of such answers, mathematical difficulties are likely to result, as the equations give rise to attempts to find square roots of negative numbers. This can be avoided by minimising a function  $f(\underline{w})$ , where

$$\underline{w} = \begin{pmatrix} n_1^{\frac{1}{2}} \\ k_1^{\frac{1}{2}} \\ d^{\frac{1}{2}} \end{pmatrix}$$

With this modification, the algorithm successfully found solutions for  $n_2$ ,  $k_2$  and  $d$  for an experimental system of  $\text{TiO}_2$  on silicon, with  $d = 65\text{nm}$ ,  $\lambda = 500\text{nm}$ , and employing six angles of incidence. Since derivatives are not needed when using Powell's procedure, it is a simple matter to vary the choice of adjustable parameters according to the amount of data available. Thus in the new program, the vector  $w$  may be selected at run-time from any of the elements of

$$(n_0^{1/2} \quad k_0^{1/2} \quad n_1^{1/2} \quad k_1^{1/2} \quad n_3^{1/2} \quad k_3^{1/2} \quad d^{1/2})^T$$

'T' indicates the column vector.

As found by Schueler, difficulty occurs if  $k_1$  is small ( $\sim 0.05$ ) and unknown, making it impossible to obtain  $n_1$  and  $k_1$  to great accuracy. However, if  $k_1 = 0$ , and this is known a priori, only  $n_1$  and  $d$  need be found, and this can be done quite precisely. Thus for the  $\text{TiO}_2/\text{Si}$  system, a wavelength in the range 700-800nm was employed, at which  $k_1$  could safely be set to zero. The thickness so computed was then used at shorter wavelengths to provide a spectrum of  $n_1$ ,  $k_1$  values. This technique was much more robust than that of finding all three parameters simultaneously by multiple angle measurements, giving rise to no extra confusing solutions. As a further refinement, Oldham's idea of using two films of different thickness but (assumedly) the same refractive index to reduce indeterminacy was incorporated in a generalised way into the multi-angle program.

The new error function was then

$$f(\underline{w}) = \sum_{i=1}^n \sum_{j=1}^m (\psi_{ij}^{\text{calc}} - \psi_{ij}^{\text{expt}})^2 + (\Delta_{ij}^{\text{calc}} - \Delta_{ij}^{\text{expt}})^2$$

Note that as  $\Delta$  is a periodic function, it is necessary to evaluate  $\Delta^{\text{calc}} - \Delta^{\text{expt}}$  modulo  $2\pi$ . Now  $\underline{w}$  is selected from

$$(n_0 \dots k_3, d_1 \ d_2 \dots d_n)^T$$

It must be remembered that the assumption of similarity between two or more films of differing thickness is - at best - tentative, perhaps unlikely to be frequently correct in practice.

Another way of reducing the possibility of finding a local minimum in the error function (which may be far removed from the optimal solution) is to constrain the values that the unknown quantities may take, but this has not been incorporated in the final algorithm. This may be done by constant inequality constraints of the form  $a_j < x_j < b_j$ , where  $x_j$  is an element of  $\underline{x}$  (ie.  $n$ ,  $k$  or  $d$ ) and  $a_j$  and  $b_j$  represent reasonable lower and upper limits the quantity  $x_j$  may take. Use of a general purpose unconstrained optimization algorithm may be retained by a further transformation of variables (Box, 1966):

$$w_j = \left[ \frac{b_j - a_j}{x_j - a_j} - 1 \right]^{-1} \quad \text{so that} \quad -\infty < w_j < \infty$$

Reduction of film growth curve data

A commonly used method (for example, Osborne 1979, Ross 1978, Hayfield 1961) of obtaining film optical constants involves measurement of  $(\Psi, \Delta)$  pairs at many stages during growth of the film. A family of  $(\Psi, \Delta)$  loci is then calculated for various assumed film refractive indices, and that which most closely corresponds to the experimental curve supposedly indicates the correct R.I. It was hypothesised that this tedious and inaccurate method could now be replaced by an optimisation approach based on minimising the error function

$$f(n_1, k_1) = \sum_{j=1}^n |\text{Im } \hat{d}_j|$$

by adjustment of  $n_1$  and  $k_1$ . The complex film thickness  $\hat{d}_j$  is calculated for each pair of  $(\Psi, \Delta)$  measured using an inversion of equation 4.22. In practice this approach is fraught with pitfalls, as many values of the optical constants satisfy the error condition. This can be understood in the graphical picture, for suitable (very small) values of  $k$  result in the locus of film-growth values passing very close to all points in the  $(\Psi, \Delta)$  plane. The method can be made to work only by applying very tight constraints to the range of permitted values of  $n$  and  $k$ .

Spectral Ellipsometric Measurements - Lorentzian function fitting.

Little interest in spectral ellipsometry seems to have been shown from the early work of Bartell and Churchill (1961) until recently (Aspnes 1976, Roth et al 1975). An isolated paper by McBee and Kruger (1969) discussed the application of this technique to the problem of thin film characterisation, but without the success that was hoped for. It was found that even with an independent thickness determination, there was still difficulty in obtaining a unique result for each film refractive <sup>index</sup> spectrum, using the then current techniques of analysis. A continuity condition on  $n_1$  and  $k_1$  was inadequate to resolve all the ambiguities in data interpretation. Roth et al (1975) have since shown that the independent thickness measurement is unnecessary, since assumption of an incorrect film thickness leads to non-causally related  $n_1$  and  $k_1$  spectra. Thus, by the Least-Squares (LSQ) fitting of a Lorentzian function to describe the film, it was possible to calculate  $n_1(\lambda)$ ,  $k_1(\lambda)$  and  $d$ . Of particular interest here is their demonstration that their method is applicable to the  $\text{Ag}_2\text{O}$  on Ag system. In the present study Roth's method has been extended to include the possibility of data at several angles of incidence as well as at many wavelengths. Particular values of the Lorentzian function at each wavelength may be used as starting guesses in a similar LSQ fitting of each data point, and further serve to rule out alternative solutions.

The form of the Lorentzian function used is similar to that of Verleur (1968) who used it in connection with the reduction

of reflection data. Unlike Roth, a transformation has been used to prevent the oscillator parameters from taking unphysical negative values. Again, this has two effects - some non-optimal solutions are eliminated and calculation errors are avoided. For a single oscillator fit, the vector of adjustable parameters consists of

$$\begin{pmatrix} s^{\frac{1}{2}} \\ \lambda_0^{\frac{1}{2}} \\ \Gamma^{\frac{1}{2}} \\ \epsilon_\infty^{\frac{1}{2}} \end{pmatrix}$$

These scalars are of order unity except for  $\lambda_0$  (500nm for visible data) so appropriate scale factors were used. The quantities are the oscillator strength ( $s$ ), centre wavelength ( $\lambda_0$ ), relative width ( $\Gamma$ ) and the high frequency contribution to the dielectric function ( $\epsilon_\infty$ ).

## 5.2 Calculation of Optical Functions

Once substrate and film dielectric functions have been calculated by the methods of section 5.1, it is possible to compute many functions of the constants of the system ( $n_0$ ,  $\hat{n}_1$  and  $\hat{n}_2$ ) and of the geometry ( $\phi$ ,  $\frac{d}{\lambda}$ ), which describe the effect of the system on specularly reflected light. These include  $R_N$  (normal reflectivity),  $R_S$  (intensity reflection coefficient for light polarised perpendicular to the plane of incidence),  $R_P$  (ditto for parallel polarization),  $\Psi$  and  $\Delta$  (the ellipsometric parameters) and A and P (the ellipsometer analyser and polarizer readings).

The calculation, using the equations of Chapter 4, is straightforward using a digital computer. In the present application, complications again rise because of the spectral nature of the data. Since the amount of data involved precludes a once-and-for-all production of comprehensive tables of these functions, and since the computation is now relatively cheap, a computer program has been devised which scans loosely formatted 'command strings' - run-time data - and then performs the required calculation. The same program which reduces clean substrate ellipsometric data to a dielectric function may be used to obtain graphical or tabulated output of optical functions, for instance by a command such as -

LIST WAVELENGTH, RNORMAL, PSI, DELTA

It may happen that substrate data is very much more highly structured than the film dielectric function, or vice-versa, so that while ~100 data points between  $\lambda = 250\text{nm}$  and  $\lambda = 850\text{nm}$  may be needed to accurately define  $\hat{n}_2(\lambda)$  for copper, fewer than this may be enough for  $\hat{n}_1(\lambda)$  of  $\text{Cu}_2\text{O}$ . Again, it may be simply that only an incomplete, albeit still useful, film spectrum is available, or that the available spectra have been measured at different wavelengths. In the early part of this study measurements were made using the several lines of a high pressure mercury lamp, the wavelengths of which have not been used subsequently. Monochromator recalib-

ration may also cause incompatibilities. The computer program has been devised so that when a request is made to perform a calculation involving incompatible sets of data, quadratic interpolation is automatically used to furnish values of  $n_0$ ,  $\hat{n}_1$  and  $\hat{n}_2$  at each wavelength. Whenever this is done, a warning message is printed to indicate the necessarily approximate nature of the results.

The same procedure is applied when computing an effective dielectric function, for example using Maxwell Garnet's theory.

### 5.3 Intrinsic Spectral Substrate Functions

There are several other functions related to the dielectric function of interest to the solid state physicist. These include  $\epsilon_2^f$  (the 'free', conduction electron or intra-band contribution to  $\epsilon_2$ ),  $\epsilon_2^b$  (the 'bound' or inter-band component),  $\text{Im}^1/\hat{\epsilon}$  (the bulk plasmon energy loss function),  $\text{Im} \frac{1}{\hat{\epsilon} + 1}$  (the surface plasmon energy loss function) and  $\sigma$  (the optical conductivity). Computation of these values may likewise be requested of the same computer program using function mnemonics -

eg.            PLOT        WAVELENGTH, E2B

Separation of  $\epsilon_2$  into  $\epsilon_2^f$  and  $\epsilon_2^b$  is possible for noble metal alloys if the data extends to a region ( $\lambda \gtrsim 650\text{nm}$ ) where  $\epsilon_2^b \sim 0$ . Simple theory indicates that in this case

$$\epsilon_2 \sim \epsilon_2^f \propto 1/\lambda^3$$

In practice cubic behaviour of  $\epsilon_2(\lambda)$  has not been observed, but a power law dependence has -

$$\epsilon_2 \propto \lambda^N$$

Values of N between 1 and 2.7 have been found here, while Beaglehole and Erlbach (1972) report values  $\sim 2$ . Graphical techniques have previously been used (Steel and Treherne, 1972) to measure the constant of proportionality and N, but in the present work the process has been automated. A linear least squares fit, which may be performed exactly, was used on the function

$$\ln \epsilon_2 = a + N \ln \lambda$$

The constants so obtained were used to define

$$\epsilon_2^f = a \lambda^N$$

which was then extrapolated to shorter wavelengths and subtracted from  $\epsilon_2$  to yield  $\epsilon_2^b$ . The correlation coefficient and values of the constants were also available.

Output from the computer program was possible as functions of  $\hbar\omega$ , the photon energy, rather than wavelength. Graphical output could thus be produced with  $\lambda$  or  $\hbar\omega$  as abscissa, and by a change of scale results of other workers given as functions of  $\omega$  could be compared. A facility was provided so that  $\lambda^{-2}$  or  $\lambda^{-3}$  could be used, or logarithmic graphs plotted, to establish the form of intraband absorption.

#### 5.4 Non-spectral intrinsic substrate functions

Intraband electronic relaxation time and plasma frequency,  $\tau$  and  $\omega_p$  respectively, could be computed from the form of the dielectric function. The Drude theory was used despite the fact that its prediction of cubic dependence of  $\epsilon_2^f(\lambda)$  has not been borne out. Relaxation time was obtained from a linear least squares fit in the region  $650\text{nm} > \lambda > 800\text{nm}$ , involving the relation of  $\epsilon_1$  and  $\epsilon_2/\lambda$ . For this it was not necessary to assume  $\omega\tau \gg 1$ , but it was required that  $\epsilon_1^b$ , the bound electron contribution to  $\epsilon_1$ , be independent of wavelength over this region. This is a doubtful assumption as the absorption <sup>edge</sup> is very close, between 300 and 570nm depending on composition. A further straight line fit, for which  $\omega\tau \gg 1$  was assumed, enabled  $\omega_p$  to be computed. For such short wavelengths the assumption was generally justified, but computed values of  $\epsilon_1^b$  (often  $\sim 100$ ) indicated that use of a constant for this term was not.

#### 5.5 Colorimetry

Colours of light reflected by filmed or clean systems, under the usual assumptions, were computed using the C.I.E 1931 Standard System or 1960 Uniform Colour System, and one of the reflectances as in section 5.2.

The response functions  $\bar{x}(\lambda)$ ,  $\bar{y}(\lambda)$  and  $\bar{z}(\lambda)$ , and lamp intensity  $s(\lambda)$ , were tabulated at 5nm intervals from 380-770nm. These functions were combined with the computed  $R(\lambda)$  by linear interpolation and extrapolation, were necessary, during integration. This facility was not required for the majority

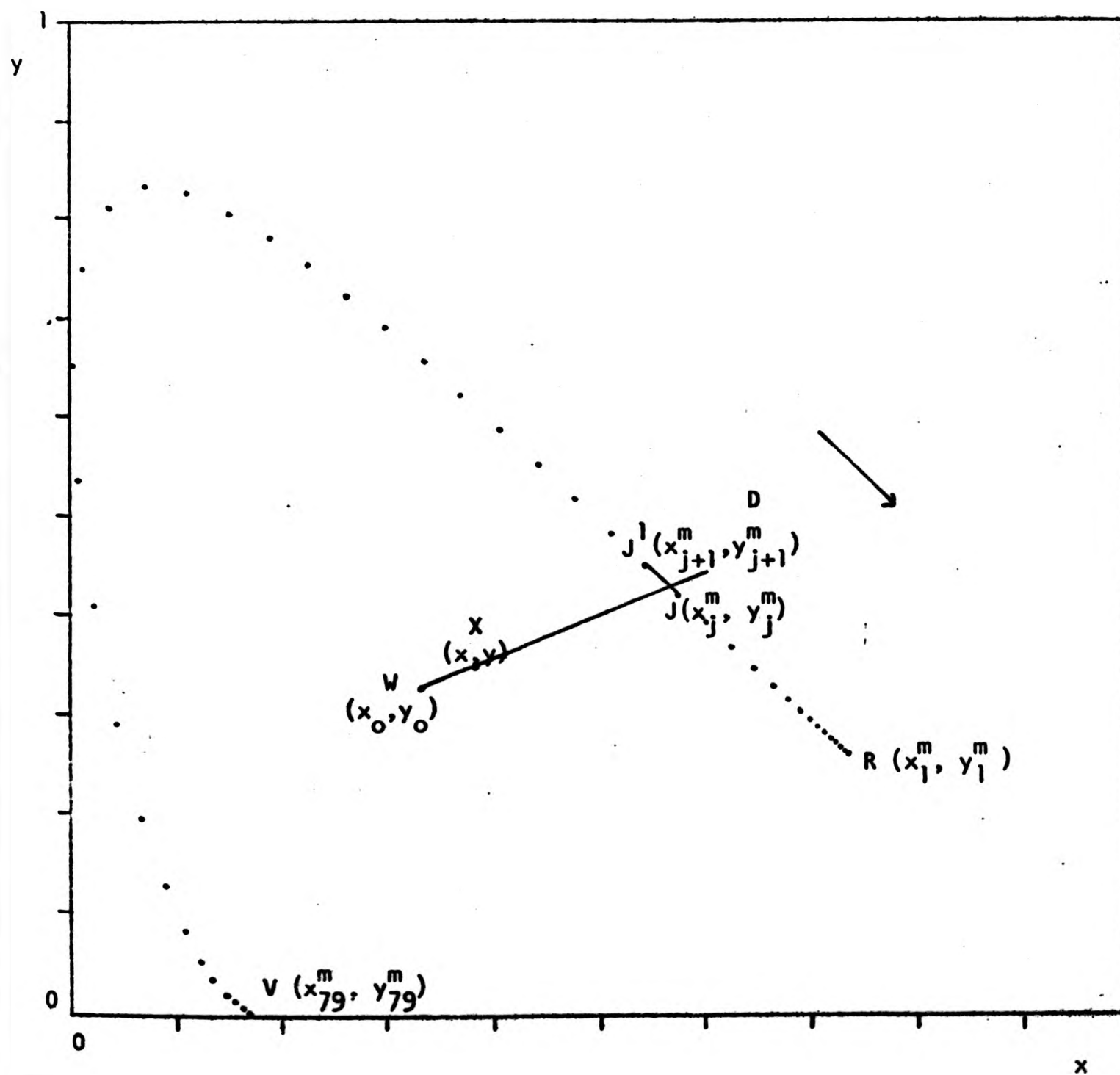
of data as the reflectance was evaluated at all the tabulated wavelengths in most cases.

It was arranged that the effect of angle of incidence, film thickness (if necessary) and number of reflections could be computed by varying these quantities as data.

#### Saturation and Dominant Wavelength

The colour co-ordinates  $(x^m, y^m)$  for monochromatic light of each of the tabulated wavelengths were also tabulated. At the extreme red end of the visible we denoted these  $(x_1^m, y_1^m)$ , whilst at the blue end they were denoted  $(x_{79}^m, y_{79}^m)$ . The curved locus joining these points is called the 'locus of monochromatic radiations'. The wavelength corresponding to the point on this locus where a straight line, drawn from the neutral ('white',  $(x_0, y_0)$  point), through some point  $(x, y)$  and extended to the locus, is called the dominant wavelength  $(\lambda_d)$  of the colour stimulus  $(x, y)$ . Using Cartesian geometry, the equation of the straight line WX from the neutral to the experimental point was calculated. That of the line WR from the neutral point to  $(x_1^m, y_1^m)$  was also computed, and the angle  $\theta$  between these lines determined. A pair of tabulated points on the locus, say  $J(x_j^m, y_j^m)$  and  $J'(x_{j+1}^m, y_{j+1}^m)$ , were then found such that  $\theta$  lay between the angles  $\phi_j = \text{JOR}$  and  $\phi_{j+1} = \text{J'OR}$  formed at  $(x_0, y_0)$  by each of these points and  $(x_1^m, y_1^m)$ . Next, the straight line between this pair of points was calculated and the position of the intercept D between J'J and the extended

WX obtained. Linear interpolation between the wavelengths corresponding to J and J' finally gave the dominant wavelength of the point X. Knowing the co-ordinates of W, X and D the saturation  $WX/WD$  was easily found.



## 6.0 RESULTS

### 6.1 The primary metals: Silver, Gold and Copper

In this section measurements on each of the primaries are presented. In addition to the calculated functions ( $\epsilon_2^b(h\nu)$  and  $R_N(h\nu)$ ; colour co-ordinates, relaxation times and plasma frequencies) that will form the basis of most of the later discussion, other results are given to illustrate the basis of the calculations or to illustrate points that do not require reiteration for each of the alloys measured.

#### The ellipsometric results

The ellipsometric curves for pure silver, sample No.30R,  $\Psi(h\nu)$  and  $\Delta(h\nu)$  are shown in Figure 6.1. It will be recalled that in Section 3, an experimental procedure requiring two photomultipliers and two core materials for the Faraday modulators was described. One arrangement enabled the range 250-540nm ( $\sim 2.3 - 5\text{eV}$ ) to be studied while another was necessary to cover the range 480 - 850nm ( $\sim 1.4 - 2.6\text{eV}$ ). Measurements made in the region of overlap did not exactly co-incide, the curves for Ag being typical. The difference in  $\Delta$  was  $\sim 0.1^\circ$ , and that in  $\Psi \sim 0.3^\circ$ . These changes are much greater than the resolution of the instrument ( $\sim 0.01^\circ$ ). For the purpose of computing C.I.E co-ordinates and other properties, a 'correction' of half the average difference in the centre of the overlap region (500 - 540nm) was made to each of the measurements under the alternative systems to bring them into line. The effect of this was always smaller than that due to sample preparation, when experiments were repeated.

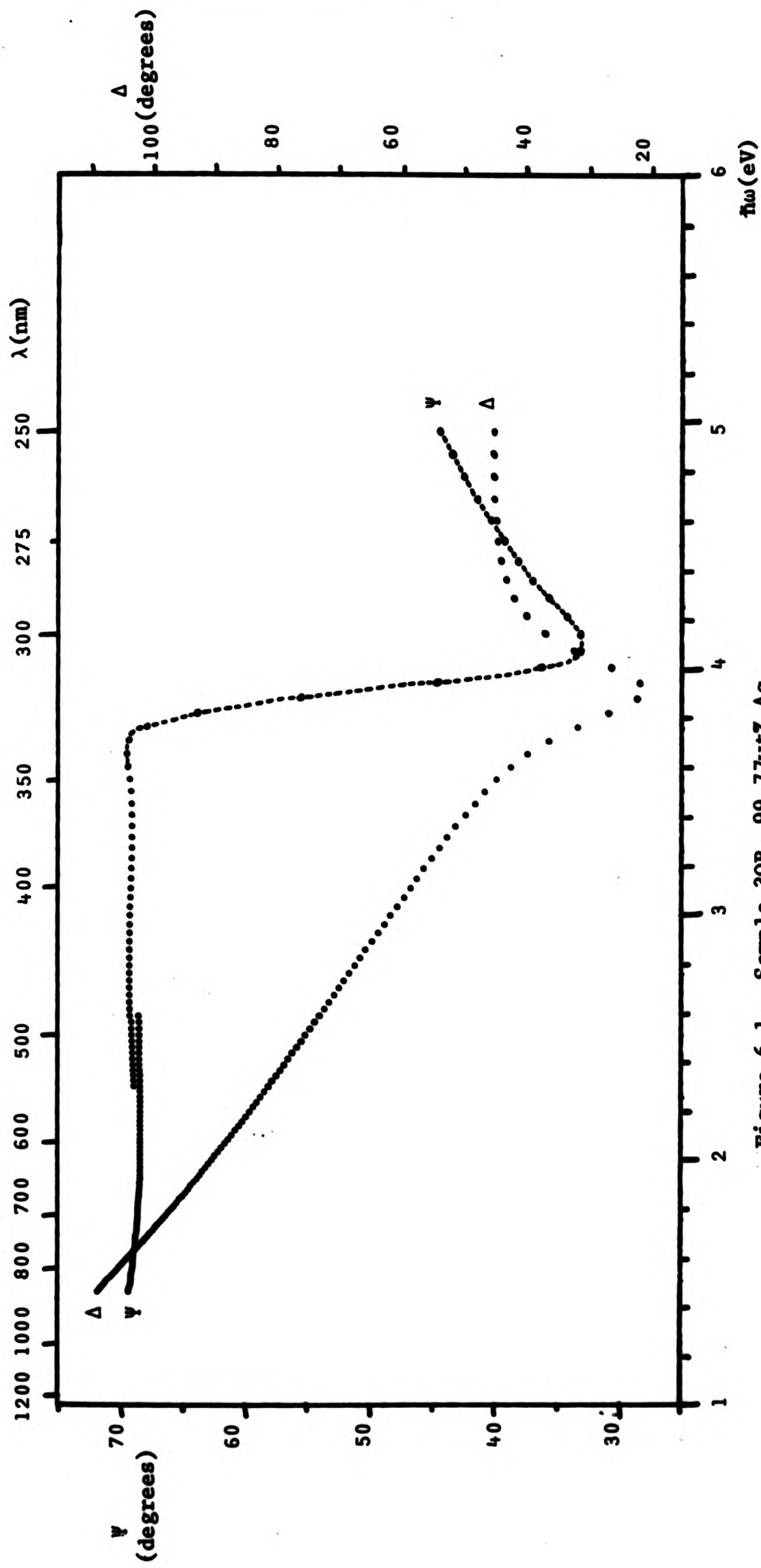


Figure 6.1. Sample 30R, 99.77wt% Ag. The ellipsometric functions  $\Psi(\omega)$  and  $\Delta(\omega)$ , showing the region of overlap of the detectors (see Section 3.3).

Inspection of this figure shows that the abrupt fall in  $\Psi$  corresponds closely with the minimum in  $\Delta$ , at about 3.9eV.

The Dielectric function and Reflectance.

Figures 6.2 and 6.4 show the computed normal reflectance  $R_N(\hbar\omega)$ , along with the real and imaginary parts of the dielectric function,  $\epsilon_1(\hbar\omega)$  and  $\epsilon_2(\hbar\omega)$ . Comparison of Figures 6.1 and 6.2a indicates a similarity in overall shape between  $R_N(\hbar\omega)$  and  $\Psi(\hbar\omega)$ , and between  $\epsilon_1(\hbar\omega)$  and an inverted  $\Delta(\hbar\omega)$ .

The reflectance of Ag (Figure 6.2a) is high at low energies,  $\sim 90\%$ , falling slowly through the visible to  $\sim 70\%$  at 3.6eV and then abruptly to  $\sim 5\%$  at 3.9eV. The sharp drop occurs at an energy when  $\epsilon_2(\omega)$  is almost constant, and when  $\epsilon_1(\omega)$  is passing through zero. Since normal reflectance is uniquely determined by  $\hat{\epsilon} = \epsilon_1 - i\epsilon_2$ , it is apparent that the change in  $R_N$  is related to the shape of  $\epsilon_1$ . Indeed, the highly reflecting region is that where  $\epsilon_1 \ll 0$ .  $\epsilon_1(\hbar\omega)$  itself shows little structure, a single peak at  $\sim 3.9$ eV co-inciding with a step in  $\epsilon_2(\hbar\omega)$ . Referring now to Figure 6.2b, a rather more complicated behaviour can be seen. This shows the same functions for sample No.30, computed from measurements made on a non-planar sample. Although a highly polished surface was achieved, this was superimposed on scratches remaining from a stage of grinding on 600 grit wet carbide. There was therefore an undulation of  $\sim 25\mu\text{m}$  period in the surface of the sample. This has given rise to a double step in  $R_N$  and a broad peak in  $\epsilon_2$  between 2.8 and 3.5eV. Interestingly, the calculated reflectance for the 'rough' sample is generally greater than that for

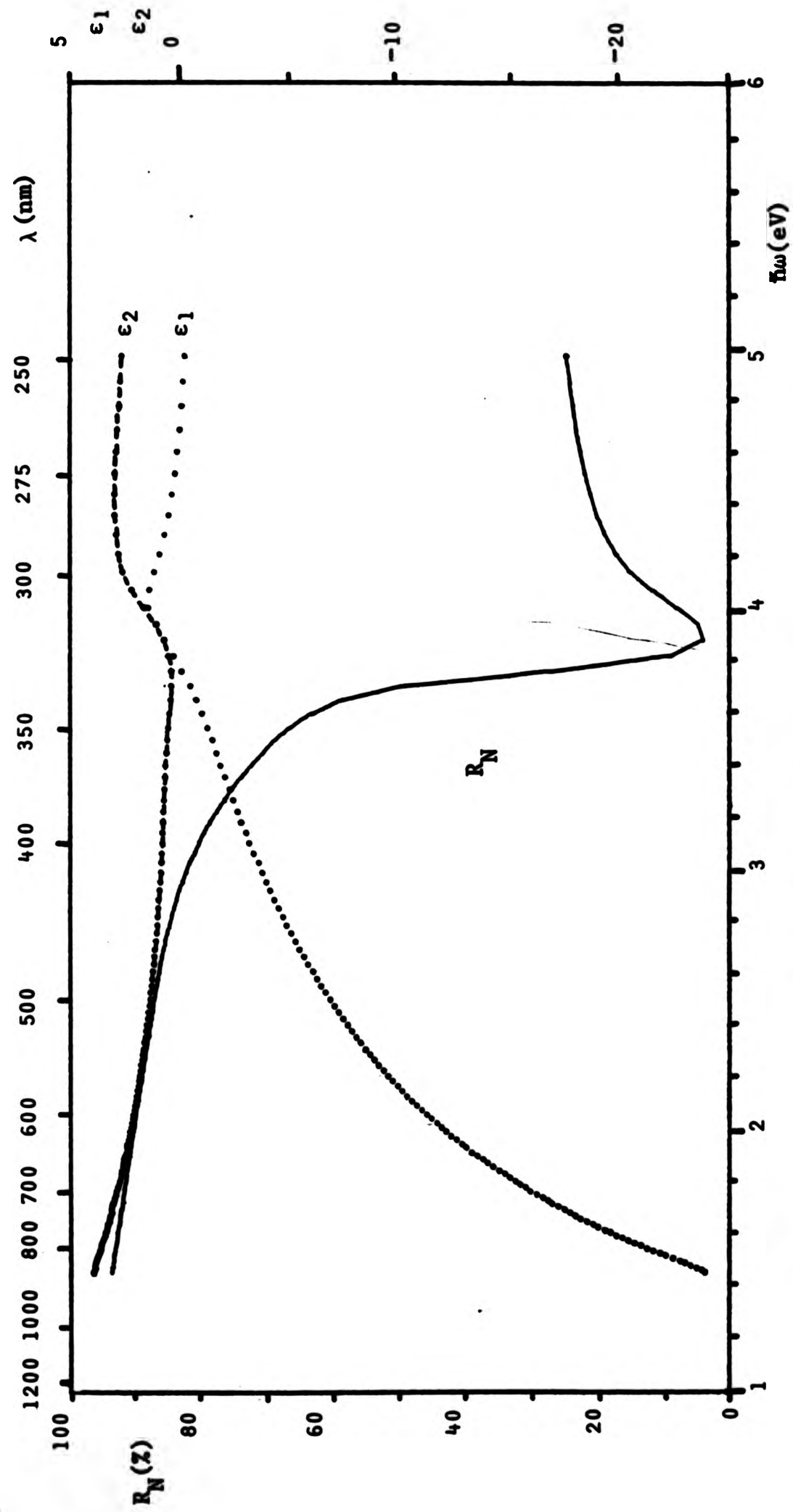


Figure 6.2a. Sample 30R, 99.97 wt.% Ag.  
 Normal reflectance ( $R_N$ ) and dielectric function  $\hat{\epsilon}(\omega) = \epsilon_1(\omega) - i\epsilon_2(\omega)$ .  
 The imaginary part of the dielectric function ( $\epsilon_2$ ) is shown more clearly in Figure 6.9.

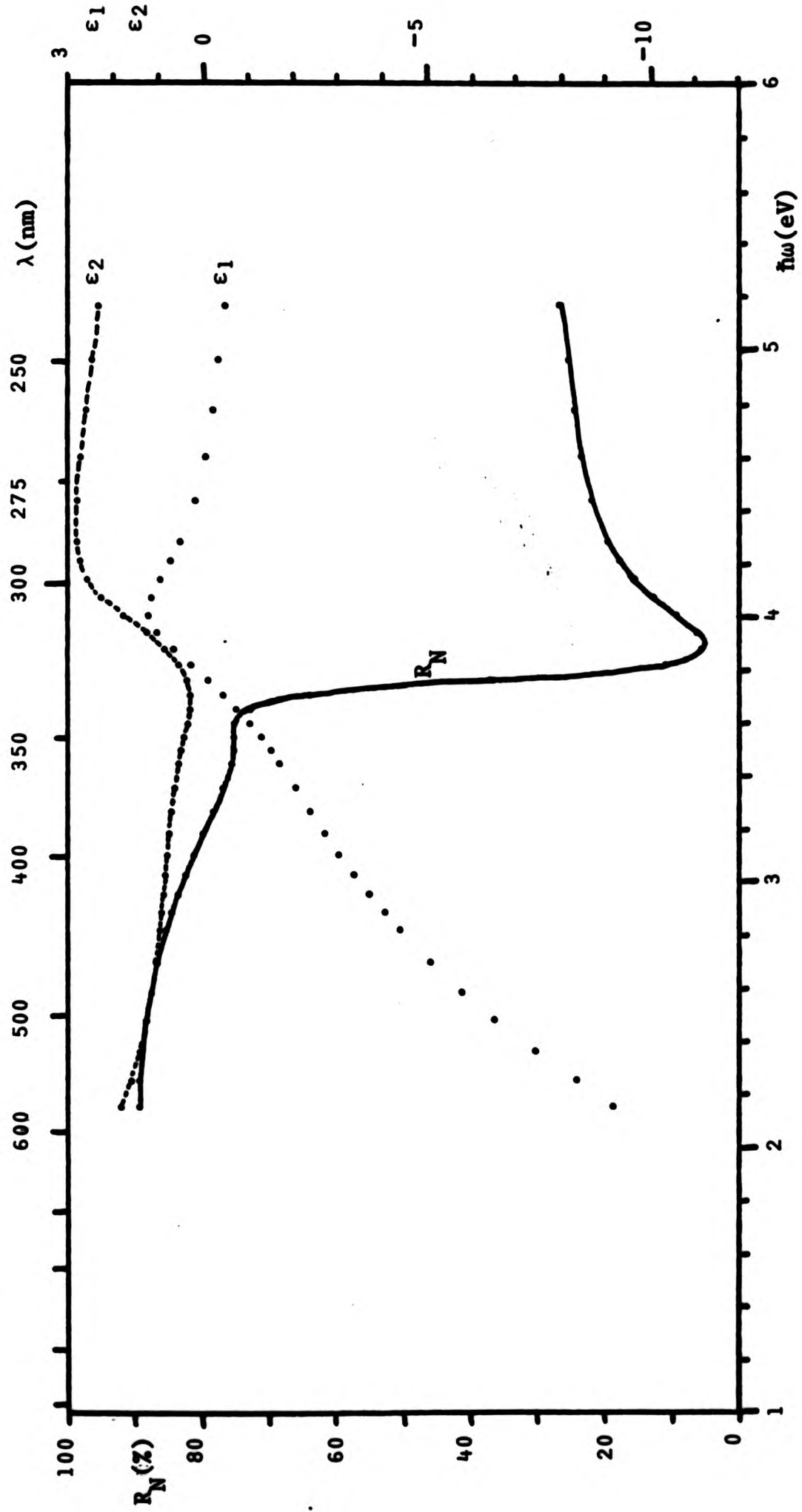


Figure 6.2b. Sample 30A. 99.9 wt.%Ag. Normal reflectance and dielectric function of a silver sample having long-period surface roughness.

the 'smooth' one; although since the calculation assumes plane surfaces, and more particularly disregards losses due to scattering out of the specular beam, the value of this computation is doubtful.

The results for gold show a much less pronounced drop, to only 35% reflectance (Figure 6.3), compared with silver. This is at about 2.3eV; before the rise in  $\epsilon_2$  ( $\sim 2.5\text{eV}$ , when  $R_N$  is already near to its minimum value) and when  $\epsilon_1 \sim -3$ . Reflectance remains nearly constant throughout the visible, indeed up to the limit of the experiment at 5eV. All three spectral curves show weak structure at energies greater than 2.6eV but in general the picture is much the same as for silver.

In Figure 6.4 a similar pattern is repeated by the curves for copper. A very high reflectance,  $\sim 95\%$ , at 1.5eV drops abruptly to  $\sim 60\%$  at  $\sim 2.2\text{eV}$ . At this energy  $\epsilon_1 \sim -5$  and  $\epsilon_2$  has already begun to increase. A steady fall in  $R_N$  continues until a minimum of 30% is reached at 4.3eV, after which there is a slight rise. The falling reflectance between 2.2 and 4.3eV is associated with a rising  $\epsilon_1(\omega)$ . This may be contrasted with the situation for Ag ( $\epsilon_1$  decreasing,  $R_N$  increasing) and Au ( $\epsilon_1$  and  $R_N$  more or less constant).

#### Energy-Loss Spectra

Calculated plasmon energy-loss spectra for both the bulk plasma and surface plasma modes are given in Figures 6.5 - 6.6. These represent the magnitude of collective oscillations of the electrons in the samples in response

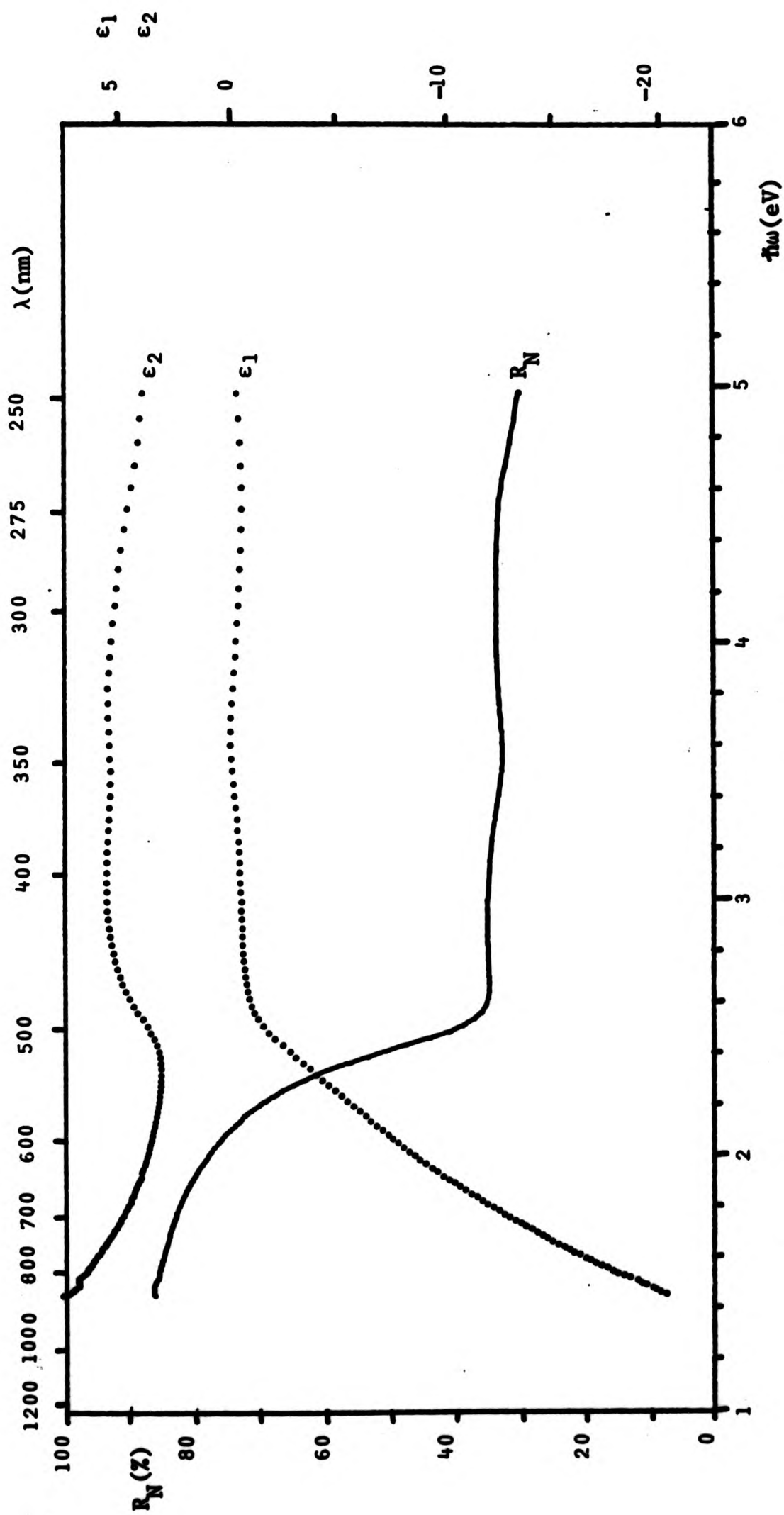


Figure 6.3. Fine gold sample purchased from Johnson-Matthey. Normal reflectance and dielectric function of fine gold.

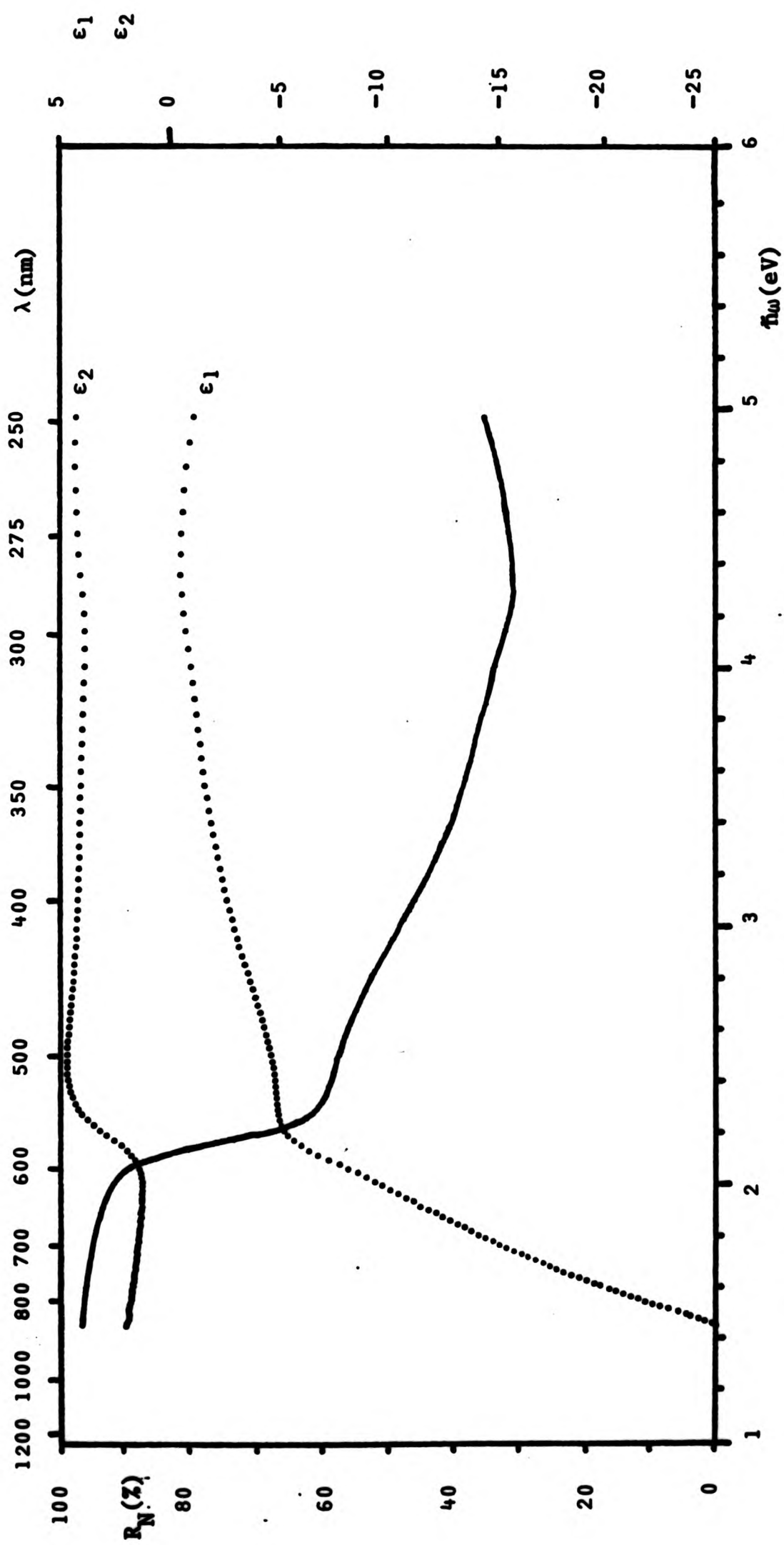


Figure 6.4. Nominal 100Cu donated by the Goldsmith's Research Foundation. Normal reflectance and dielectric function.

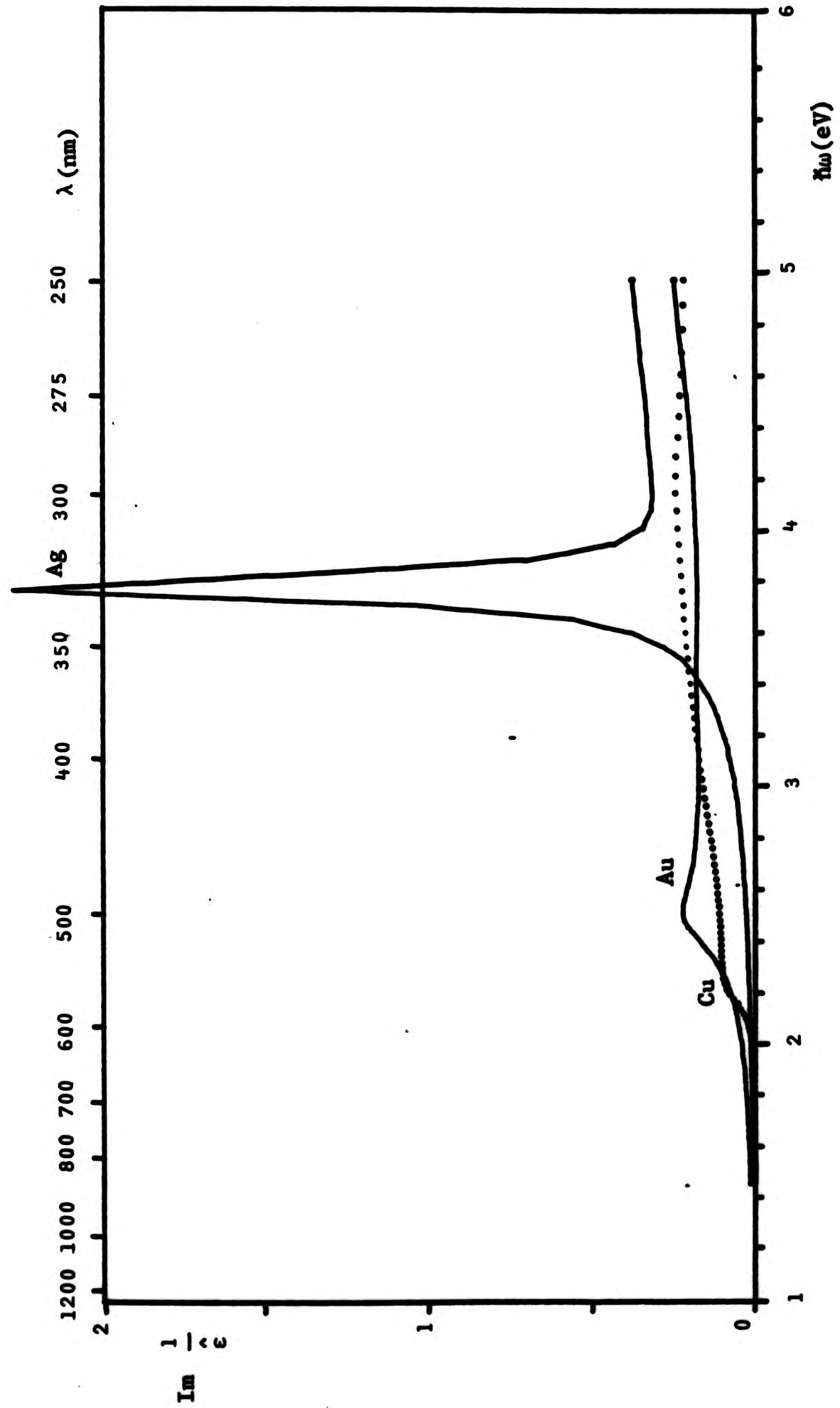
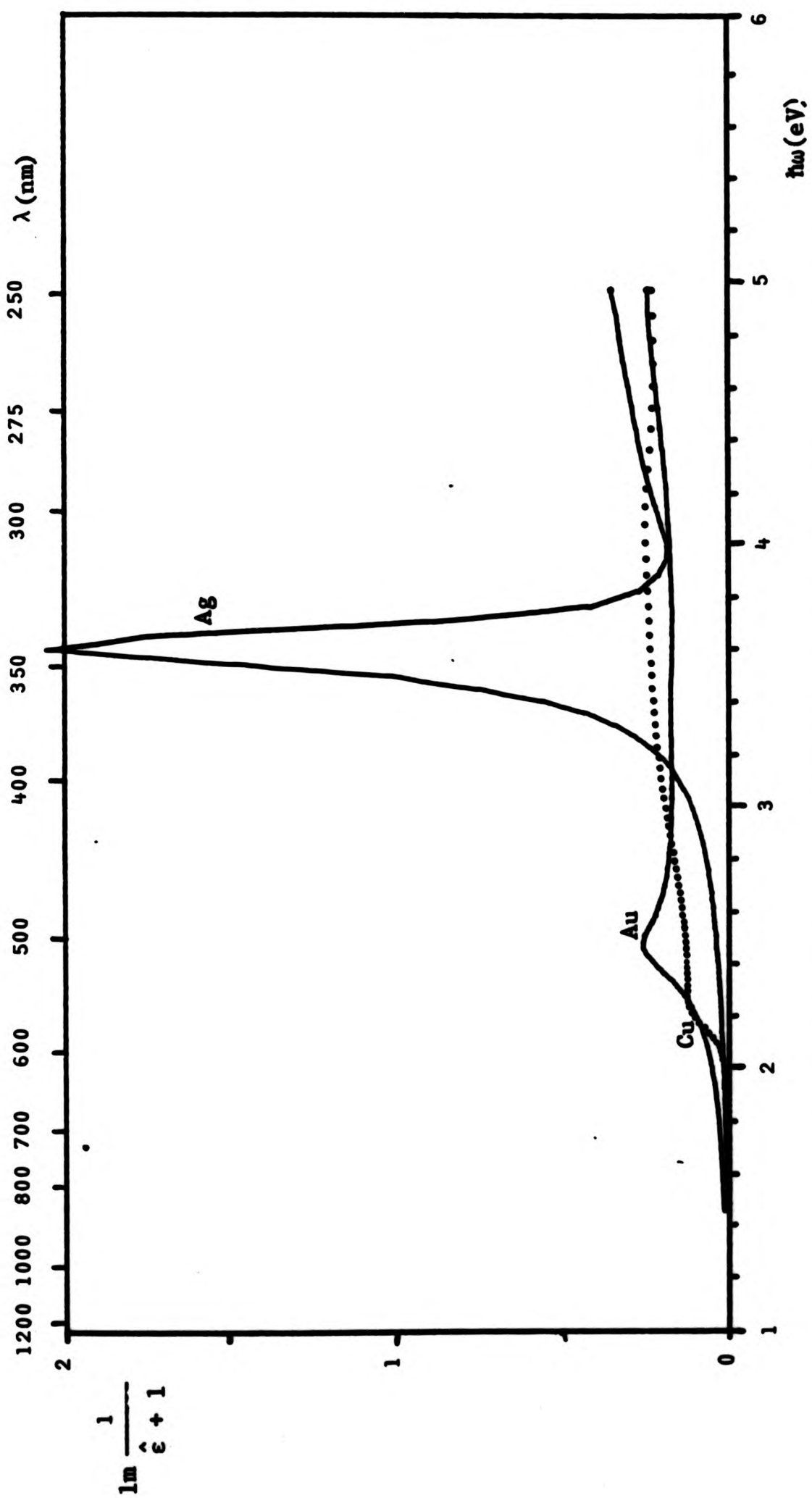


Figure 6.5. Bulk plasmon energy loss function for the samples of Figures 6.2a, 6.3 and 6.4. The initial rise for copper is at 2.2eV, gold at 2.4eV while silver shows a strong maximum at 3.8eV.



**Figure 6.6.** Surface plasmon energy loss functions for the samples of Figures 6.2a, 6.3 and 6.4. The sharp maximum for silver is at 3.6eV (cf. 3.8eV for the bulk plasmon).

to an external stimulus. It can be seen that these plasmon losses are much larger for silver than for either gold or copper; for all three materials the functions take very small values for energies less than those of the 'edges' of  $\epsilon_2$  and  $R_N$  described above - 3.8, 2.4 and 2.2eV respectively.

The shape of these curves has been shown to correlate strongly with the attenuation of a beam of electrons passing through foils of these materials. Photons, however, do not interact with plasmons as readily as electrons, so that generally absorption by generation of plasmons may be ignored. For rough surfaces on bulk samples, it is possible for the light beam to generate surface plasmons, when the surface plasmon energy loss function is large. In this case extra absorption ( $\epsilon_2$ ) may be observed close to the energy of the surface plasmon peak. Computation of this function may thus assist in identifying some component of the absorption.

#### Conduction band absorption

The Drude 'free-electron' model of optical absorption predicts that, for a free-electron gas  $\epsilon_2 \propto \omega^{-3}$ . In quantum mechanical terms, little modification is needed to apply this (classical) theory to materials having a spherical Fermi-surface. Assuming that all absorption, in some energy range, is due to excitation of conduction electrons to other states within the same band, the only contribution of electrons in lower-lying bands is to  $\epsilon_1$ . Furthermore this contribution, say  $\delta\epsilon_1$ , will be constant for photon energies much less than some threshold. Thus,

for the purpose of extending the results to include free-electron, Drude or intraband absorption, it is assumed that

- (a) The Fermi surfaces of these metals are spherical;
- (b) that  $\delta\epsilon_1$  is constant.

Also, to simplify the calculation, we assume

- (c)  $\omega\tau \gg 1$ , where  $\tau$  is the relaxation time of the conduction electrons.

In order to test the validity of these assumptions, Figure 6.7 is a plot of  $\epsilon_2$  versus  $(\hbar\omega)^{-3}$ . Departure of the curves from straight lines indicates that free-electron behaviour cannot be assumed. All three curves show high energy regions where the absorption is not at all Drude-like and a low energy region where the assumption may be tenable. A slight curve in the graph for silver implies some deviation from exact cubic behaviour. Accordingly, following previous workers, the assumptions were relaxed and a power-law dependence

$$\epsilon_2 \propto (\hbar\omega)^N$$

was tried. The value of  $N$  could be determined from a plot of  $\log \epsilon_2$  vs  $\log \hbar\omega$ . Again, deviations from a straight line would demonstrate the falseness of the assumptions. The graphs are given on Figure 6.8. Other experiments have yielded values for  $N$  ranging from 0.9 for one Cu sample to 2.7, compared with the predicted 3. The value obtained strongly depends on the preparation of the sample.

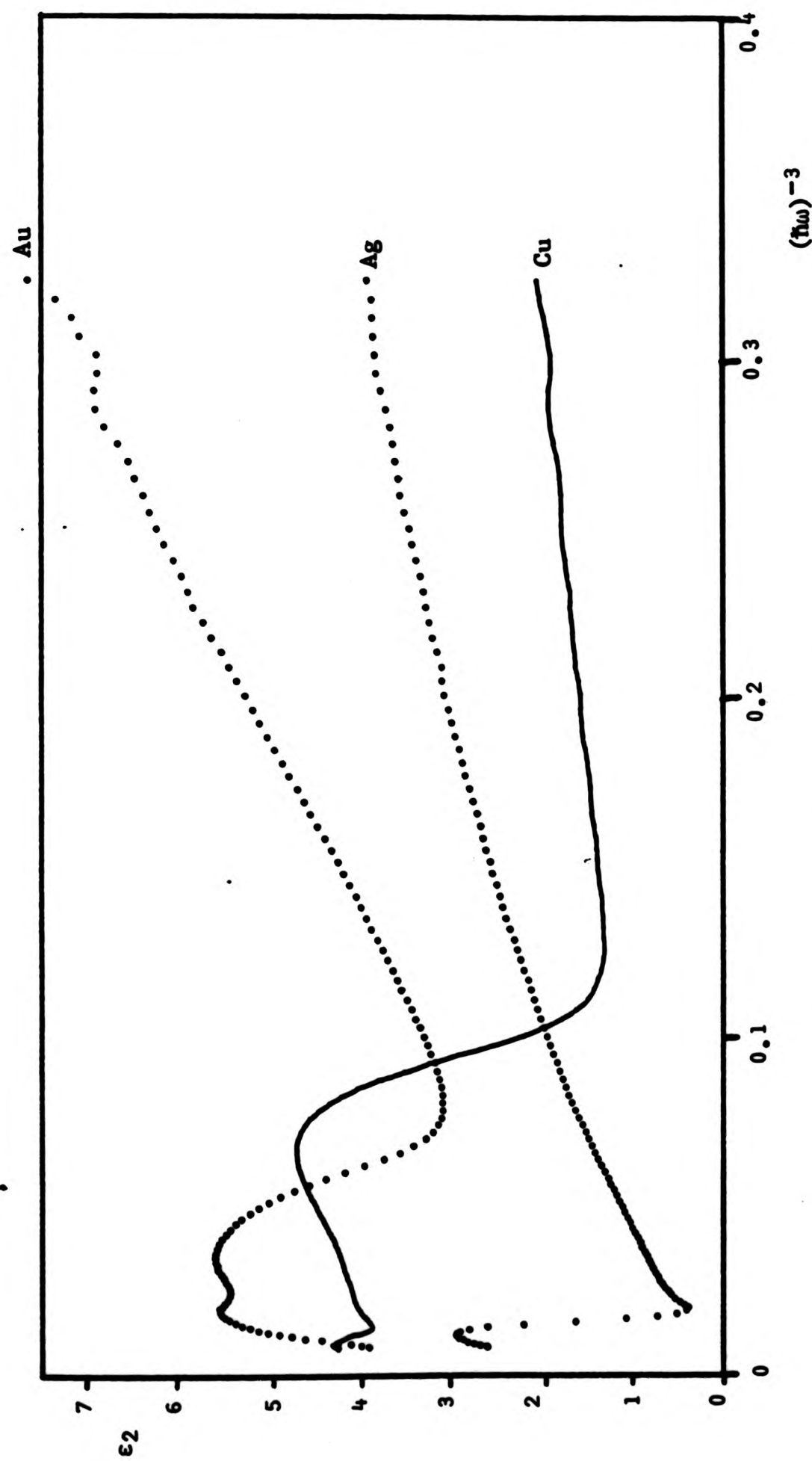


Figure 6.7. Illustrating the region of Drude-like absorption,  $\epsilon_2 \propto \omega^{-3}$ , for Ag, Au and Cu.

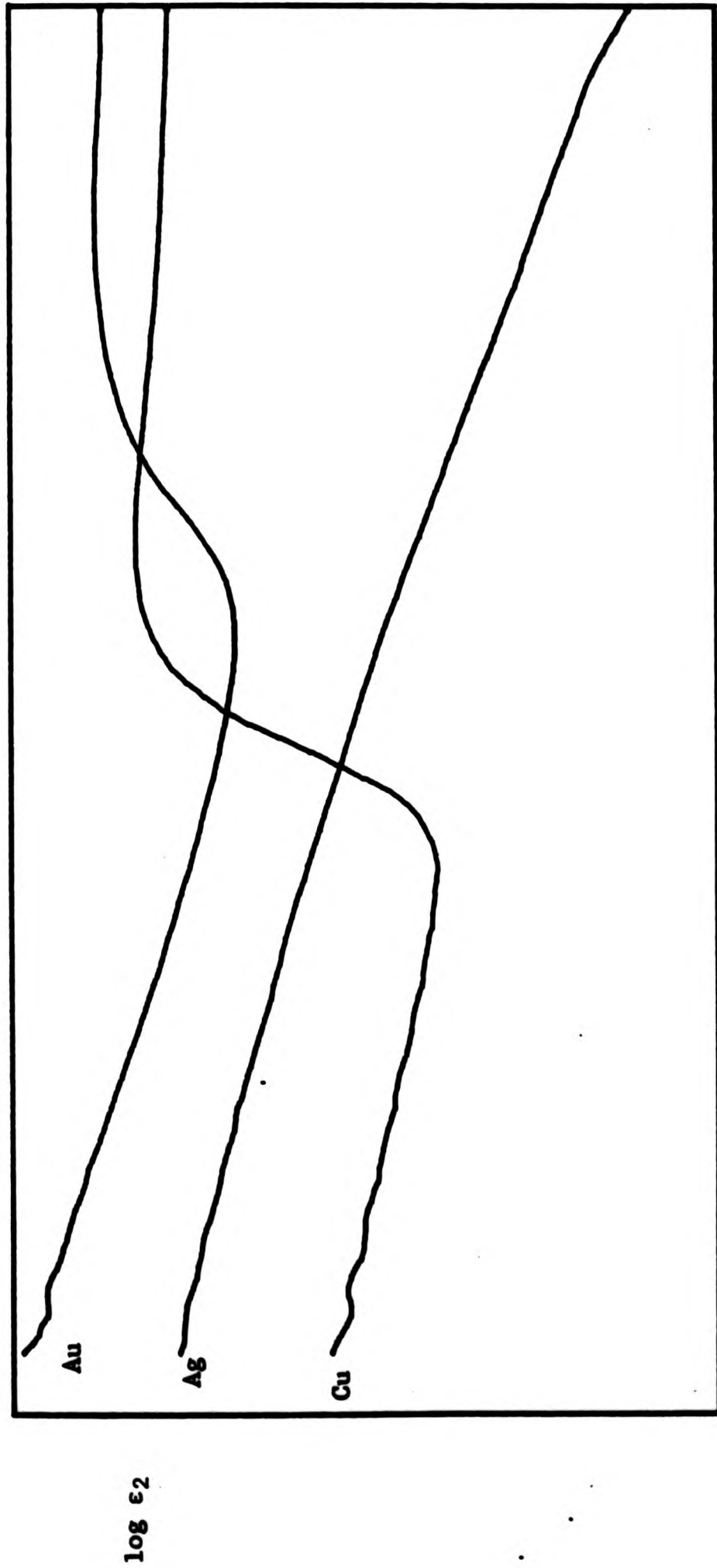


Figure 6.8.  $\epsilon_2(h\omega)$  on logarithmic axes, showing the region of free-electron absorption governed by a power law of the form  $\epsilon_2 \propto h\omega^N$ . The gradients of these functions give the power law coefficient  $N$  (-2.09, -2.21 and -1.50 for these Ag, Au and Cu samples, respectively).

### Separation of absorption processes

The coefficients of the log-log graphs, obtained by linear least-squares fitting, were used to calculate  $\epsilon_2^f(\hbar\omega)$ , the free-electron absorption, for the full energy range. This function was then subtracted from the experimental  $\epsilon_2$  to give  $\epsilon_2^b$ . The results of this exercise are shown in Figures 6.9 - 6.11. For silver, the results show that this fit is not altogether satisfactory, sometimes being ten percent of the value of  $\epsilon_2^b$  (ie. 0.3) out. For gold and copper the fit is much better, although a much smaller interval is being considered. For gold, it appears there is some absorption at  $\sim 2.2\text{eV}$ , just below the edge, which cannot be attributed to  $\epsilon_2^f$ . However, the magnitude of the absorption is within the observed fitting accuracy for silver.

Silver shows only a single peak in  $\epsilon_2^b$  within the measurement range, at 4.4eV. Gold has two, at 3.0 and 3.8eV, while copper has three, at 2.4, 3.6 and 4.7eV. Gold has the largest  $\epsilon_2$ , while copper has much the steepest rise in  $\epsilon_2^b$ .

### Numerical Derivatives

Numerical derivatives  $D^1\epsilon_2^b(\hbar\omega)$  and  $D^2\epsilon_2^b(\hbar\omega)$  are shown in Figures 6.12 and 6.13. These have been produced by fitting an quadratic to  $\epsilon_2^b(\hbar\omega)$  exactly over three adjacent measured values -

$$\epsilon_2^b(\hbar\omega) = a(\hbar\omega)^2 + b(\hbar\omega) + c$$

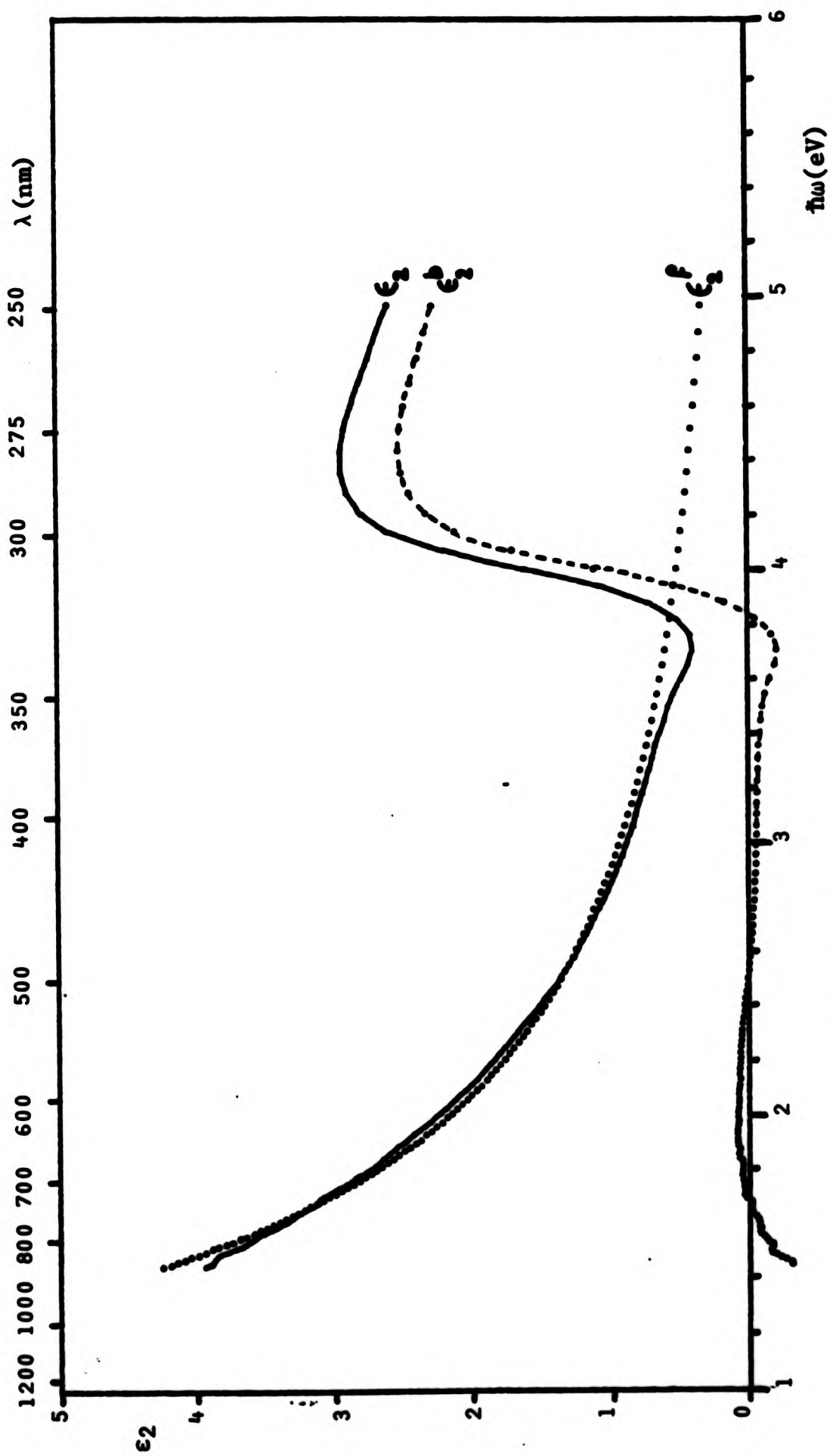


**Figure 6.9.** Sample 30R, 99.97 wt.% Ag. The separation of  $\epsilon_2$  into free-electron (intraband) and bound electron (interband) components  $\epsilon_2^a$  and  $\epsilon_2^b$ . A linear least squares fit of  $\log \epsilon_2$  vs.  $\log \lambda$  was carried out for  $\lambda$  400-850nm ( $\sim 1.4 - 3.1$ eV).

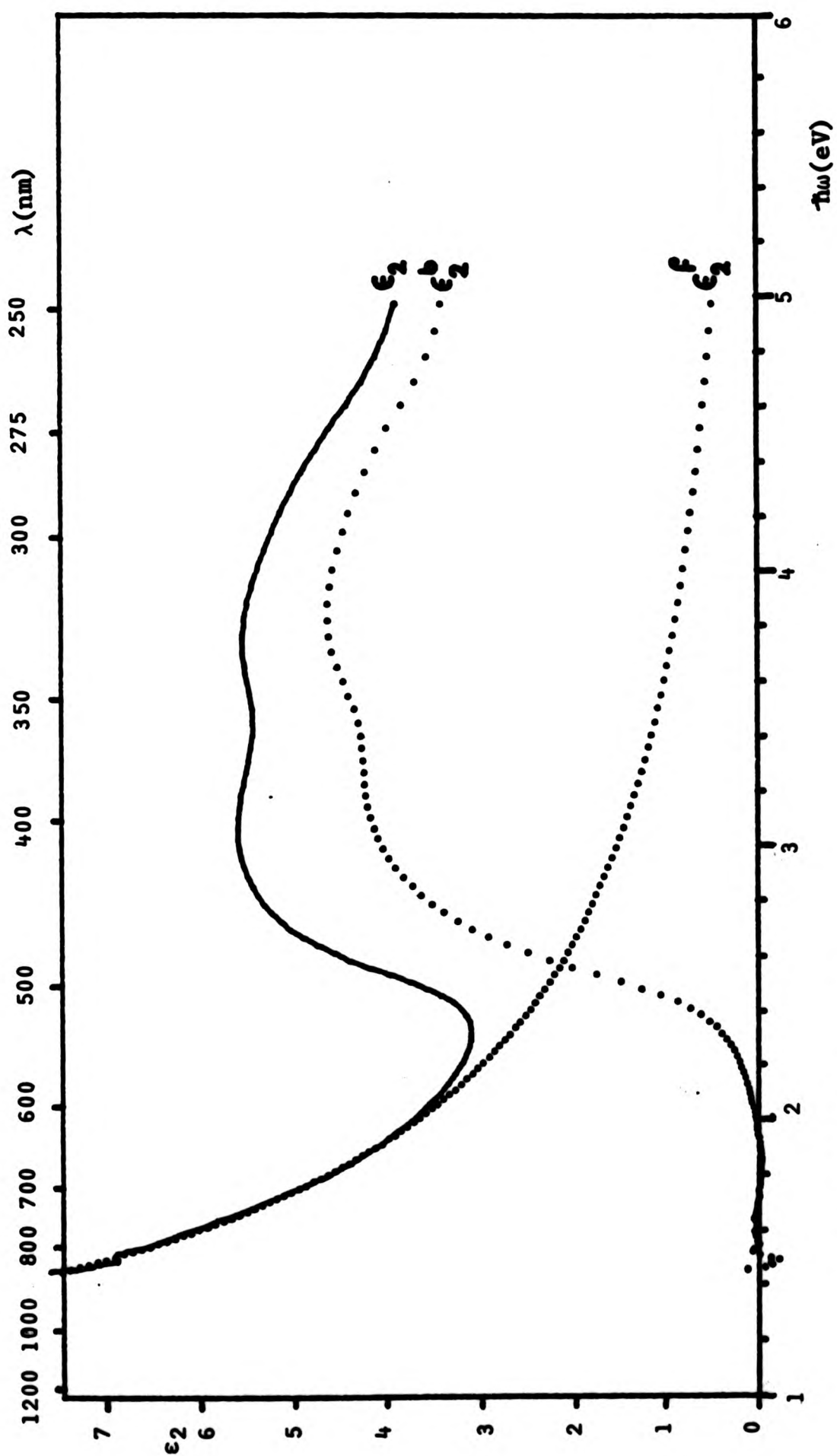
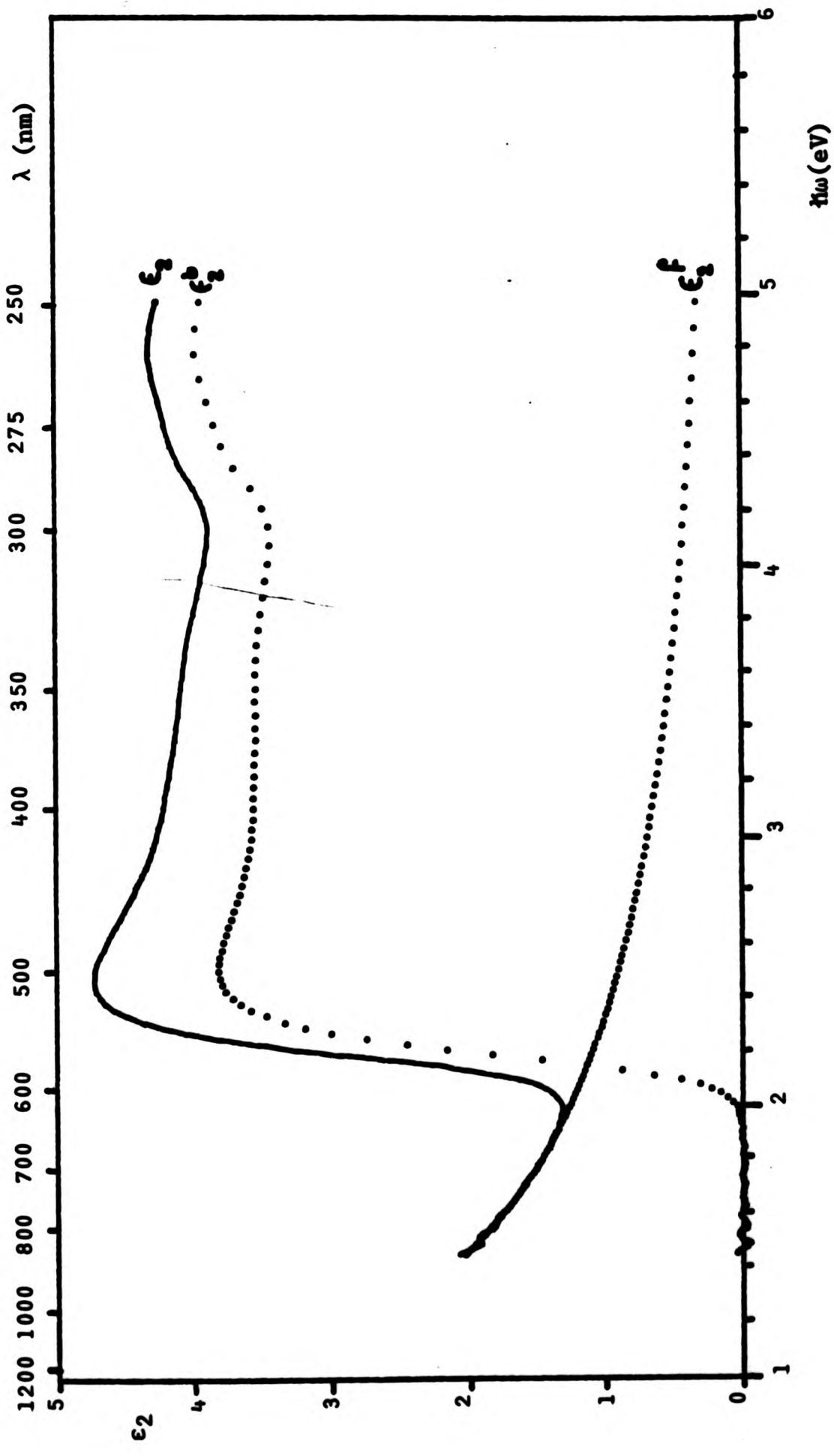


Figure 6.10. Fine gold.  $\epsilon_2 = \epsilon_2^a + \epsilon_2^b$ , by a power law fit for  $\lambda$  650 - 850nm  
 (  $h\nu$  1.4 - 2.0eV ).



**Figure 6.11.** 100Cu.  
 Decomposition of  $\epsilon_2 = \epsilon_2^a + \epsilon_2^b$  by a power law fit of  $\epsilon_2(\lambda)$  for  $\lambda$  650-850nm.  
 ( $\hbar\omega$  1.4 - 2.0eV).

and then computing the derivative -

$$\frac{1}{h} \frac{d\epsilon_2^b}{d\omega} = 2a h\omega + b$$

to give the gradient at the central point. Application of this procedure recursively enabled derivatives of any order to be built up. Thus the second derivative at any energy was obtained from measured values of  $\epsilon_2^b$  at five adjacent energies.

Figure 6.12 clearly shows the positions of the main edges, and also indicates plainly the subsidiary maxima for Au and Cu. That for Cu at 4.7eV is resolved into two, at 4.5 and 4.8eV. The exact position of an absorption edge may conveniently be defined as the point of maximum slope, which is to say one of the zeroes of the second derivative. Thus Figure 6.13 should enable accurate values for these positions to be interpolated. In practice, the inaccuracy of the data can be seen to have defeated this aim for energies less than 3.5eV. There appears to be superimposed on the spectra a periodic ripple about 0.1eV wide. The origin of this structure will be discussed later, but it is possibly due to multiple reflections in one or more of the optical elements producing interference effects, or to spectral variation of the ellipsometer sensitivity.

#### Colour calculations

These are presented in Figures 6.14 - 6.18, for a variety of schemes. The first are for the C.I.E 1931 Standard system, and the second for the 1960 Uniform Colour System. Also shown are the effects of using equal-energy distribution

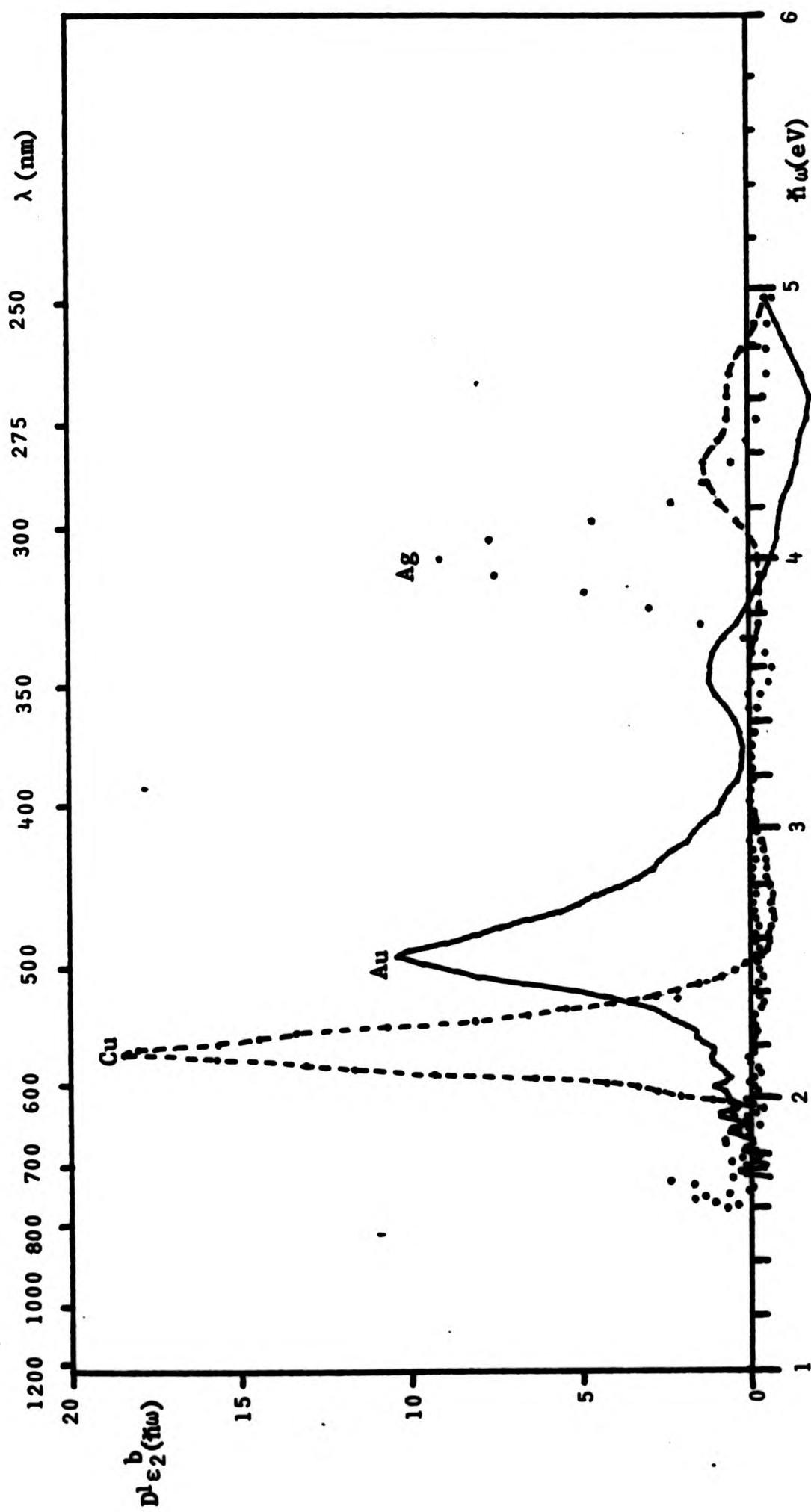


Figure 6.12. First derivative of  $\epsilon_2^b(\hbar\omega)$  for Ag, Au and Cu. These have been obtained numerically from the curves of Figures 6.9, 6.10 and 6.11.

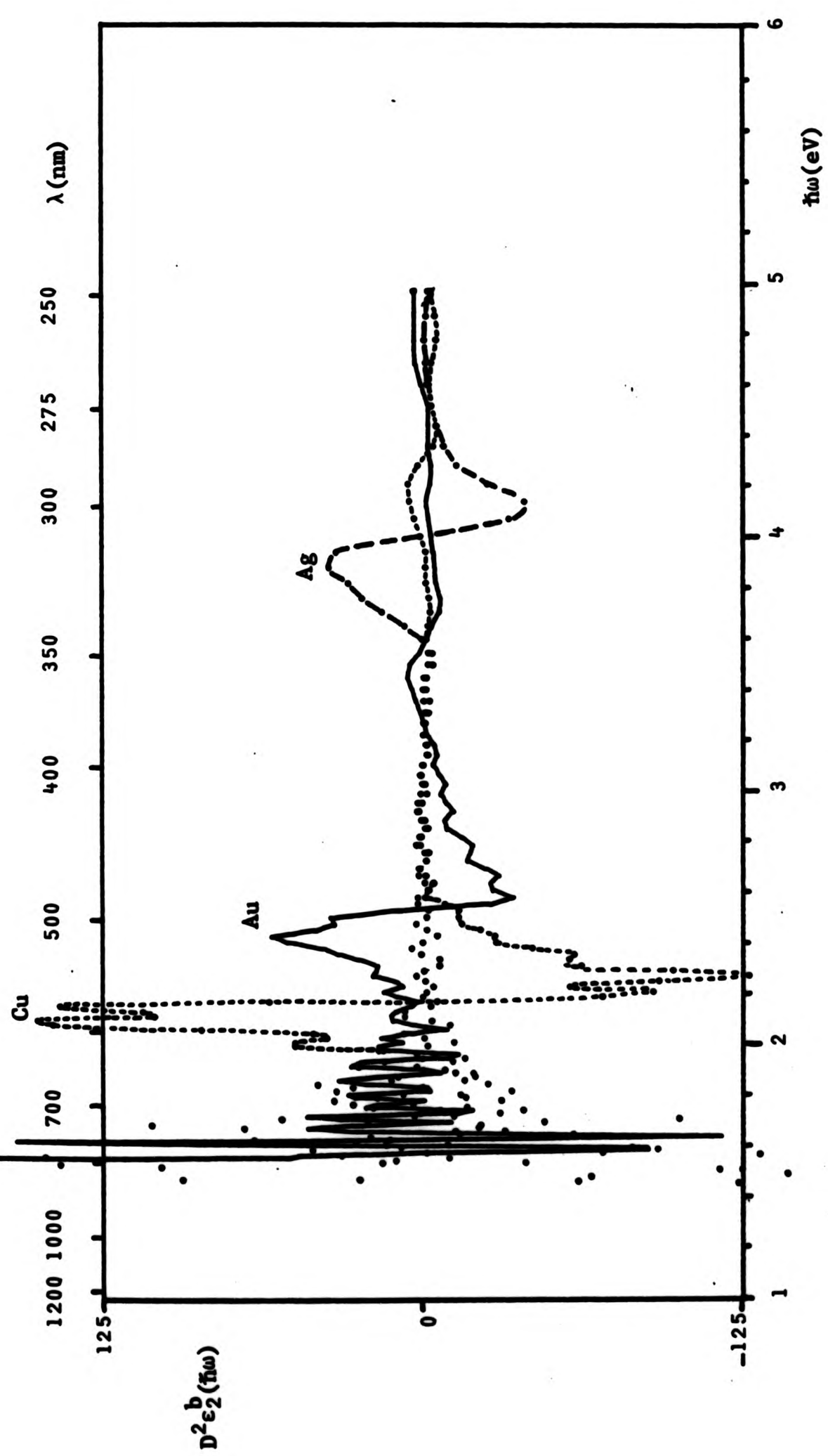
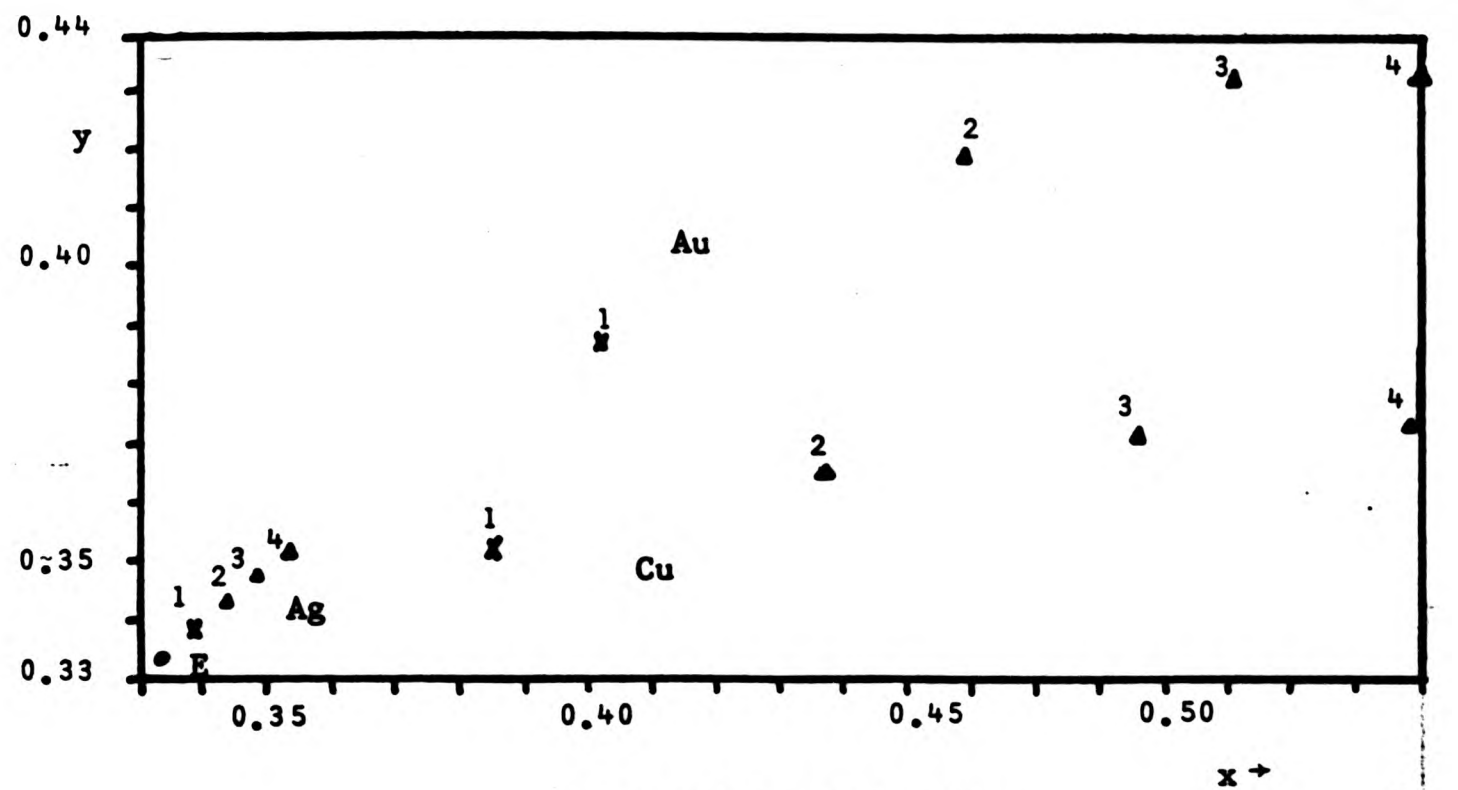


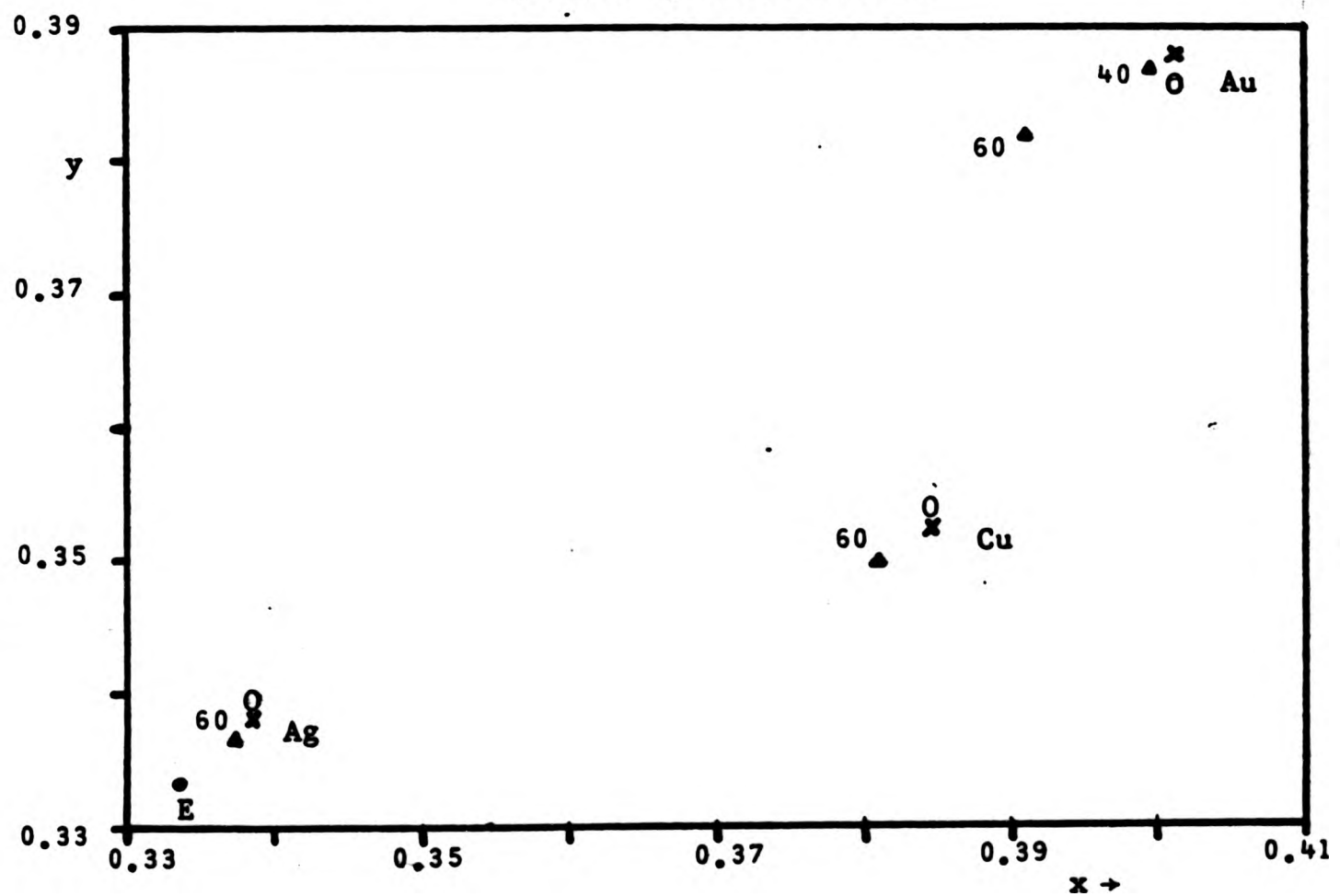
Figure 6.13. Second derivative  $\epsilon_2^b(h\omega)$  for Ag, Au and Cu.

-----Ag;    ———— Au;    ..... Cu.

Note the anomalous structure at low energies.



(a) Multiple reflections

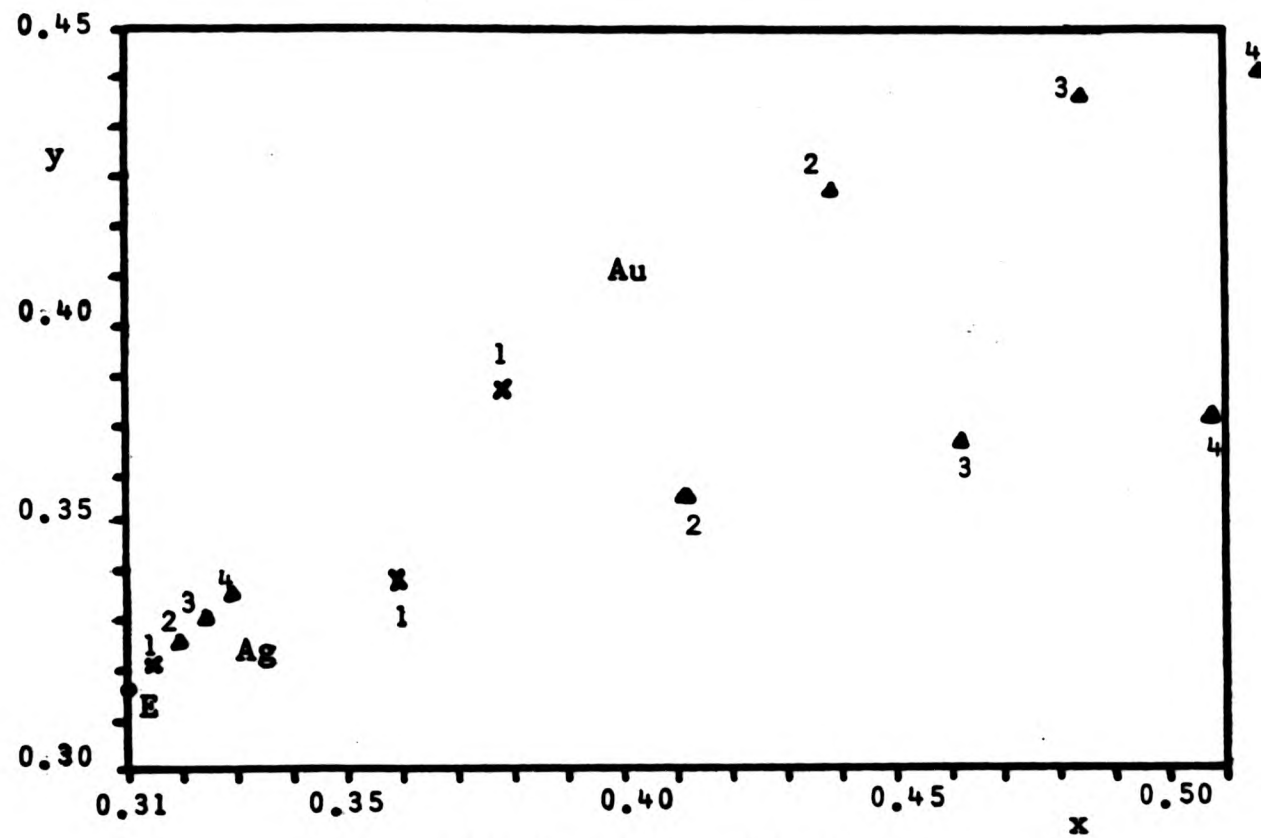


(b) Variation of angle of incidence

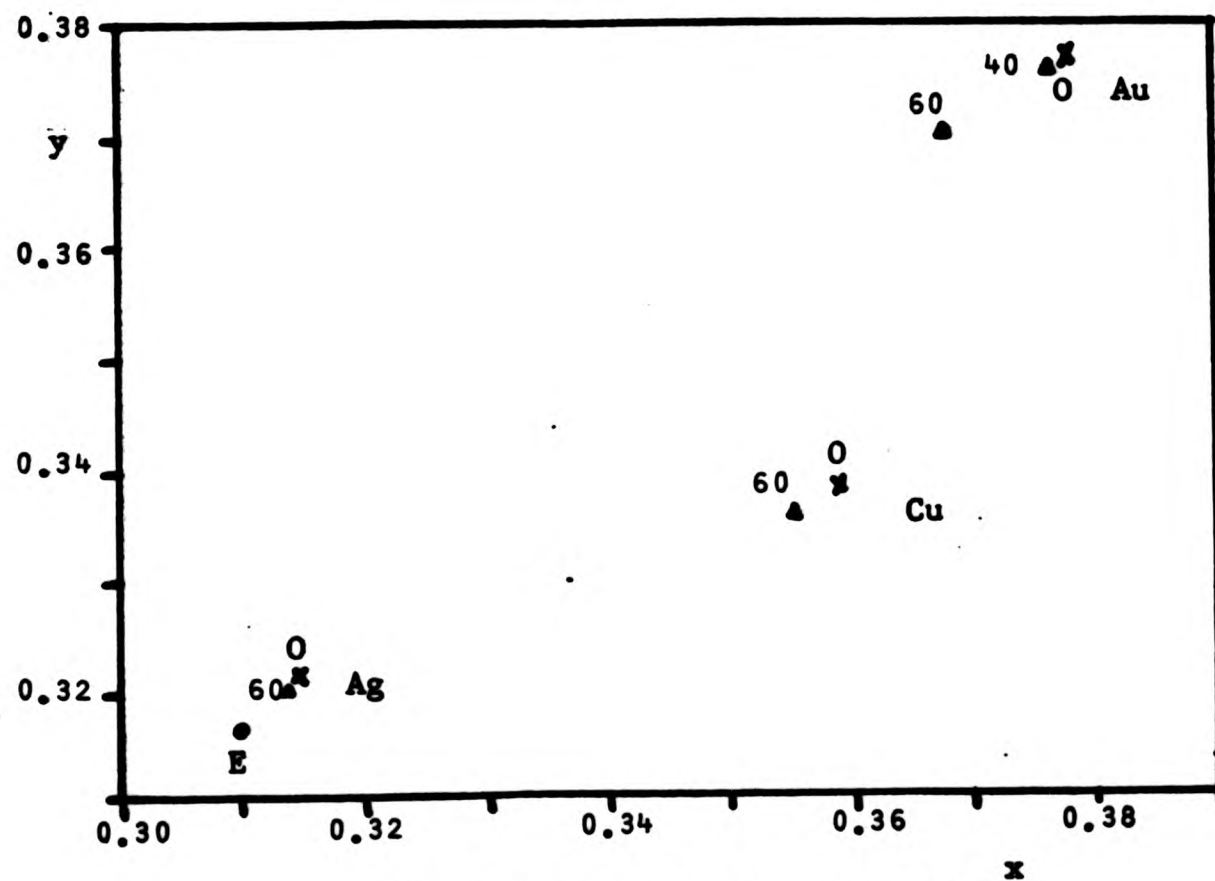
Figure 6.14. C.I.E colour co-ordinates in the 1931 Standard System, equal energy illumination.

(a) for 1, 2, 3 and 4 reflections (b) reflection at  $0^\circ$ ,  $40^\circ$  and  $60^\circ$  incidence.

The  $40^\circ$  points are not resolved from those at normal incidence in the cases of Ag and Cu.



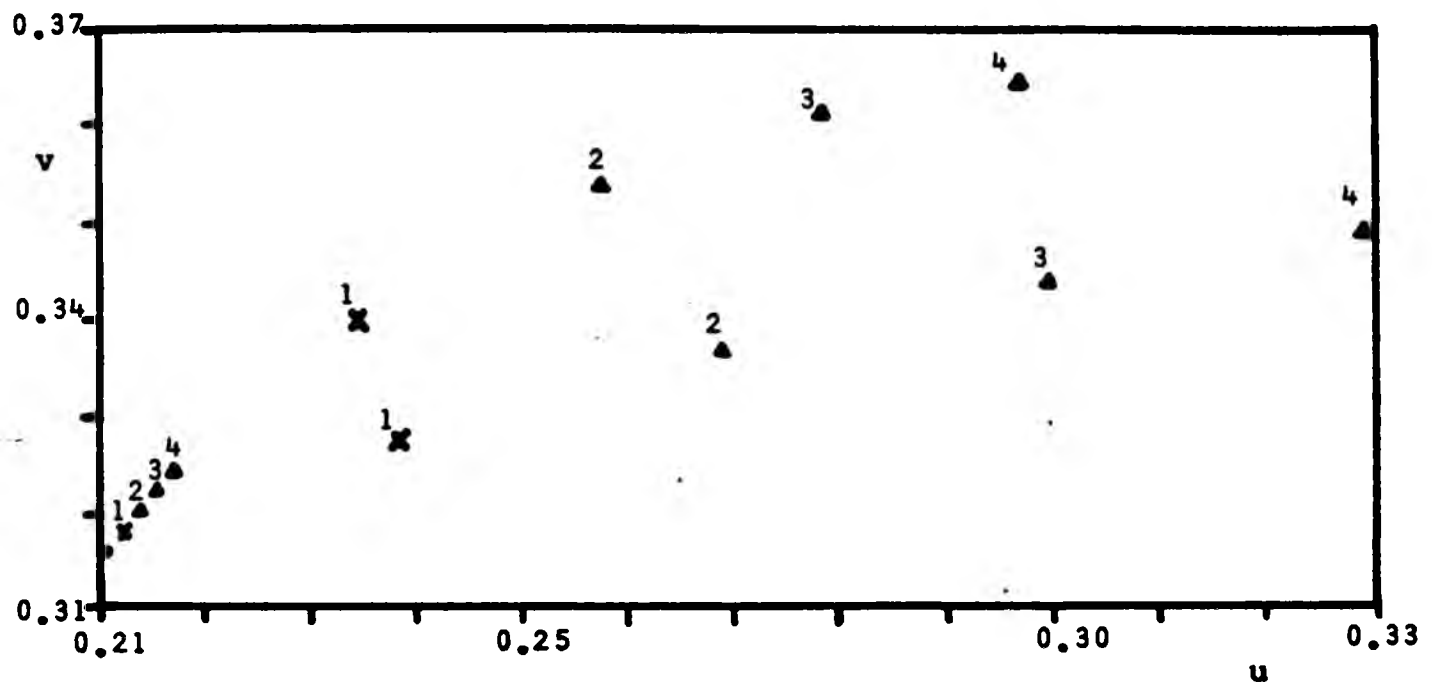
(a) Multiple reflections



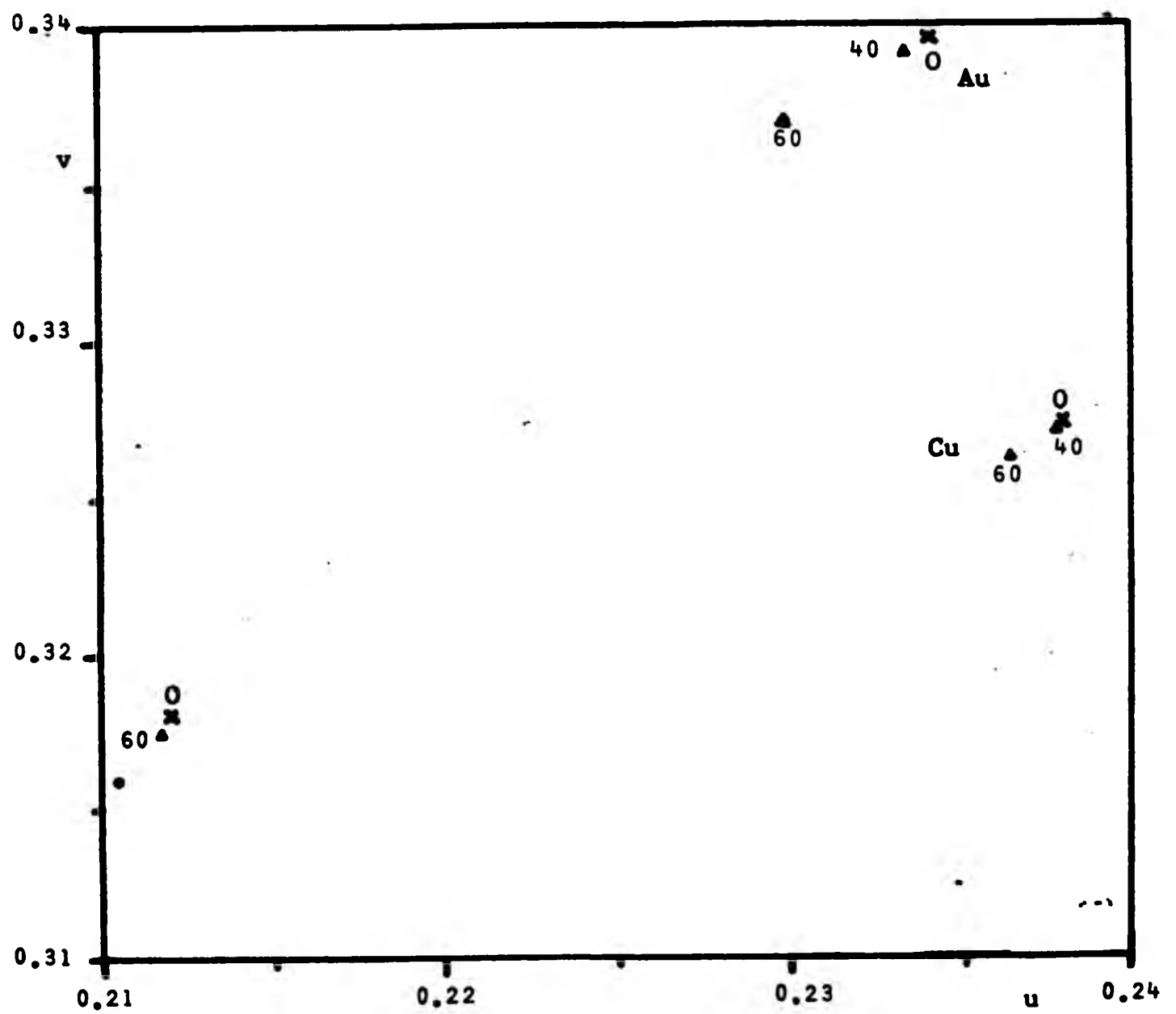
(b) Variation of angle of incidence

**Figure 6.15.** Colour co-ordinates in the C.I.E 1931 Standard System - Standard Illuminant C.

(a) for 1,2,3 and 4 reflections (b) for  $0^\circ$ ,  $40^\circ$  and  $60^\circ$  incidence.

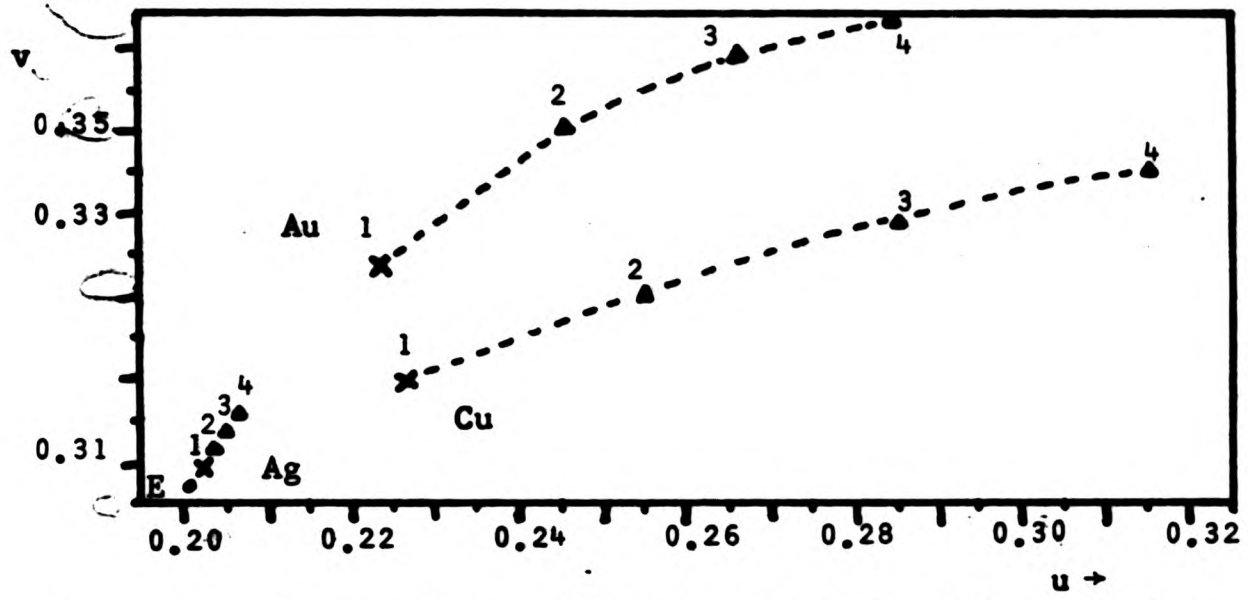


(a) Multiple reflections - 1,2,3 and 4 reflections

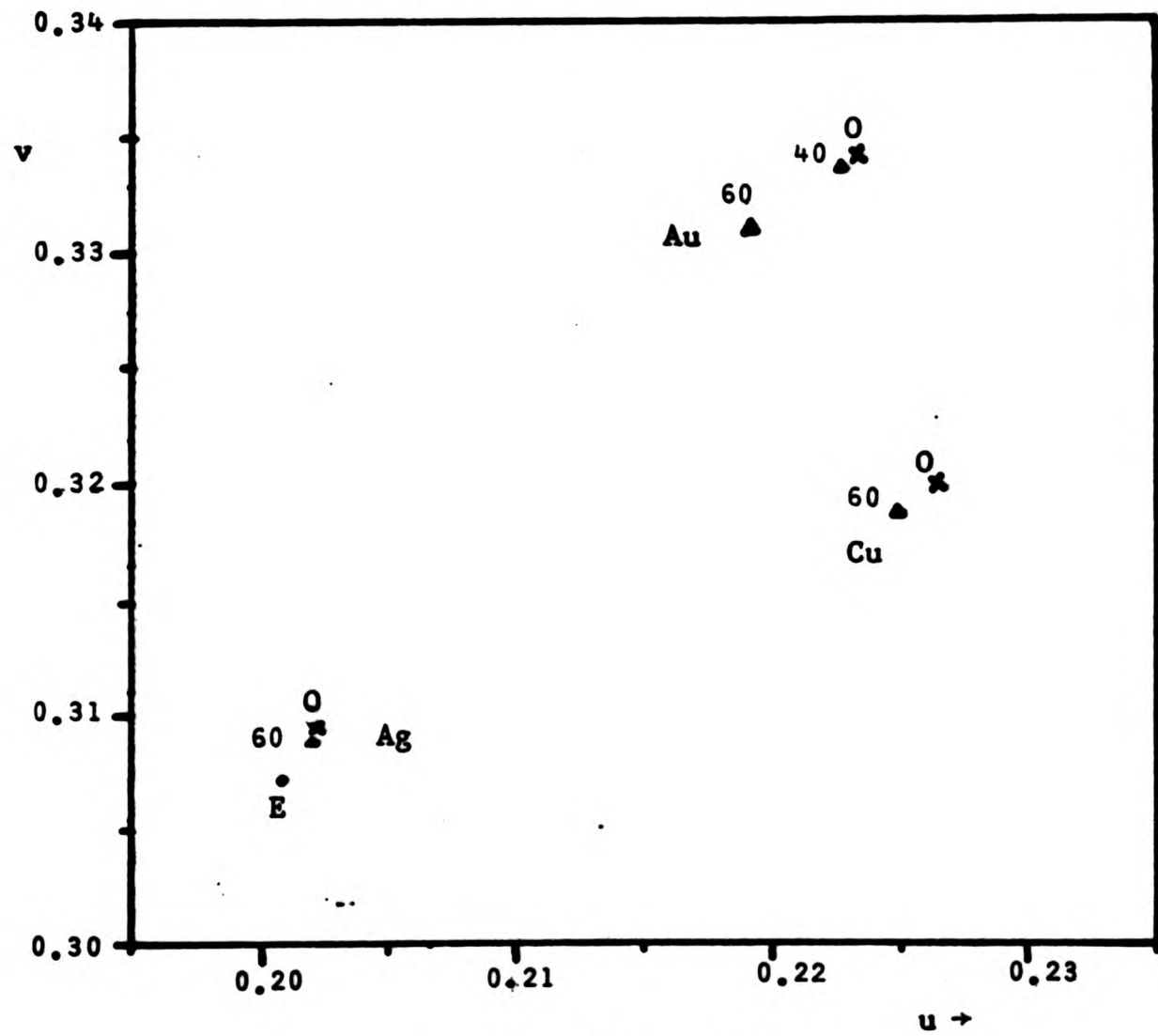


(b) Variation of angle of incidence - 0°, 40° and 60°.

Figure 6.16. C.I.E colour co-ordinates - 1960 Uniform Colour System, equal energy illumination.



(a) Multiple reflections - 1,2,3 and 4 reflections.



(b) 0°, 40° and 60° incidence.

Figure 6.17. C.I.E colour co-ordinates in the 1960 Uniform Colour System - Standard Illuminant C.

illumination, or C.I.E Standard Illuminant C, which corresponds to daylight and is slightly blue. The relative effect of varying the illuminant can be seen to be small - there is certainly no danger of metamerism in this type of lighting. The effect of varying the angle of incidence is also shown to be small, slight decreases in saturation being found for all three materials at large angles of incidence (greater than  $40^\circ$ ). Angles within  $30^\circ$  of normal incidence give an insignificant effect. Increasing the number of reflections from the surface has the opposite effect - co-ordinates move rapidly away from the 'white' point. For two reflections (each at near-normal incidence) the saturation is approximately doubled. A small increase in colour between the samples is increased by increasing the number of reflections - more so for Ag/Au and Ag/Cu than for Au/Cu.

#### Effect of oxidation on copper

The change in  $\Delta(\tilde{n}_u)$  caused by five months of oxidation in the laboratory atmosphere can be seen in Figure 6.18. The largest change,  $\sim 15^\circ$ , was at the longest wavelength, and may correspond to a film  $\sim 200\text{\AA}$  thick. Attempts were made to characterise this film by fitting the ellipsometric data, so that the effect of film growth on colour could be computed. This is discussed in Section 7.3.2.

#### 6.2 Ag-Au Binary Alloys

In this section results are presented in such a way that the colour calculations may be interpreted from the simplest to steadily more fundamental levels. Thus colorimetric loci

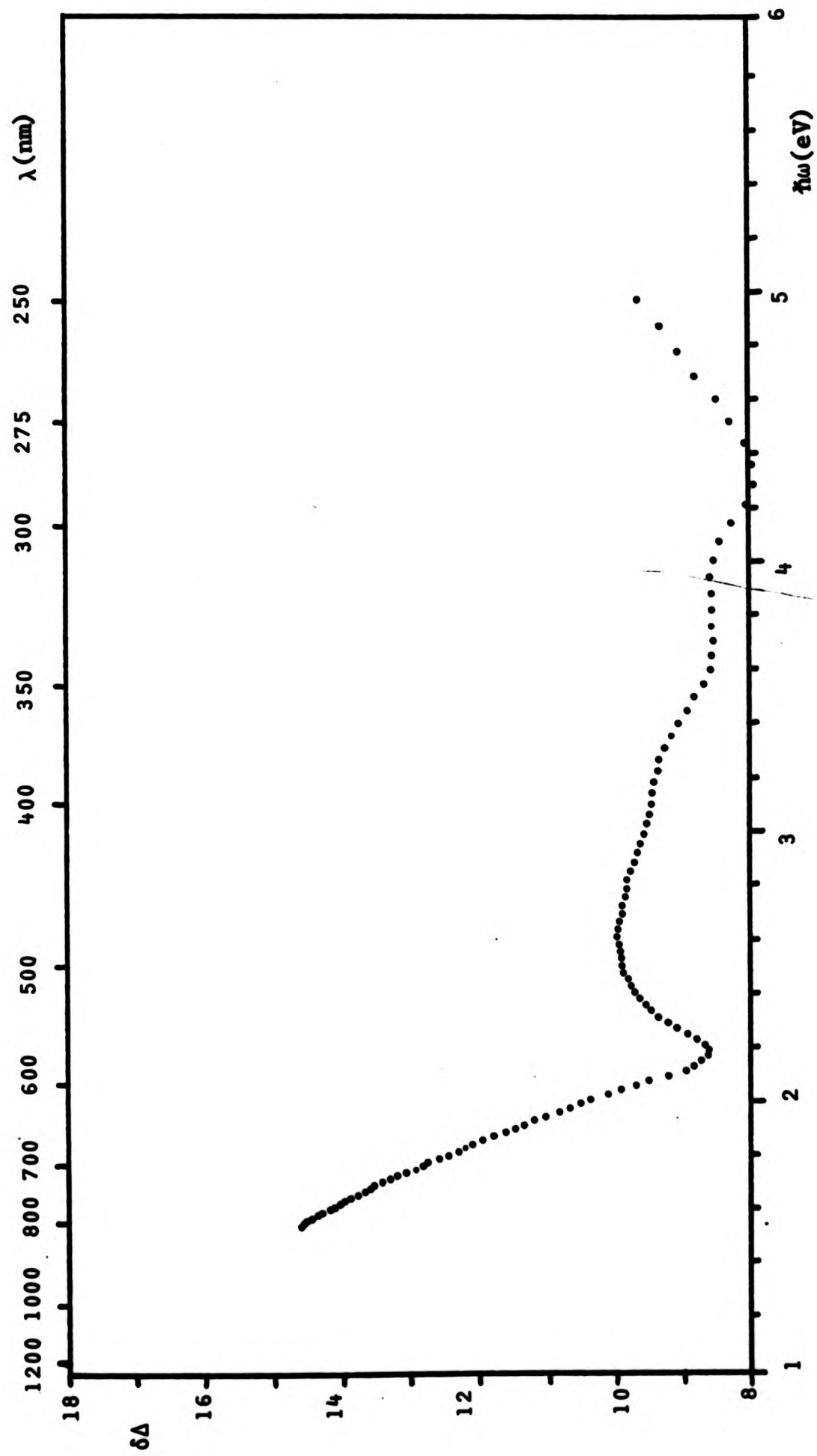


Figure 6.18. Change in the ellipsometric parameter  $\Delta$ , on room-temperature oxidation of copper for a period of five months.

Table 6.1 Some properties of Ag-Au alloys as a function of concentration.

Reference Number	Atomic % Au	Weight % Au	C.I.E. Colour Co-ordinates $\times 10^4$ Normal Reflectance			1960 Uniform Colour System Standard Illuminant C			1931 Standard System Equal Energy Illumination			Relaxation time $10^{-15}$ s.	$h\nu_p$ (plasma freq.) eV	$d\epsilon/d\lambda$ absorp. edge eV	$\epsilon_p(0)$	
			1931 Standard System Equal-Energy Illumination		y	u	v	$\lambda_d$ nm	s	z	L					z
			x	y												
21	83.4	90.2	3884	3989		2111	3362	575.9	36.31	80.98						
22	68.7	80.0	3756	3919		2058	3323	574.1	30.36	81.32						
23	56.3	70.2	3621	3789		2022	3265	572.6	22.41	85.02						
24	45.3	60.2	3519	3613		2022	3193	573.1	14.03	85.66						
25	35.4	50.0	3429	3504		2006	3144	571.3	8.06	89.76						
26	26.7	39.9	3386	3442		2002	3118	579.7	4.89	90.04						
27	19.0	30.0	3379	3406		2011	3104	572.6	3.60	90.20						
28	12.4	20.6	3344	3369		2002	3087	565.1	1.42	86.91						
29	12.7	21.0	3379	3375		2019	3093	577.3	2.47	86.12						
29R	5.8	10.1	3363	3363		2016	3087	577.8	1.81	93.75		5.52	9.91	12.9		
68			3352	3350		2014	3081	578.8	1.08	94.78		7.17	9.97	14.0		
78	90.7	94.7	3989	3945		2193	3361	578.9	38.14	70.91		3.92	10.9	28.8	2.56	

not available

functions and finally the electronic parameters. Where possible, spectral curves are summarised in terms of scalar quantities that can be given as functions of composition.

#### Colorimetry

The C.I.E 1960 Uniform Colour System has been chosen to show the main colorimetric results, using C.I.E Standard Illuminant C. This leads to a colour diagram in which the geometric separation of any pair of points most closely corresponds to the perceived colour difference between the associated stimuli, ie. observation of a pair of samples in diffuse daylight. The  $(u, v)$  locus for Ag-Au binary alloys is given in Figure 6.19. Since this does not include a quantity relating to perceived brightness, a graph (Figure 6.20) of luminance versus composition is also given. This was computed using the 1931 Standard System.

Saturation and Dominant Wavelength ( $\lambda_d$ ) are also presented on this figure, calculated for equi-energy illumination. In this system the hue is most similar to that of the monochromatic stimulus equal to  $\lambda_d$ .

#### Spectral Reflectance

Figure 6.21 is a composite of the normal reflectance curves for a representative selection of the alloys. For this particular system it is possible to give all eleven curves for the nominal 10% by weight intervals, without unduly crowding the graph. In order to show more precisely the effect of each 10% alloying addition, difference curves for adjacent alloy compositions are presented in Figure 6.22.

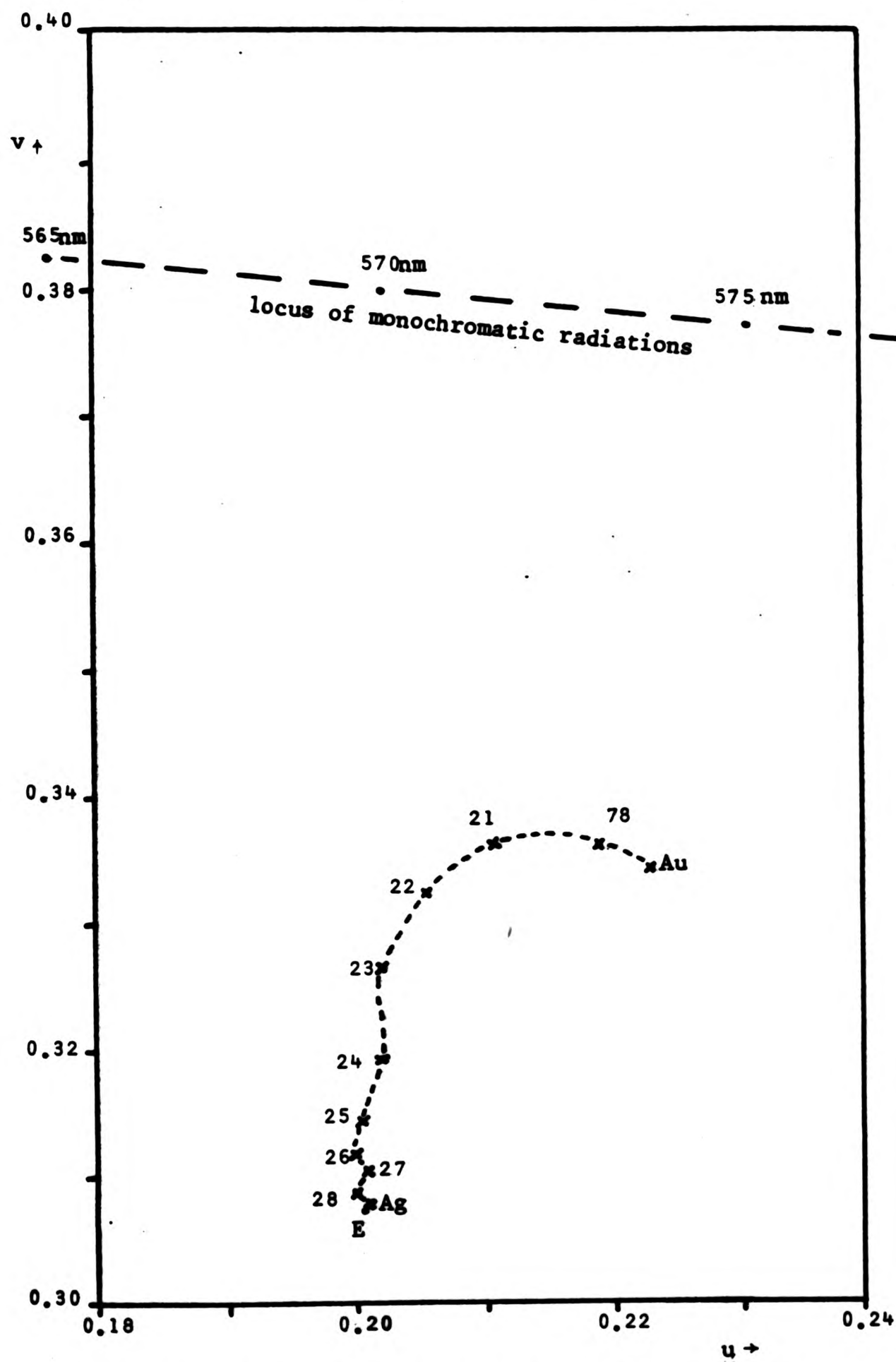


**Figure 6.19.** Colour co-ordinates of Ag-Au binary alloys, C.I.E 1960 Uniform Colour System, Normal Reflectance, Standard Illuminant C. The numbers on the curve (-----) refer to the sample melt number. Ag and Au results are for Johnson Matthey samples.

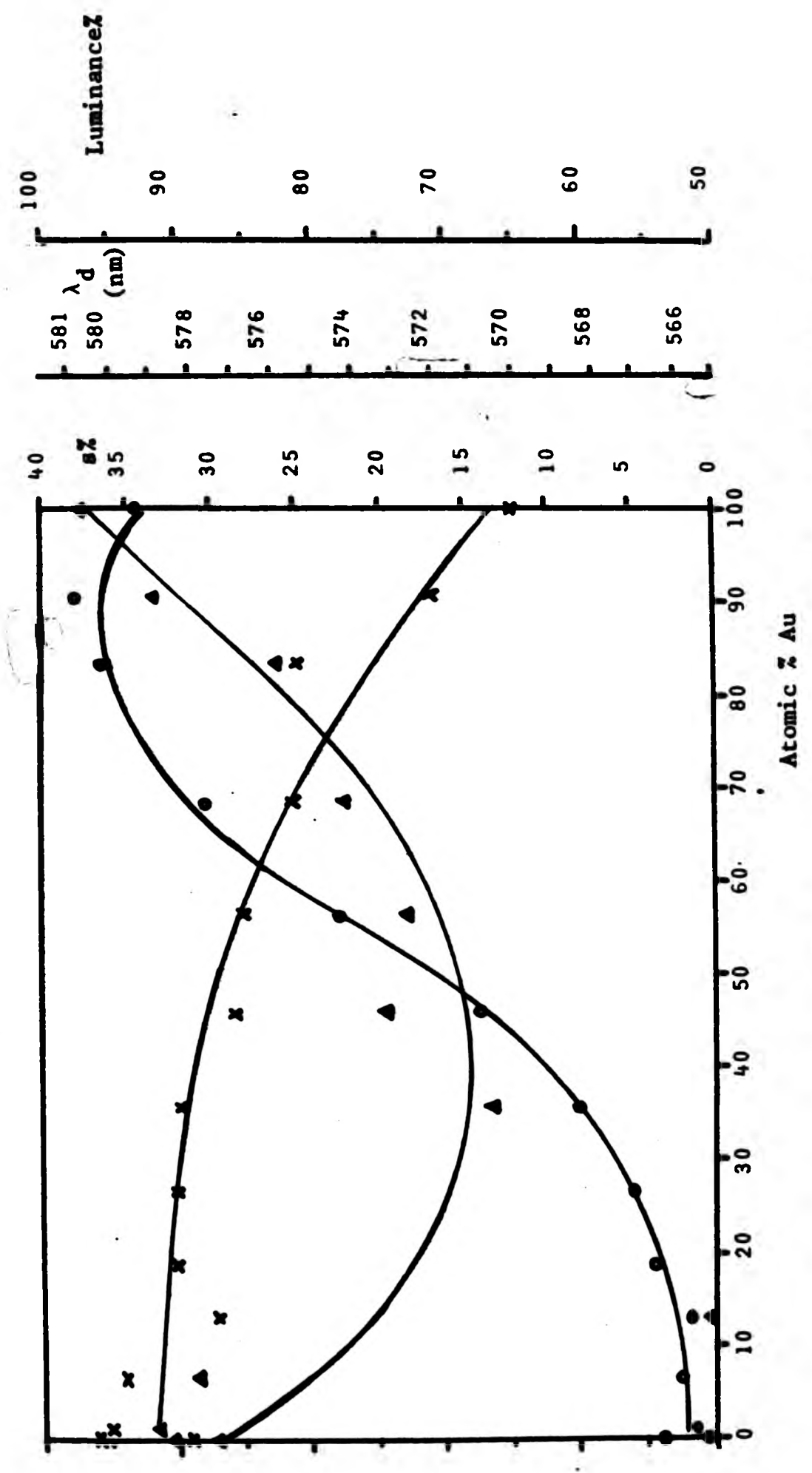


Figure 6.20. Saturation (●-●-●), Luminance (x-x-x) and Dominant Wavelength (▲-▲-▲), of Ag-Au alloys. C.I.E. 1931 Standard System, Equal-Energy Illumination.

These will be used to provide the basis for discussion of colour changes, and in combination with the derivative spectra of Figure 6.22, to furnish shifts in the absorption edges.

Data summarising the movements of the reflectance edge are tabulated in Table 6.2.

#### The dielectric functions

Figure 6.24 shows the measured values for the imaginary part of the dielectric function,  $\epsilon_2(\omega)$ , for various compositions of Ag-Au alloys. The difference between these curves ( $\delta\epsilon_2$ ) for each pair of alloys of adjacent composition are given in Figure 6.25. Also shown are the first derivative spectra,  $\frac{\partial\epsilon_2}{\partial\omega}$  (Figure 6.26). Again, shifts in the position of the main absorption edge,  $\delta\omega$ , have been computed using  $\delta\epsilon_2 + \frac{\partial\epsilon_2}{\partial\omega}$ , and tabulated in Table 6.3.

Data for alloys No.21 to 28 inclusive were obtained before the RCA 8852 red-sensitive photo-multiplier tube became available, and therefore do not extend below 2eV. These samples cover the range of composition from 10% to 80% Ag, by weight.

Systematic variation with composition for samples 21 to 28 can be seen, while the samples measured much later (Johnson Matthey Ag, Au; 5.8 at.% Au (29R) and 90.7 at.% Au (78)), appear also to form a distinct group.

There is a monotonic shift in the position of the edge in  $\epsilon_2(\omega)$  with composition (Table 6.3 and Figure 6.34), while

Table 6.2. Edges of  $R_N(\omega)$ , Ag-Au alloys

Sample No.	Atomic % Au	zero of D <sup>2</sup> $R_N(\omega)$ eV	D <sup>1</sup> $R_N(\omega)$ max % per eV	$R_N$ (same value of $h\omega$ ) %	e $h\omega$ eV	$R_N$ of adjacent alloy at same $h\omega$	$\delta R_N$ %	$\delta h\omega = \delta R_N + \frac{\partial R_N}{\partial h\omega}$ eV	$\delta h\omega$ from zero of eV 2nd derivative	shift per unit charge in concent- ration	@ concentration % (av. of adj. val. used)
J-M	100	2.43	-142	47.6	2.43	55.8	-8.2	0.059	0.02	0.006	95
78	90.7	2.45	-129	52.6	2.45	68.2	-15.6	0.12	0.08	0.014	87
21	83.4	2.53	-128	59.0	2.53	67.1	-8.1	0.06	0.08	0.005	76
22	68.7	2.61	-105	61.5	2.58	72.4	-10.9	0.10	0.13	0.01	62
23	56.3	2.74	-101	56.5	2.75	68.6	-12.1	0.12	0.15	0.01	50
24	45.3	2.89	-94.6	57.1	2.88	70.3	-13.2	0.14	0.12	0.013	40
25	35.4	3.01	-103	56.2	3.02	67.6	-11.4	0.11	0.15	0.015	30
26	26.7	3.16	-105	52.0	3.18	62.5	-10.5	0.10	0.13	0.016	23
27	19.0	3.29	-116	53.1	3.26	64.0	-6.9	0.06	0.11	0.009	16
28	12.4	3.40	-138	47.8	3.40	72.0	-22.2	0.16	0.20	0.024	9
29R	5.8	3.60	-190	43.8	3.59	( 70.4 ( 82.3	-26.6	0.14	0.12	0.026	3.5 **
68	0.95	3.72	-337	47.3	3.70	( 49.6 ( 71.4	-2.3	0.0065	0.02	0.01	**0.5 ****
30R	0	3.74	-355	27.3	3.76						
JmAg	0	3.77	-502	44.7	3.77						

\* Compared with sample No.68

\*\* " " " JmAg

\*\*\* " " " 30R

\*\*\*\* " " " JmAg

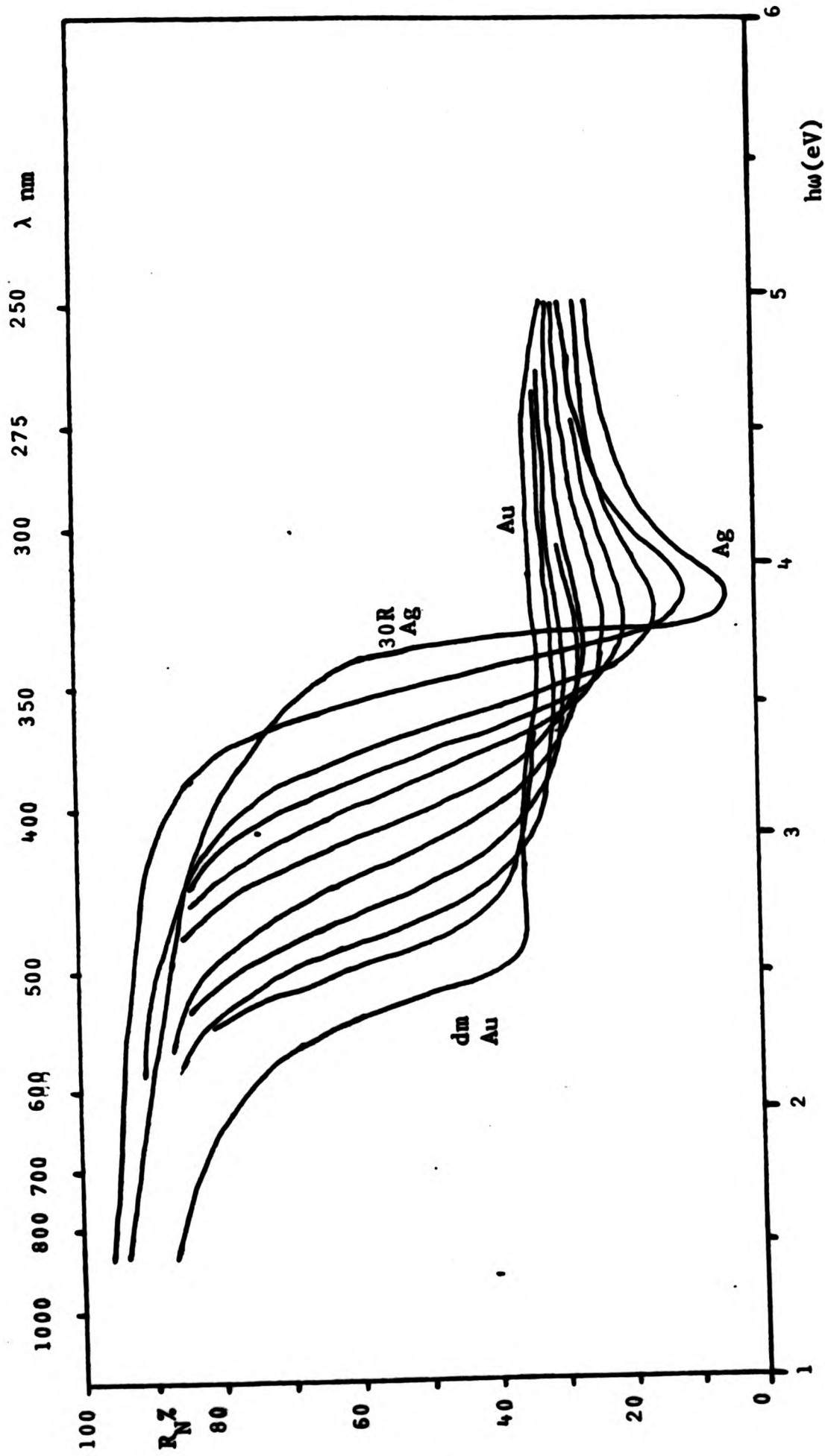


Figure 6.21. Normal Reflectance of Ag-Au alloys. The absorption edge moves monotonically to higher energies with increasing silver content, while the depth of the minimum monotonically increases. Curves shown are for samples (from left to right): J-M Au, 21, 22, 23, 24, 25, 26, 27, 28, 29R, 30R, 30R.

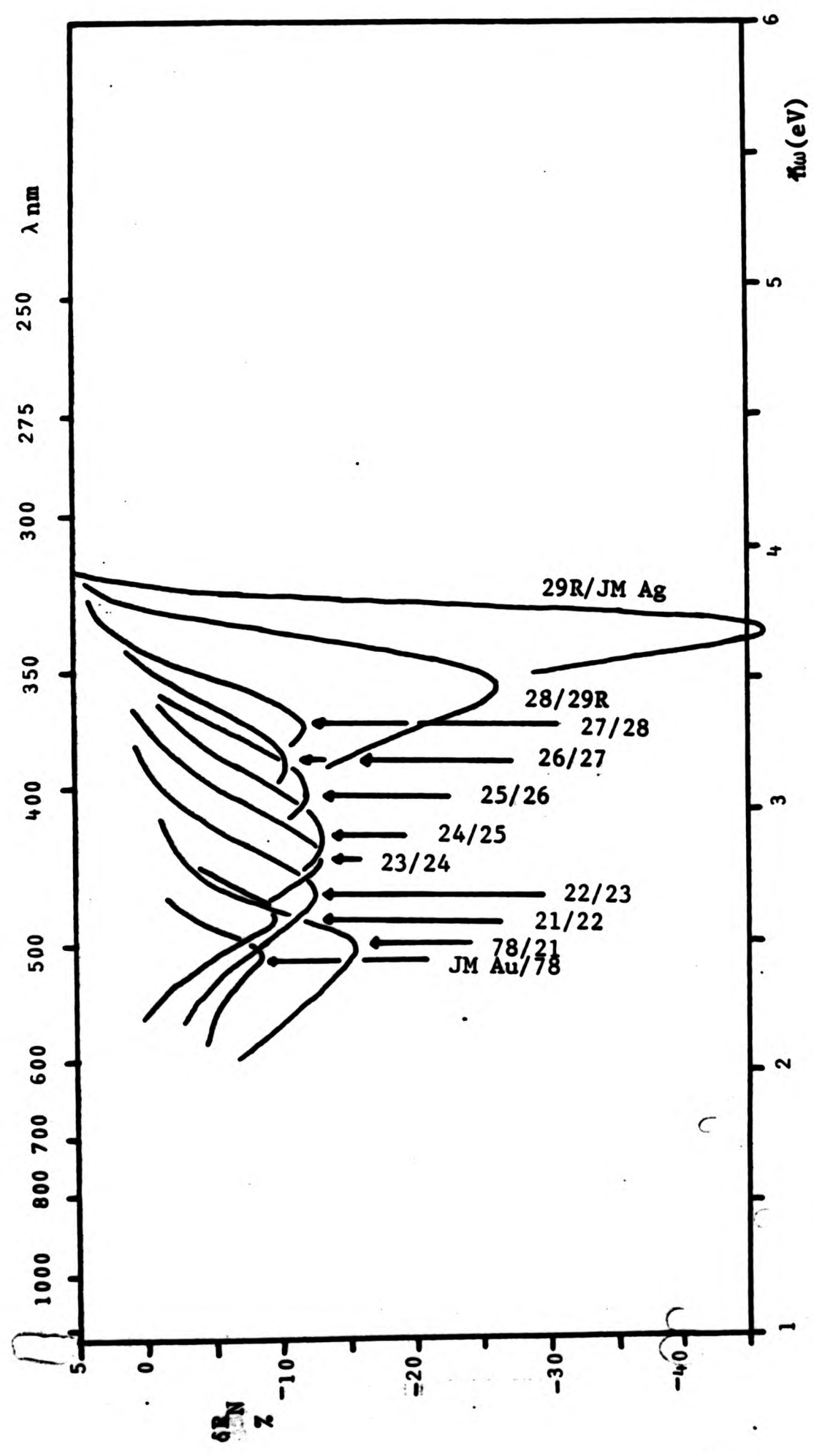


Figure 6.22. Change in normal reflectance on addition of Au; Ag-Au alloys.  
Notation: eg. 78/21 implies the reflectance of sample 21 subtracted from that of sample 78. For numerical values of the minima, see Table 6.2.

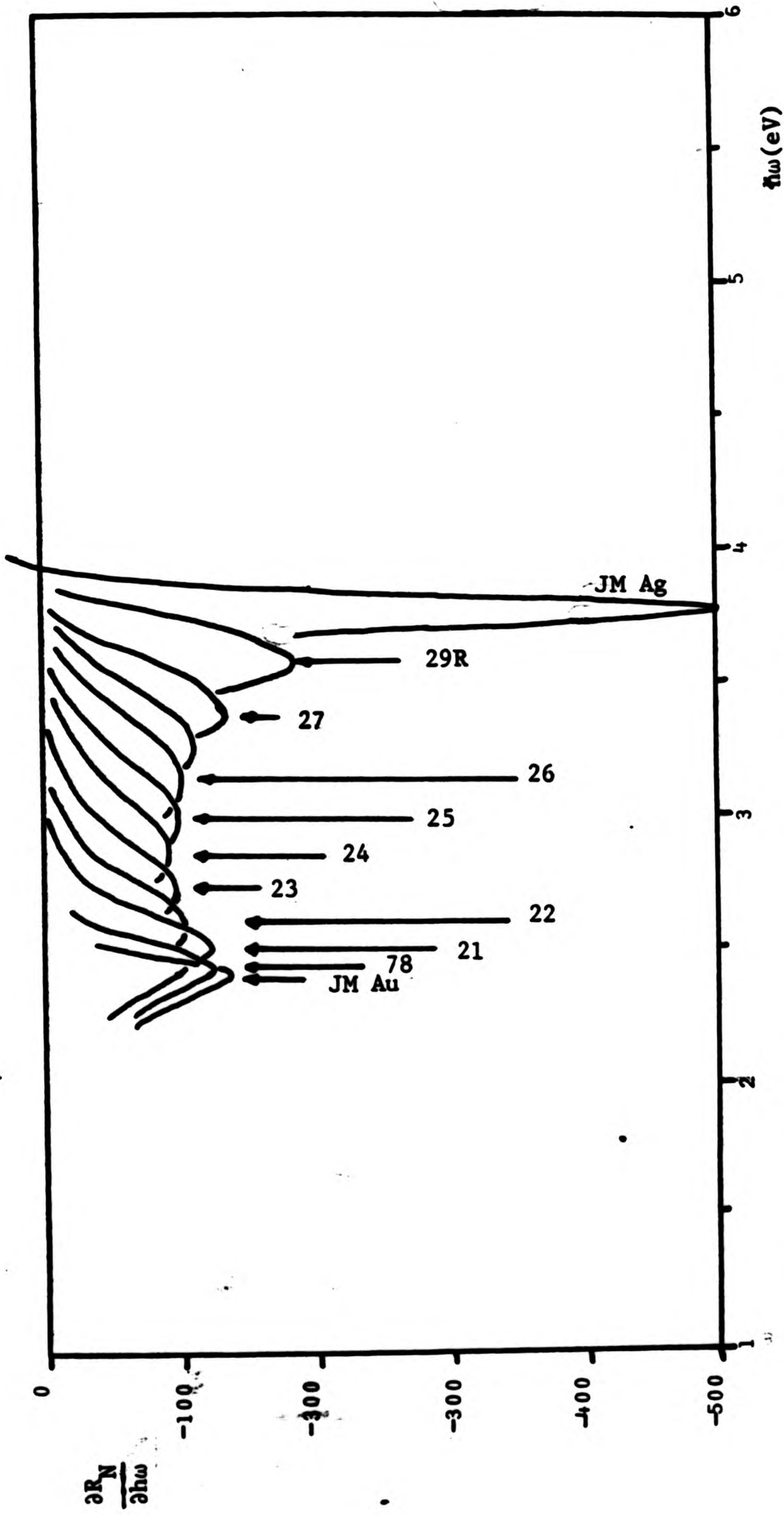


Figure 6.23. First derivative of normal reflectance (percent  $eV^{-1}$ ), Ag-Au alloys. Samples 23 and 24 (56.3 and 45.3 at.7 Au) have the smallest minimum gradient (-101 and -94.6).

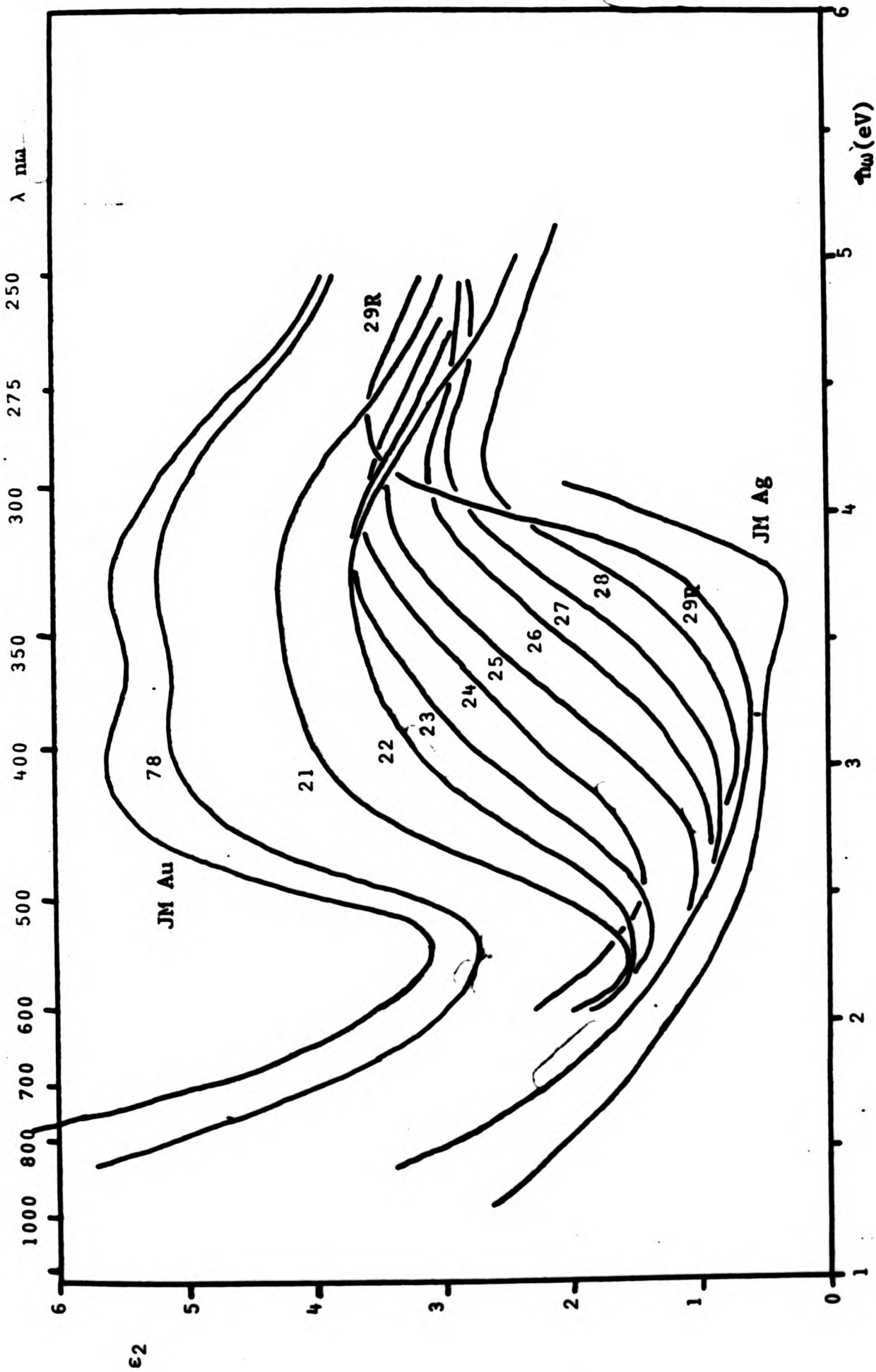


Figure 6.24. Imaginary part of the dielectric function, Ag-Au alloys.

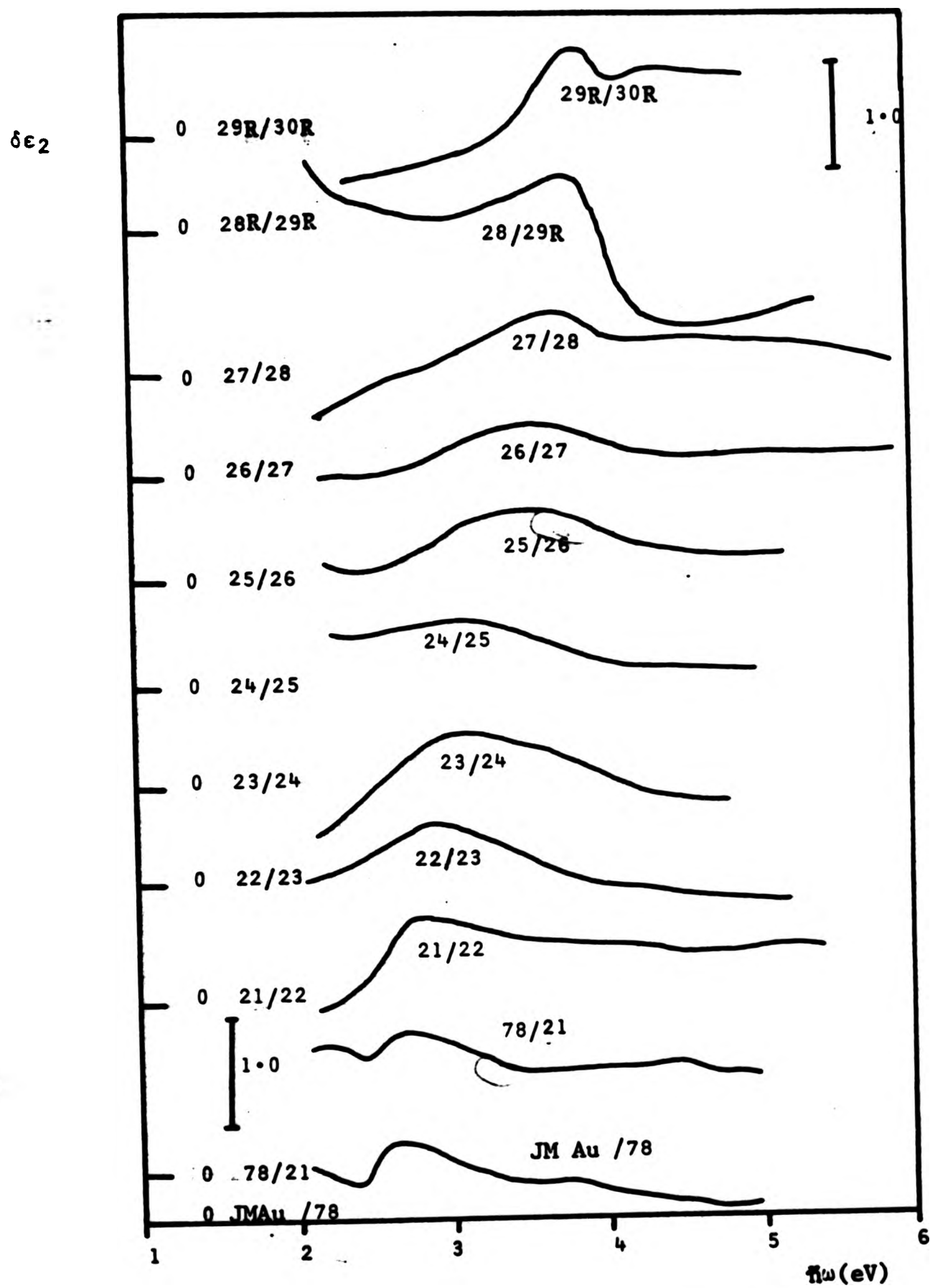


Figure 6.25. Changes in  $\epsilon_2$ , Ag-Au alloys, on addition of Au. Notation as in Figure 6.22.

The vertical bars show the scale, while each graph has its own origin.

the gradient at the edge shows a well-defined minimum at about 50 at.% Au (Table 6.3, Figure 6.26).

The curve shown for pure Ag covers 1.4 + 4.1eV, which does not include the maximum in  $\epsilon_2(\omega)$  at  $\sim 4.5\text{eV}$ . Later experiments, up to 5eV, gave a calculated normal reflectance of 89% compared with 95% (at 2eV), and so were not preferred to this result.

#### The Interband Dielectric Function

Figure 6.27 shows  $\epsilon_2^b(\omega)$ , separated as described in Section 6.1. 'Free electron' absorption in each case was considered to start  $\sim 0.3\text{eV}$  below the maximum in  $\frac{\partial \epsilon_2}{\partial \omega}$  for that alloy. Due to lack of data, these curves can be presented only for fine gold and 90.7 at.% Au at the gold-rich end; 12.4 at.% Au, 5.8 at.% Au and fine silver at the silver-rich end. This includes only one - No.28, 12.4 at.% Au - of the set Nos. 21 to 28. Apart from this sample, quite systematic behaviour was again found.

#### Surface Plasmon Absorption

The surface plasmon energy loss functions are given in Figure 6.30. It is clear that even at low Au concentrations ( $\sim 20$  at.%) surface plasmon effects, even for rough samples, may be safely neglected.

Table 6.3 Edges of  $\epsilon_2(\omega)$ , Ag-Au alloys

Sample No.	Atomic % Au	zeroes $D^2\epsilon_2(\omega)$ eV	$D^1\epsilon_2(\omega)$ max per eV	$\epsilon_2$ (same value of $h\omega$ )	$e$ $h\omega$	$\epsilon_2$ of adjacent alloy at same $h\omega$	$\delta\epsilon_2$	$\delta h\omega = \delta\epsilon_2 = \frac{d\epsilon_2}{dh\omega}$	$\delta h\omega$ from zeroes of $D^2$
J-M	100	2.54	8.48	3.98	2.53	3.33	0.65	0.077	0.02
78	90.7	2.56	6.30	3.50	2.56	2.27*	1.23	0.20	0.06
21	83.4	2.62	4.84	2.66	2.64	1.99	0.67	0.14	0.13
22	68.7	2.75	3.22	2.36	2.75	1.87	0.49	0.15	0.12
23	56.3	2.87	2.73	2.21	2.88	1.75	0.46	0.17	0.18
24	45.3	3.05	2.18	2.05	3.02	1.49	0.56	0.26	0.13
25	35.4	3.18	2.29	1.84	3.18	1.31	0.53	0.23	0.46
26	26.7	3.64	2.32	2.27	3.65	1.83	0.44	0.19	0.11
27	19.0	3.75	2.57	2.11	3.76	1.57	0.54	0.21	0.11
28	12.4	3.86	3.21	1.94	3.87	1.52	0.42	0.13	0.15
29R	5.8	4.01	7.11	2.27	4.00	1.81	0.46	0.065	0.00
68	0.95	4.01	9.06	1.81	4.00	(1.64 1.2)	(0.15 0.6)	(0.017 0.068)	(-0.001 0.08)***
30R	0	4.00	8.82	1.64	4.00				
J-M	0	4.09	7.90	1.62	4.06				

\* interpolated

\*\* cf 30R

\*\*\* cf J-M Ag

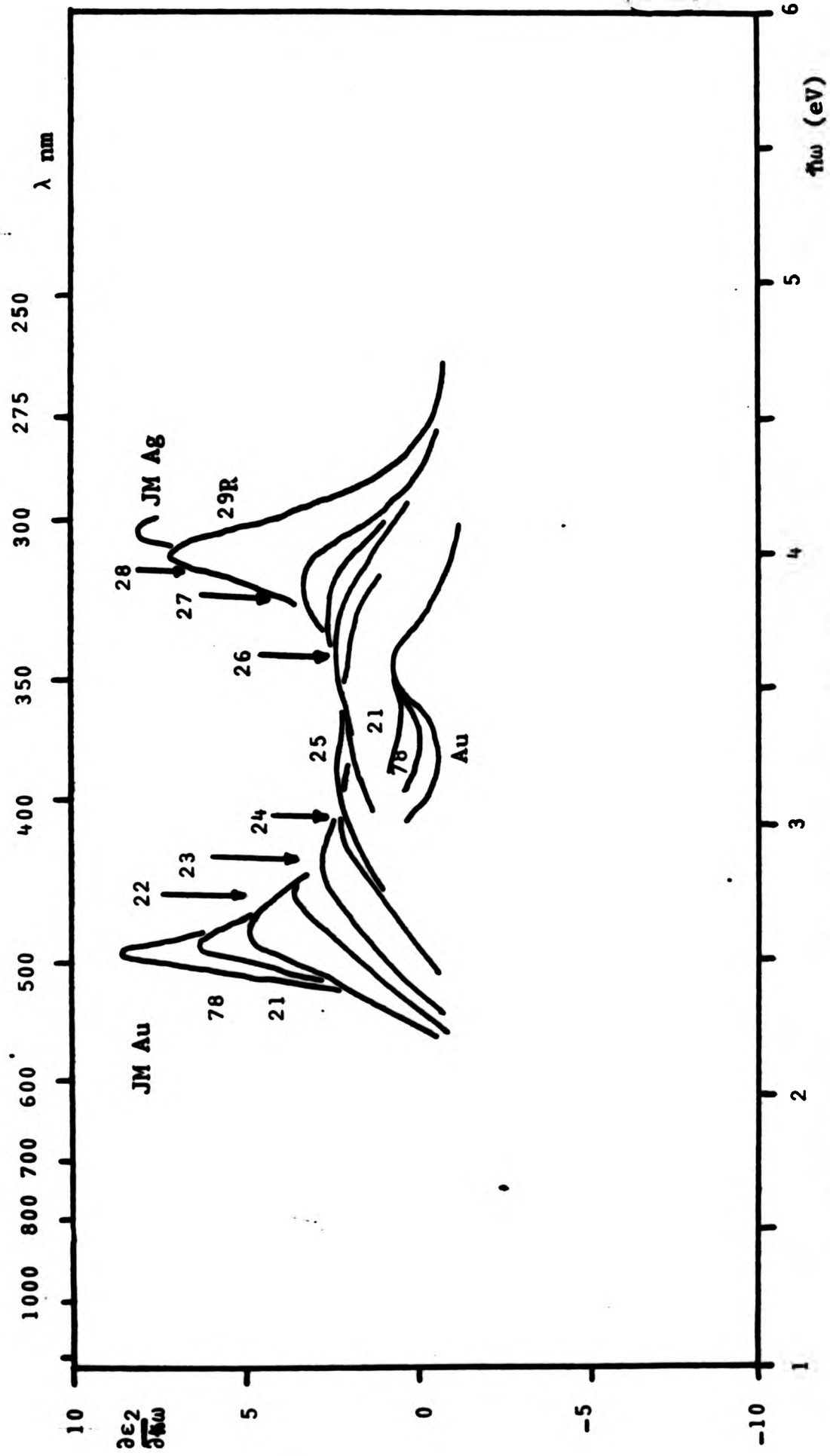


Figure 6.26. First derivative of  $\epsilon_2(\omega)$  ( $\text{eV}^{-1}$ ), Ag-Au alloys. The low energy maximum ( $d \rightarrow$  FS) is shown for each sample. For the gold-rich alloys, a second maximum at 3.7eV is also given. This is not discernible for alloys less than  $\sim 83$  at.% Au.

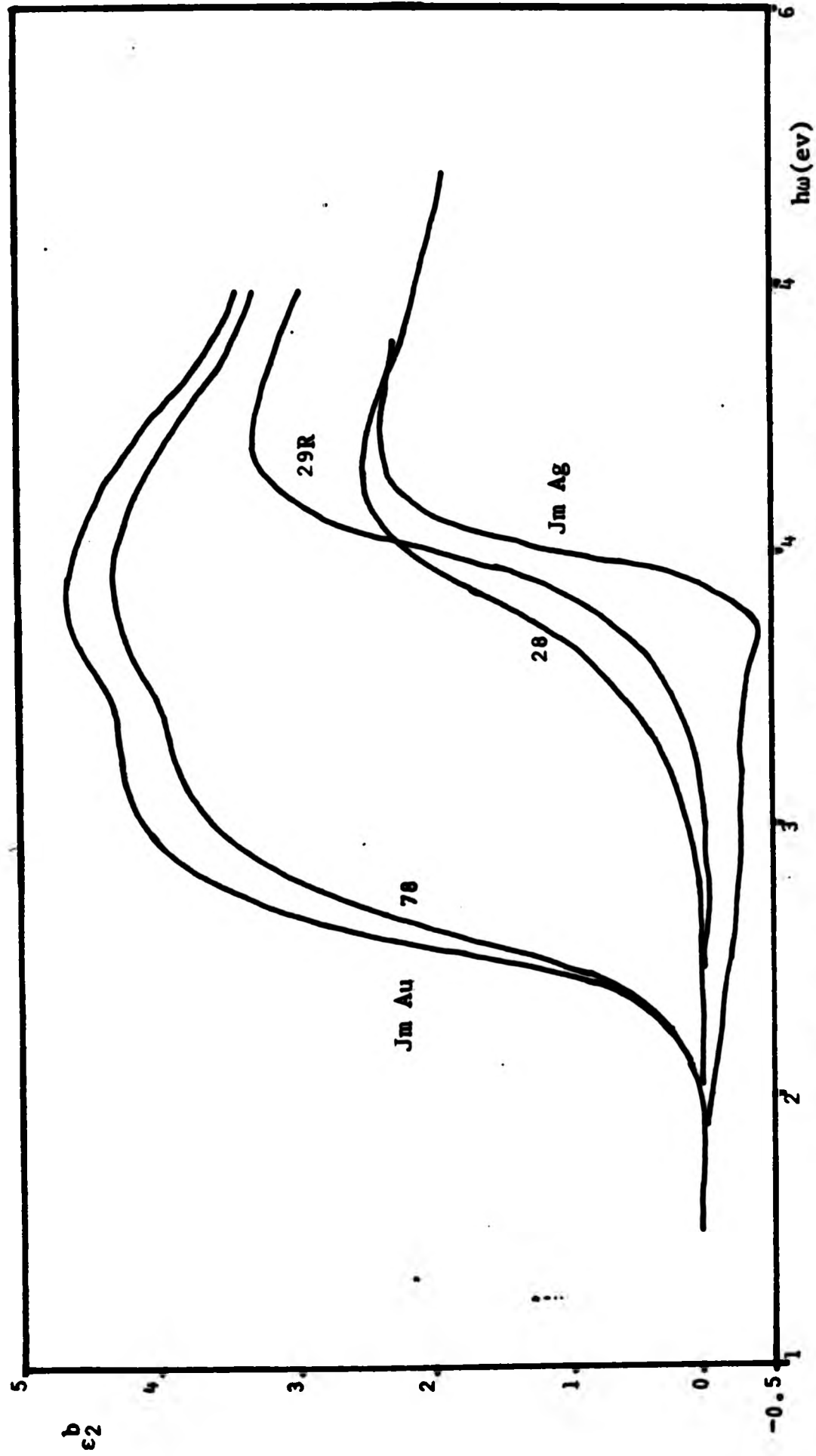
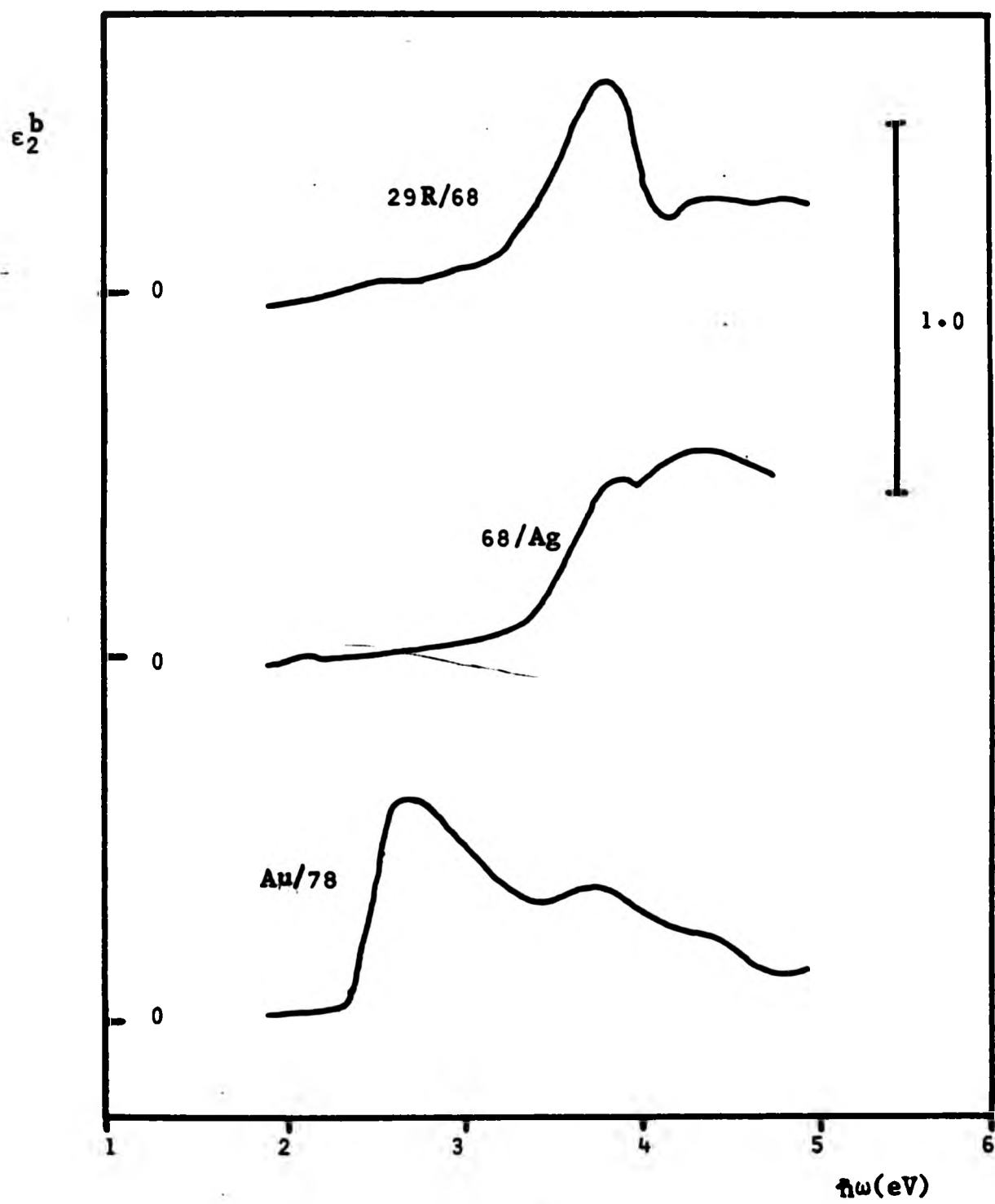


Figure 6.27. Interband contribution to the dielectric function,  $\epsilon_2^b$ , versus photon energy,  $\hbar\omega$  (eV), for Ag-Au alloys. The conduction electron contribution has been fitted in the range 650 - 850 nm. for each alloy.

Table 6.4. Edges of  $\epsilon_2^b(\omega)$ , Ag-Au

Alloy Melt No.	Atomic % Au	zeros of $D^2\epsilon_2^b(\omega)$ eV	$(D^1\epsilon_2^b(\omega))_{\max}$ per eV	$\epsilon_2^b$ (same $\hbar\omega$ )	$\hbar\omega$ eV	$\epsilon_2^b$ next alloy, same $\omega$	$\delta\epsilon_2^b$	$\delta\hbar\omega = \delta\epsilon_2^b = \frac{d\epsilon_2^b}{d\hbar\omega}$	$\delta\hbar\omega$ from zeros of $D^2\epsilon_2^b(\omega)$	$\delta\hbar\omega/\text{unit conc}$
J-M	100	2.54	10.4	1.76	2.53	1.32	0.44	0.04	0.02	0.004
78	90.7	2.56	7.78	1.52	2.56	not available				
29R	5.8	4.01	7.30	1.95	4.00					
	(cf 68					1.55	0.40	0.05	0	0.01
	(cf 30R					1.09	0.84	0.10	-0.01	0.02
	(cf JM					1.00	0.95	0.11	0.08	0.02
68	0.95	4.01	9.21	1.55	4.00					
	(cf 30R					1.09	0.44	0.05	-0.01	0.05
	(cf JM					1.00	0.55	0.06	0.08	0.06
30R	0	4.00	9.10	1.09	4.00					
J-M	0	4.09	7.99	1.17	4.06					



**Figure 6.28.** Change in  $\epsilon_2^b$  on addition of Au; Ag-Au alloys. The scale is shown by the bar (top right). Each graph has its own origin.

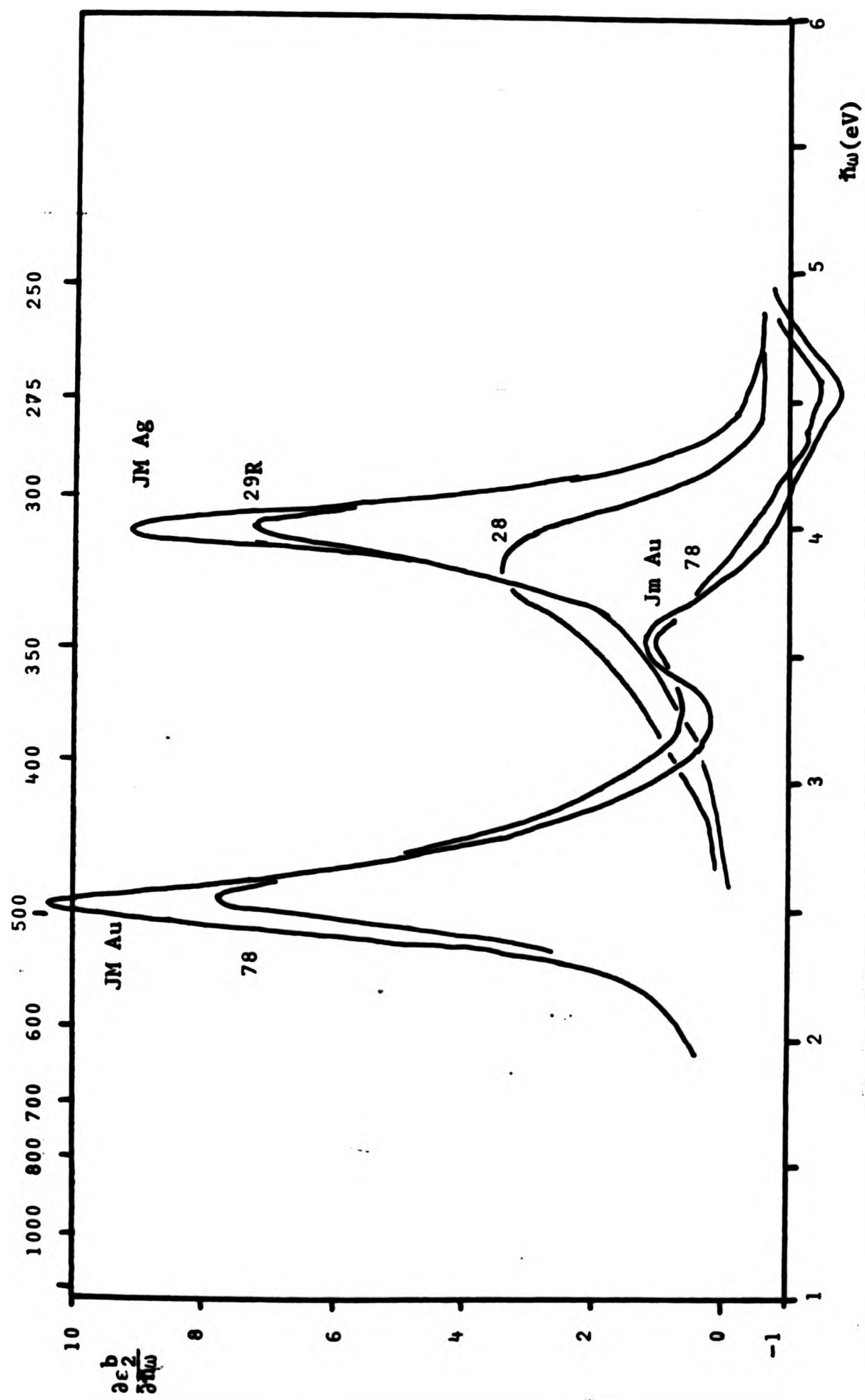


Figure 6.29. First derivative of  $\epsilon_2^b(\omega)$  ( $\text{eV}^{-1}$ ), Ag-Au alloys.

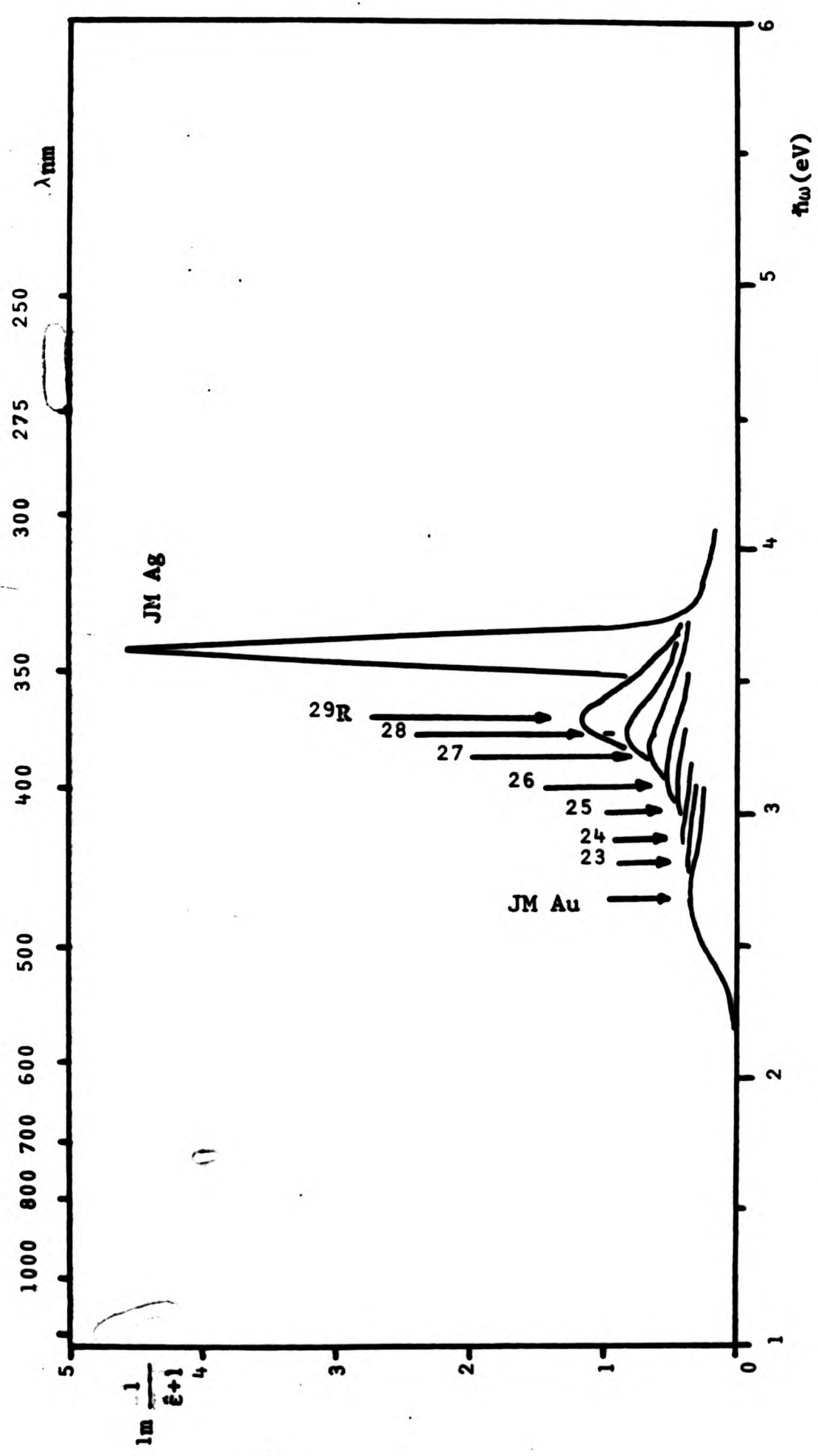


Figure 6.30. Surface plasmon energy loss function, Ag-Au alloys. Sample 30R (not shown) had a peak value of 2.1, despite having a composition of 99.97 wt % Ag. See Figure 6.31.

### Alloying effects

Figures 6.31 - 35 show various derived scalar quantities as functions of alloy concentration. The conduction electron properties  $\tau$  (Drude-like relaxation time) and  $\hbar\omega_p$  (Drude-like plasma frequency) show no discernible concentration effects. As outlined in Section 4, the low frequency value of  $\epsilon_1^b$ , the interband contribution to the real part of the low frequency dielectric function, is also available from the behaviour of  $\hat{\epsilon}(\omega)$ , provided that again Drude-like behaviour of  $\hat{\epsilon}^f(\omega)$  can be assumed. Apart from this, it is likely that  $\epsilon_1^b$  is not constant at  $\sim 1.5\text{eV}$  for alloys where  $\left|\frac{\partial\epsilon_2^b}{\partial\omega}\right|_{\text{max}}$  occurs at  $\sim 2\text{eV}$ . For the few samples where results were available (Figure 6.34) no systematic behaviour was observed.

The 'position of the absorption edge' ( $E_{\text{gap}}$ ), which is equal to the size of a band-gap in the electronic structure of the material, has been defined as the value of  $\hbar\omega$  where  $\frac{\partial\epsilon_2^b}{\partial\omega}$  is a maximum. These values are given in Table 6.1 and Figure 6.35. When  $\epsilon_2^b(\omega)$  could not be evaluated - which was the case for most of the Ag-Au alloys - values of  $\hbar\omega$  deduced from  $\epsilon_2^f(\omega)$  have been given instead. These might be expected to be affected by  $\epsilon_2^f$ , but in practice whenever both functions were available they gave the same result to  $\sim 0.01\text{ eV}$ .

### 6.3 Au-Cu binary alloys

The results for these alloys are presented in the same format as those for the Ag-Au alloys above, as a similar metallurgical system has been studied, namely, the system of disordered solid-solutions.

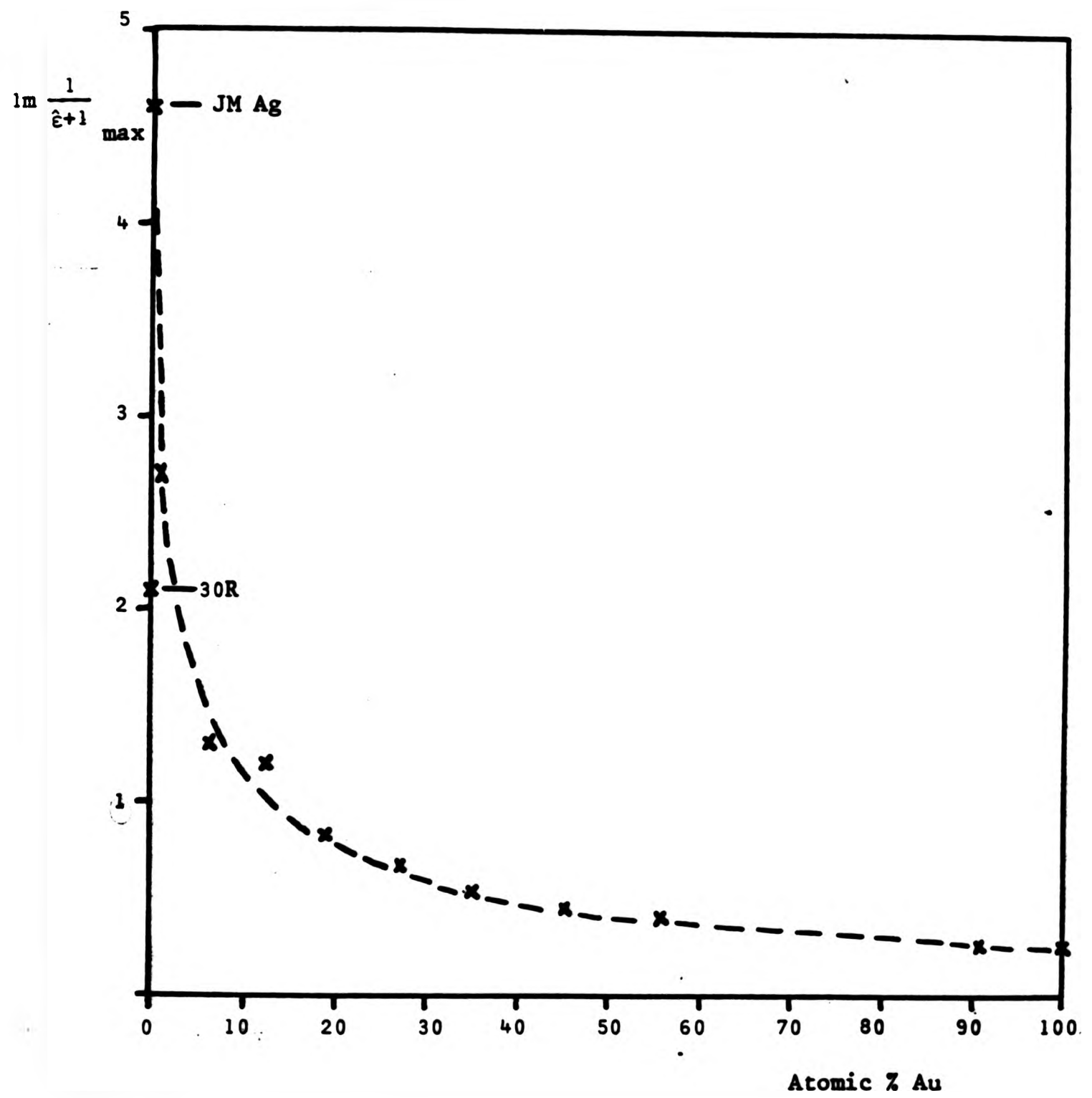


Figure 6.31. Maximum values of the surface plasmon energy loss function as a function of composition.

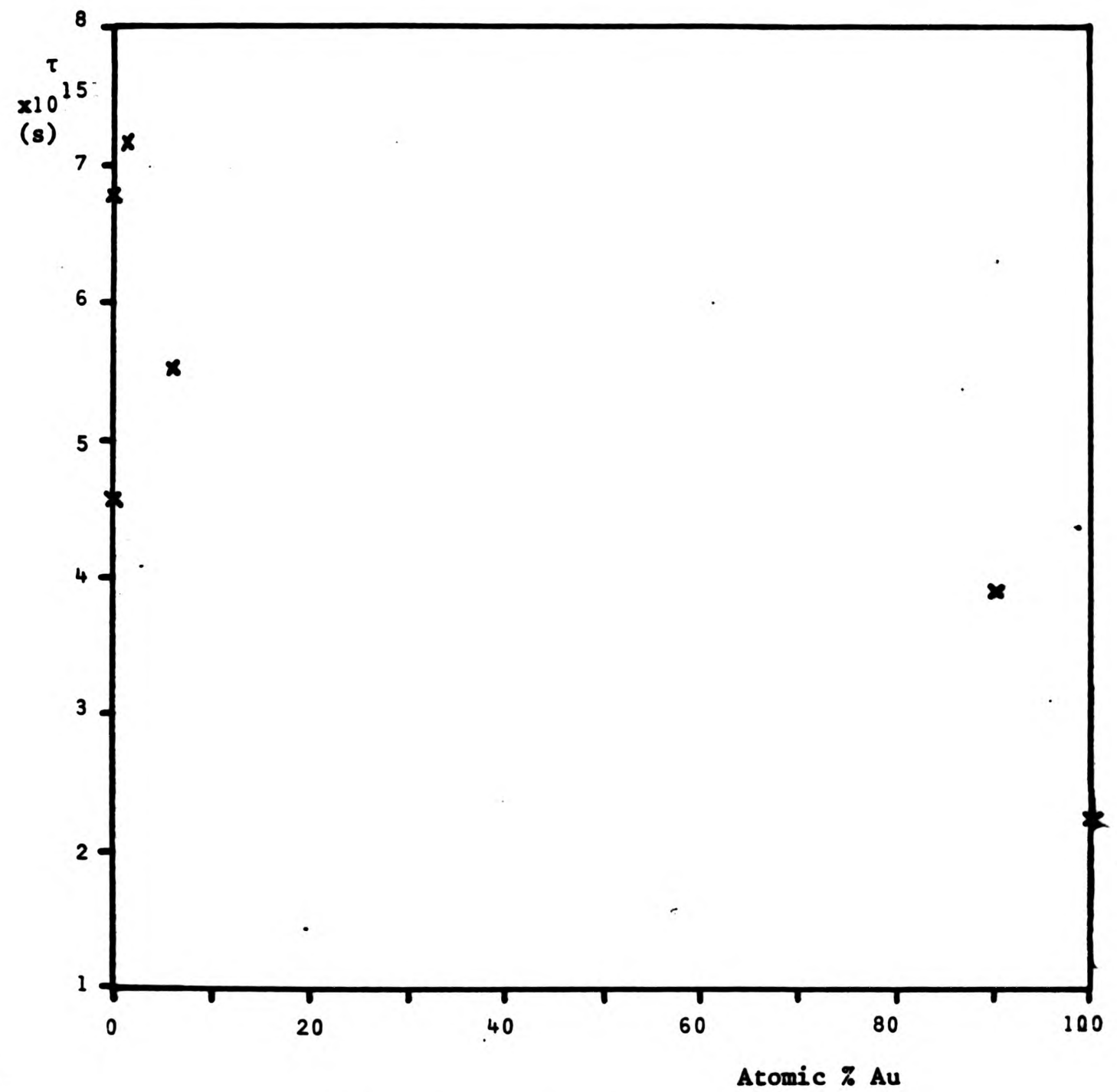


Figure 6.32. Conduction electron relaxation time, Ag-Au alloys. Calculated according to the theory of Drude.

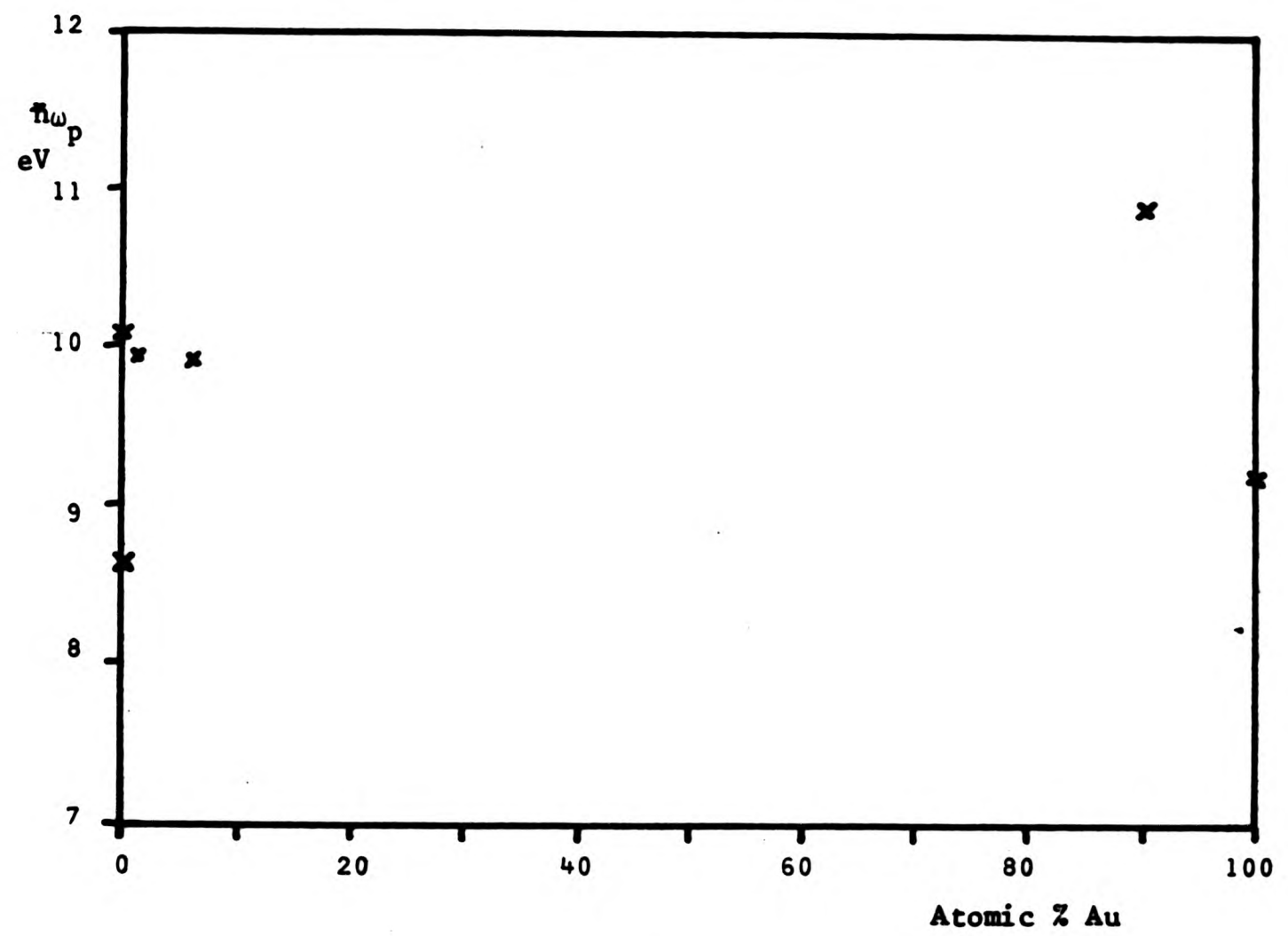


Figure 6.33. Conduction electron plasma frequency, Ag-Au alloys.

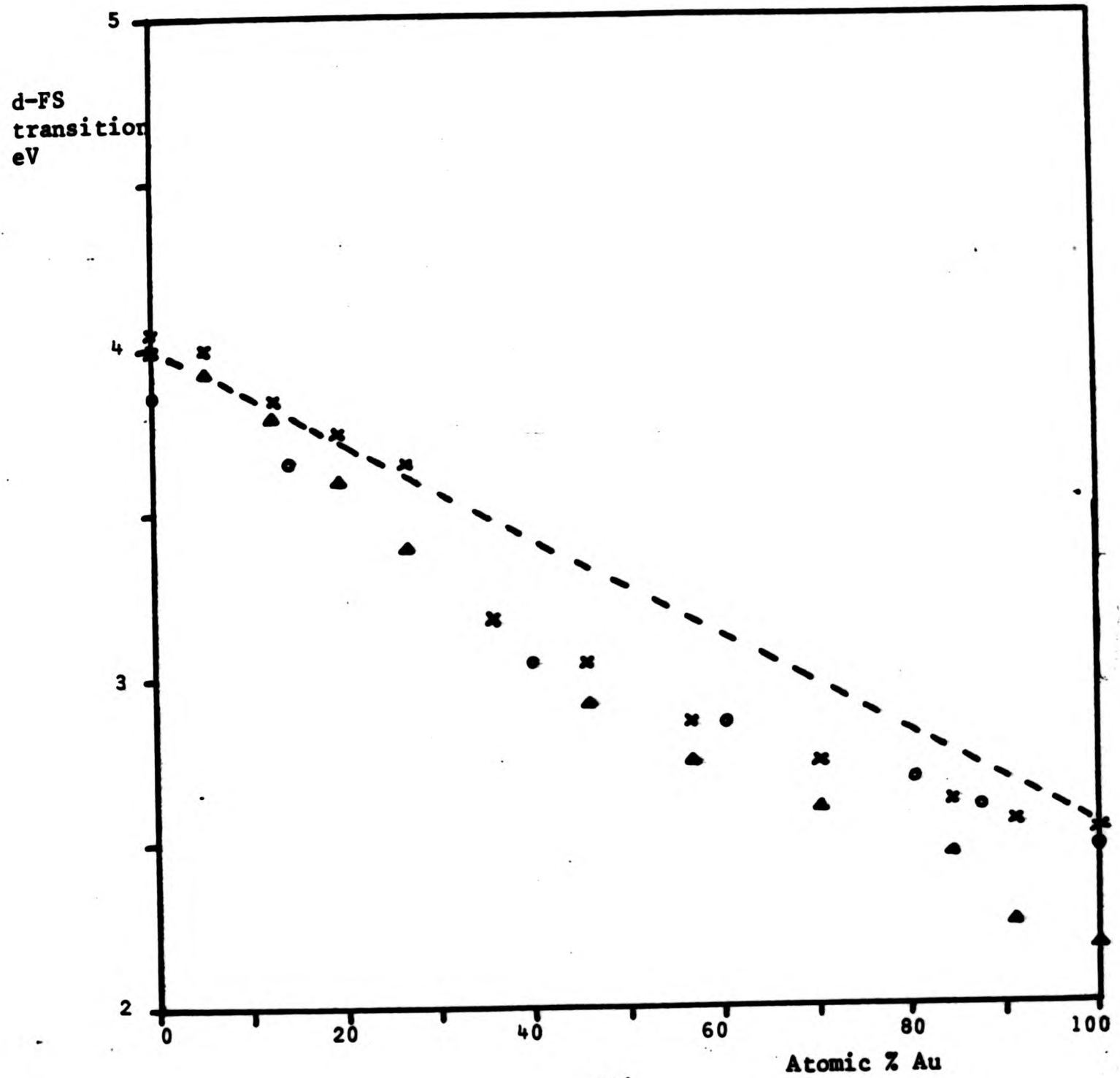


Figure 6.34. Position of the low energy absorption edge, Ag-Au alloys. See Tables 6.2, 6.3.

x - from zeroes of  $\frac{\partial^2 \epsilon_2}{\partial \hbar \omega^2}$

△ - from  $\delta \hbar \omega = \delta \epsilon_2 \div \frac{\partial \epsilon_2}{\partial \hbar \omega}$  starting from a value of 4.00eV for sample 30R (Ag)

● - from J Rivory (1977).

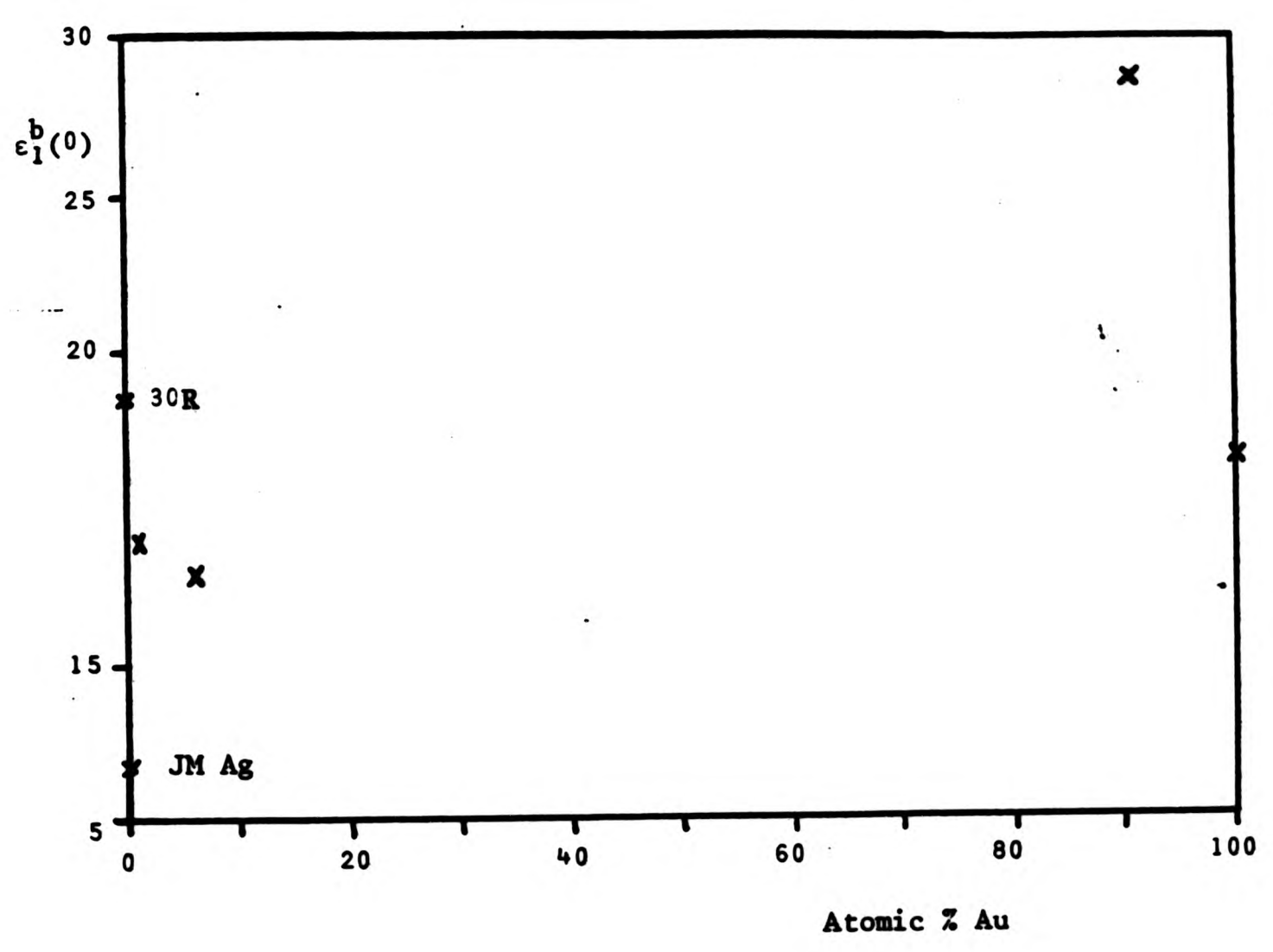


Figure 6.35. The low energy value of the interband part of  $\epsilon_1(\omega)$ , Ag-Au alloys. See text and Table 6.1.

Table 6.5 Some properties of Au-Cu alloys as a function of composition

Reference No.	Atomic % Au	Weight % Au	CIE Colour Co-ordinates $\times 10^4$ Normal Reflectance			$\lambda_d$ nm	1931 Standard System Equal Energy Illumination			Relaxation time $10^{-15}$ s	h $\nu_p$ (plasma freq) eV	d + $\epsilon_2$ absorp. eV	$\epsilon_1$ (o) eV
			1931 Standard System Equal Energy Illumination				L %	s %	z %				
			x	y	u								
Jm Au	100	99.99	4011	3877	2233	3342	580.8	39.53	65.01	2.22	9.20	2.54	16.5
77	86.4	95.2	4005	3806	2256	3318	582.5	34.43	68.58	7.36	13.1	2.44	48.4
10R	73.2	89.5	3869	3617	2243	3237	586.0	24.66	70.07	3.60	10.2	2.29	18.2
10	66.5	86.1	3874	3686	2221	3261	583.5	26.81	73.02	4.41	10.4	2.31	20.7
9R	56.7	80.3	3847	3500	2236	3229	586.2	23.49	68.58	3.46	9.27	2.26	14.3
9	56.4	80.1	3804	3571	2219	3213	586.5	21.32	70.78	2.91	9.05	2.26	11.6
8	42.8	70.0	3760	3514	2213	3188	588.6	18.27	69.70	3.11	9.77	2.19	16.0
7	35.4	63.1	3753	3506	2212	3184	589.0	17.83	70.59	3.41	9.73	2.19	15.3
6	23.2	48.5	3759	3495	2220	3180	589.9	17.68	68.73	2.85	9.38	2.19	13.5
5	14.7	34.9	3772	3493	2229	3181	590.4	17.98	70.87	5.05	10.5	2.19	21.8
4	12.7	31.2	3787	3500	2236	3185	590.2	18.69	70.10	5.45	10.7	2.20	24.9
3	6.7	18.2	3793	3503	2239	3187	590.2	18.94	69.99	4.51	10.2	2.17	20.4
2	3.4	9.9	3814	3510	2250	3192	590.2	19.77	71.26	4.98	9.89	2.19	17.9
Cu	-	-	3839	3521	2261	3199	590.1	20.86	72.05	9.5	10.5	2.18	25.3

### Colorimetry

Figure 6.36 shows the locus obtained using the C.I.E 1960 Uniform Colour System to plot the chromaticity co-ordinates of Au, Cu and several Au-Cu alloys. The results given in this section are for alloys 2, 3, 4, 5, 6, 7, 8, 9R, 10R and 77 of Table 3.1; in addition certain figures show results for samples 9 and 10. It will be seen that for these alloys curvature of the colour locus is even more pronounced than for the Ag-Au system. These and other colorimetric values are given also in Table 6.5, while saturation (S), dominant wavelength ( $\lambda_d$ ) and luminance (L) are plotted on Figure 6.37. A distinct trend is noticeable in S and  $\lambda_d$  - as is implicit in the smoothness of the (u, v) locus - but L, which is not represented in the chromaticity diagram, shows a degree of unsystematic variation.

### Spectral Reflectance

Normal reflectance of these alloys is shown in Figure 6.38. There is but a small change in structure with composition, in order to avoid obscuring the graph it has been necessary to plot the values of each alloy with a separate origin and therefore with a much reduced scale. To convey better the small shifts in edge position, a graph showing  $R(\lambda)$  in the visible region (Figure 6.38b) has been provided in addition to that showing  $R(\omega)$ , Figure 6.38a.

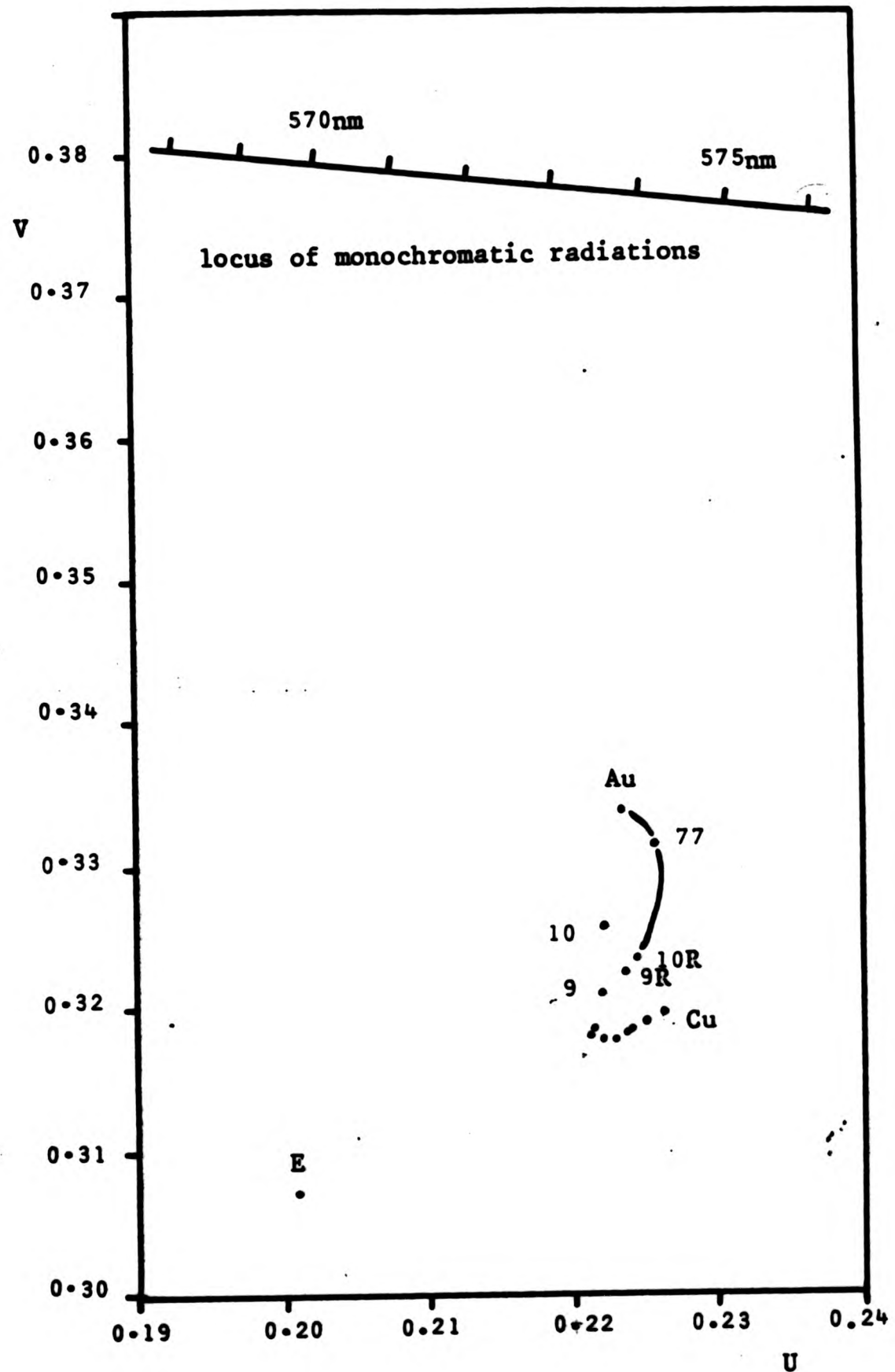


Figure 6.36. CIE Chromaticity Co-ordinates, 1960 Uniform Colour System, Standard Illuminant C. The point E marks the neutral stimulus, while the curve is the locus for the Au-Cu alloys. The points on this locus are for the alloys in the order Au, 77, 10R etc., as in Figure 6.38 below.

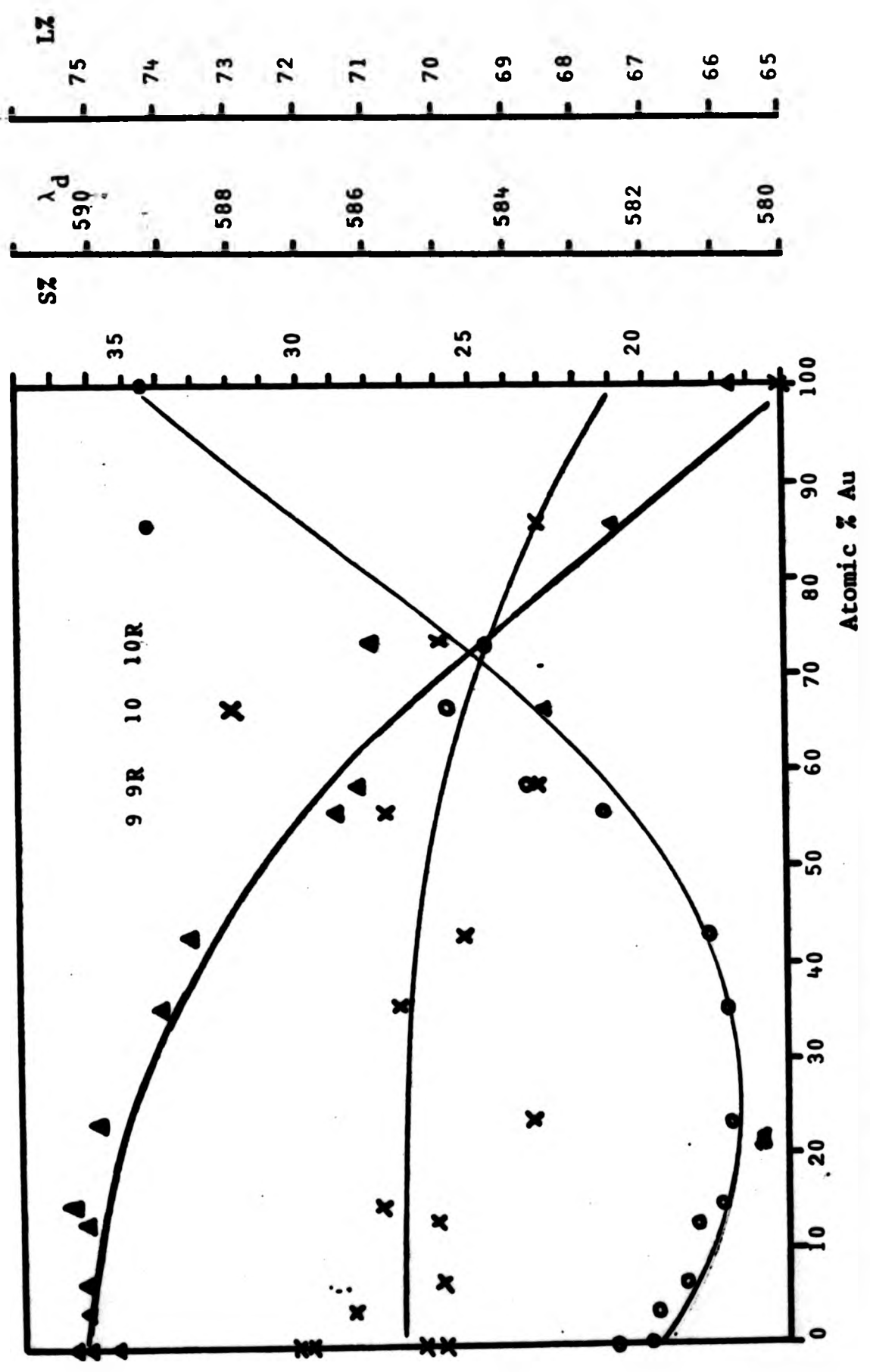
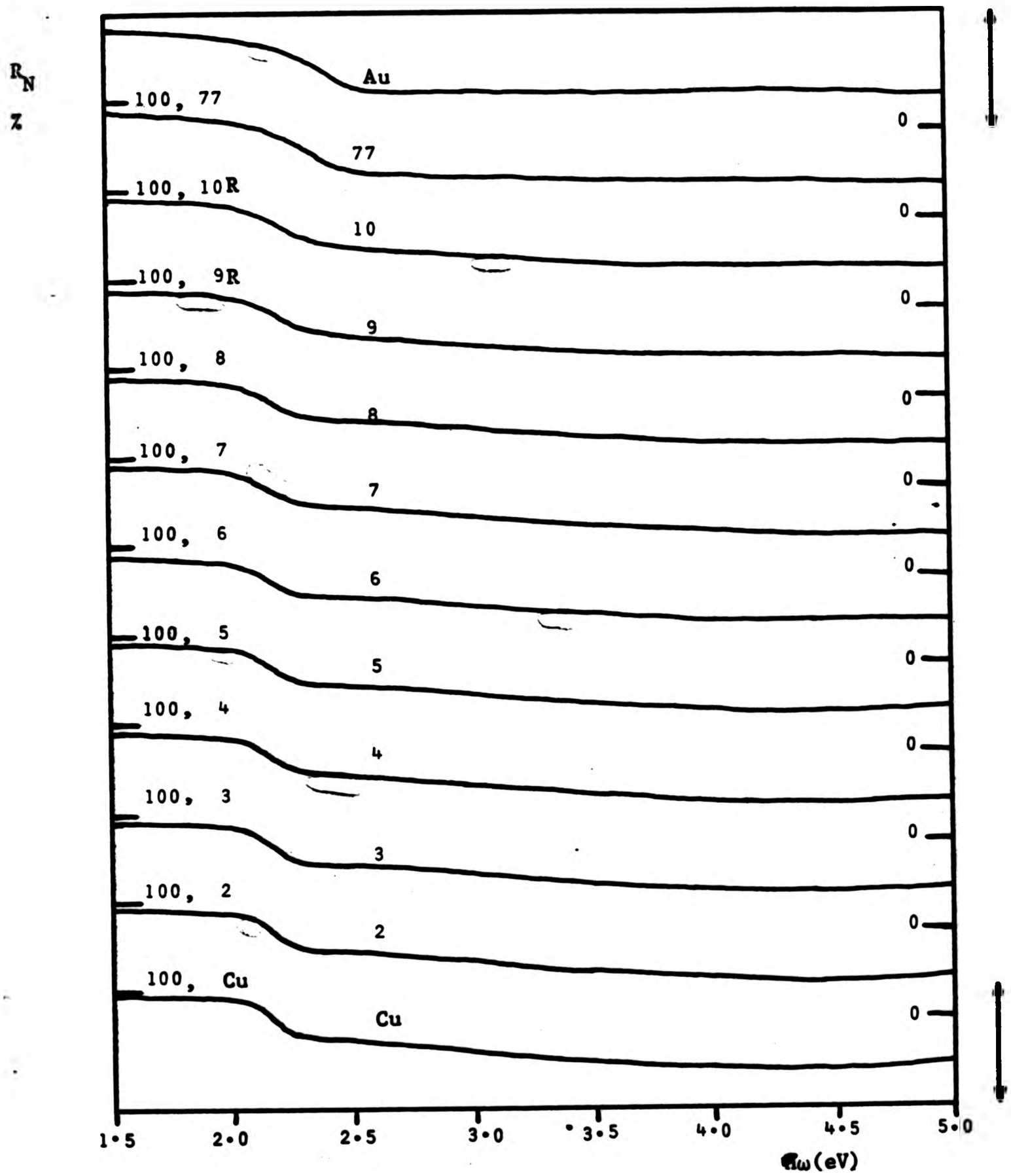


Figure 6.37. Au-Cu alloys. Saturation (S; e-e-e), Dominant wavelength ( $\lambda_d$ ;  $\Delta$ - $\Delta$ - $\Delta$ ) and Luminance (L; x-x-x). CIE 1931 Standard System, Equal-energy distribution illumination.

Table 6.6 Edges of  $R_N(\omega)$ , Au-Cu alloys

Melt Number	Atomic % Au	Width of edges	Zero of $D^2R_N(\omega)$ eV	$D^1R_N(\omega)$ min % eV <sup>-1</sup>	$R_N$ at same $\hbar\omega$ %	at $\hbar\omega$ eV	$R_N$ of adj. alloy	$\delta R_N$	$\delta \hbar\omega = \delta R_N = \frac{\partial R_N}{\partial \hbar\omega}$	$\delta \hbar\omega$ from zeroes of $D^2$
JM Au	100	0.16	2.43	-142	47.64	2.43	48.16	-0.42	+0.003	-0.09
77	86.4	0.22	2.34	-133	58.75	2.34	57.8 (10R)	+1	-0.007	-0.11
10R	73.2	0.20	2.23	-110	67.11	2.25	65.6 (9R)	+1.5	-0.014	+0.01
10	66.5	0.19	2.27	-110	71.21	2.25	66.8 (10R)	+4.41	-0.040	-0.08
9R	56.7	0.12	2.24	-112	65.64	2.25	64.59	+1.05	-0.01	-0.06
9	56.4	0.19	2.19	-105	72.83	2.19	69.95	+2.88	-0.027	-0.01
8	42.8	0.17	2.18	-112	72.15	2.18	72.73	-0.58	+0.005	0
7	35.4	0.17	2.18	-114	72.73	2.18	70.41	+2.32	-0.020	-0.01
6	23.2	0.11	2.17	-122	70.41	2.18	72.56	-2.15	+0.018	0
5	14.7	0.19	2.17	-145	72.56	2.18	71.89	+0.67	-0.005	0
4	12.7	0.13	2.17	-147	71.89	2.18	72.14	-0.25	+0.002	0
3	6.7	0.11	2.17	-156	72.14	2.18				
2	3.4	0.11	2.17	-178	73.18	2.18	73.5	-0.32	+0.002	-0.01
Cu	0	0.12	2.16	-193	73.80	2.18				



**Figure 6.38a.** Normal reflectance of Au-Cu alloys. The numbers given here are the sample melt reference numbers. Au is a sample of fine gold from Johnson-Matthey, Cu is a piece of cathode copper (4N pure). The vertical arrows (right) indicate 0 - 100%.

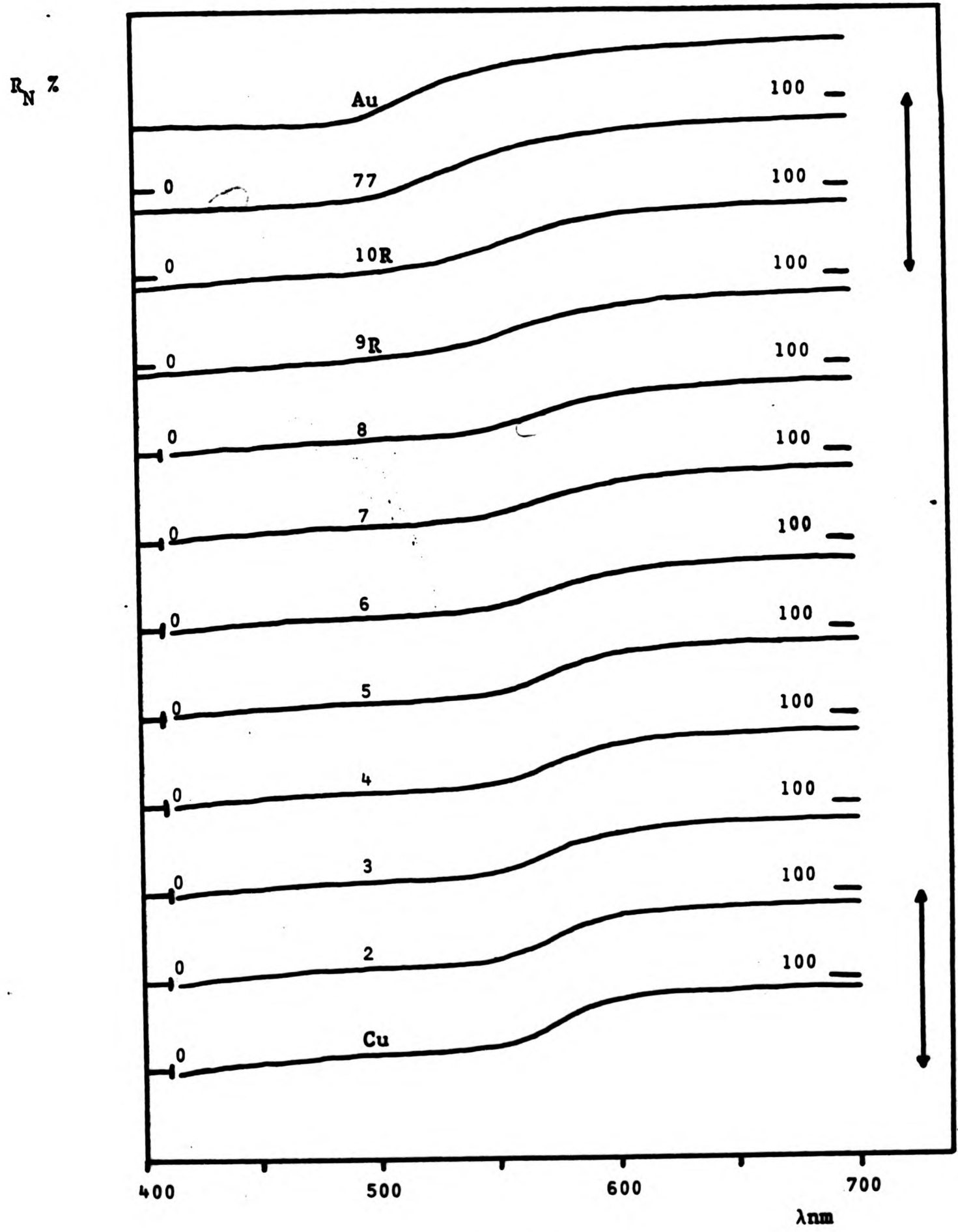


Figure 6.38b. Normal reflectance of Au-Cu alloys. As for Figure 6.38a, but with a wavelength axis over the visible region.

Again, difference curves ( $\delta R_N$ ) are given to emphasise the trend with composition (Figure 6.39). These enable the colour differences to be interpreted at the level of specific spectral features.

The first derivative spectra with respect to energy,  $\frac{1}{\hbar} \frac{\partial R}{\partial \omega}$ , are shown in Figure 6.40. Numerical data is presented in Table 6.6.

#### The Inter-band Dielectric Function, $\epsilon_2^b$

Graphs of  $\epsilon_2^b(\omega)$  only are given, Figure 6.41, since the conduction electron effects can be conveniently summarised in terms of a few non-spectral quantities, and sufficient data was available for the separation to be carried out on all the alloys.

Difference curves ( $\delta \epsilon_2^b(\omega)$ ) are given in Figure 6.42 and numerical derivatives  $\frac{1}{\hbar} \frac{\partial \epsilon_2^b}{\partial \omega}$  in Figure 6.43. These figures show a tendency to increasing width in the peaks at  $\sim 2.5\text{eV}$ , with increasing gold content. This is shown more clearly in Table 6.8, where a column is devoted to the difference (in eV) between the energy of the point of maximum slope on the low-energy side of the peak in  $\frac{\partial \epsilon_2^b}{\partial \omega}$ , and the energy of the gradient minimum on the high energy side. This has been obtained by numerically computing second derivatives and considering their minima and maxima.

#### Alloying Effects

The same quantities - namely  $\tau$ ,  $\hbar\omega_p$ ,  $E_{\text{gap}}$  and  $\epsilon_1^b(0)$  - as were derived for certain Ag-Au alloys are given here for all the Au-Cu alloys measured. Systematic variation is

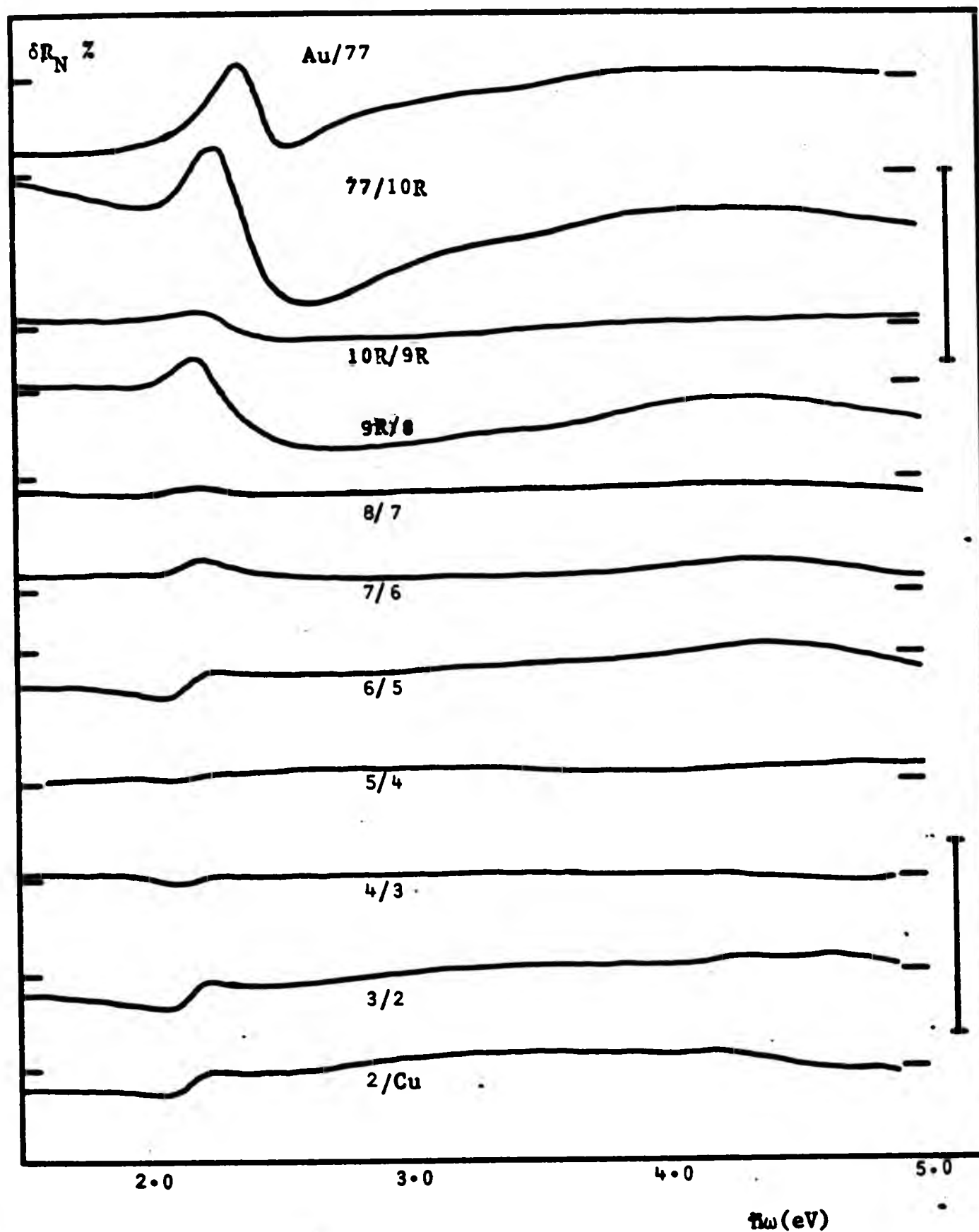


Figure 6.39a.  $\delta R_N(\omega)$ , the change in normal reflectance on addition of Cu, for Au-Cu alloys.

$$\delta R_N = R_N(\text{Au rich alloy}) - R_N(\text{Cu rich alloy})$$
 for pairs of alloys of similar composition, eg. Melt 3 (6.7 at% Au) and Melt 2 (3.4 at% Au). Notation is as in Figure 6.22. The zero of each curve is shown by short horizontal lines. The scale is shown by the bars (right) which represent 15%.

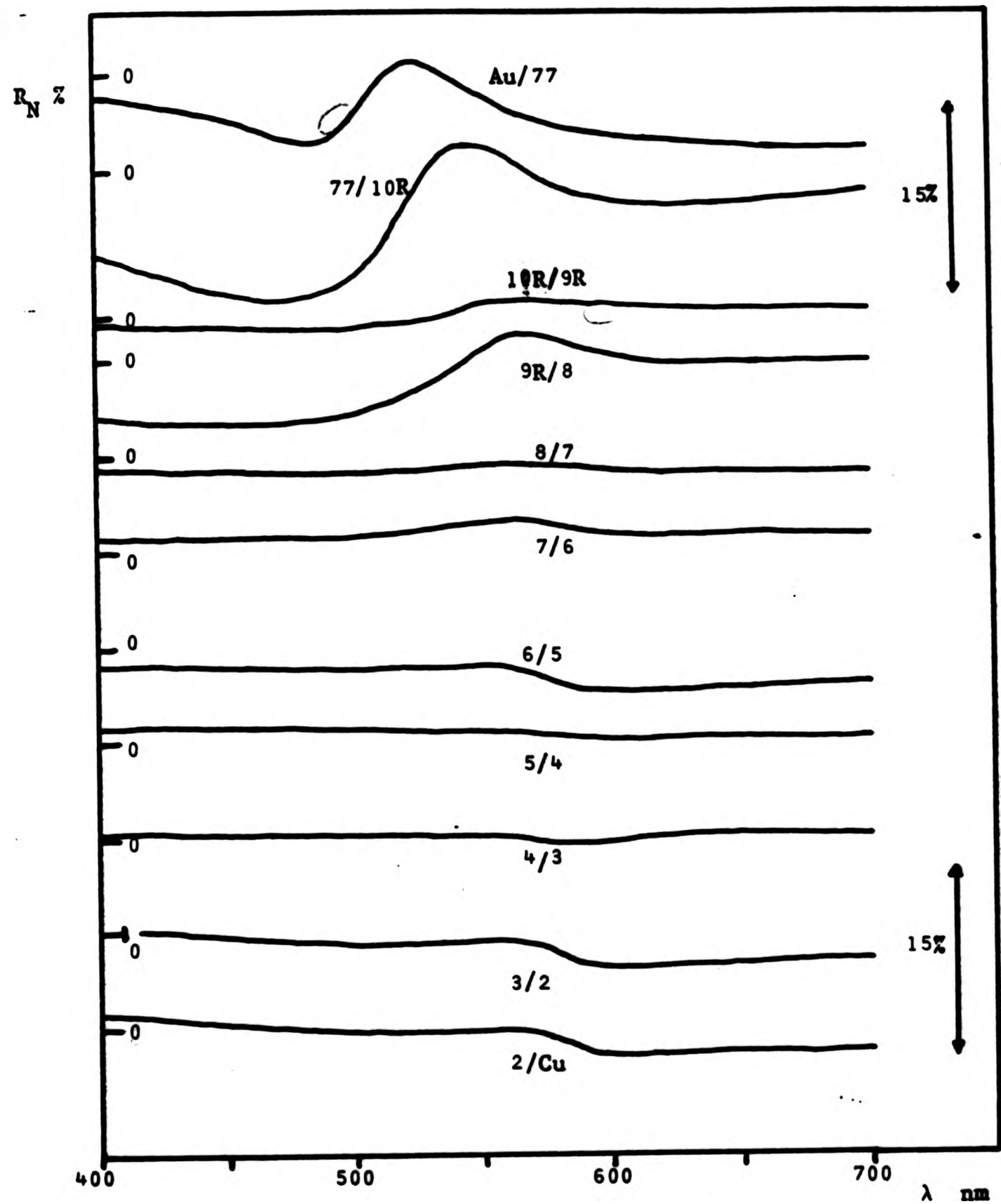


Figure 6.39b.  $\delta R_N(\lambda)$ , the change in normal reflectance on addition of copper, Au-Cu alloys.  $R_N$  is defined by

$$\delta R_N = R_N(\text{Au rich}) - R_N(\text{Cu rich})$$

for alloys of similar composition. The notation is as in Figure 6.22. The zero for each curve is marked on the left, while the arrows (right) show the scale.

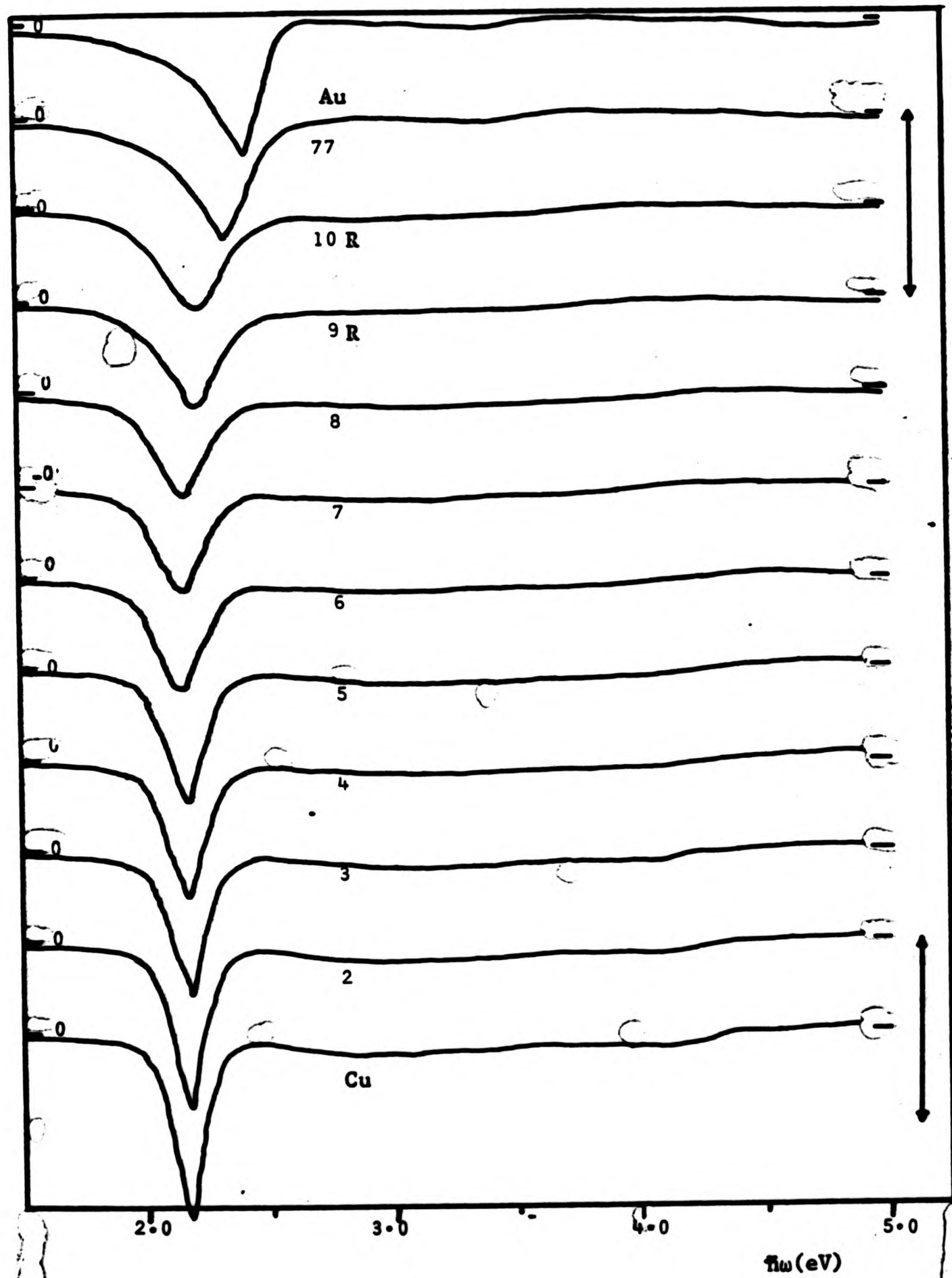


Figure 6.40.  $\frac{\delta R_{II}}{\delta \hbar\omega}$ , Au - Cu alloys

The scale is shown by the bars (right), which are 200 units (% eV<sup>-1</sup>). The zeroes for each curve are indicated on the left.

Table 6.7 Edges of  $\epsilon_2(\omega)$ , Au-Cu alloys.

The 'adjacent alloy' melt number, with respect to which the change in  $\epsilon_2$  is calculated, is shown in parenthesis in cases where confusion could arise, eg. 4.39 (10A).

Melt Number	Atomic % Au	Width of edge	Zero of $D^2\epsilon_2(\omega)$ eV	$D^1\epsilon_2(\omega)$ max eV <sup>-1</sup>	$\epsilon_2$ (at same $h\omega$ )	at $h\omega$	$\epsilon_2$ of adj. alloy	$\delta\epsilon_2$	$\frac{\partial\epsilon_2}{\partial h\omega} = \frac{\partial\epsilon_2}{\partial h\omega}$	$\delta h\omega$ zeroes
JM Au	100	0.32	2.54	8.48	3.94	2.53	4.24	-0.30	-0.03	-0.10
77	86.4	0.24	2.44	7.15	3.62	2.43	4.39 (10A)	-0.77	-0.11	-0.13
10R	73.2	0.35	2.29	9.24	4.19	2.30	3.87 (9R)	-0.39	-0.053	-0.03
10	66.5	0.22	2.31	7.40	3.48	2.30	4.18 (9A)	-0.70	-0.095	-0.05
9R	56.7	0.20	2.26	8.53	3.52	2.25	4.57 (8)	-1.05	-0.12	0
9	56.4	0.21	2.26	8.72	3.82	2.25	4.57 (8)	-0.75	-0.086	-0.01
8	42.8	0.19	2.25	10.6	4.57	2.25	4.60	-0.03	-0.0028	-0.06
7	35.4	0.17	2.19	11.5	3.94	2.19	4.08	-0.14	-0.012	+0.01
6	23.2	0.17	2.20	12.0	4.08	2.19	3.65	+0.43	0.036	-0.01
5	14.7	0.17	2.19	14.2	3.37	2.18	3.20	+0.17	0.012	+0.01
4	12.7	0.12	2.20	14.0	3.73	2.21	3.78	-0.05	-0.0036	-0.01
3	6.7	0.12	2.19	14.6	3.50	2.19	3.19	+0.31	0.021	0
2	3.4	0.12	2.19	16.3	2.87	2.18	2.50	+0.37	0.023	0
Cu	0	0.17	2.18	16.2	2.43	2.18				

Table 6.8 Edges of  $\epsilon_2^b(\omega)$ , Au-Cu alloys

Melt Number	Atomic % Au	Width of edge	Zero of $D^2\epsilon_2^b(\omega)$ eV	$D^1\epsilon_2(\omega)$ max eV <sup>-1</sup>	$\epsilon_2$ (at same $\omega$ )	$h\omega$	$\epsilon_2$ of adj.alloy	$\delta\epsilon_2$	$\delta h\omega = \delta\epsilon_2 + \frac{\partial\epsilon_2}{\partial h\omega}$	$\delta h\omega$ from the b zeros of $D^2\epsilon_2$
JH Au	100	0.15	2.54	10.4	1.755	2.53	2.50	-0.74	-0.07	-0.10
77	86.4	0.24	2.44	3.47	1.750	2.43	3.52	-1.77	-0.21	-0.15
10R	73.2	0.35	2.29	11.2	2.31	2.30	2.20 (9R)	+0.11	+0.01	-0.03
10A	66.5	0.22	2.31	9.10	1.776	2.30	2.44 (9A)	-0.66	-0.06	-0.05
9R	56.7	0.21	2.26	10.5	1.74	2.25	2.46	-0.72	-0.07	-0.07
9A	56.4	0.21	2.26	10.9	1.99	2.25	2.46	-0.47	-0.04	-0.07
8	42.8	0.19	2.19	13.1	1.72	2.19	1.93	-0.21	-0.026	0
7	35.4	0.17	2.19	13.8	1.93	2.19	1.88	+0.05	+0.003	0
6	23.2	0.17	2.19	14.5	1.88	2.19	1.63	+0.15	+0.01	0
5	14.7	0.17	2.19	16.0	1.63	2.18	1.44	+0.19	+0.01	+0.01
4	12.7	0.12	2.20	15.6	2.03	2.21	2.00	+0.03	+0.002	-0.03
3	6.7	0.12	2.17	16.4	1.68	2.19	1.84	-0.16	-0.01	+0.02
2	3.4	0.12	2.19	17.8	1.44	2.18	1.45	+0.04	+0.002	-0.01
Cu	0	0.17	2.18	17.2	1.45	2.18				

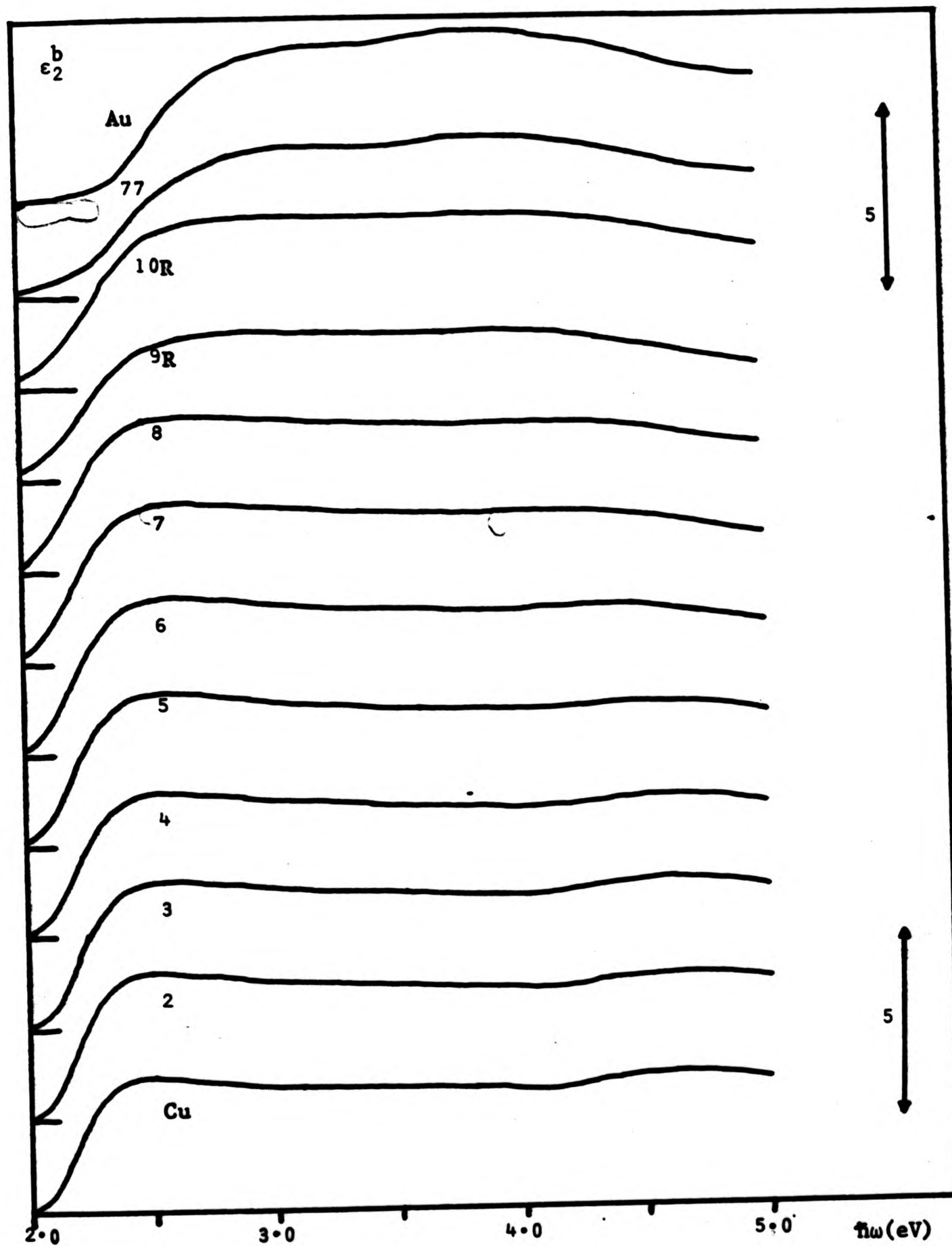
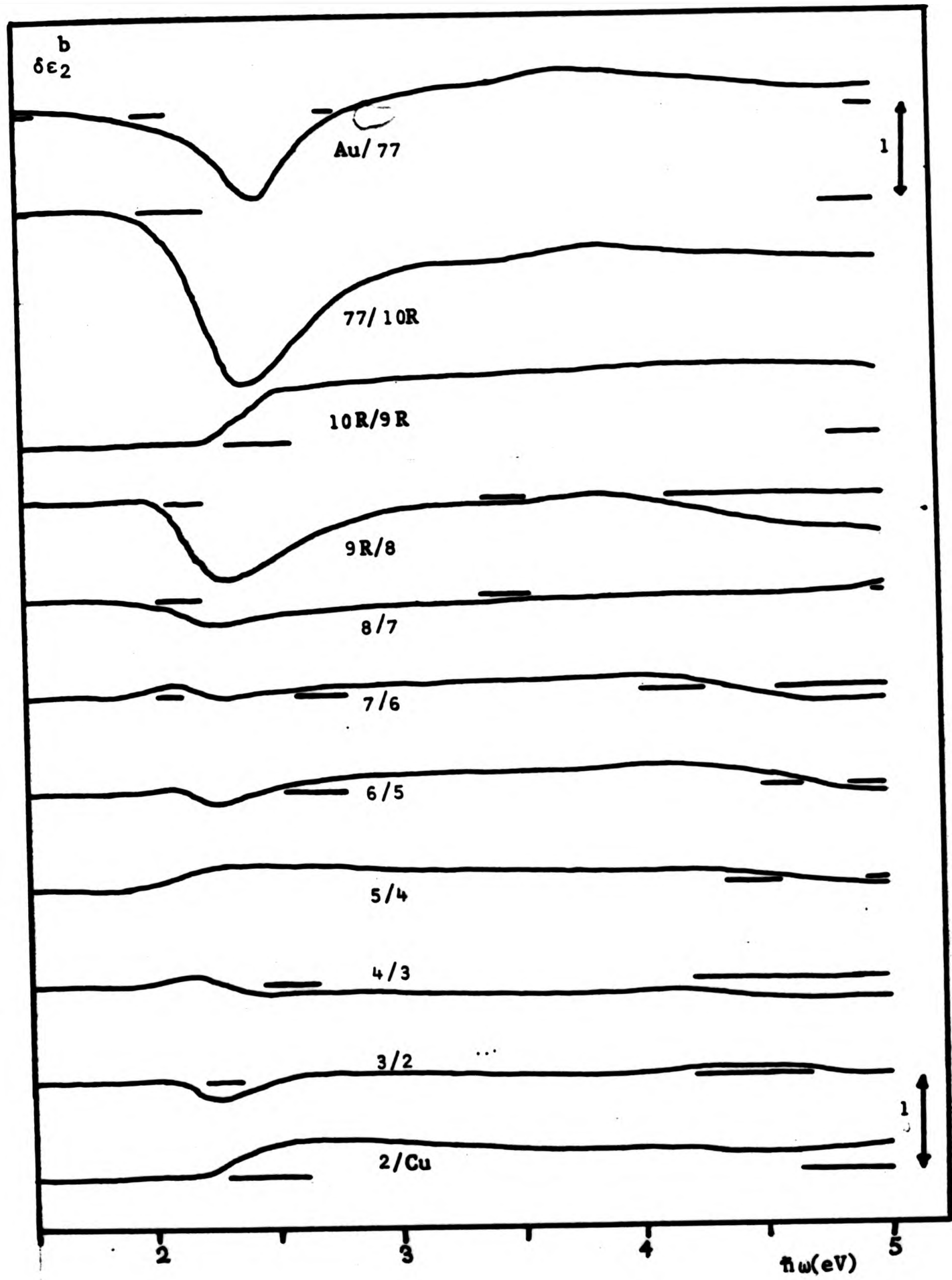


Figure 6.41.  $\epsilon_2^b(\omega)$ , Au-Cu alloys.  
 The zero for each curve is given on the left. The scale is  
 on the right.



**Figure 6.42.** The change in the interband part of  $\epsilon_2, \delta\epsilon_2^b$ , Au-Cu alloys. The horizontal lines indicate the zeroes for each curve.

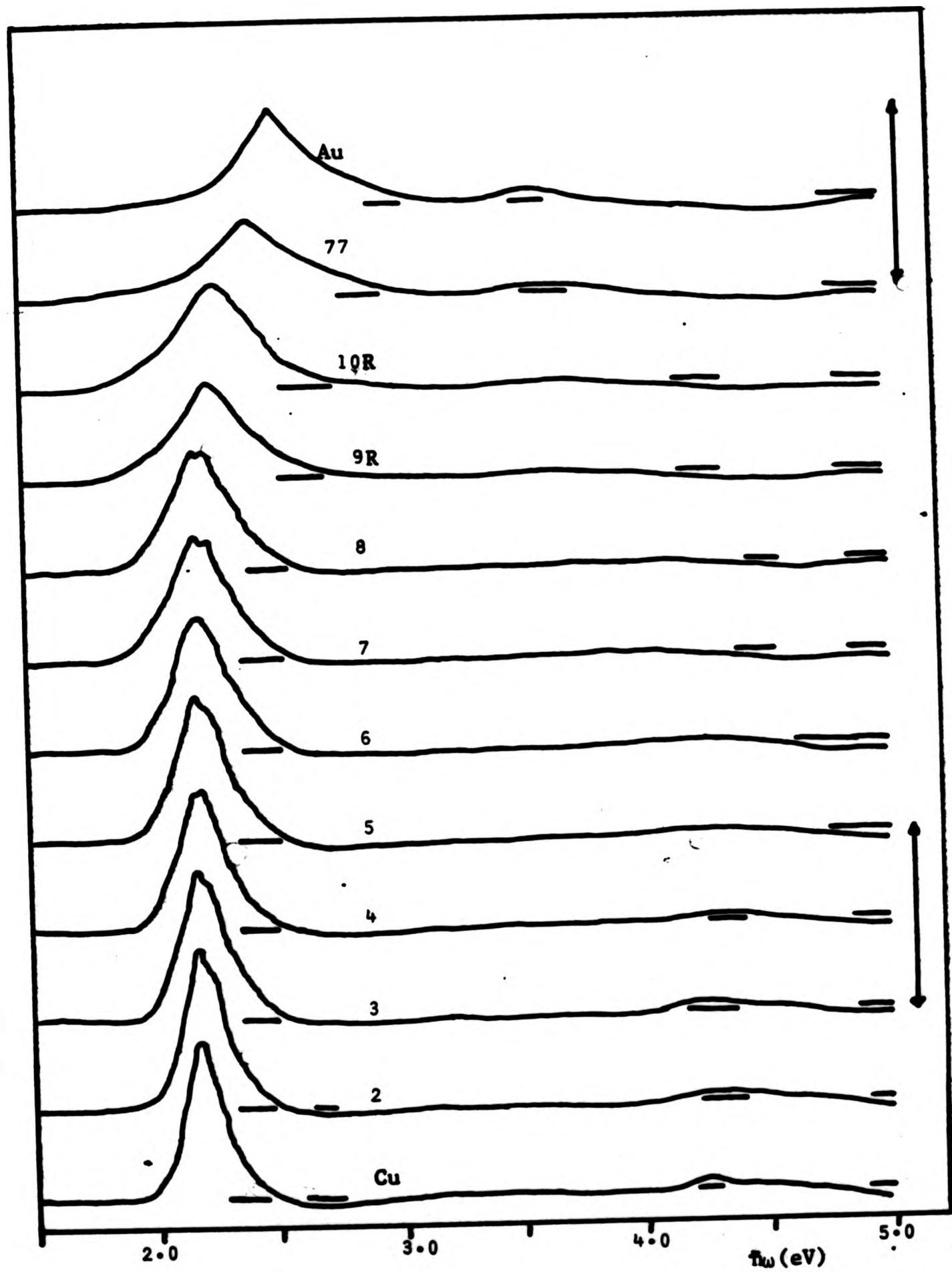


Figure 6.43.  $\frac{\partial \epsilon_2^b}{\partial \hbar\omega}$ , Au-Cu alloys. The bars (right) indicate the scale ( $20 \text{ eV}^{-1}$ ). The horizontal lines show the zero for each curve.

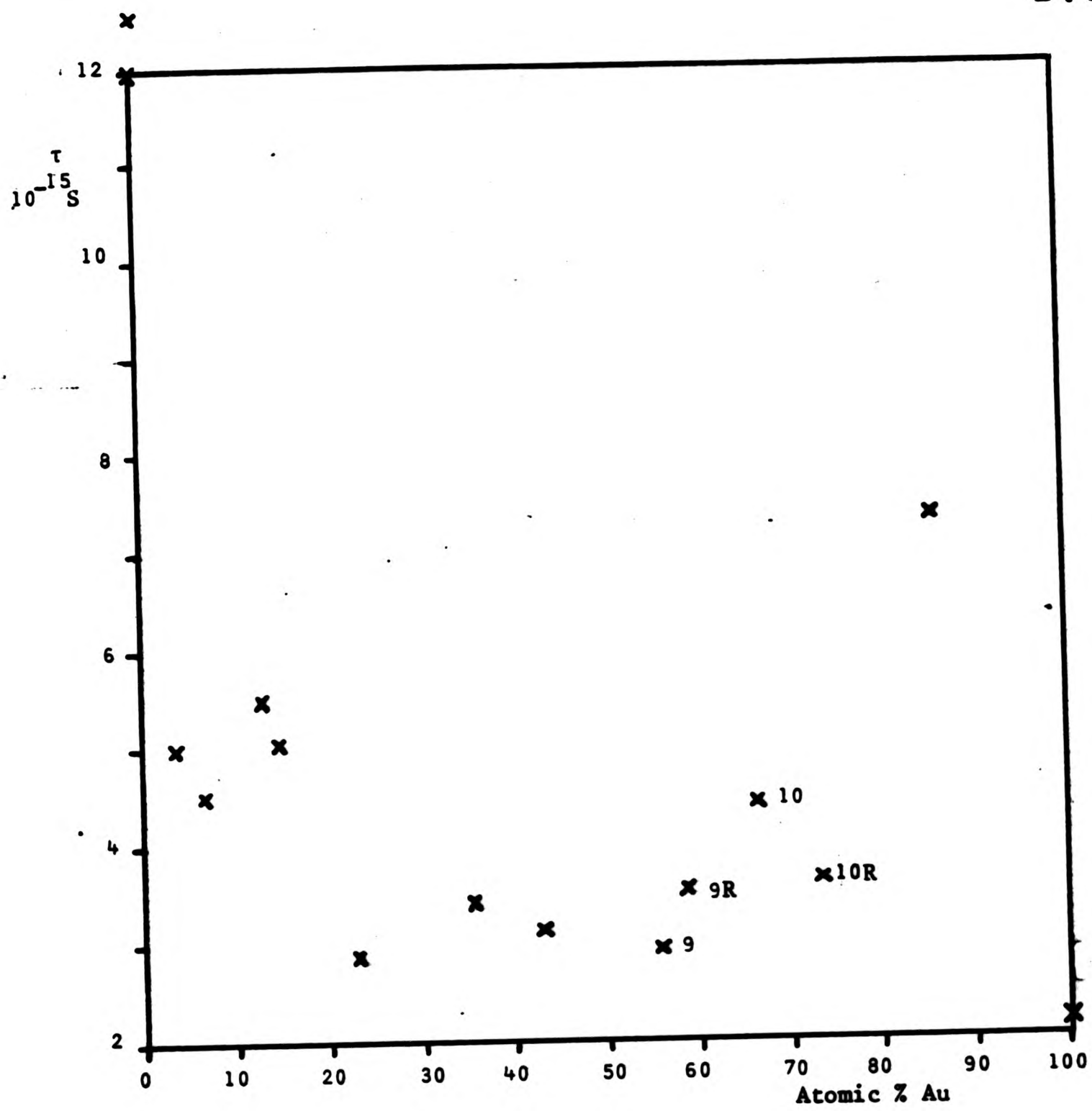


Figure 6.44. The Drude-like conduction electron relaxation time, Au-Cu alloys.

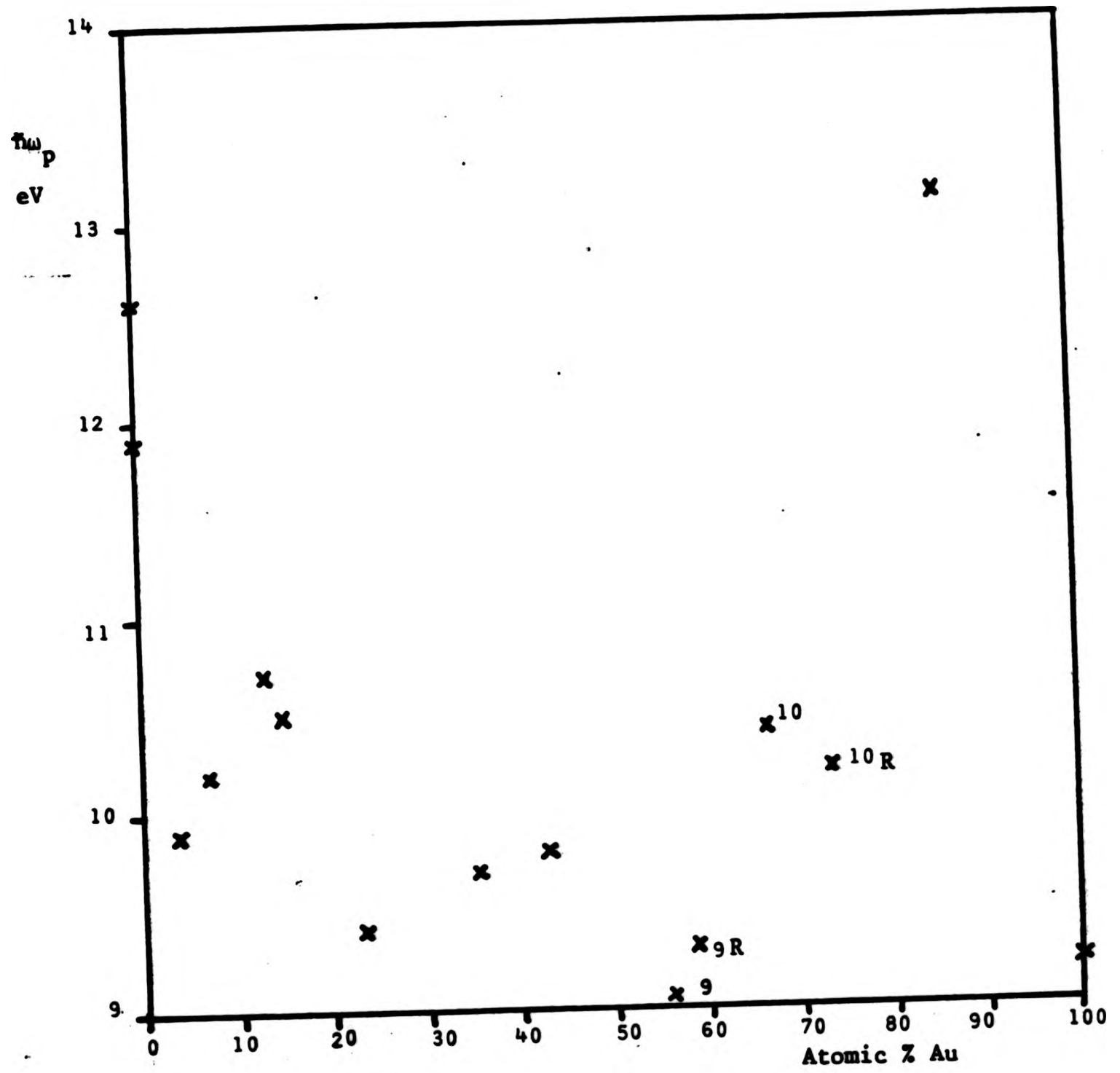


Figure 6.45. The conduction electron plasma frequency, Au-Cu alloys.

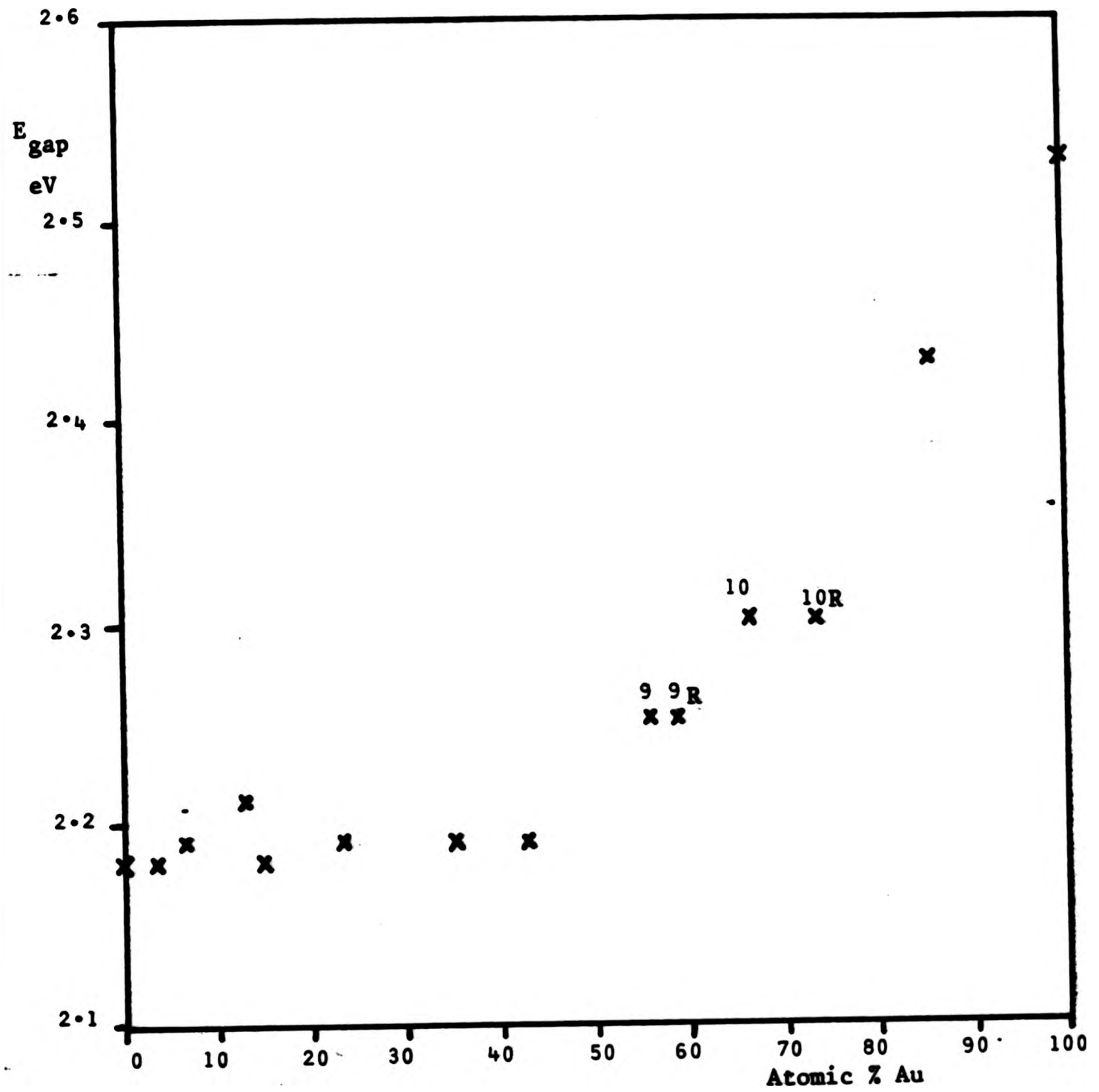
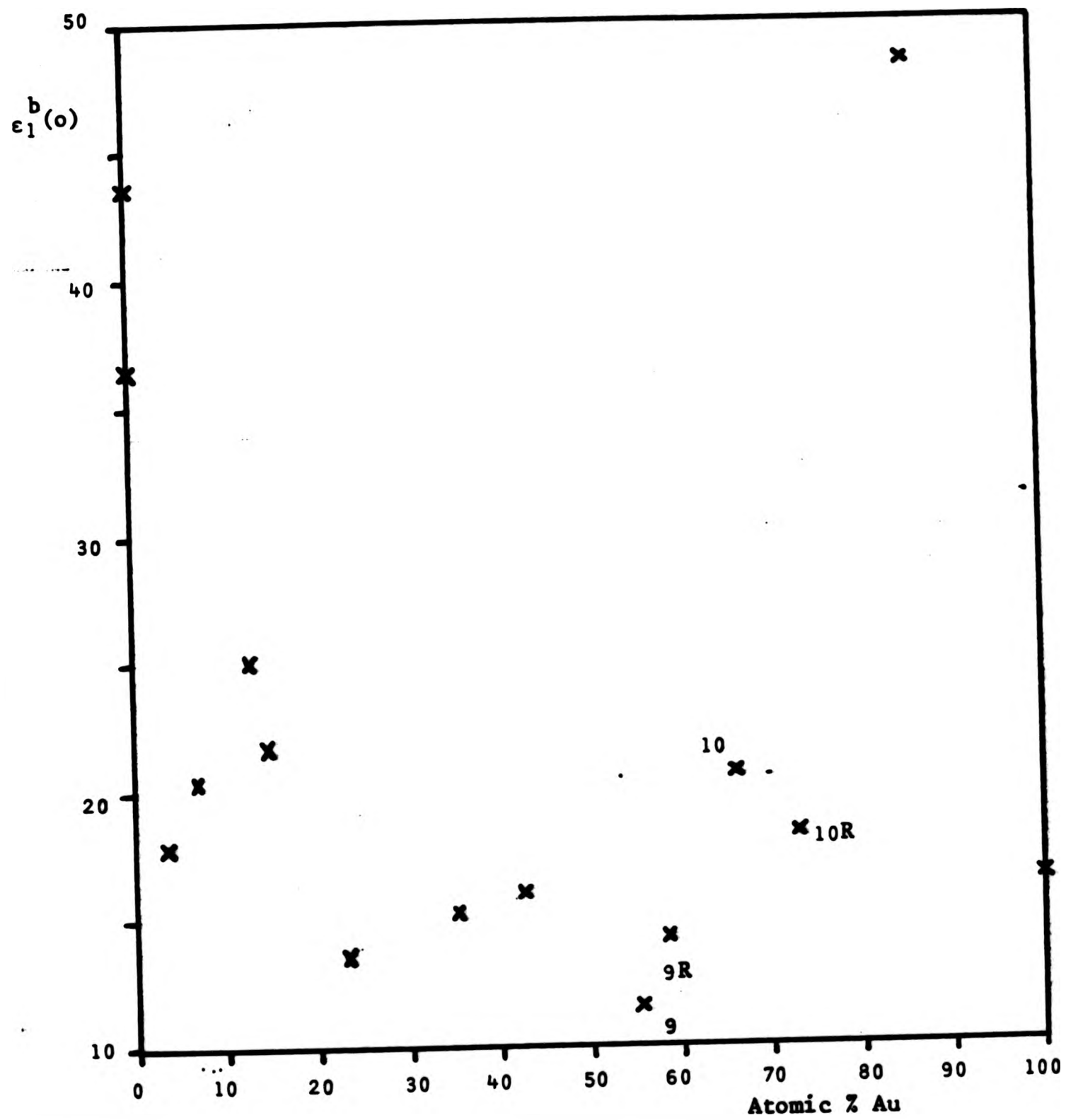


Figure 6.46. The energy  $E_{\text{gap}}$ , of the absorption edge in  $\epsilon_2^b(\omega)$ , Au-Cu alloys. This is the energy where  $\frac{\partial \epsilon_2^b}{\partial \omega}$  is a maximum.



**Figure 6.47.** The low frequency contribution of interband transitions to  $\epsilon_1$ ,  $\epsilon_1^b(\omega)$ , Au-Cu alloys.

absent from the plots of these as a function of Au concentration (Figures 6.44 - 6.47), with the exception of  $E_{\text{gap}}$ . Figure 6.46, which clearly shows little or no variation for Au content 0-50 at.%, and rapid shift subsequently. Analysis of the curves  $\delta\epsilon_2^b(\omega)$  will be used in the Discussion to examine these measurements more closely.

#### 6.4 Ag-Cu alloys

This alloy system has only an extremely narrow range of solid solution at 600°C (the annealing temperature used for this study) - only ~ 5 at.% Cu dissolving in Ag, and less than 1.5 at.% Ag dissolving in Cu. Nevertheless, several single phase samples were prepared. Those of the 600°C saturated solid solution composition (melt numbers 75 and 76) were annealed and quenched from 750°C to ensure that no second phase precipitated. Another alloy, melt number 70, approximately  $\text{Ag}_{99}\text{Cu}_1$ , was made, and also a sample of melt number 16 was remade by liquid-quenching as a metastable single phase alloy of 37.4 at.% Ag.

Some relevant properties of both the single- and duplex-phase samples are presented together here. Sections 6.4.1 will deal with the solid solutions and Section 6.4.2 the others. Table 6.9 lists colorimetric and electronic properties.

#### Colorimetry

Figure 6.48 shows the CIE 1960 Uniform Colour System co-ordinates, for C.I.E Standard Illuminant C, for all the

Table 6.9 Some properties of Ag-Cu alloys as a function of concentration

Melt number	Atomic % Ag	Weight % Ag	CIE Colour Co-ordinates			1931 Standard System			Relaxation time (10 <sup>-15</sup> sec)	Plasma freq. (eV)	d-PS transit ion energy (eV)	E <sub>p</sub> (eV)	
			(x10 <sup>4</sup> ) Normal Reflectance			Equal Energy Illumination							
			x	y	z	λ <sub>d</sub> nm	S	Z					L
JM Ag	-	99.99	3344	3344	2011	3078	577.4	0.67	95.9	6.76	3.66	4.09	6.82
30R	-	99.97	3383	3381	2023	3096	578.5	2.96	89.1	4.54	10.1	4.00	18.4
70	99.0	99.4	3380	3376	2023	3093	579.1	2.7	88.9	7.57	12.8	4.01	43.8
76	93.4	96.0	3371	3382	2014	3094	574.9	2.6	93.6	6.66	10.6	4.02	20.4
12	83.4	89.5	3390	3391	2024	3100	578.0	3.5	95.4	67.8	19.9	2.14	1.35
13	70.1	79.9	3435	3412	2044	3113	581.2	5.5	91.5	-	50.5	2.14	-
14	57.0	69.2	3496	3428	2077	3125	584.8	7.8	87.1	7.85	9.63	2.17	15.5
15	47.7	60.8	3551	3476	2094	3149	583.3	10.9	87.3	8.92	8.96	2.17	10.9
16	37.4	50.3	3631	3527	2125	3177	583.5	14.8	84.9	33.3	14.8	2.17	65.5
16 (splat)			3711	3612	2145	3217	581.9	19.7	79.3	4.25	9.19	-	14.8
17	28.1	39.9	3682	3534	2155	3185	584.9	16.5	84.4	50.8	13.6	2.18	52.0
18	20.2	30.1	3739	3555	2184	3199	585.6	18.9	80.9	17.7	11.6	2.19	32.3
19	12.4	19.4	3755	3545	2198	3198	586.6	19.1	80.4	18.7	11.8	2.19	32.5
20	6.5	10.6	3832	3549	2246	3208	588.4	21.5	74.9	23.8	13.6	2.19	54.4
75	1.25	2.1	3847	3534	2261	3204	589.6	21.5	71.5	9.40	11.7	2.19	32.9
Cu			3839	3521	2261	3199	590.1	20.9	72.0	9.5	10.5	2.18	25.3

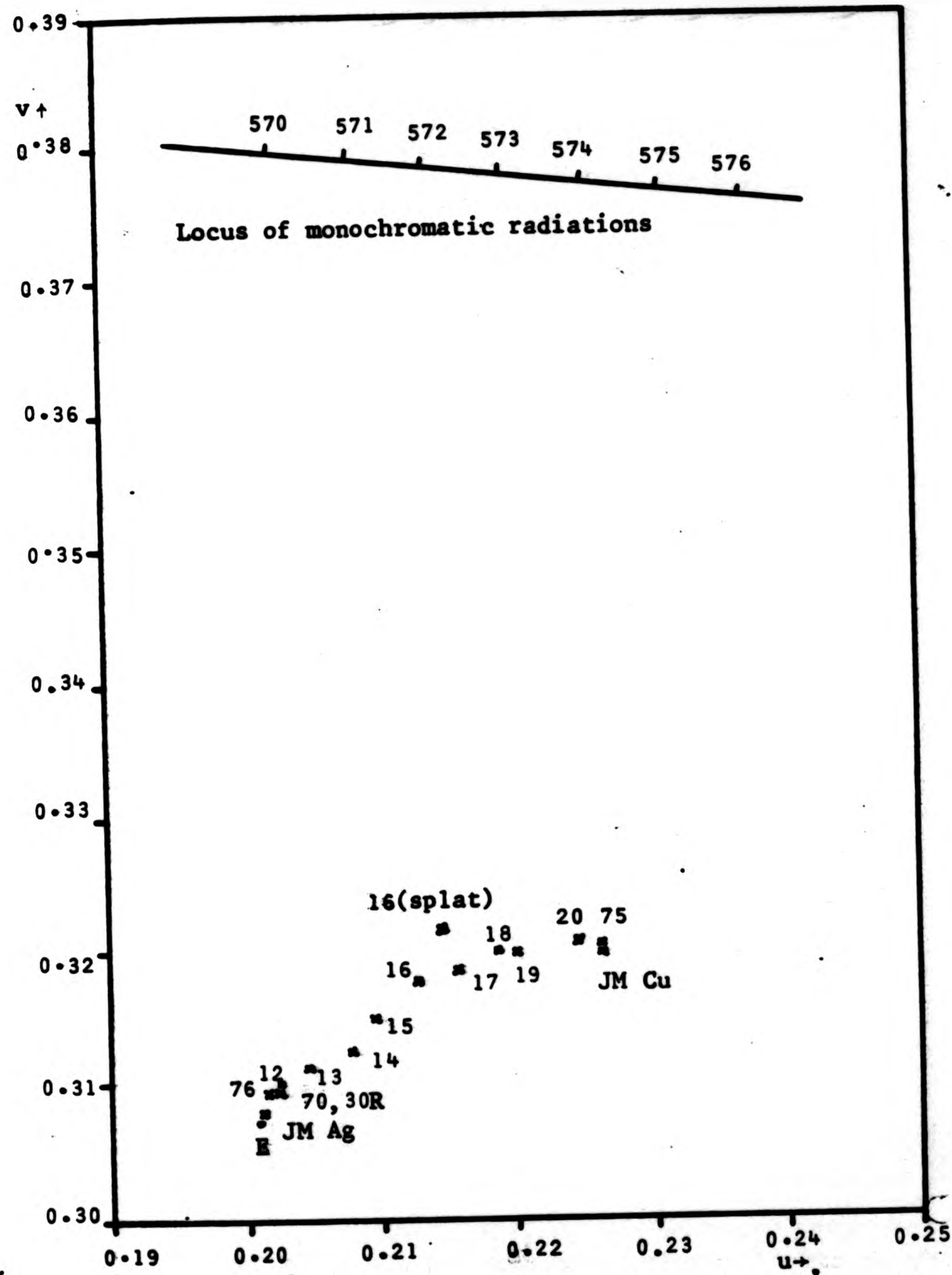


Figure 6.48. Colour Coordinates of Ag-Cu alloys.  
 Values calculated in the C.I.E 1960 Uniform Colour  
 System for C.I.E Standard Illuminant C.

The numbers on the locus are sample melt reference  
 numbers. The point E is the equal energy point.

Ag-Cu alloys measured. The colour locus takes the form of an upward-curving arc; the results which fit least well on this curve are those of the eutectic and of the splat-cooled sample. Note that the results for the 2-phase samples have been obtained as described in Chapter 4, taking no account of any inhomogeneity. Figure 4.49 gives these results as functions of composition.

#### Electronic Properties

The computed dielectric functions of all these alloys show the 'Drude-like' tail characteristic of solid solution noble metal alloys. The optical relaxation time, plasma energy and low frequency part of  $\epsilon_1^b$  are plotted as functions of concentration in Figures 6.50 - 6.52. Sample 13 gave a negative value for the relaxation time (as also did one pure copper sample), so that results from this alloy, in the infra-red, have been discounted. Overall these results do not display a marked relationship, but are similar enough to those for the Ag-Au and Au-Cu systems. It can be seen from Table 6.15 that the absorption edge position does not change significantly.

#### 6.4.1 Single phase Ag-Cu alloys

##### Reflectance Curves

Figure 6.53 shows the spectral reflectance of a range of Ag-Cu solid solutions, as well as curves for pure Ag and Cu. These divide into Ag rich alloys 100 + 95 at.% Ag, and Cu rich, 37.4 + 0 at.% Ag. The measured absorption edge for a silver sample from Johnson-Matthey was at a higher energy than that

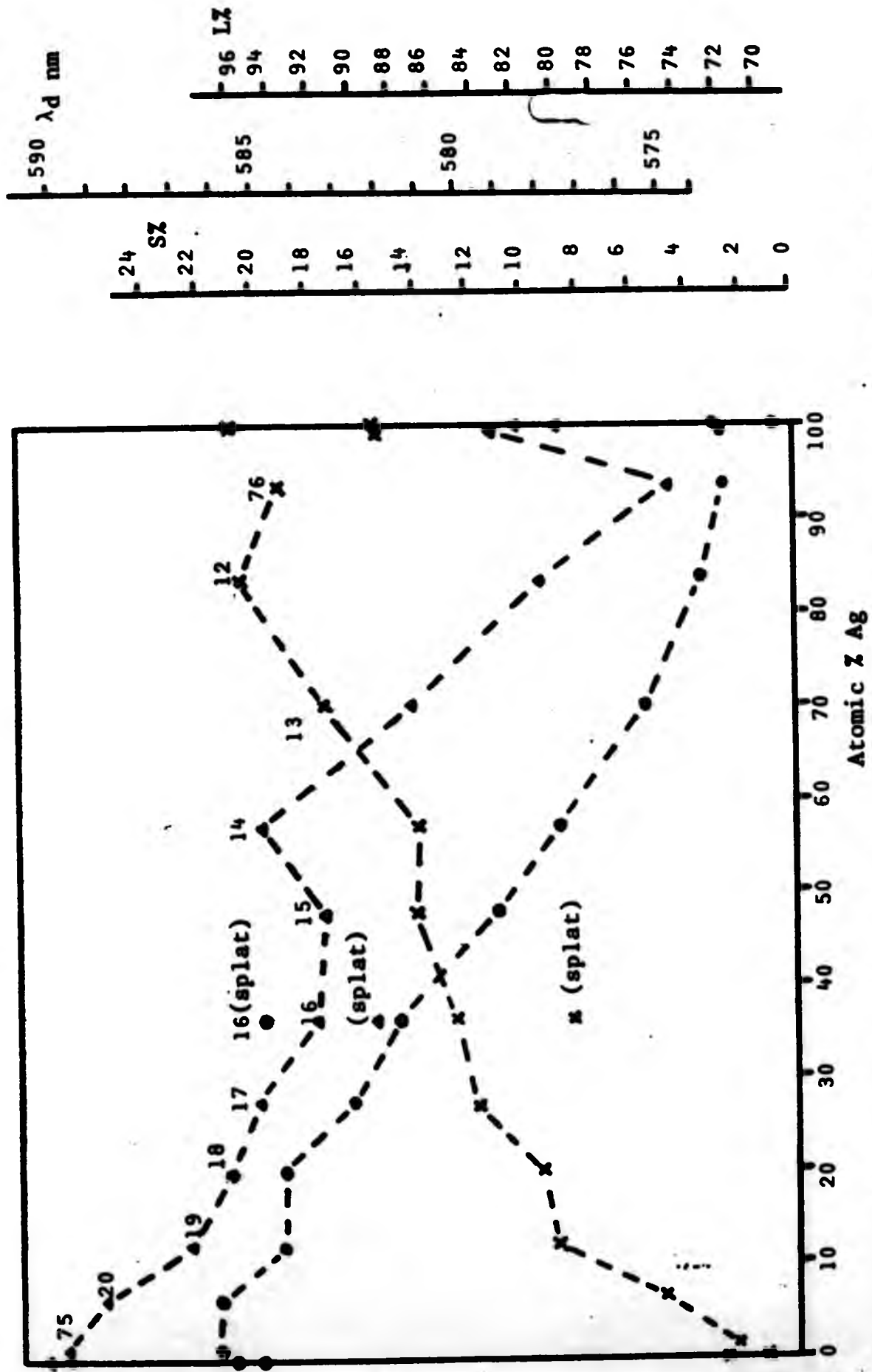


Figure 6.49. Saturation (e-e-e), Luminance (x-x-x) and Dominance Wavelength (---), Ag-Cu alloys. Calculated in the C.I.E 1931 Standard System for equal-energy distribution illumination.

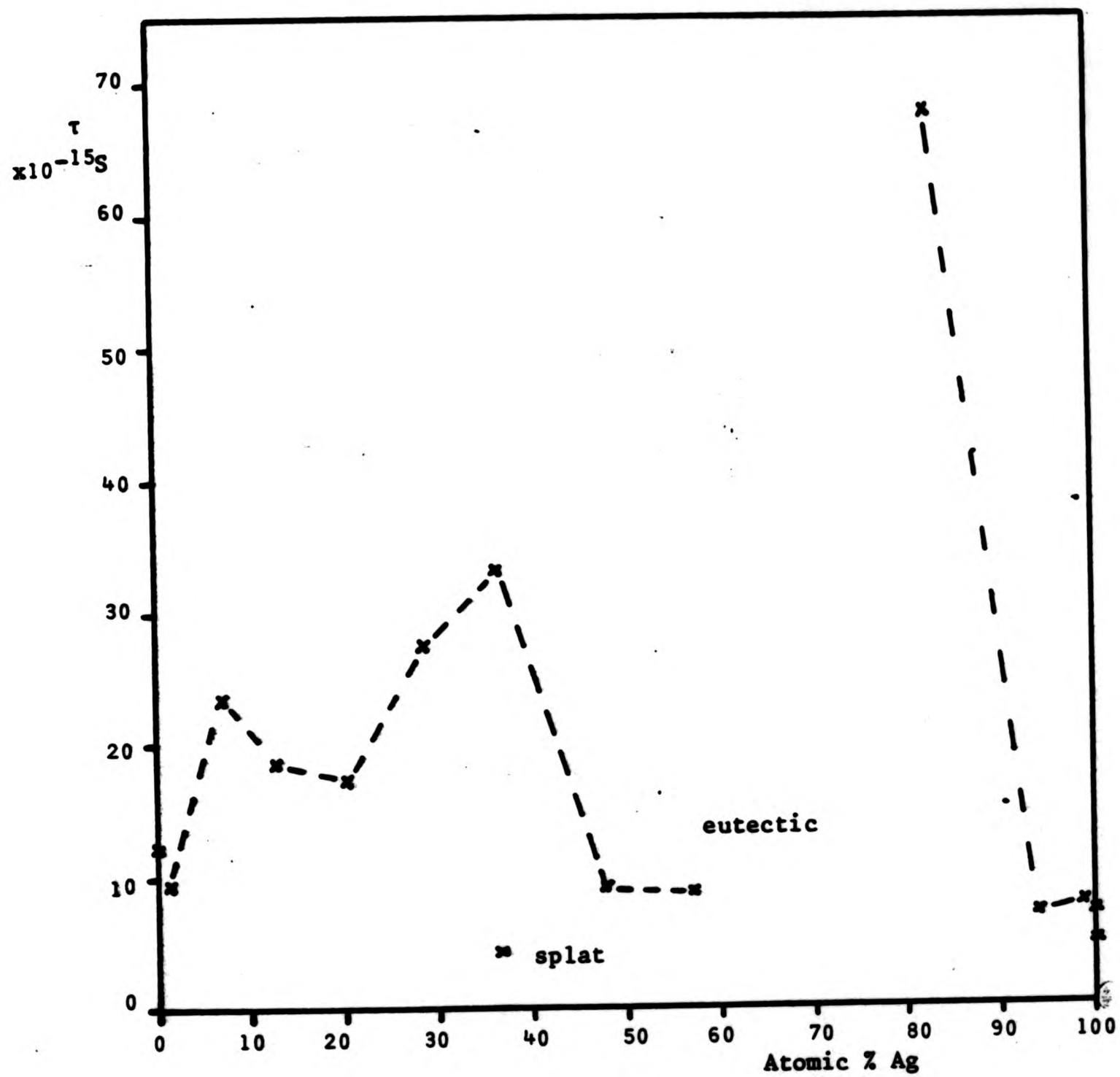
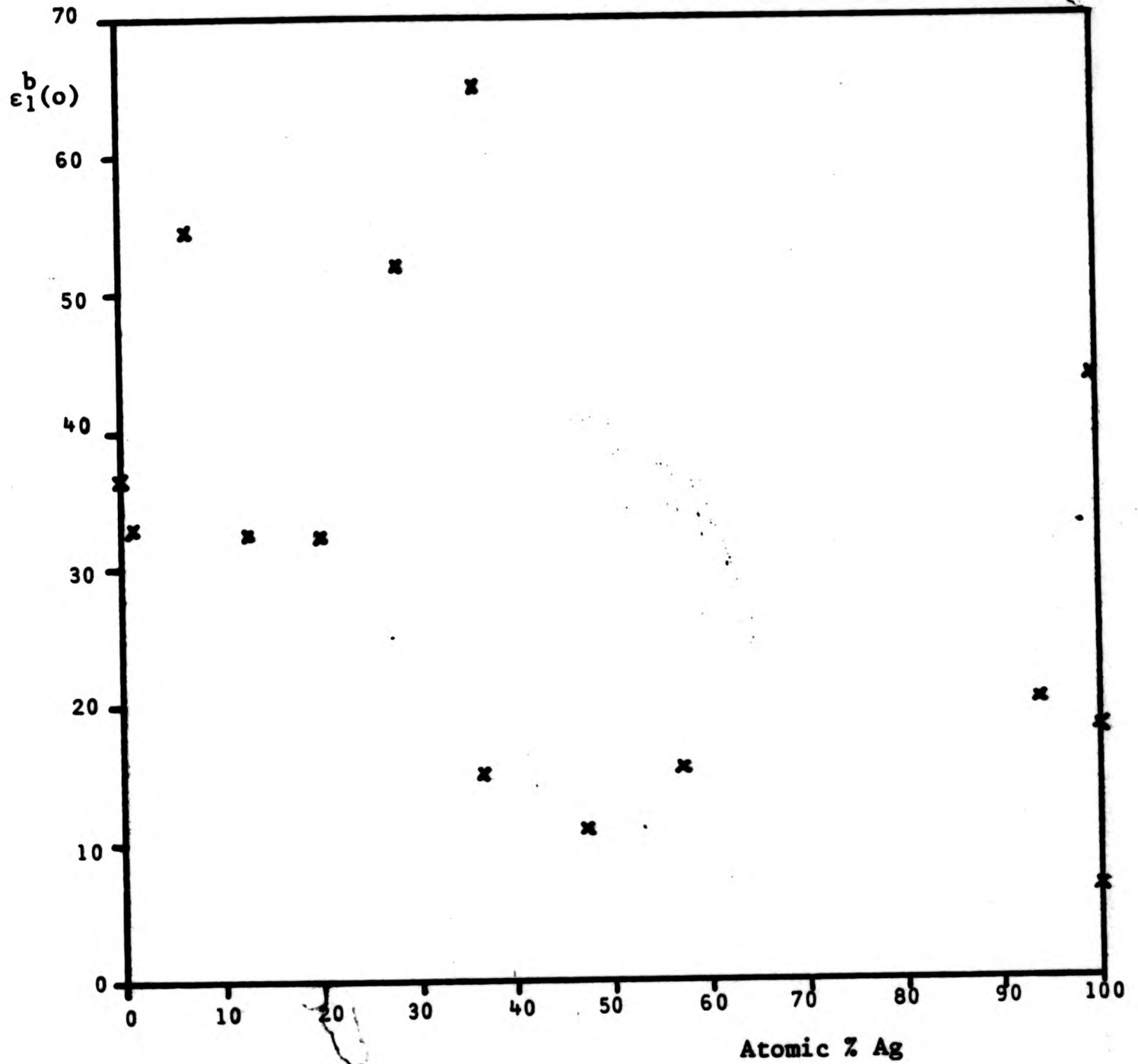
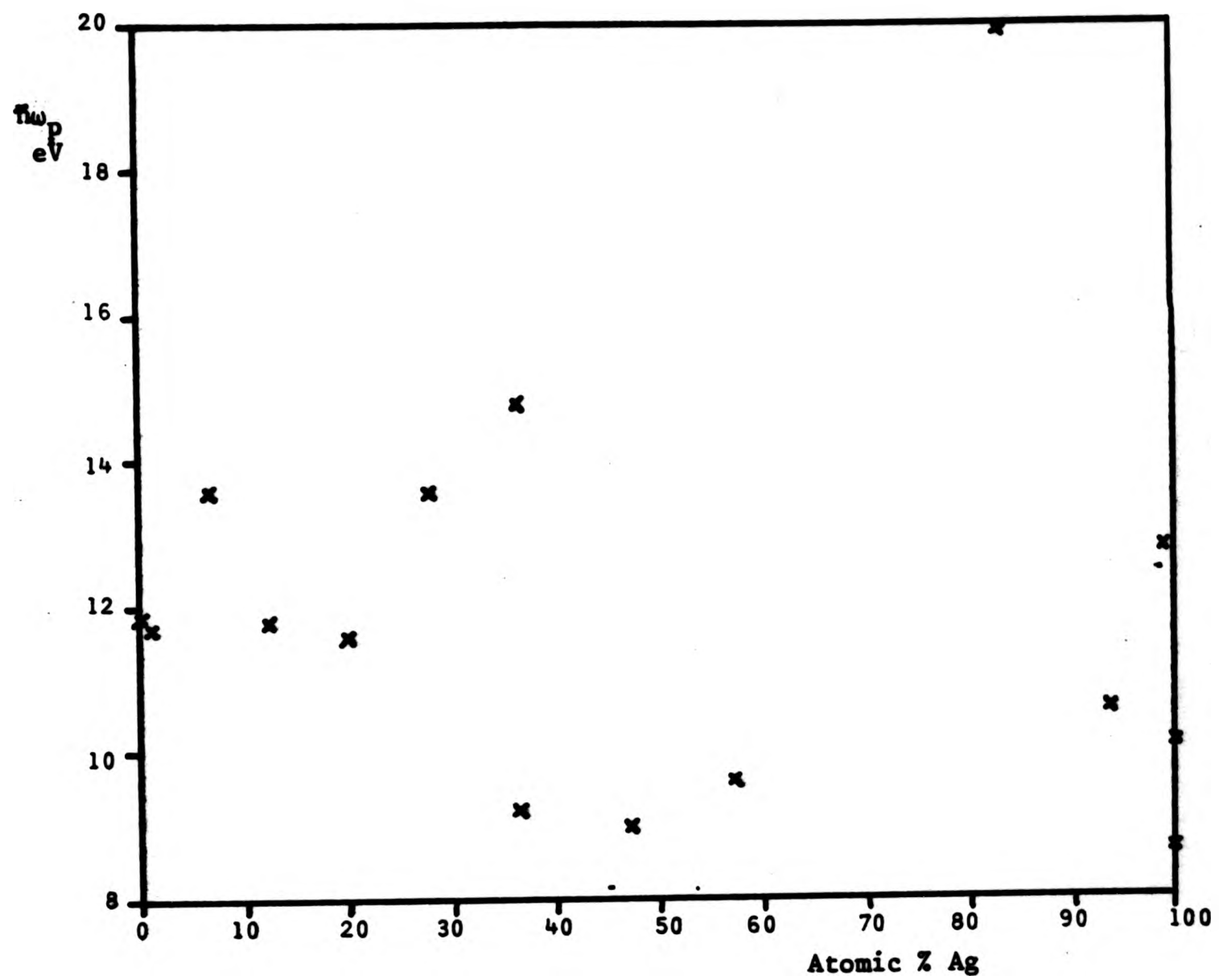


Figure 6.50. Optical (Drude-like) relaxation time of Ag-Cu alloys. The calculated value for sample number 13 (not shown) was negative. See also Table 6.9.



**Figure 6.51.** Low frequency interband component of the real part of the dielectric function, Ag-Cu alloys.

These values are unexpectedly large. The value for sample number 12 (not shown) was 135; that for sample number 13 was not calculated.



**Figure 6.52.** The intraband plasma frequency, Ag-Cu alloys. The value computed for sample number 13 (not shown) was 50.5.

Table 6.10 Edges of reflectance curves (solid solutions)

Melt number	Atomic % Ag	Edge width	zero of $D^2$	max gdt	$h\omega$	$R_N$ this alloy at $h\omega$	$R_N$ adj.alloy at $h\omega$	shift ( $\delta R$ ) eV	shift(zeroes) eV
Jm Ag	100	0.12	3.77	-502	3.77	44.7			
30R	100	0.11	3.74	-355	3.76	27.3	29.1	+0.005	0
70	99.0	0.11	3.74	-340	3.76	29.1	31.0	+0.003	0
76	93.4	0.23	3.74	-218	3.76	31.0			
16 (splat)	37.4	0.12	2.25	-85.2	2.25	77.6			
75	1.25	0.13	2.17	-192	2.18	73.8	73.5	-0.001	0
Cu		0.11	2.16	-190	2.18	73.5			

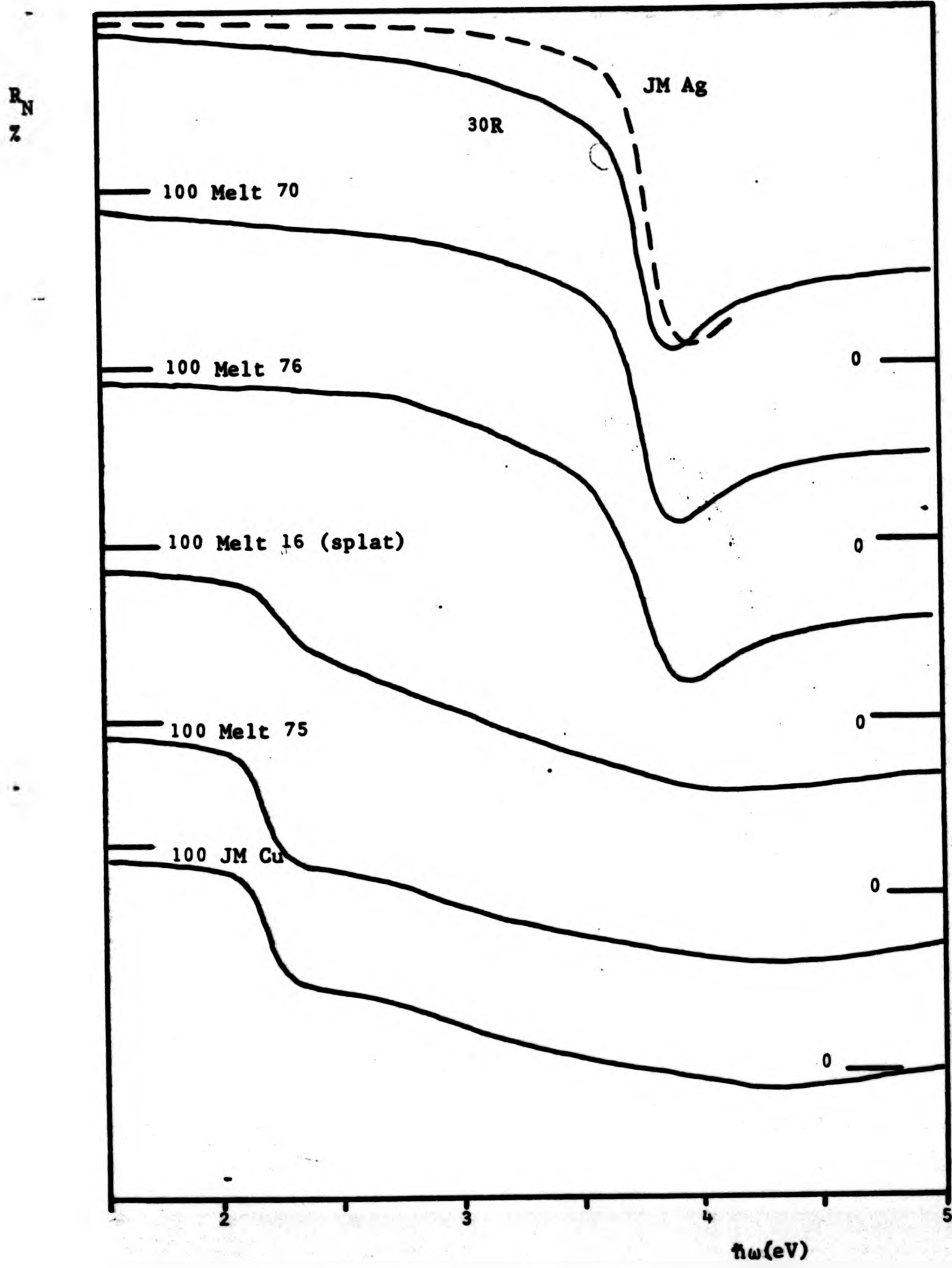


Figure 6.53. Normal reflectance of single phase Ag-Cu alloys.

for any of the samples 30R, 70 and 76; namely, 4.09 eV to 0.1 eV compared with 4.00 eV. At this energy, the difference corresponds to approximately 10 nm wavelength difference. However, the optical configuration of the ellipsometer was realigned after this result. Also, it proved impossible to complete the experiment by making measurements for energies  $\sim 4.3 \rightarrow 5$  eV due to poor ellipsometer performance. The possible significance of this on the validity of these results that were obtained will be discussed again later. The measured curves for the other Ag-rich alloys are very similar. Difference curves (changes in reflectance with alloying additions) and numerical derivatives show more structure (Figures 6.54, 6.55). Change in reflectance is roughly proportional to alloying concentration, near the absorption edge, that is, 2% for a 1% Cu addition, 8% for a 5 at.% Cu addition. There is also a weak structure near 3 eV. The derivative curve shows discernible structure between 2.5 and 3 eV in the case of the more concentrated alloy.

Turning to the Cu-rich alloys, these are characterised by an edge at 2.17 eV in the case of Cu and sample No. 75 (1.25 at.% Ag), or at 2.25 eV in the case of the metastable alloy No. 16 (37.4 at.% Ag). A difference plot has been produced for Cu and No. 75, by subtracting the values for Cu from those for No. 75. This follows the method for the Ag-rich alloys, since always the values for the alloy with relatively more copper are subtracted from the values for the alloy having less copper. Structure is clear (1%, compared with  $\sim 0.1\%$  scatter) at 2.17 eV, at  $\sim 4.1$  eV ( $\sim 0.3\%$ ), and possibly at 3.3 eV. The derivative curves emphasise the lack of sharpness in the edge for the splat-cooled

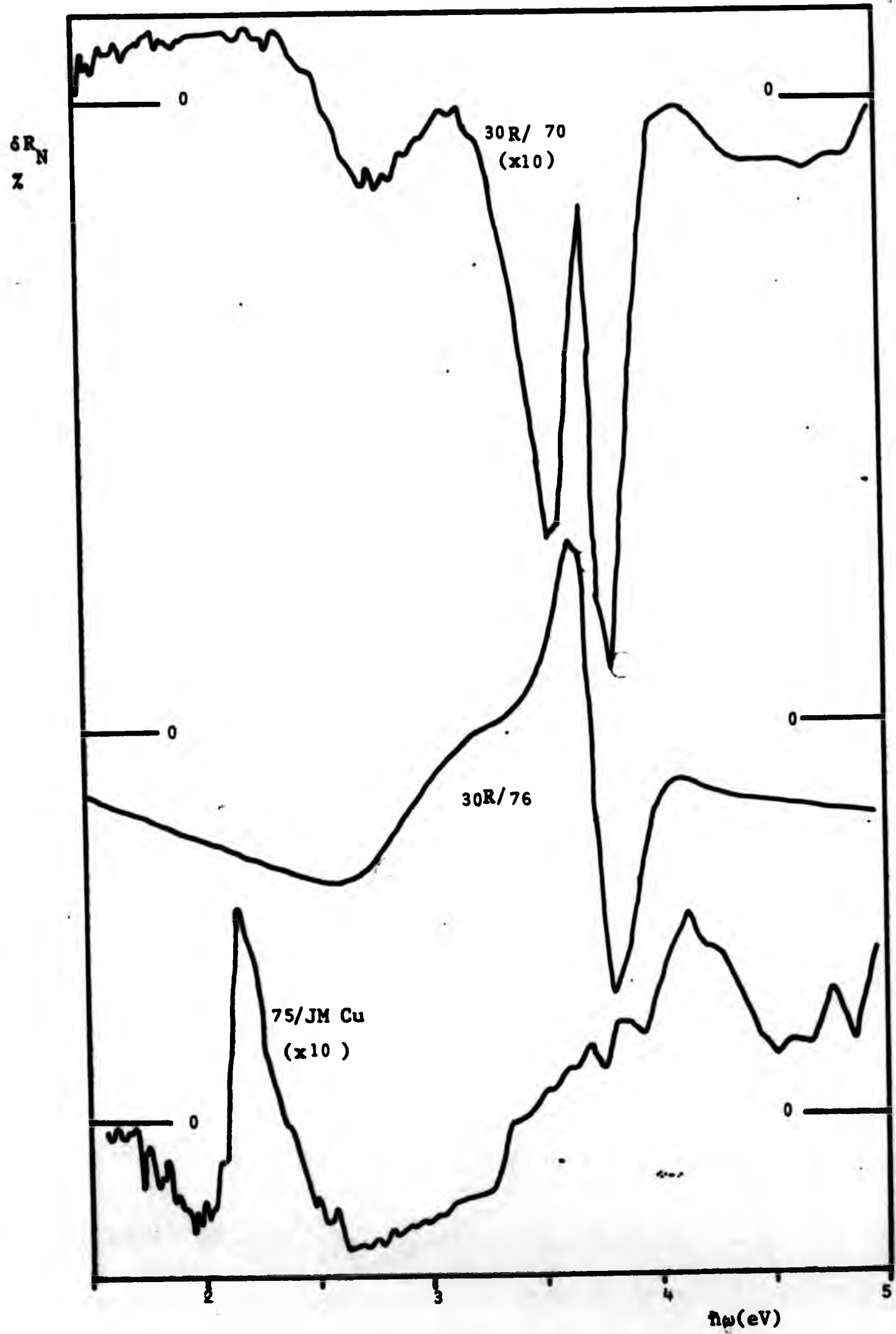
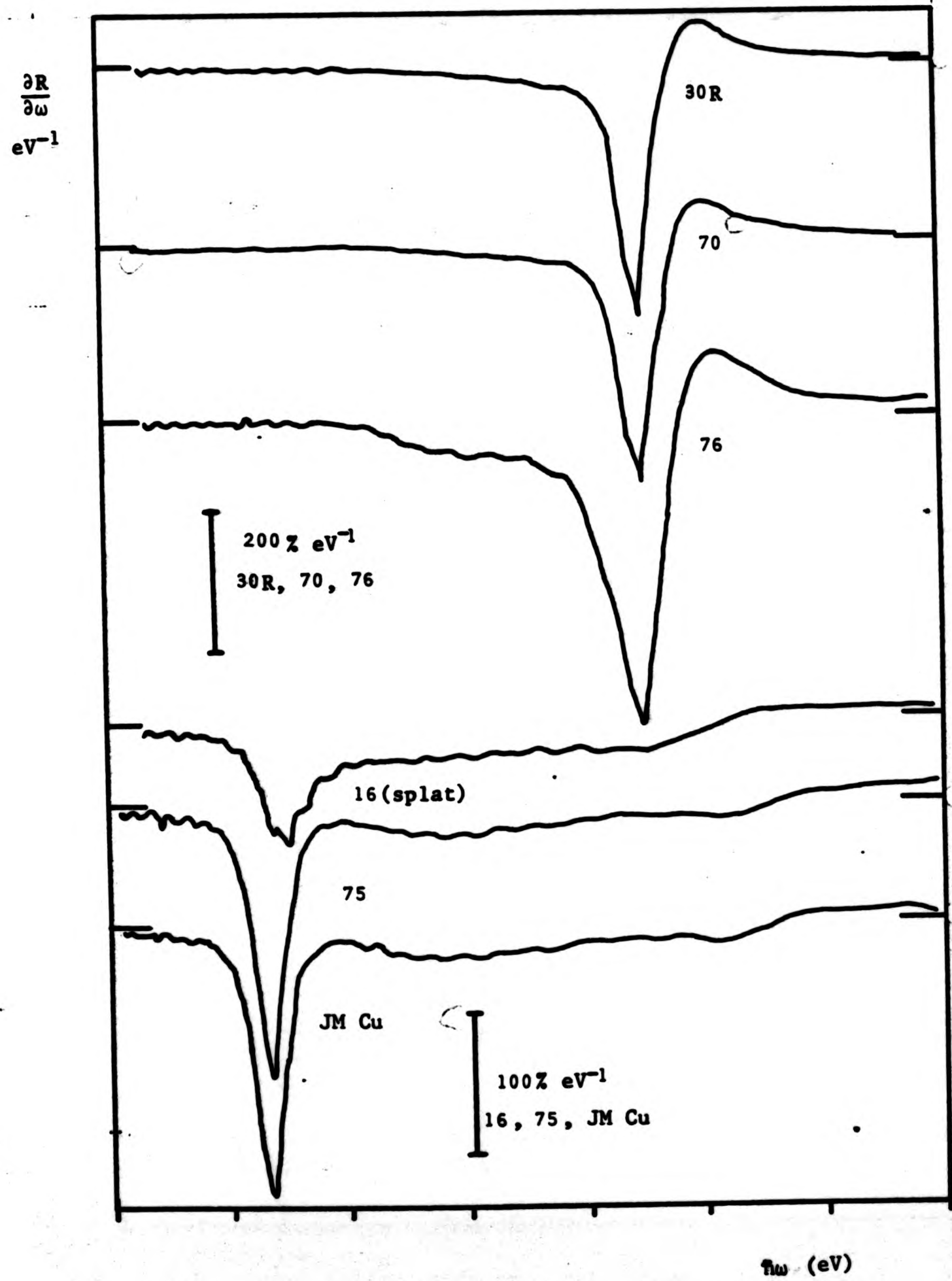


Figure 6.54. Change in reflectance on addition of Cu, single phase Ag-Cu alloys.



**Figure 6.55.** Numerical derivative of the reflectance, single phase Ag-Cu.

Table 6.11 Edges of  $\epsilon_2(\omega)$ , Ag-Cu solid solutions

Melt number	Atomic % Au	Edge width	Zero of $D^2$	Max gdt.	$h\omega$	$\epsilon_2$ this alloy at $h\omega$	$\epsilon_2$ next alloy at $h\omega$	Shift $\delta h\omega$ from $\delta\epsilon_2$	$\delta h\omega$ from zeroes
JM Ag	100	n.a	4.09	7.90	4.06	1.62			
30R	100	n.a	4.00	8.82	4.00	1.64	1.62 <sup>(70)</sup>	+0.0025	+0.01
							1.82 <sup>(76)</sup>	-0.225	+0.02
70	99.0	0.26	4.01	8.23	4.00	1.62			
76	93.4	0.20	4.02	6.96	4.00	1.82			
16 (splat)	37.4				4.00( $\alpha$ ) 2.18( $\beta$ )				
75	1.25	0.12	2.19	16.8	2.18	2.68	2.50	+0.01	-0.01
Cu	0	0.17	2.18	16.3	2.18	2.50			

Table 6.12 Edges of  $\epsilon_2^b(\omega)$ , Ag-Cu solutions

Melt number	Atomic % Au	Edge width	Zero of $D^2$	Max gdt.	$h\omega$	$\epsilon_2^b$ this alloy at $h\omega$	$\epsilon_2^b$ next alloy at $h\omega$	Shift from $\delta\epsilon_2^b$	Shift from zeroes
JM Ag	100		4.09	7.99	4.06	1.47	not calculated		
30R	100		4.00	9.10	4.00	1.09	0.84 <sup>(70)</sup>	+0.025	+0.01
							1.43 <sup>(76)</sup>	-0.035	+0.02
70	99.0	0.26	4.01	8.58	4.00	0.84			
76	93.4	0.20	4.02	7.16	4.00	1.43			
16 (splat)	37.4	not calculated			4.00 <sup>(A)</sup>				
					2.18 <sup>(B)</sup>				
75	1.25	0.12	2.19	17.9	2.18	1.41	1.476	-0.003	-0.01
Cu	0	0.17	2.18	18.4	2.18	1.47			



sample, the latter has only half the gradient of the other samples. The width of the peaks of the derivative seem to be fairly constant. Structure may also be seen at  $\sim 4\text{eV}$  in these curves.

#### The Interband Dielectric Function

This function is plotted as Figure 6.56 for each of the single phase alloys. Those for Ag-rich samples are characterised by a single, sharp rise at  $4.00\text{eV}$  for all three compositions. For the Johnson-Matthey Ag sample, which is not shown, an  $\epsilon_2^b(\omega)$  edge position of  $4.06\text{eV}$  was calculated. The negative values of  $\epsilon_2^b$  at low energies are the result of the inadequacy of the expression used to fit  $\epsilon_2^f$  over a wide range.

Interestingly, the magnitude of the absorption at the edge varies considerably (Table 6.12). The Johnson Matthey Ag and 93.4 at.% Ag (No.76) samples have absorptions of 1.47 and 1.43 respectively, while samples 30R and 70 (Ag and 99.0 at at.% Ag) have absorptions of 1.09 and 0.84 respectively. Sample 76 has broad absorption centred at  $\sim 3.1\text{eV}$ . The difference curves show structure at  $4\text{eV}$  and  $3.1\text{eV}$ , again in proportion to the change in concentration (Figure 6.57). Derivative spectra in Figure 6.58 show a little more clearly the absorption at  $\sim 3.1\text{eV}$  for those samples containing Cu.

#### 6.4.2 Two-phase alloys

##### Reflectance Curves

Spectral reflectance of a set of two-phase Ag-Cu alloys, is given in Figure 6.59, together with results for two samples representing the terminal solid solutions  $\alpha$  and  $\beta$ .

This shows the variation of strength of the absorption edge

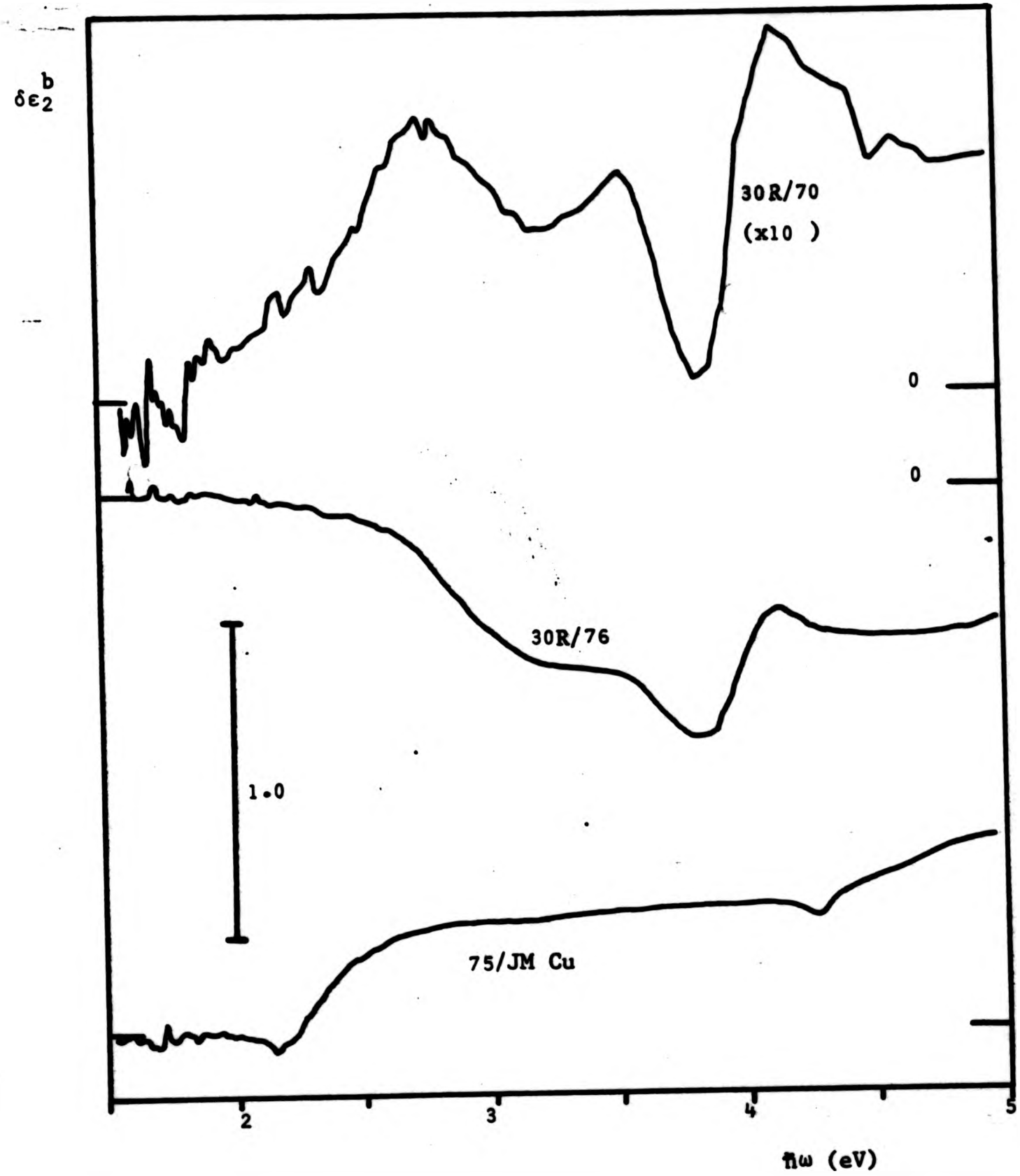


**Figure 6.57.** Change in interband absorption on addition of Cu, single phase Ag-Cu alloys.

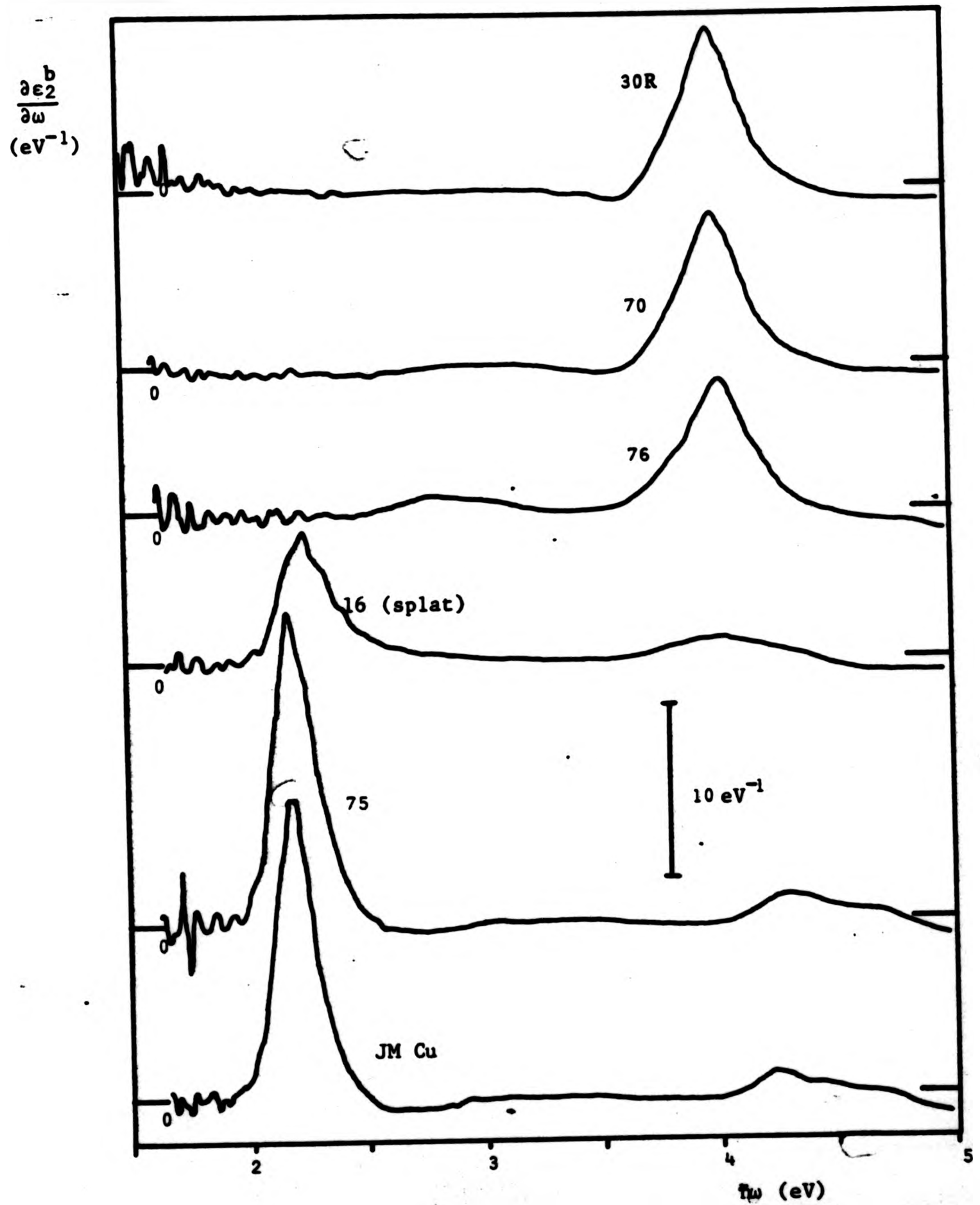


Figure 6.58. Derivative of the interband absorption, single phase Ag-Cu.

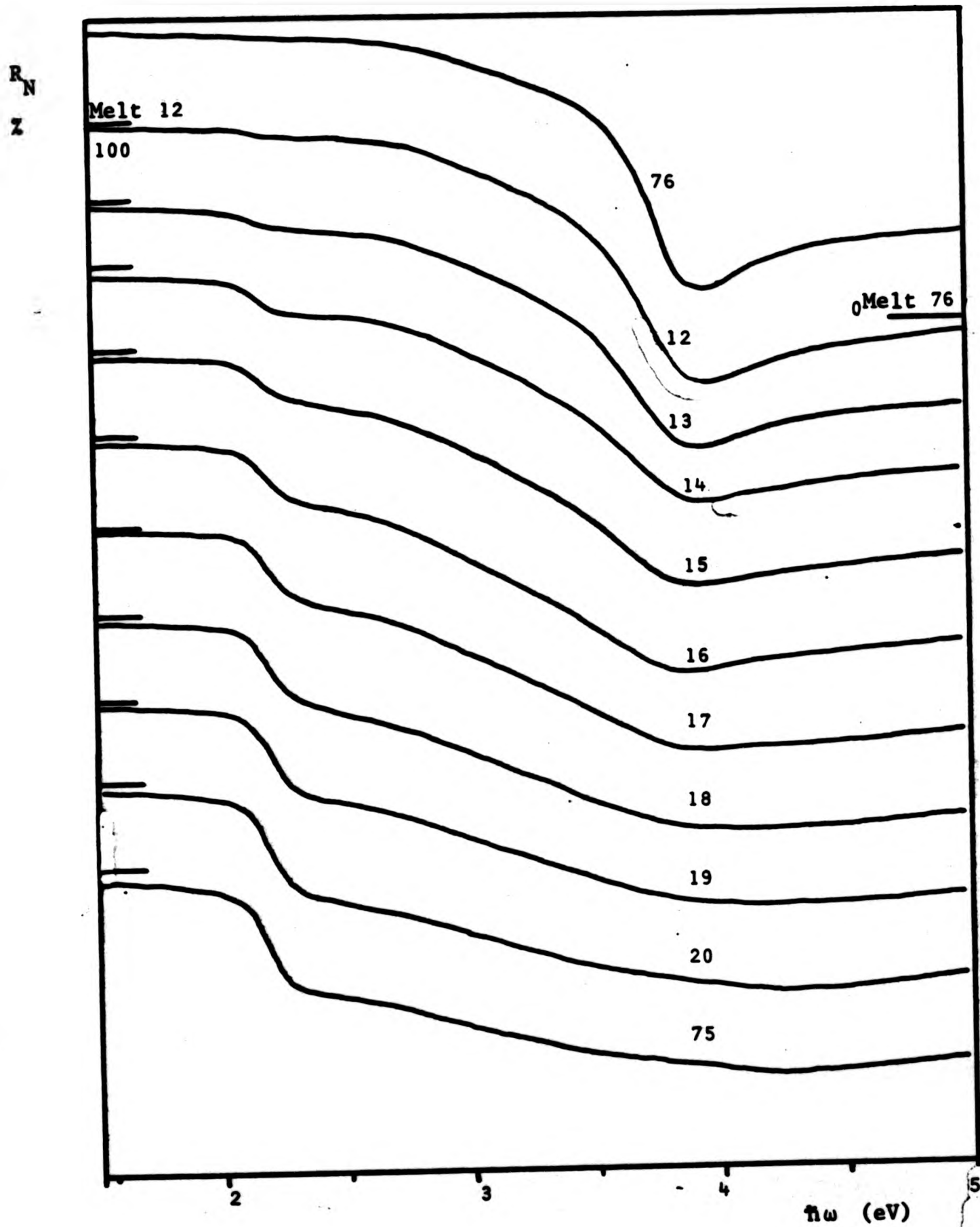


Figure 6.59. Calculated normal reflectance of 2-phase Ag-Cu alloys.

Table 6.13 Edges of reflectance curves, 2-phase Ag-Cu alloys,  $\beta$ -phase edge.

The change in edge position has not been calculated by consideration of  $\delta R_N$ .

Melt No.	Atomic % Ag	Volume fraction $\alpha$ phase %	Edge width	Zero of $D^2$	Max gdt. % $\text{eV}^{-1}$	$h\nu$	$R_N$
76	93.4	100*					
12	83.4	91.2	0.11	2.16	-13.3	2.18	95.6
13	70.1	79.8	0.11	2.15	-30.5	2.16	92.2
14	57.0	67.6	0.13	2.17	-65.1	2.18	87.3
15	47.7	58.3	0.13	2.17	-71.4	2.18	88.4
16	37.4	46.9	0.11	2.17	-92.0	2.18	87.0
17	28.1	36.1	0.11	2.18	-123	2.18	87.3
18	20.2	26.2	0.06	2.18	-135	2.18	84.8
19	12.4	15.7	0.10	2.19	-149	2.18	84.8
20	6.5	7.3	0.11	2.18	-179	2.18	78.4
75	1.25	0*	0.13	2.17	-192	2.18	73.8

\* annealed at 750°C to ensure solid solution

with composition. In the following chapter an attempt will be made to relate these strengths to the volume fractions of the phases present. The difference curves ( $\delta R_N$ , Figure 6.60) have a wide variety of shapes. These suggest changes of edge-width, strength and possibly position in a complicated manner. The derivative curves ( $\partial R_N / \partial \omega$ , Figure 6.61) show structure at 2.17eV and 4.00eV. In the case of the Ag-rich samples, additional weak structure is present at  $\sim 2.7$ eV, while in the case of the Cu-rich samples the 4eV minimum transforms to a small step at  $\sim 4.3$ eV.

#### The Interband Dielectric Function

These are given in Figure 6.62. Structure is present at the same energies as in the reflectance curves, and the overall impression is similar. The low energy edge in the pure  $\beta$ -phase (bottom curve) is rather stronger than that in the pure  $\alpha$ -phase (top curve). The difference curves ( $\delta \epsilon_2^b$ , Figure 6.63) show a negative-going step at low energies (2.17eV) and a positive-going step at high energies (4.00eV), with the exception of that for  $\delta \epsilon_2^b = \epsilon_2^b$  12.4 at.% Ag -  $\epsilon_2^b$  6.5 at.% Ag, which has two positive steps. The shape of all of these curves implies a composition-dependant transition strength, with, in general, the low energy transition increasing in strength with decreasing Ag content while the high energy transition decreases. In the Ag-rich alloys varying absorption between  $\sim 2.5 - 4.5$ eV is also apparent. The derivatives (Figure 6.64) exhibit approximately constant-width peaks of varying strength corresponding to the two main edges. The 4eV peak is somewhat broader than that at  $\sim 2$ eV.

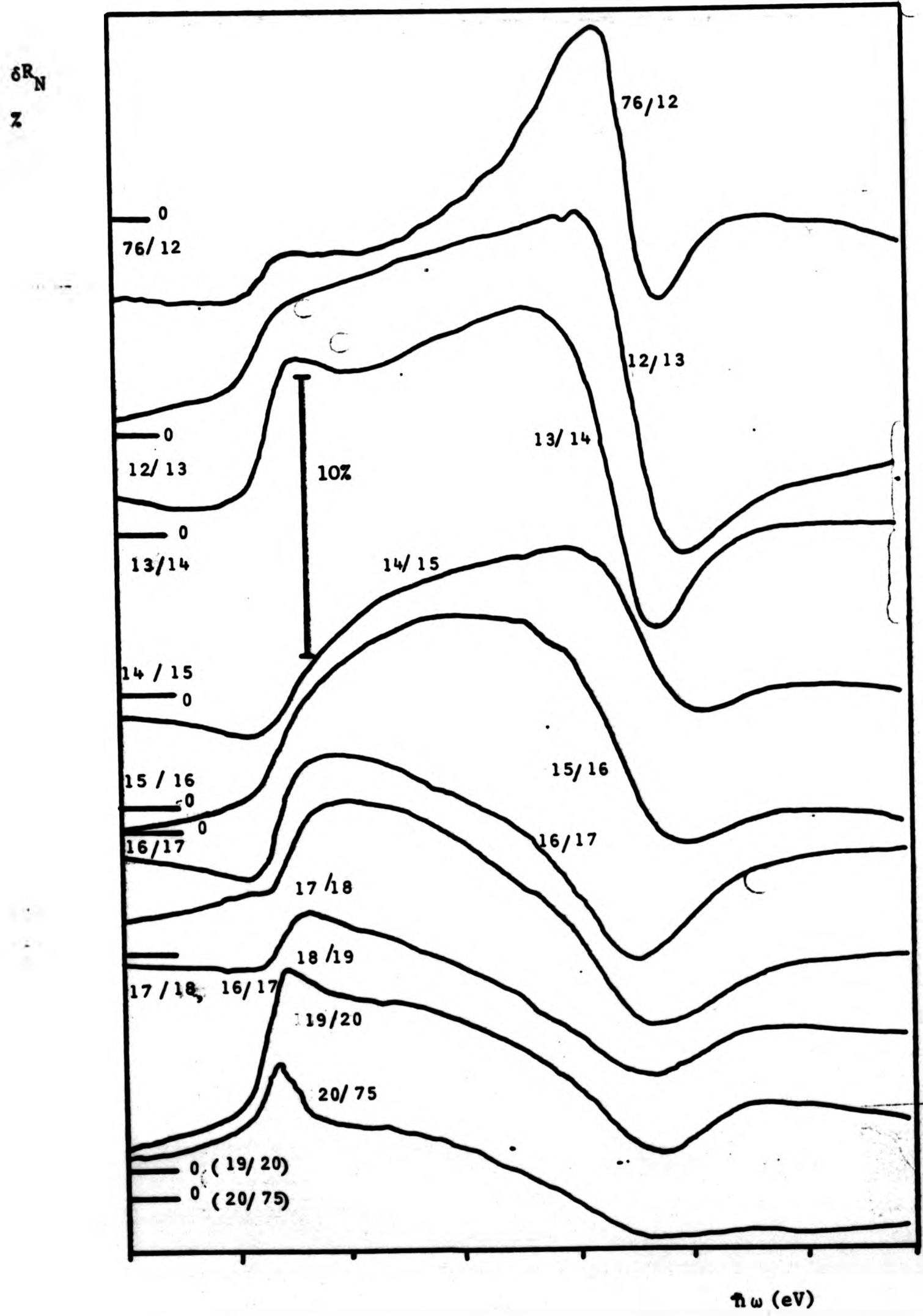
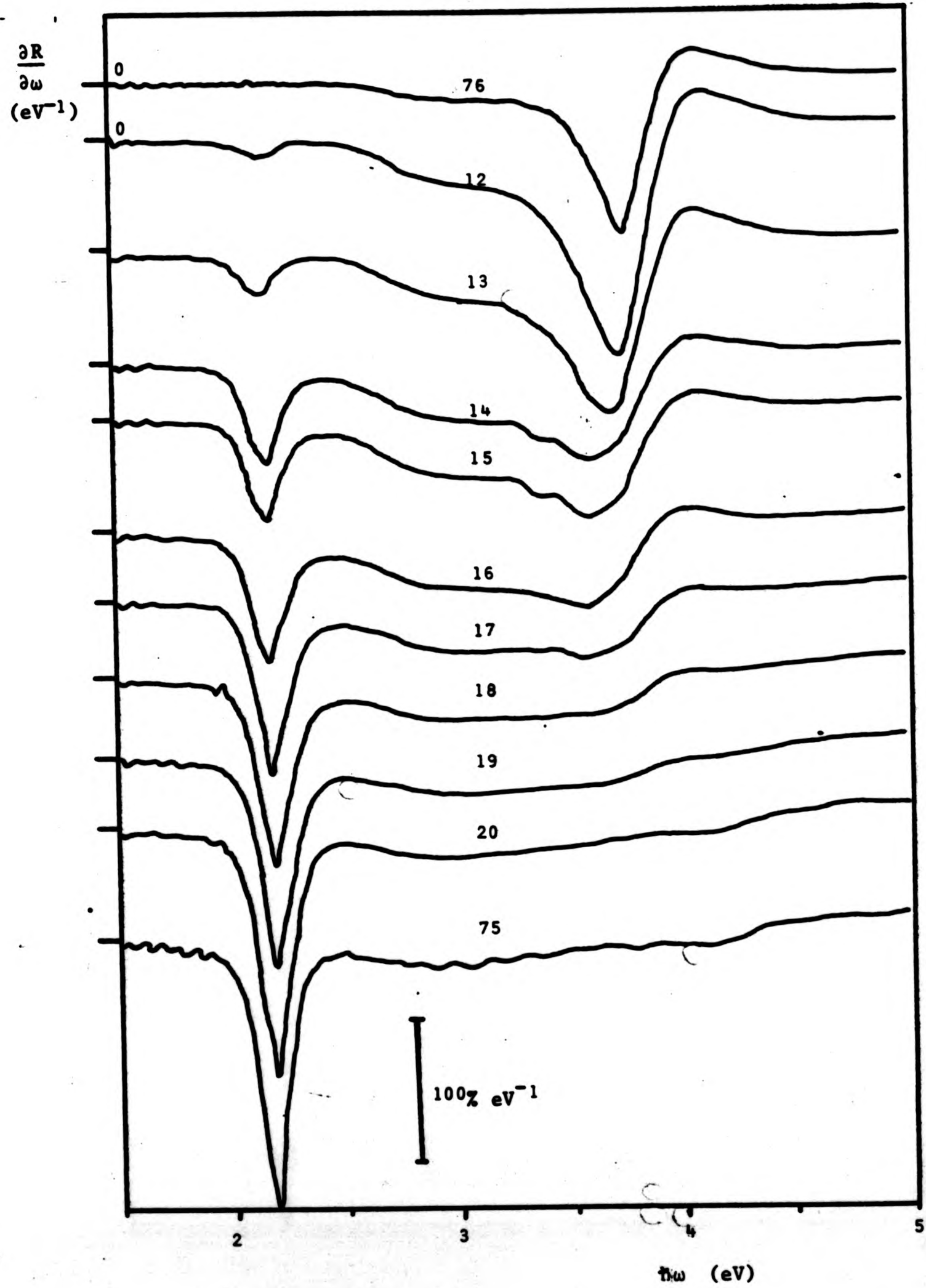


Figure 6.60. Change in reflectance on addition of Cu, 2-phase Ag-Cu alloys.



**Figure 6.61.** Derivative of reflectance, 2-phase Ag-Cu alloys.

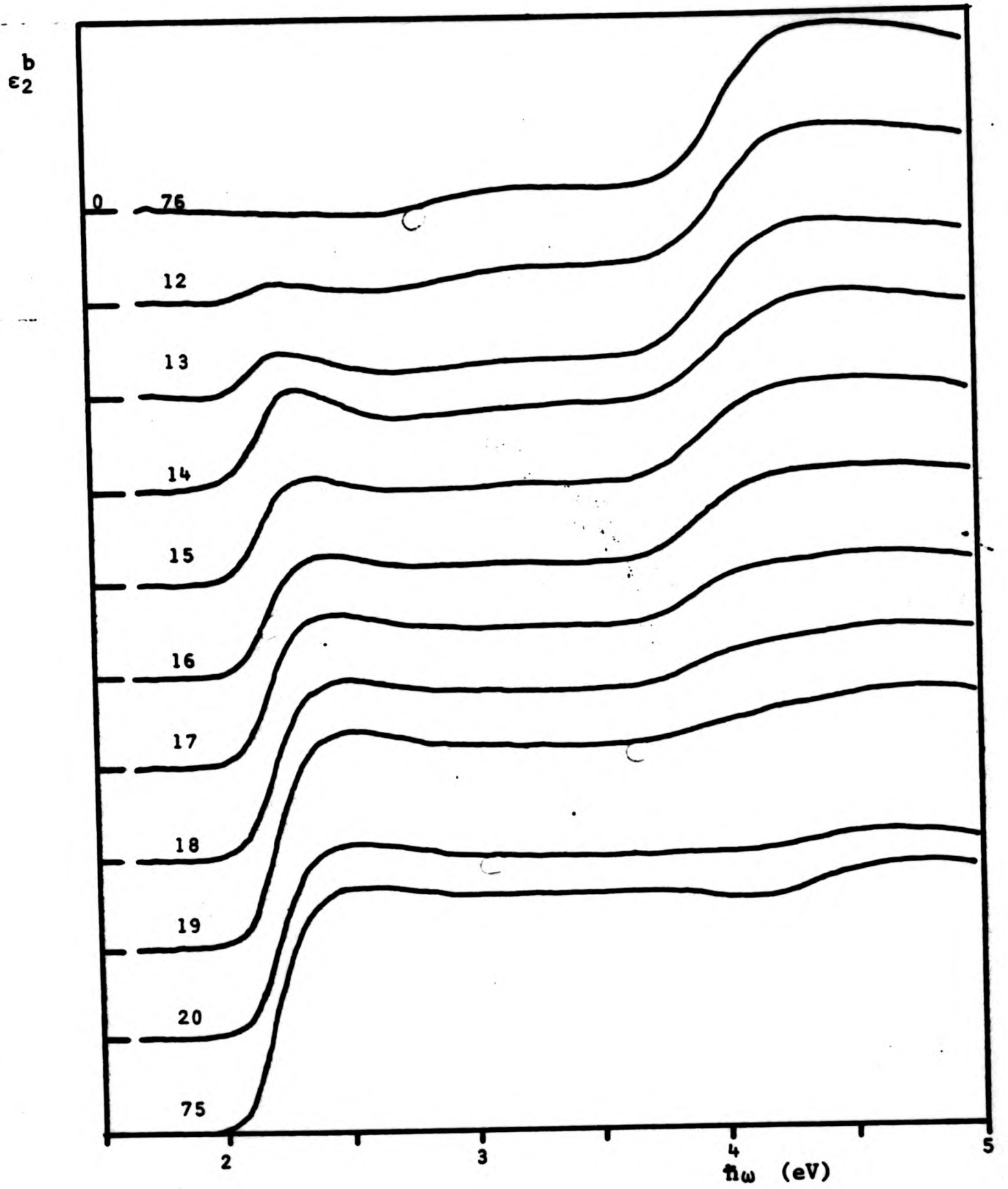


Figure 6.62. Interband absorption of 2-phase Ag-Cu alloys.

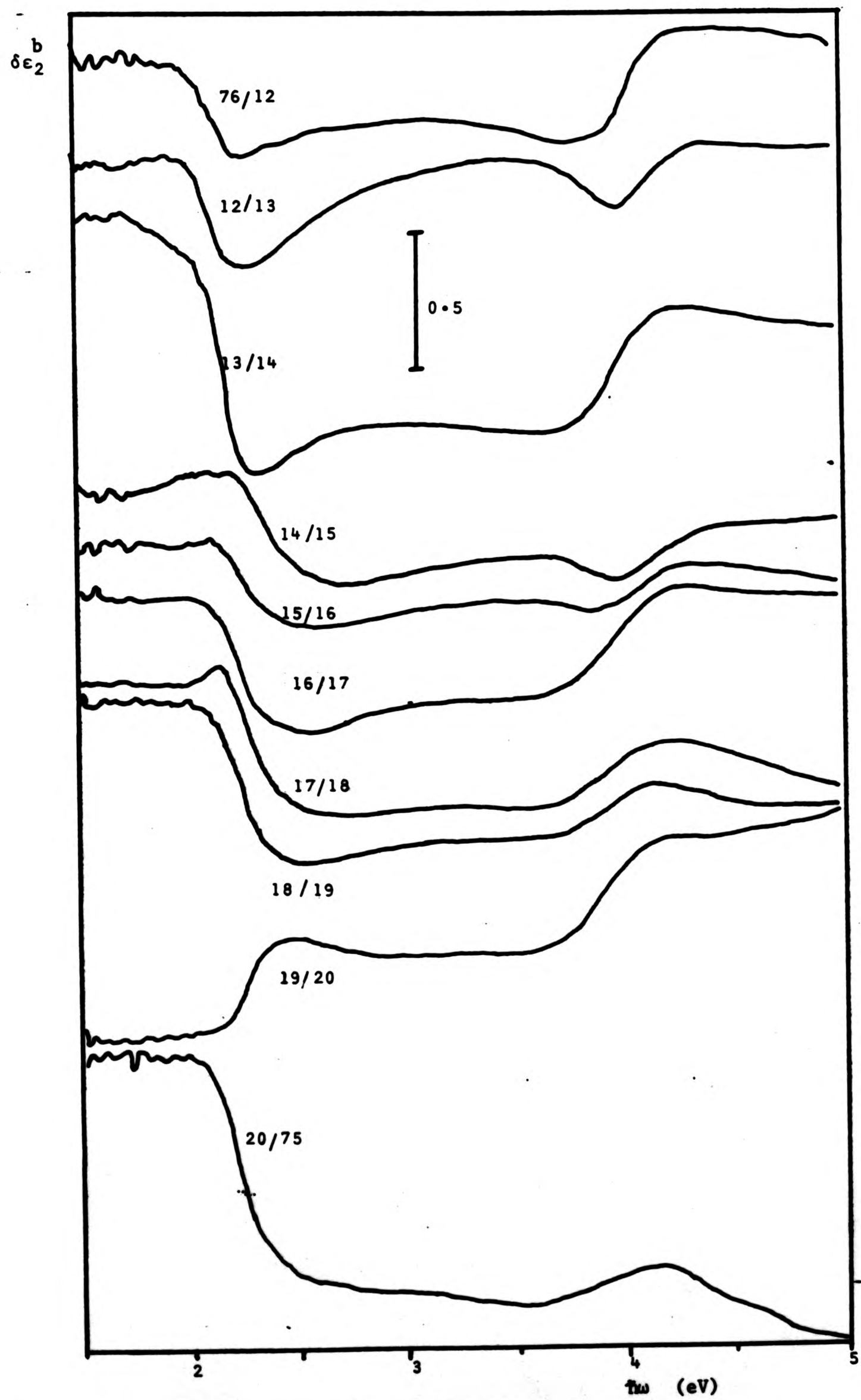


Figure 6.63. Change in interband absorption on addition of Cu, 2-phase Ag-Cu alloys.

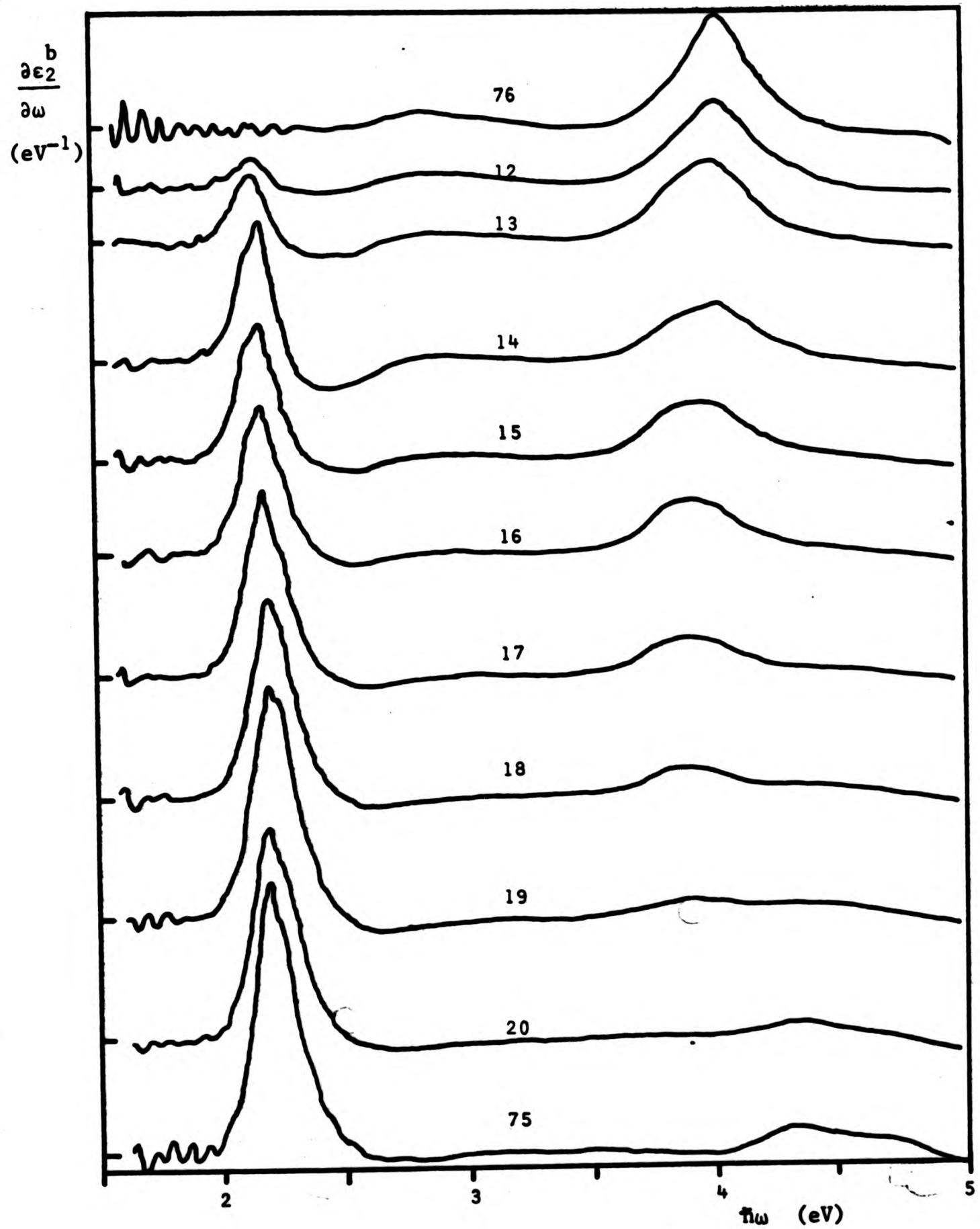


Figure 6.64. Derivative of the interband absorption, 2-phase Ag-Cu alloys.

Table 6.14 Edges of  $\epsilon_2(\omega)$ , 2 phase Ag-Cu alloys,  $\beta$ -phase edge.

Melt No.	Atomic % Ag	Vol. fraction $\beta$ (%)	Edge width eV	Zero of $D^2\epsilon_2(\omega)$ eV	Max gdt $eV^{-1}$	$h\omega$ eV	$\epsilon_2$	$\epsilon'_2 = \epsilon_2 - \epsilon_2(\alpha)$	$\epsilon'_2/vol.fract.\beta$
76	93.4	0	(no absorption edge)			2.14	1.381	-	-
12	83.4	8.8	0.23	2.14	1.44	2.14	0.781	-0.600	-6.82
13	70.1	20.2	0.11	2.15	3.84	2.16	1.51	0.129	0.68
14	57.0	32.4	0.11	2.17	8.23	2.18	1.97	0.589	1.82
15	47.7	41.7	0.13	2.17	8.08	2.18	1.63	0.249	0.597
16	37.4	53.1	0.11	2.17	9.41	2.18	1.64	0.259	0.487
17	28.1	63.9	0.11	2.18	12.0	2.18	1.45	0.069	0.107
18	20.2	73.8	0.14	2.19	12.5	2.19	1.97	0.589	0.798
19	12.4	84.3	0.14	2.19	14.9	2.19	2.13	0.749	0.888
20	6.5	92.7	0.19	2.19	13.3	2.19	2.14	0.759	0.818
75	1.25	100	0.12	2.19	16.8	2.18	2.50	1.12	1.12

Table 6.15 Edges of  $\epsilon_2^b(\omega)$ , 2-phase Ag-Cu alloys,  $\beta$ -phase edge.

Melt No.	Atomic % Ag	Vol. fraction $\beta$ phase %	Edge width eV	Zero of $D^2\epsilon_2^b(\omega)$ eV	Max gdt $\text{eV}^{-1}$	$h\omega$ eV	$\epsilon_2^b$	$\epsilon_2^b/\epsilon_2^b(\text{Melt } 75)$	$\epsilon_2^b/\epsilon_2^b(75) + \text{vol. fract. } \beta$
12	83.4	8.8	0.23	2.14	1.84	2.14	0.128	0.0908	1.03
13	70.1	20.8	0.11	2.14	4.27	2.16	0.426	0.302	1.37
14	57.0	32.4	0.11	2.17	9.22	2.18	1.03	0.73	2.25
15	47.7	41.7	0.13	2.17	8.85	2.18	0.965	0.684	1.64
16	37.4	53.1	0.11	2.17	9.87	2.18	0.985	0.699	1.32
17	28.1	63.9	0.11	2.18	12.2	2.18	1.10	0.780	1.22
18	20.2	73.8	0.14	2.19	13.1	2.19	1.30	0.922	1.25
19	12.4	84.3	0.14	2.19	15.4	2.19	1.50	1.06	1.26
20	6.5	92.7	0.19	2.19	13.9	2.19	1.39	0.986	1.06
75	1.25	100	0.12	2.19	17.9	2.18	1.41	1	1

## 7. DISCUSSION

### 7.1 Experimental Method

The principal aim of the investigation was to provide objective information concerning colours of a commercial alloy system along with physical measurements that would provide background concerning the fundamental processes giving rise to these colours. The commercial application of the work required that mechanically polished surfaces be studied, as these are the type of surface encountered in the industry. For this reason bulk samples were prepared as described in Chapter 3. The method adopted gave samples that were flat and homogeneous, and that could be accurately assayed by conventional techniques. The expense of gold alloy samples prepared in this way meant that only one alloy of each composition was available, but when time allowed repolishing was possible so that this did not necessarily limit the number of surfaces studied. Hardness measurements made on some samples after polishing indicated an unexpected degree of hardening, which could have been quench-hardening or a result of deformation during grinding and polishing. X-ray diffraction measurements indicated no ordering of the AuCu or AuCu<sub>3</sub> alloys, showing that the anneal quench procedure satisfactorily retained the disordered structures. It has often been suggested in the literature that mechanically polished surfaces are unsuitable for providing data on electronic properties due to the existence of the Beilby-like layer, but a great deal of published optical work shows that only trivial differences exist between well-prepared samples of the noble metals.

Accuracy of the optical work was sufficient to discriminate alloying changes of the order of 5 atomic percent. The chief sources of error in the early ellipsometric results were poor setting of the angle of incidence (which was subsequently improved) and birefringence in the Faraday modulator cores. The main source of error in conventional (ocular) ellipsometry is the compensator, but use of an achromatic quarter-wave rhomb minimised errors from this source making measurements in more than one zone unnecessary. Since the compensator was rarely disturbed, small errors will have affected similar alloys in the same way. Birefringence of the silica modulator cores was  $\sim 0.05^\circ$  and was neglected, as was the birefringence of the DEDF cores ( $\sim 0.5^\circ$ ). It was necessary to use both sets of cores during every experiment, so that they would have required re-calibrating each time. This was impractical. Use of a single pair of cores capable of covering the entire spectral range of interest would have made possible the calibration of this source of error in the same way as birefringent windows in electrochemical cells or vacuum apparatus are calibrated. This could be achieved by using longer silica cores with a higher modulation current. Alternatively, the use of liquid filled cores is an attractive possibility. These would be cheap to construct in any length and would be free of birefringence.

Sample alignment was a significant source of error during these experiments. The situation was improved by incorp-

oration of the dial-gauge described in Chapter 3, but this did not provide an improvement in the absolute determination of the angle of incidence. Calibration of the dial-gauge in terms of angle of incidence could be provided using accurately constructed prisms in the sample position.

### 7.2 Performance of Computer Programs

It is inappropriate to discuss the detailed performance of the computer systems developed as part of this study in terms of efficient use of computer resources (such as data storage and processor time), at a time when these can be provided cheaply compared with the user's time. The most important criterion is the level of satisfaction felt by users of the systems. Members of the Ellipsometry Group at City of London Polytechnic have been able to use the systems to analyse ellipsometric data with no need of programming knowledge and after only minutes rather than hours of instruction.

The most serious shortcoming of the computer programs is their lack of portability. In general, it is obviously preferable that computer programs should be usable on many different machines so that as wide as possible a community can take advantage of the effort spent in their production. In the present case this aim has been sacrificed in order to provide maximum ease and security of use by taking advantage of language facilities not available in any of the common programming languages available. Also, development time was greatly reduced

by using the most suitable rather than the most universal languages.

As far as possible, techniques were used that generated concise and relevant computer output. Thus graphical output, particularly of spectral data, was preferred to the printing of large tables. Least-squares methods were used to analyse experimental data obtained on filmed systems, as this is much more convenient than methods which rely on visual inspection of large quantities of theoretical results (as in the well-known program of McCrackin, 1969), and also much more reliable than mathematically primitive techniques such as pattern searches for 'best' values of film thickness and refractive indices, used by, eg. Schewchur and Rowe (1970). Multiple-angle-of-incidence (Schueler 1969), multiple-film (Oldham 1969) and Lorentzian function fitting techniques (Roth et al 1974) have all been implemented, using the non-linear optimisation method of Powell (1964) in all cases. This provides excellent convergence (at some cost in increased computer time) even when initial guesses for the unknown parameters are as much as 50% above or below the optimal values. Use of these programs has been limited by the necessity of extreme absolute accuracy in the ellipsometric data. This made it impractical to pursue the study of tarnishing effects as part of this project, in view of the peripheral nature of the problem. Initial study (Section 7.3.2) showed that room-temperature tarnishing over periods of  $\sim 2$  hours could

not affect the colours of these alloys to any significant degree.

Full documentation of the computer programs has been provided elsewhere (Clarke 1978).

### 7.3 Effects of Sample Preparation

#### 7.3.0 Comparison of results from two experiments

The results of different experiments are influenced by various causes; notably sample preparation (considered in this section) and composition (which will be considered subsequently). It is necessary only to discuss variations in  $\epsilon_2(\omega)$ , as  $\epsilon_1(\omega)$  is causally related. Differences in the shape of  $\epsilon_2(\omega)$ , due to intraband effects, can be analysed in terms of differing  $\tau$  and  $m^*$ , but differences in interband absorption are more difficult to treat. The simplest analysis is in terms of the absorption strength (magnitude of  $\epsilon_1$  peaks in  $\epsilon_2^b$ ), and the position and widths of structure, such as peaks and edges in  $\epsilon_2^b$ . The latter two effects are more easily identified if the spectra which are being compared are normalised to have the same overall strength. This can be done by choosing a photon energy and using the ratio of the two  $\epsilon_2(\omega)$  at this energy to scale one of the spectra. Alternatively, a scale factor can be chosen to minimise the difference between the spectra over a range of energies. The least-squares optimal scale factor  $s$  is here defined as that which minimises the sum-of-squares residual

$$\sum_i (s\epsilon_{2i} - \epsilon'_{2i})^2$$

where  $\epsilon_{2i}$  and  $\epsilon'_{2i}$  are also the values of the two spectra at energy  $\hbar\omega_i$ . Consideration of the derivative of this expression with respect to  $s$  leads to an equation

$$s = \frac{\sum_i \epsilon'_{2i} \epsilon_{2i}}{\sum_i \epsilon_{2i}^2}$$

### 7.3.1 Effects of sample finish

#### Comparison of results for fine gold with data from J Rivory

Rivory's gold data were obtained using non-opaque thin films prepared in vacuo and annealed. The films were microcrystalline but annealing will have reduced the amount of structural disorder and deposition strains within the grains. However annealing will also assist surface segregation of impurities. Our data has been obtained on a mechanically polished gold sample, which is expected to have resulted in a heavily deformed layer, having a large number of defects within each grain (but quite possibly room temperature recrystallization might occur in pure gold at room temperature).

The computed colour of an opaque sample having the same optical constants as Rivory's is both brighter and more saturated than our own; also, the dominant wavelength is shorter. In terms of reflectance, the difference in luminance (14%) is accounted for by the much greater reflectance of the annealed sample - 16% larger (in absolute terms) just below the absorption edge where the

eye is most sensitive. The difference in saturation is a result of the increased magnitude of the step in  $R(\lambda)$  - a 12% greater step, despite the fact that Rivory's sample is still reflecting 4% more than ours at short wavelengths. When one turns to the function  $\epsilon_2(\omega)$ , it appears that her sample has a greatly reduced absorption in the red where free electron effects dominate, but a larger absorption in the blue (interband) region. In terms of the parameters  $m^*$  and  $\tau$ , the difference in optical mass appears negligible, but our relaxation time is a factor of 5 shorter than Rivory's, suggesting much increased conduction electron scattering by defects and grain boundaries in our samples. This accounts for the reflectance difference for  $\omega < 2.5\text{eV}$  ( $\lambda > 500\text{nm}$ )

Shorter wavelengths are dominated by the term  $\epsilon_2^b(\omega)$  in  $\epsilon_2(\omega)$ . Rivory's sample has an  $\epsilon_2^b(\text{max})$  of  $\sim 6.7$  compared with 4.7 for our own, (both samples have this maximum at 3.87eV), explaining the larger step in  $R(\lambda)$  and the reflectance difference in the blue and ultra-violet. Also, structure in  $\epsilon_2^b(\omega)$  is marginally sharper in her sample than in ours, which is also understandable in terms of reduced disorder. It has previously been noted that increasing disorder increases  $\epsilon_2$ , but this is necessarily true only of 'free electron' absorption (which dominates  $\epsilon_2$  in copper in the visible), particularly when  $\tau$  is relatively large. The implication of this work is that disorder reduces  $\epsilon_2^b$ , but the mechanism in this case is

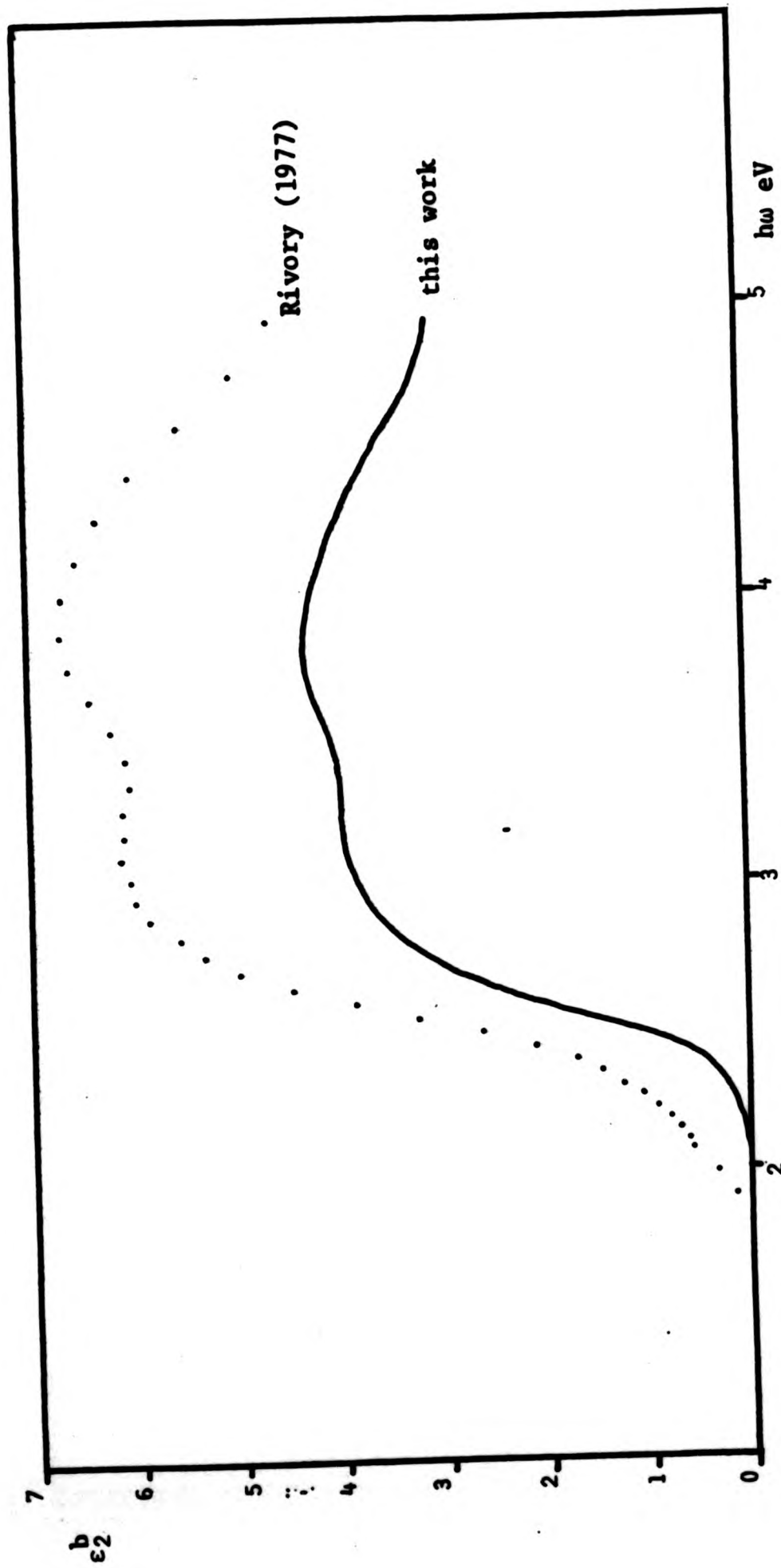


Figure 7.1 Interband absorption of fine gold. Both functions were obtained by fitting the experimental  $\epsilon_2$  in the interval  $650 < \lambda < 850 \text{nm}$  by a function of the form  $\epsilon_2/\lambda = a\lambda^2 + b$ .

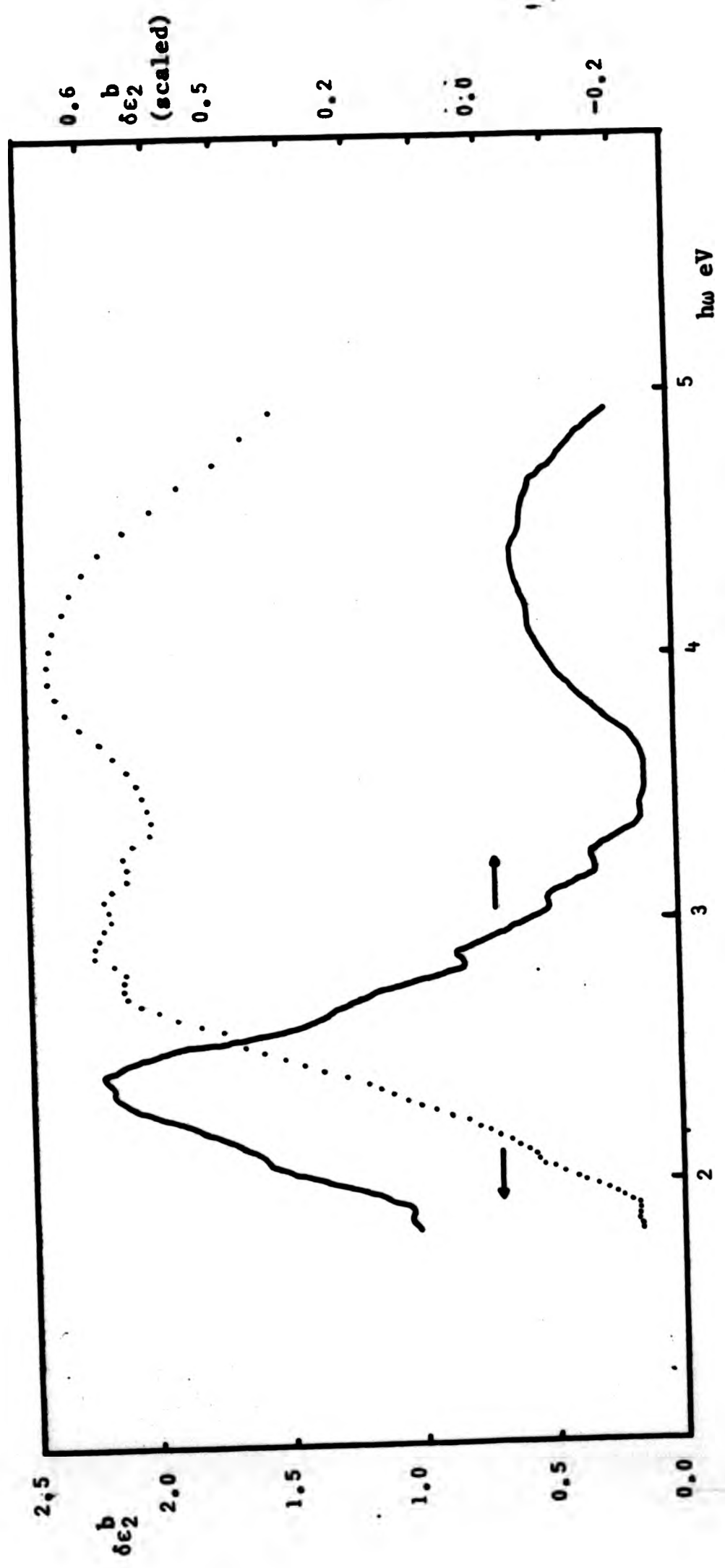


Figure 7.2. The difference between the interband absorption measured by Rivory (1977) and that of this work, for fine gold. Dotted curve (left axis) difference between the curves of Figure 7.1. Full curve (right axis), difference when Rivory's data is scale by 0.62, to match it to this work at 3eV. The low energy peak implies a difference in the edge position of 0.06eV.

not clear. Electronic states giving rise to interband absorption must be dependant on the degree of crystal perfection, so that in a grossly defective surface, from which all periodicity is absent, certain states and their associated absorption peaks could be completely suppressed. The ratio 4.7:6.7 is equal to 0.69, giving the scale difference at 3.87eV. It has previously been commented (eg. Beaglehole 1972) that variations in sample preparation, in the same laboratory, produced variations in reflectance of up to 5%, but without changing the structure of the spectral curves. Contrary evidence is provided by Miller (1970) who found that the strength of  $\epsilon_2^b$  for gold was unaffected by melting, which will produce a larger increase in long-range disorder than can exist in a room-temperature sample.

#### Comparison of results for copper

In the case of fine gold, it has been established that interband absorption begins near 1.5eV (Theye 1971, Rivory 1977), increasing slowly up to 2.5eV where there is the well-known sudden rise. It is not, therefore, surprising that calculations of  $\tau$  and  $m^*$  assuming intraband absorption between 2eV and 1.7eV (the low energy limit of our data) give different results from those calculated over the range 0.5 to 1.0eV; even so, the variation is not large. In the case of copper, our results give widely different results (for the intraband absorption) from those in the literature. The differ-

Table 7.1 Comparison of Results for Fine Gold

	$\epsilon_2^b(2.53\text{eV})$	$\epsilon_2^b(3.26\text{eV})$	$\epsilon_2^b(3.87\text{eV})$
This work	1.76	4.26	4.65
Rivory (1977)	3.26	6.15	6.75
Ratio	1.6	1.5	1.3

	$\frac{\partial \epsilon_2^b(2.53)}{\partial \omega}^{(1)}$	edge width <sup>(2)</sup>	$\delta \epsilon_2^b(3.87\text{eV})^{(3)}$
This work	10.2		
Rivory (1977)	11.9		

(1) per electron volt

(2) difference between the energies where the second derivative has its minimum and maximum (d-FS)

(3) after subtraction of the background due to d → FS transitions starting at 2.5eV.

ences cannot be explained in terms of reasonable variations in the parameters; rather an explanation must be sought in tarnishing effects leading to incorrect values of  $\epsilon_2(\omega)$  or in the nearness of the absorption edge. These points are amplified in the following sections, but it is appropriate to mention here that Rivory's data corroborates results found in the literature when analysed at the lowest energies, but gives results similar to the present ones in the energy interval 1.7  $\rightarrow$  2eV. (See Table 7.2 for values of  $\tau$  etc., from Rivory at  $\sim 2\mu$  and  $\sim 0.75\mu$ ).

### 7.3.2 Effects of Tarnishing

It is well-known that room temperature tarnishes form on silver- and copper-rich alloys, having a profound effect on the surface colour of these metals. On silver (and sterling silver) a black sulphide tarnish forms, which can cause yellow interference effects during the early stages of its growth. On copper a reddish cuprite phase appears, and again interference effects are produced; in this case the pink hue of the fresh copper surface is made more intense, to an orange-red. Other workers have shown that cuprite is the thermodynamically favoured oxide on Au-Cu alloys for gold concentrations up to 70 atomic percent. Higher carat alloys tarnish so slowly that the oxide formed is negligible.

Burge et al (1969) found an initial tarnishing rate for air-formed  $\text{Ag}_2\text{S}$  on silver of  $0.6\text{\AA} \text{ hr}^{-1}$ , for a measured concentration of atmospheric  $\text{H}_2\text{S}$  and  $\text{SO}_2$  of 0.2 parts per billion. Johnson and Bashara (1971) give the film

thickness of air formed  $\text{Ag}_2\text{S}$  on silver as only  $\sim 13\text{\AA}$  after seven days, but do not state the laboratory atmosphere concentration of  $\text{H}_2\text{S}$  and  $\text{SO}_2$ . Given this slow rate of growth, sulphide tarnishes on the silver rich alloys have been neglected, but it is worth pointing out that the surface plasma frequency is expected to be shifted to lower energies, compared with the peak in  $\text{Im}(1/\epsilon + 1)$ , by the presence of a surface film.

The influence of an oxide layer on copper-rich samples has received attention from several points of view. Firstly, the appearance of these alloys when viewed in air is strongly modified by the presence of films which may be  $15 - 20\text{\AA}$  after only a few hours exposure. The limiting film thickness is about  $45\text{\AA}$  at room temperature (Winterbottom 1955.)

As described in Chapter 3, copper samples were finished by polishing with  $\frac{1}{2}$  micron diamond paste, washing with pure soap solution ('Teepol') and rinsing with distilled water. At this point, an adsorbed layer some  $5\text{\AA}$  thick consisting of  $\text{O}_2$  and  $\text{H}_2\text{O}$  can be expected; during the course of the experiment this will be replaced by up to  $20\text{\AA}$  of  $\text{Cu}_2\text{O}$ . Pells and Shiga (1969) measured the optical constants of copper at room temperature, using electro-polished samples given a reducing anneal at high temperatures and low pressures to remove contamination. Rivory (1977) prepared continuous thin films of copper in vacuum and measured the refractive index by a combination of reflection and transmission measurements. It was not stated, however,

whether the films were exposed to air before or during the optical work. Calculations have been made using the numerical data of Pells and Shiga and of Rivory, for comparison with and interpretation of the current results. The spectral refractive index  $\hat{n}(\omega)$  for bulk cuprite obtained by Roberts and Rastall (1979) has been used to represent the film, and Pells' and Shiga's data for the substrate, as this is known to have been obtained on clean copper. Table 7.3 shows the variation of colour for this system with film thickness, and the computed colours using the data of Rivory for an alloy  $\text{Ag}_6\text{Cu}_{94}$ . From our own data, we find no significant difference between copper and a Ag-Cu alloy of 1.25 at.% silver; nevertheless, these results may not be directly comparable, particularly as Rivory's sample was in a vapour-quenched metastable form.

Luminance can be seen to fall rapidly and saturation increases rapidly as the film thickness increases. Dominant wavelength decreases, but slowly. Copper samples measured here had a luminance (computed assuming no film to be present) corresponding to between  $20\text{\AA}$  and  $30\text{\AA}$  of  $\text{Cu}_2\text{O}$  on copper. The saturation implies a film thickness of  $20\text{\AA}$ . One sample was polished and left in the laboratory unprotected for several months, after which time the oxide film caused noticeable reddening of the sample. Similar calculations gave a luminance corresponding to a film thickness of  $45\text{\AA}$  to  $50\text{\AA}$  but a saturation suggesting  $20\text{\AA}$  again. The thicker the oxide layer, then the less acceptable is the use of the pseudo-constants to compute the

**Table 7.2 Rate of change of Drude-like conduction electron parameters with contaminant film thickness. Substrate  $\text{Ag}_6\text{Cu}_9$  (Rivory 1977) and film  $\text{Cu}_2\text{O}$  (Roberts and Rastall 1979). The results of the calculation depend on the energy or wavelength interval over which the fitting is performed.**

Interval	$\frac{\partial \tau}{\partial d}$ (s nm <sup>-1</sup> )	$\frac{\partial \epsilon_1^b(0)}{\partial d}$ (nm <sup>-1</sup> )	$\frac{\partial \hbar\omega_p}{\partial d}$ (eV nm <sup>-1</sup> )
650-850nm	$0.62 \times 10^{-15}$	2.77	0.12
1 $\mu$ -2 $\mu$	$0.22 \times 10^{-15}$	0.29	-0.30

**Table 7.3a Rate of change of computed colorimetric values with contaminant cuprous oxide thickness.**

These were obtained by using clean substrate data for  $\text{Ag}_6\text{Cu}_9$  (Rivory 1977) and copper (Pells and Shiga 1969), and comparing these results with those obtained using the pseudo-refractive indices corresponding to  $20\text{\AA}$  of film.

CIE 1931 Standard System, Illuminant C, Normal Reflectance

	$\frac{\partial x}{\partial d} (\text{nm}^{-1})$	$\frac{\partial y}{\partial d} (\text{nm}^{-1})$	$\frac{\partial L(\% \text{ nm}^{-1})}{\partial d}$	$\frac{\partial \lambda d}{\partial d}$	$\frac{\partial s(\% \text{ nm}^{-1})}{\partial d}$
Rivory	0.0056	0.0038	-1.81	-0.5	2.51
Pells and Shiga	0.0041	0.0026	-1.82	-0.6	1.77

**Table 7.3b Rate of change of computed absorption, calculated as above for a Ag Cu substrate.**

$\lambda$ nm	$\frac{\partial \epsilon_2 (\text{nm}^{-1})}{\partial d}$	$\frac{\partial \epsilon_2^f (\text{nm}^{-1})}{\partial d}$	$\frac{\partial \epsilon_2^b (\text{nm}^{-1})}{\partial d}$
250	-0.073(-1.1%)	-0.032(-5%)	-0.041(-0.7%)
500	-	-0.124(-6%)	-0.417(-8%)
800	-0.40 (-9%)	-	-

reflectance. The exact equations have been used to compute the ellipsometric parameters  $\Psi(\omega)$  and  $\Delta(\omega)$  for systems of  $\text{Cu}_2\text{O}$  on copper, which have then been used to derive pseudo-constants, reflectance and colour coordinates. This indicates that for a  $20\text{\AA}$  film, use of the pseudo-constants would cause the film thickness to be under-estimated by  $2-3\text{\AA}$ , from the calculated luminance and saturation. Using  $\lambda_d$ , the thickness would be overestimated by  $\sim 10\text{\AA}$  but due to the small changes ( $\delta\lambda_d \sim 2\text{\AA}$ ) this figure could vary widely.

The sensitivity of chromaticity, luminance etc. to film thickness is further illustrated by the partial derivatives (w.r.t thickness) of these parameters, in Table 7.3. A just-noticeable-colour-difference would result from  $\sim 10\text{nm}$  of oxide. The variation shown is that found using a range of different substrate-and film-constants including those of Rivory (1977) for  $\text{Ag}_6\text{Cu}_9$  and Pells and Shiga (1967) for copper.

Variation of computed free-electron parameters with thickness of oxide film.

Copper data of Rivory (1977) and cuprite data of Roberts and Rastall (1979) have been used to calculate ellipsometric data for systems of cuprite on copper in the wavelength range  $2.5\mu$  to  $620\text{nm}$ . In turn these have furnished pseudo- $\hat{n}$  values which have been analysed to give  $\tau$ ,  $m^*$  and  $\epsilon_1^b(0)$ . Thus the variation of these parameters with contaminant film thickness has been obtained. The change in apparent Drude-like relaxation time is about 10% of the measured value per nanometre

of oxide, in the wavelength interval 650 - 850nm, and about 5% in the interval 1 - 2  $\mu$ . At the shorter wavelengths Rivory's copper data yields a value some 10% larger than at the longer wavelengths; a possible explanation for this would therefore be the presence of some 2nm of cuprite tarnish. The effect of contamination on the apparent value of  $\epsilon_1^b(0)$  is much less - 1% of the measured value - whereas the effect of using the shorter wavelength interval to calculate this quantity is to increase it by about 30%. It seems likely, therefore, that anomalously large values of  $\epsilon_1^b(0)$  are not the result of using tarnished samples. Calculated values of the plasma energy are much greater between 650 and 850nm than between 1 $\mu$  and 2.5 $\mu$ . The tarnish acts to depress values at long wavelengths and increase them at shorter wavelengths, but the effect is too small by a factor of four to account for the discrepancy.

Computed values of the conduction electron relaxation time have been shown to increase with oxide film thickness, by about 10% of the typical value per nanometre of film. However, measurements on a sample allowed to age for several months in the laboratory atmosphere at room temperature yielded a value only 50% of the typical value for a fresh sample. This is inexplicable in terms of oxide formation (clearly visible) or self-annealing, which both act in the opposite direction. Unfortunately, it was not possible to obtain infra-red measurements of this sample in its original condition as the equipment

**Table 7.4** Sample-to-sample variation of  $h\omega_p$ ,  $\epsilon_1^b(0)$   
 ( $\lambda = 500\text{nm}$ ). Free-electron fitting was performed over  
 $650 < \lambda < 850\text{nm}$ . Although a clear correlation exists  
 between  $h\omega_p$  and  $\epsilon_1^b(0)$ , these are not correlated with  
 $\epsilon_2^b$ , ie. the interband absorption strength.

	$\epsilon_2^b$	$h\omega_p$	$\epsilon_1^b(0)$
Copper(this work)	3.537	9.32	15.60
" (tarnished)	1.8	10.00	25.00
" (this work)	3.717	12.05	37.33
Ag <sub>6</sub> Cu <sub>94</sub> (Rivory)	3.4	12.59	43.76
Copper (this work)	4.694	12.93	40.67
" ( " " )	3.317	14.58	64.97
" ( " " )	3.8	17.33	96.30

had not then been obtained, and so there remains the possibility that this particular copper surface was much more damaged than those produced subsequently. It is also important to bear in mind the possible variations in  $\text{Cu}_2\text{O}$  optical properties as a result of differing growth conditions. It has been observed that a positive correlation exists between the values of  $\epsilon_1^b(0)$  and  $h\omega_p$  (see particularly the various values for pure copper in Section 6.3). In view of the fact that Beaglehole (1966) obtained a reasonable value for the effective free electron mass using only short wavelength data, it seems most probable that the assumption of constant  $\epsilon_1^b(\omega)$  is breaking down near the absorption edge. If this were the whole explanation, one would expect a correlation between the magnitude of the interband absorption near the absorption edge, and  $\epsilon_1^b(0)$ . However, not only do  $\epsilon_1^b(0)$  and  $h\omega_p$  vary by as much as, or more than 100% between samples of the same composition for changes in  $\epsilon_2^b$  at 500nm of  $\sim 5\%$ , but no correlation at all is observed within this range of variation.

### 7.3.3 Optical effective masses of the f.c.c metals Ag, Au and Cu Theory.

For any free-electron gas, there exists a frequency  $\omega_p$  such that  $\epsilon_1(\omega_p) \sim n(\omega_p) \sim 0$ . This frequency can be measured using optical techniques, and is related to the microscopic properties of the metal:

$$\omega_p^2 = \frac{4\pi Ne^2}{m}$$

Table 7.5a Numerical values (from 'The Science Data Book' by R M Tennent 1971).

$\hbar$	6.5821845	$\times 10^{-16}$	eV s
e	4.80325	$\times 10^{-10}$	e.s.u
$m_0$	9.10956	$\times 10^{-28}$	g

Table 7.5b Lattice parameters and electronic density of Ag, Au and Cu from 'Alphabetical Index of Work on Metals and Alloys'.

	$a(\text{\AA})$	$a^{-3}(\text{\AA}^{-3})$	$a^{-3}(\text{\AA}^{-3}/2)$	$N(=4a^{-3})(\text{cm}^{-3})$
Ag	4.0862	$1.4657 \times 10^{-22}$	0.12106	$5.8628 \times 10^{22}$
Au	4.07833	$1.4742 \times 10^{-22}$	0.12142	$5.8968 \times 10^{22}$
Cu	3.6147	$2.1173 \times 10^{-22}$	0.14551	$8.4692 \times 10^{22}$

Table 7.5c Electronic density using bulk values for the density

	At.wt. (g mol <sup>-1</sup> )	At.wt. (g)	$\rho$ (g cm <sup>-3</sup> )	$N(\text{cm}^{-3})$
Ag	107.87	$1.7912 \times 10^{-22}$	10.494 <sup>(1)</sup>	$5.8586 \times 10^{22}$
Au	196.97	$3.2707 \times 10^{-22}$	19.32 <sup>(2)</sup>	$5.9069 \times 10^{22}$
Cu	63.55	$1.0553 \times 10^{-22}$	8.95 <sup>(3)</sup>	$8.4813 \times 10^{22}$

Avagadros's No.  $6.0222 \times 10^{23}$  at.mol<sup>-1</sup>

(1) Silver, vacuum annealed for 24 hrs at 600°C (Vette and Foote, 1935)

(2) Weast (1971)

(3) Scientific Encyclopaedia, Van Nostrand, 1971.

where c.g.s units are used; note that  $\omega_p$  is a circular frequency.  $N$  is the conduction electron concentration ( $\text{cm}^{-3}$ ),  $e$  the electronic charge (e.s.u) and  $m$  the electronic mass (g). In practice, the periodic potential of the lattice causes the relation between energy and momentum for the electrons to depart from the parabolic behaviour expected for free electrons:

$$E \neq \frac{p^2}{2m_0}$$

In order to use a classical description of conduction behaviour it is therefore essential to use an effective mass  $m^*$ ,

$$E = \frac{p^2}{2m^* m_0}$$

This is conventionally measured in electronic masses and not grams, so that values of  $m^*$  of order unity can be expected.

The quantity  $N$  can be calculated from crystallographic data. For an f.c.c lattice there are four atoms per unit cell, and the volume of a unit cell is simply equal to the cube of the lattice spacing ( $a$ , cm).

Thus

$$N = 4a^{-3} \text{ cm}^{-3}$$

We may therefore write

$$\hbar\omega_p = \hbar \left( \frac{16\pi e^2}{m_0} \right) \left( \frac{1}{m^* a} \right) = b \left( \frac{1}{m^* a} \right)$$

$$b = 4\hbar e \sqrt{\frac{\pi}{m_0}} \quad m^* = \left( \frac{b}{\hbar\omega_p} \right)^2 \cdot \frac{1}{a^3}$$

When  $\hbar\omega_p$  is measured in eV,  $m^*$  in electronic masses and  $a$  in Å, the quantity  $b$  has the value 74.2658. Writing  $\omega_{p1}$  for the plasma frequency, computed assuming unity effective mass,

$$m^* = \left( \frac{\hbar\omega_{p1}}{\hbar\omega_p} \right)^2$$

Using published values of the lattice constants, one obtains values of 8.9906, 9.0174 and 10.8064 eV for the plasma frequencies of silver, gold and copper respectively. However, structural imperfections may alter the actual value of  $N$  by a few percent (invariably downwards) introducing uncertainty into calculated values of  $\hbar\omega_p$ .

Typical values given in the literature are  $m^* \sim 1$  for silver and gold,  $m^* \sim 1.45$  for copper. The experimental values of  $\hbar\omega_p$  are similar ( $\sim 8.8$  eV) for all three metals.

#### Experiment

$\hbar\omega_p$  is deduced from experimental data for  $\hat{\epsilon}(\omega)$  for  $\hbar\omega < \hbar\omega_0$ , where  $\hbar\omega_0$  is the energy of the onset of interband transitions.

Using the Drude free-electron theory, the experimental

$\hat{\epsilon}(\omega) = \epsilon_1(\omega) + i\epsilon_2(\omega)$  can be decomposed into 'free'

$\hat{\epsilon}^f(\omega)$  and 'bound'  $\hat{\epsilon}^b(\omega)$  parts:

$$\epsilon_1(\omega) = \epsilon_1^b(\omega) - \frac{\omega_p^2 \tau^2}{(1 + \omega^2 \tau^2)}$$

$$\epsilon_2(\omega) = \epsilon_2^b(\omega) + \frac{\omega_p^2 \tau}{\omega(1 + \omega^2 \tau^2)}$$

These are used to deduce the relation

$$\omega \epsilon_2(\omega) = -\frac{1}{\tau} \epsilon_1(\omega) + \frac{\epsilon_1^b(\omega)}{\tau}$$

As  $\omega \rightarrow 0$ ,  $\epsilon_1^b(\omega) \rightarrow \text{const.}$ , so that this describes a straight line at low frequencies. Also,  $\epsilon_2^b(\omega) \rightarrow 0$  as  $\omega \rightarrow 0$ . Assuming  $\omega\tau \gg 1$ ,

$$\epsilon_2(\omega) = \frac{\omega_p^2}{\tau \omega^3}$$

Thus  $\omega_p$ ,  $\tau$  and  $\epsilon_1^b(\omega \rightarrow 0)$  are obtained. The problems with this method are that  $\epsilon_2(\omega)$  does not show cubic behaviour,  $\epsilon_1^b(\omega)$  does not become constant within the experimental range and for some materials  $\omega\tau \sim 1$ .

As a new approach, it is suggested that the relaxation time be replaced by an empirical expression used by Theye (1970)

$$\frac{1}{\tau(\omega)} = \frac{1}{\tau_0} + b\omega^2$$

And that a Kramers-Kronig transformation of  $\epsilon_2^b(\omega)$  in the experimental range is used to compute a term  $\delta\epsilon_1^b(\omega)$ . The remaining contribution to  $\epsilon_1$ , from  $\epsilon_2^b$  for energies  $\hbar\omega > 5\text{eV}$ , would indeed be constant.

$$\epsilon_1(\omega) = A + \delta\epsilon_1^b(\omega) = \frac{\omega_p^2 \tau^2}{(1 + \omega^2 \tau^2)}$$

$$\delta\epsilon_1(\omega) = \frac{2}{\pi} \int_{\omega_0}^{\omega_{\max}} \frac{\omega \epsilon_2^b d\omega}{\omega^2 - \omega^2}$$

since  $\omega > \omega_0$ , the integral is non-singular.

The only parameters to be determined would then be  $\omega_p$ ,  $A$ ,  $\tau_0$  and  $b$ .

The experimental data for silver and gold give  $m^* 0.98 \pm 0.09$  and approximately 0.95, respectively. In the case of copper, values ranging from 0.8 to 1.1 have been found, compared with values in the literature of  $\sim 1.45$ .

The values of  $\hat{\epsilon}(\omega)$  used in these calculations ( $1.6 < h\omega < 1.9\text{eV}$ ) were for higher  $h\omega$  than those used in most studies ( $0.5 < h\omega < 1\text{eV}$ ). In consequence the spectral variation of  $\epsilon_1^b(\omega)$  will complicate the measured spectrum. If  $\epsilon_1^b$  is assumed to be constant (when, in fact, it is interesting with increasing frequency), then  $\epsilon_1^f(\omega)$  will appear to decrease less rapidly with increasing frequency than is really the case. At these energies, despite the short relaxation times observed,  $\omega\tau > 1$  and therefore

$$\epsilon_1 \sim \epsilon_1^b - \frac{\omega_p^2}{\omega^2}$$

A reduction in the frequency dependence of  $\epsilon_1$  will therefore cause  $\omega_p^2$  to be underestimated, and therefore the optical effective mass to be overestimated. Ehrenreich and Philipp (1962), re-analysing the data of Roberts (1960), suggested correcting the values of  $m^*$  downwards from 1.44 to 1.42 to allow for this effect. Another explanation must therefore be sought for the anomalous

low values of  $m^*$  found in this report.

Data of J Rivory for a thin film composition  $\text{Ag}_6\text{Cu}_4$  has been analysed using the computer program (Clarke 1978) developed for this study to solve the equations of Chapter 4. Pearson (1958) gives the rate of change of volume on alloying silver into copper as  $0.0049 \text{ at.}\%^{-1}$ . Thus  $h\nu_{p1}$ , the plasma frequency, assuming unity effective mass, must be decreased by  $\sim 0.97$  for this data. In the wavelength interval  $2\mu \rightarrow 2.5\mu$  ( $0.5 \rightarrow 1.2\text{eV}$ ) an optical mass of 1.3 is obtained, which is identical with that given by Rivory (1977). However, in the interval  $650 - 850\text{nm}$  ( $1.7 \rightarrow 2\text{eV}$ ), which is the largest available in the present study,  $m^* \sim 0.68$  is found. Clearly a similar discrepancy exists in this data as in those for copper obtained here. Also, the quantity  $\epsilon_1^b(0)$  obtained using Rivory's data is 29.3 at long wavelengths, 40.7 near the edge; presumably this can be related to the frequency dependence of  $\epsilon_1^b$  as the edge is  $\epsilon_2^b$  is approached.

#### 7.4 Effects of Alloying on the Interband Absorption

##### 7.4.1 Interband absorption of Ag-Au alloys

Data was not obtained for all these alloys at sufficiently long wavelengths to enable the function  $\epsilon_2^b(\omega)$  to be derived. For this reason the movement of the absorption edge in  $\epsilon_2(\omega)$  with composition has been studied. This is not completely satisfactory, as the result will depend on the form of  $\epsilon_2^f(\omega)$  - and hence on the relaxation time and optical effective mass - as well as on  $\epsilon_2^b(\omega)$  as determined by the band gap. This can be seen in terms of a contribution to the second

derivative of  $\epsilon_2(\omega)$  from the curvature of  $\epsilon_2^f(\omega)$ , moving the zero of this function to higher energies (Figure 7.3). There will therefore be a systematic overestimation of the band gap energy, and additional errors introduced by the sample-to-sample differences in relaxation time, optical effective mass and the deviation from exact Drude-like free electron absorption. It is apparent from the results (Section 6.2) that these quantities, at least in the samples studied here, do not show a marked dependence on composition and so these errors can be regarded as a random element. The most probable cause of this is the damaged nature of the surface, which, for example, introduces so much electron scattering from structural defects that impurity scattering appears to be negligible. It is also the case that the movement of the fundamental absorption edge in this system is so large (1.5eV) that the effect of these errors is not serious, as it would be in the Au-Cu system where the movement is only 0.4eV. The trend of the absorption edge with composition (Figure 6.34) is within  $\pm 2\%$  of the energy values reported by Rivory (1977). This is better than the experimental bandwidth of the monochromator employed (10nm) in the present study; Rivory does not state the optical bandwidth used. No significant movement of the second absorption peak (at 3.8eV) in the gold-rich alloys occurs on addition of silver; this is also remarked upon by Rivory although she reports the energy of 3.9eV. A shift to lower energies of the edge at 3.5eV was reported by Beaglehole and Erlbach (1972). This could, however, be caused by effects other than movement of the 3.8eV peak,

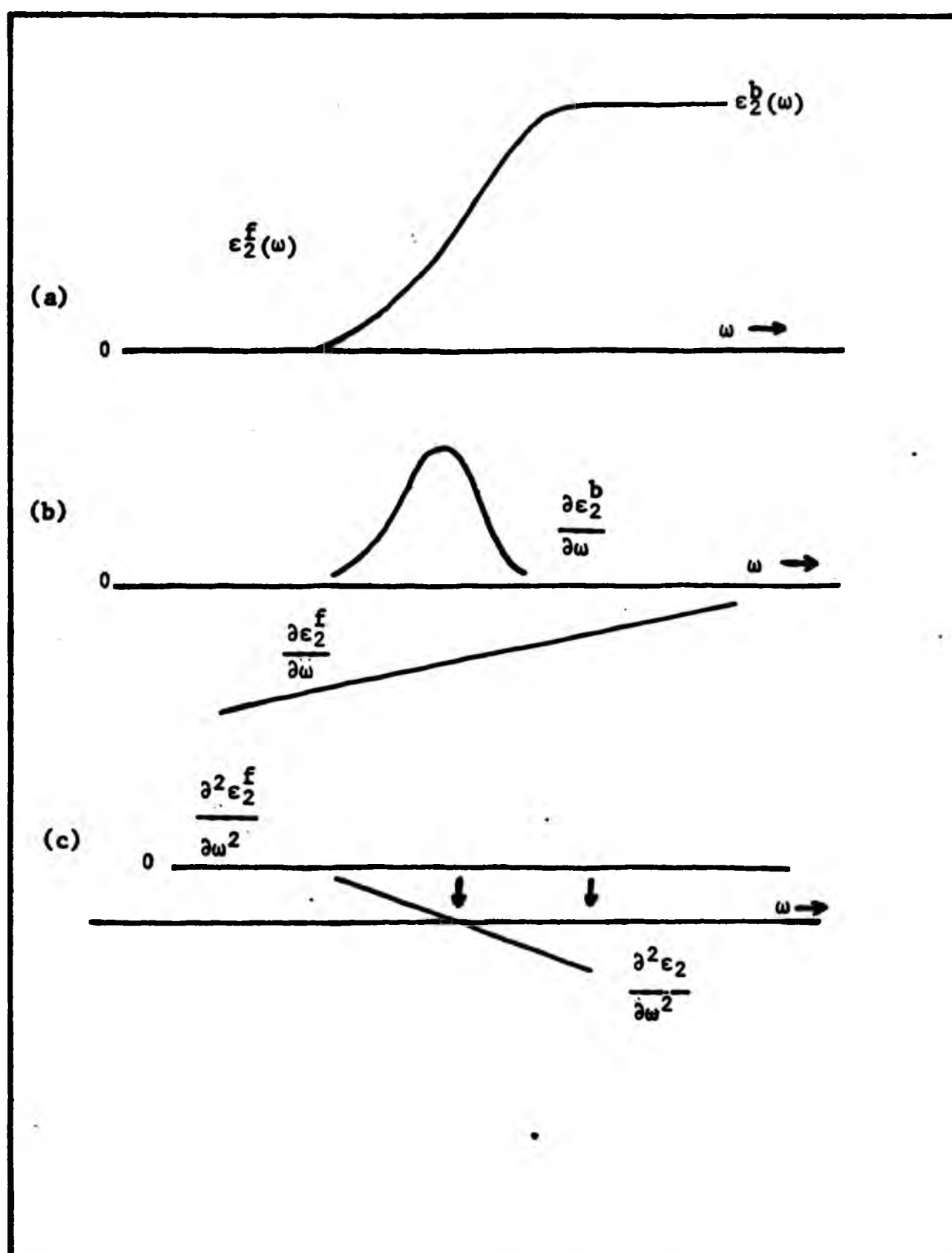


**Figure 7.3**

(a) Ideal forms of the imaginary parts of the dielectric function.

(b) Ideal forms of the first derivatives of (a).  $\epsilon_2^f(\omega)$  has been assumed to be quadratic. The actual index is typically  $\sim 2.3$ .

(c) Ideal forms of the second derivatives.  $\frac{\partial \epsilon_2^b}{\partial \omega}$  has been assumed parabolic near the maximum. Since  $\frac{\partial^2 \epsilon_2}{\partial \omega^2} = \frac{\partial^2 \epsilon_2^f}{\partial \omega^2} + \frac{\partial^2 \epsilon_2^b}{\partial \omega^2}$ , and from  $\frac{\partial \epsilon_2^b}{\partial \omega}$  the positions

of the zeroes (arrowed above) it is clear that considerable of the function  $\epsilon_2(\omega)$  rather than  $\epsilon_2^b(\omega)$  will normally cause

since there are two components (d-band to Fermi Surface and Fermi Surface to conduction band) of  $\epsilon_2^b(\omega)$  at this energy, and they are of similar magnitude. The argument illustrated by Figure 7.3 concerning the influence of  $\epsilon_2^f(\omega)$ , when this cannot be subtracted out, is equally applicable to the problem of separate but overlapping contributions to  $\epsilon_2^b(\omega)$  from different transitions. The exact onset energy of conduction electron transitions cannot be calculated without first subtracting the term due to d-FS transitions, for which a reliable lineshape would be required. This could be performed in a manner similar to that used by Antonangeli et al (1974) when analysing thermovariation data of the optical properties of silver.

The mechanically polished samples measured here show very similar absorption strengths at the two maxima (3.1 and 3.8eV) in the gold-rich alloys. This is in contrast to results on evaporated and annealed films. Beaglehole and Erlbach (1972) and Rivory (1977) both found a ratio of 1.1 for

$$\frac{\text{maximum at } \sim 3.8\text{eV}}{\text{maximum at } \sim 3.0\text{eV}}$$

As previously remarked, the present samples have values of  $\epsilon_2^b(\omega)$  smaller than those of Rivory throughout the whole wavelength range, but evidently the conduction electron transition  $L_2' + L_1$  is weakened relatively more than the d-band transition. It has already been noted (Chapter 2) that the conduction bands are more sensitive to the crystal potential than are the d-bands. Alloying effects do not cause a spread of the conduction electron transitions into the visible

(3.5eV, 380nm) and so it will not be necessary to consider the alloying behaviour of the conduction bands when discussing the colours in the Ag-Au system.

The deviation from linearity of the  $d + FS$  transition in this system can be used to infer the details of electron charge transfer between the silver and gold atoms, when used with a suitable theoretical model. Charge transfer in alloys is interesting, theoretically, as it relates directly (and often simply) to metallurgical (non-optical) properties. Unfortunately the calculation is so sensitive to the theoretical technique used that even qualitative results cannot be relied upon. The first calculation was by E Stern (1966) who employed the Virtual Crystal Model, considering only  $d$ -electrons. A large transfer from gold to silver was found. Levin and Ehrenreich (1971) used the CPA and considered only  $s$ -electrons, finding a net charge transfer, also from gold to silver, of 0.3 electrons per atom. This is in the opposite sense to that expected on the basis of electronegativity ( $Au \sim 2.4$ ;  $Ag$  and  $Cu \sim 1.9$ ), and is also much larger than indicated by Mossbauer experiments. When both  $s$ - and  $d$ -electrons were considered in the CPA (Gelatt and Ehrenreich 1974) a net charge transfer of 0.07 electrons per atom from gold to silver was found;  $d$ -states are evidently transferred from silver to gold. The latter result is in agreement with non-optical work (net charge transfer is small) but confusion still exists: Rivory (1977) implies that total charge transfer has the opposite sense.

#### 7.4.2 Au-Cu alloys

##### Magnitude of the interband absorption.

From the discussion of Section 7.3, it is apparent that sample preparation has tended to reduce the magnitude of  $\epsilon_2^b(\omega)$  from that of an undamaged clean surface. In the case of fine gold, the ratio of our result for the maximum (4.7) to that of Rivory (6.7) was 0.67; for copper the ratio is about 0.54. Koster and Stahl (1967) using sputtered films found a variation of the peak of  $\epsilon_2(\omega)$  of 4.3  $\rightarrow$  6.5 for gold and 4.7  $\rightarrow$  5.5 for copper. As previously pointed out, there may be a tendency for increasing disorder to reduce  $\epsilon_2^b$  whilst increasing  $\epsilon_2^f$ , so that a somewhat smaller variation of  $\epsilon_2$  with surface treatment may be expected. It is reasonable to suppose that the effect of disorder on the magnitude of the absorption is a function of composition, as is the absorption strength for the perfect crystal. It is therefore not possible to separate these effects, using only the present data. Steele and Treherne (1972), who also used mechanically polished samples report a rather small peak value of  $\epsilon_2^b(\omega)$  for fine gold, namely 3.8.

##### Position of the fundamental absorption edge

Discounting the possibility of a low-energy 'tail' in the absorption for gold, the presence of which cannot be confirmed in our data because of the lack of observations below 1.5eV, the onset of interband absorption in both copper and gold can be accepted as due to transitions from the top the d-bands to the Fermi surface over extended regions of the Brillouin zone. It is likely that in both

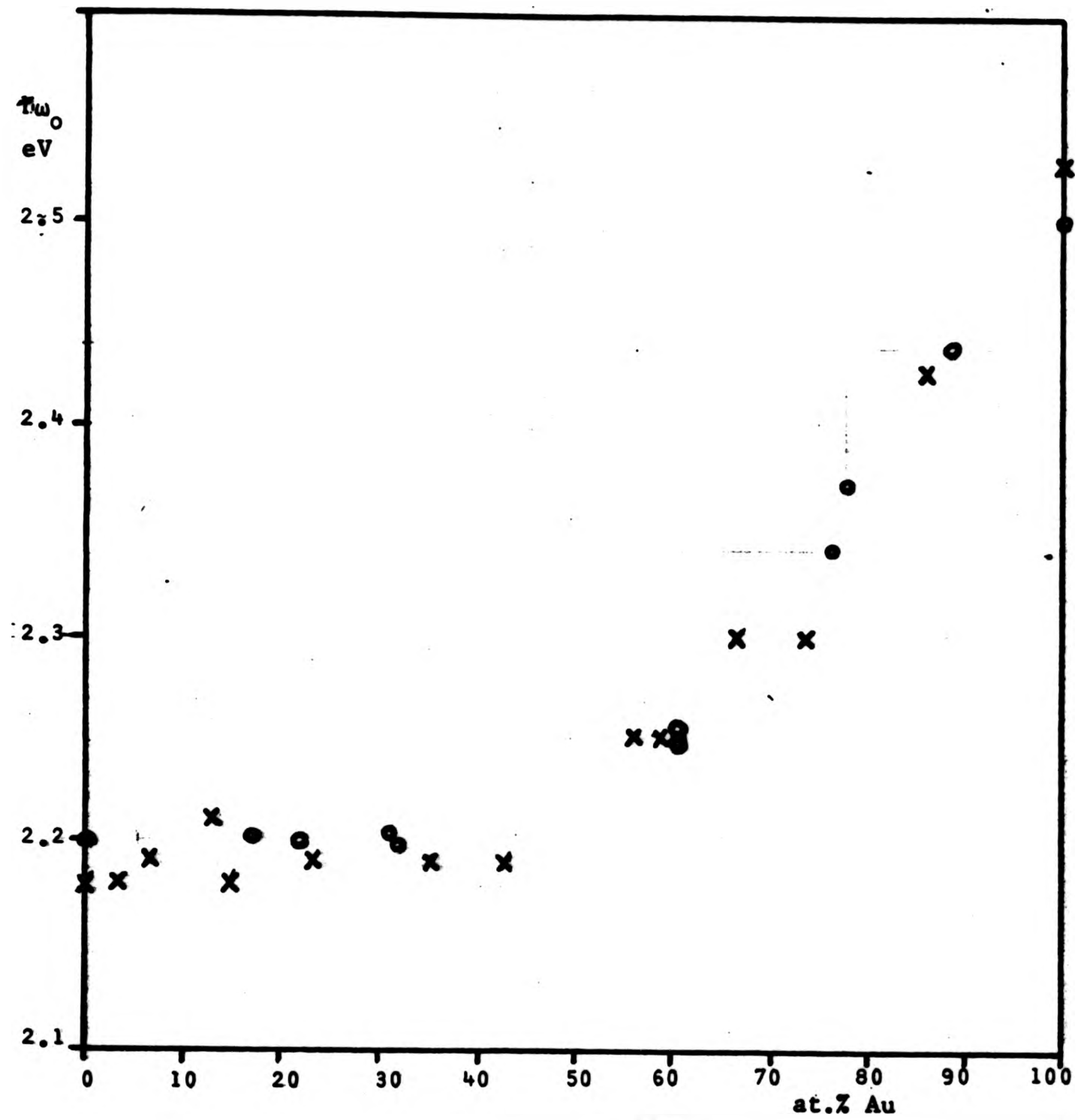


**Figure 7.4** The onset energy ( $\hbar\omega_0$ ) for interband transitions in the Au-Cu system.

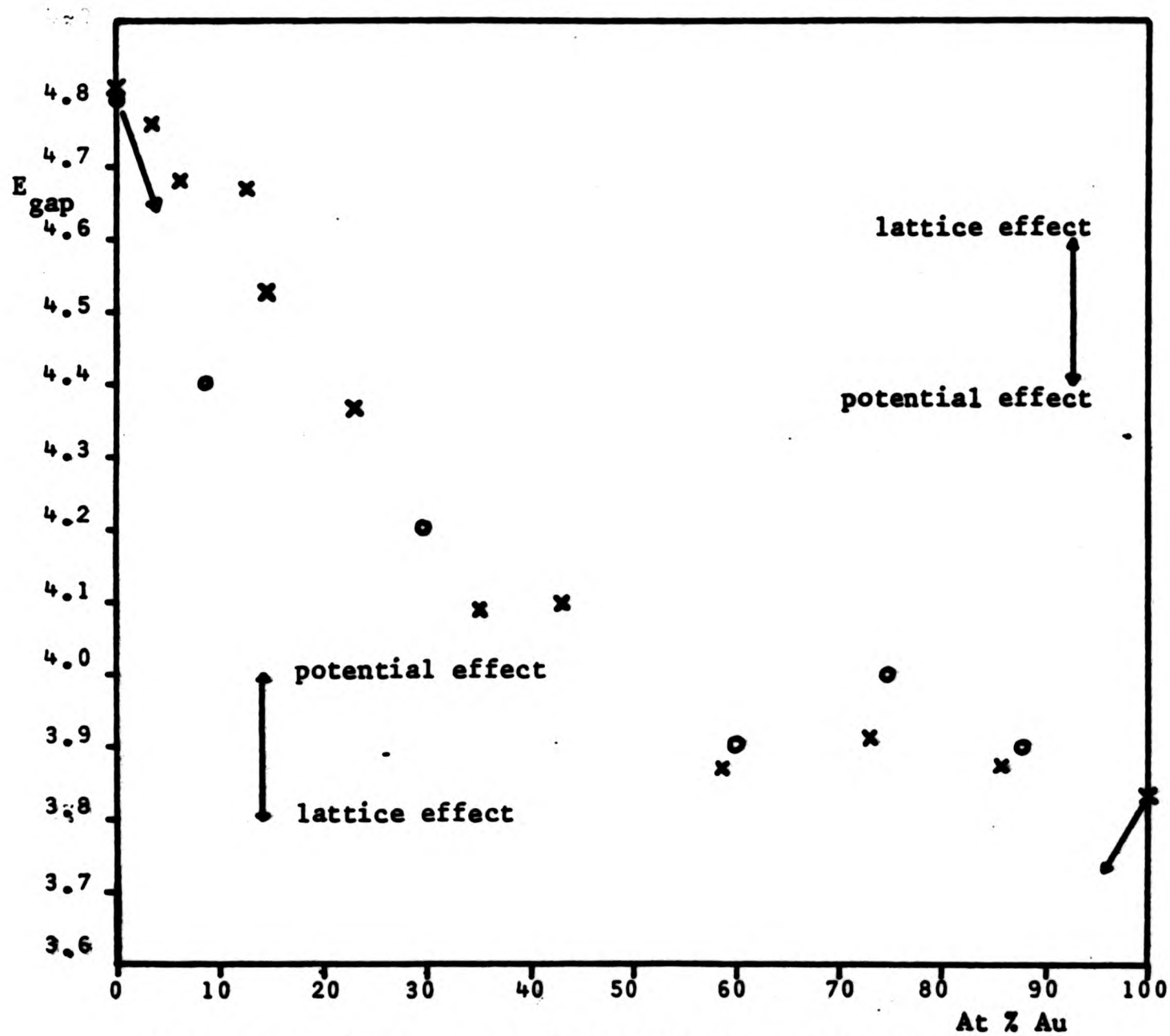


Figure 7.5. Movement of the 3.8eV(Au) - 4.8eV(Cu) peak in the Au-Cu system. Arrows show the results of Beaglehole and Erlbach (1972). Open circles are results of J Rivory (1977) and crosses are from the present work.

metals these take place near L,  $L_5^+ + 6^+ \rightarrow L_4^-$  (FS), and that the variation of onset energy shown in Figure 6.46 represents the change of the energy of this gap with composition. In the initial experiments on these alloys it appeared that the onset energy decreased when moving from pure copper to copper-rich dilute Au-Cu alloys, as reported by Beaglehole and Erlbach (1972), but this was not confirmed in any subsequent experiments. The result is now attributed to an alignment error, causing mis-calibration of the monochromator in its position following the sample. This would explain the low sensitivity of the ellipsometer noted during the particular experiment. Corroboration for this view was provided by an experiment on fine silver, in which a similarly anomalous value for the onset energy was combined with low sensitivity.

Rivory (1977) gives a graph of  $hw_0$  for a set of Au-Cu alloys, defining this quantity as the energy at which  $\epsilon_1^b(\omega)$  reached half its value at the first maximum.

Despite the fact that the energy at which  $\frac{\partial \epsilon_2^b}{\partial \omega}$  is a maximum has been preferred here, these results are consistent with the present work within the experimental scatter (Figure 7.4). No significant movement of the fundamental edge is found for alloys containing up to 50 atomic percent gold; however, the scatter is about  $\pm 0.02$  eV. This is comparable with the wavelength resolution ( $\pm 0.03$  at 2.2 eV). For gold fractions of greater than 50 at.%, the interband onset energy increases rapidly (and almost linearly) to its final value of 2.5 eV. The deviation in onset energy as a function of composition from a simple linear change can be

regarded as negative (that is, the curve lies entirely below the straight line joining the pure gold and pure copper values). This is similar to the behaviour of Ag-Au alloys. The fact that the deviation is more marked can be attributed to the variation in lattice constant in this system. When gold is added to copper, a lattice expansion takes place which, other things being equal, would tend to depress the value of the energy gap. This has been demonstrated by piezo-optical experiments for Au and Cu (Gerhardt et al 1966 and 1968). Where the rate of change of gap with lattice dilation or compression has been measured, it is possible to correct alloying data for lattice effects, leaving a term due only to the ionic potential of the alloying addition. This procedure has been followed by Beaglehole and Erlbach (1972) who assumed that in the case of very dilute alloys piezo data obtained on pure metals could be used. No studies of piezo reflectance of Au-Cu alloys appear to have been made, so that it is not possible to compare the system directly with Ag-Au, as it may be that the negative deviation discussed above is caused entirely by lattice effects, with an unknown (positive or negative) contribution from potential effects. It is therefore not possible to decide whether charge transfer is from gold to copper or vice versa without additional experimental evidence. Alternatively, theoretical calculations of the onset energy could be performed using various values of the charge transfer and specifically including the behaviour of the lattice constant in this system.

When presenting data on the Ag-Au system, calculations were included (Chapter 6) of the change in bandgap on alloying, derived from the gradient at the absorption edge and the absolute change in  $\epsilon_2$  between two samples of slightly different composition. Similar calculations for the Au-Cu system are complicated by the fact that variations of the magnitude of  $\epsilon_2^b(\omega)$  are larger. This is particularly significant when comparing sample 10R (nominal 90% by weight gold) with other alloys of similar composition. This has an absorption ( $\epsilon_2^b$ ) of  $\sim 4.5$  at the first maximum near 3.8eV, compared with  $\sim 3.5$  for the other samples. Again, sample 2 (10Au-90Cu) has a peak  $\epsilon_2^b$  of  $\sim 4$  compared with  $\sim 3.7$  for the pure copper samples. In order to make the computation of  $\delta h\omega$ , the change in bandgap, independent of simple changes in the magnitude of the absorption, the spectra have been scaled to the same value at the maximum before taking the difference (see Figure 7.2 for an example of the effect). This greatly improves the accuracy and sensitivity of the technique, instrumental resolution of the analyser and polariser values being sufficient to detect spectral shifts of about 0.001 eV. It would be necessary to use a monochromator of much higher precision than that presently employed, mounted on the incident arm to avoid resetting errors, in order to fully utilise this sensitivity.

The peak in  $\epsilon_2^b(\omega)$  for fine gold near 3.8eV can be seen to move to higher energies (Figure 6.41) on addition of copper. The mechanically polished samples measured here did not show a true maximum above the absorption edge (the structure

is not clearly defined even for annealed samples, but shows rather as a point of inflection near 3.3eV). This, in common with the edge itself, moved to lower energies upon addition of copper. Between 95Au-5Cu (Melt 77) and 10Au-90Cu (Melt 10R) the inflection develops into a true maximum/minimum at energies of  $\sim 3.0\text{eV}$  and  $3.5\text{eV}$  respectively. The double-maximum structure persists at 80Au-20Cu, becoming more complicated in the alloy 70Au-30Cu (Melt 8). For copper contents of 30% by weight or greater, the structure could be interpreted as a broad flat minimum between 3.0 and 3.5eV, or equally (within the limits of experimental error) as points of inflection at these two energies. The range of compositions (more than 50 at.% copper) over which this feature of the interband absorption does not vary coincides with that over which the main edge shows no significant movement. Some experiments showed a definite maximum near 3.5eV (Melt No.7, 3.54eV). It seems probable that samples with undamaged surfaces would show this more clearly, but the structure is so weak that a precise energy cannot be assigned to it.

The high energy peak (Figure 7.5) not only moves in the opposite sense to the low energy one, but also moves most rapidly at the copper-rich end of the alloy system. The deviation from linearity is again negative. These results may be compared with those of Beaglehole and Erlbach (1972) and Rivory (1977), shown in the same figure. The former authors discuss the movement of the edge at 4.3eV rather than the adjacent peak; this is more amenable when using their experimental technique. Data from the latter

author's work is not given explicitly and has been extracted from Figure 3 of her paper, perhaps with some loss of accuracy. Agreement is encouraging, with the exception that again, the movement of the pure copper edge in the 'wrong' direction upon addition of gold has been observed only by Beaglehole and Erlbach. The more rapid change on alloying at the copper-rich end of the system is consistent with their observation that the potential effect (which they say opposes the lattice-effect in this system) is much weaker for these alloys than for gold-rich ones.

As discussed in Chapter 2, this particular peak in the copper spectrum has been assigned by most authors to transitions from band 2 to band 1 (the first conduction band) near L, ie.  $L_2 \rightarrow L_1$ . A contribution at slightly lower energies  $L_2$  (FS)  $\rightarrow L_1$  is also likely from initial electron states on the Fermi Surface. In the case of gold it is not possible to obtain accurate results using non-relativistic theory and so the smooth shift in peak position in the Au-Cu system cannot be taken as identifying the 3.8eV peak for gold as  $L_2 \rightarrow L_1$ . Bands formed from these by relativistic splitting are  $4^-$  and  $6^-$ , and  $4^+$  and  $6^+$ . Thus the most likely assignments are  $L_{4-} \rightarrow L_{4+}$  and  $L_{6-} \rightarrow L_{6+}$ , as has frequently been suggested by many authors, on the basis of photo emission, piezo reflectance data and band theory calculations.

### 7.4.3 Single phase Ag-Cu alloys

Two silver-rich alloys in this system were prepared. Melt No.70 contained 1 at.% copper; while No.76, containing 6.6 at.% copper, corresponded to the saturated alpha-phase alloy at 600°C equilibrium concentration. Another (metastable) solid solution of approximately 50Ag-50Cu composition (No.16 37.4 at.% silver) was prepared by liquid-solution quenching, and finally Melt 75 contained 1.25 at.% silver, the composition of the saturated beta-phase alloy.

Samples No. 30R (fine silver) and No.70 are compared in Figure 6.57. The difference in interband absorption,  $\delta\epsilon_2^b$ , is nowhere greater than  $\sim 0.1$  or 2%. Structure due to broadening of the absorption edge at 4eV is visible; the centre of this coincides with the peak in  $\frac{\partial\epsilon_2^b}{\partial\omega}$  (Figure 6.58). The broadening of the edge amounts to  $\sim 0.02$ eV. A dip in  $\delta\epsilon_2^b(\omega)$  centred at  $\hbar\omega = 3$ eV corresponds to an impurity absorption band in the 1 at.% copper alloy, also noted by Rivory (1977). In our case, the absorption band has a width of  $\sim 0.5$ eV compared with  $\sim 1$ eV for the vapour quenched, 6 at.% copper sample used by Rivory. Again, the magnitude of this absorption is  $\sim 0.02$  per at.% Cu (Rivory) and 0.03 per at.% Cu (this work). In the same figure,  $\delta\epsilon_2^b$  for 100% Ag and  $\text{Ag}_{93.4}\text{Cu}_{6.6}$  is also shown. Broadening of the 4eV edge is  $\sim 0.05$ eV, with no detectable movement. A new absorption band is evident in the alloy near 3eV, having a width of  $\sim 0.7$ eV and a strength of  $\sim 0.5$ , or slightly less than 0.01 per at.% Cu. In view of the magnitude of the effect, agreement with

Rivory's data for a sample of similar composition could be better. Possibly the discrepancy is due to differences in the way  $\epsilon_2^f(\omega)$  has been fitted. It is interesting to note that the absorption due to small amounts of copper in silver is almost indistinguishable from surface plasmon absorption (induced by surface roughness). However, with larger concentrations of copper or degrees of roughness, the spectra are dissimilar.

Rivory assigns the peak to Virtual Bound State absorption, first described by Friedel(1958). The implication is that the copper d-electrons form localised states, with the occupied states below the Fermi energy but above the highest silver d-state. This existence of this type of state suggests that the width of the copper d-bands is significantly less than the difference in d + FS gaps for copper and silver. The exact formulation can be derived as a special case of the CPA (eg. Elliott 1974).

The spectrum of the 37.4 at.% silver alloy is remarkably similar to that of pure copper. The edge is broader, as would be expected in view of the highly defective lattice, and shifted slightly to higher energies. There is a weak absorption edge at about 4eV which is apparently intermediate between the 4eV silver edge and the copper edge at 4.25eV. It is possible that this relates to the inter-conduction-band contribution to the silver absorption edge ( $L_{4-}(FS) \rightarrow L_{4+}$  and  $L_{4-} \rightarrow L_{4+}$ ), as these transitions have also been cited as responsible for structure in copper at 4.31eV and 4.8eV (Antonangeli et al 1974). Superficially

the reflectance and absorption spectra of the two-phase and liqua-sol alloys of this composition are very similar. On close examination it is apparent that the structures near 2.2eV and 4eV are moved to higher energies in the homogeneous alloy, with the result that in the vicinity of 2.2eV (560nm) the reflectance is enhanced, by about 7.5%. This accounts for the larger value of saturation (18% compared with 13%) as 580nm is also the dominant wavelength of these alloys. The energy difference at 2.2eV is approximately 0.01eV. Rivory (1977) found a shift of this absorption edge of 0.06eV to higher energies, when comparing copper with an alloy containing 44 at.% silver.

Alloy number 74 represents the saturated solid solution at the  $\beta$ -phase boundary, with 1.25 at.% silver. This has an interband absorption 5% greater at 3eV than that of a typical copper sample, which cannot be interpreted as an alloying effect. In order to make the experiments more readily comparable,  $\epsilon_2^b(\omega)$  was scaled to have the same value at 3eV and the difference spectrum recalculated. Without scaling, the peak value of  $\delta\epsilon_2^b$  was  $\sim 0.07$  at 2.2eV, while with scaling the value was 0.2. These results correspond to a shift of the absorption edge of  $\sim 0.003$  and 0.01eV, respectively, to higher energies, on alloying. Even in the Ag-Au system, where large movements of the absorption edge are well established, the effect of a 1 at.% composition change would be only of the order of 0.01eV. It is clear that the experimental technique was

unable to give useful information concerning such dilute alloys, and so this difference is not regarded as significant. Sample-to-sample variation of the edge position for pure copper is also of the order of 0.01eV.

## 7.5 Effects of Alloying on the Intraband Absorption

### 7.5.1 Optical Effective Masses

These have been calculated for dilute Ag-Au alloys, the full range of Au-Cu alloys and for the single-phase Ag-Cu alloys. In general, the experimental values of the plasma energy  $h\nu_p$  are higher than expected for all the samples studied. Possible reasons for this have already been discussed in Section 7.3.3; the presence of superficial contamination and use of energies too close to the absorption edge have been mentioned. In view of the likely decrease in tarnishing rate as the gold content is increased it would be unwise to try to identify alloying effects operating directly on the effective mass in the low carat alloys. Addition of silver to gold appears to raise the plasma frequency (reduce the effective mass); this has also been noted by Beaglehole and Erlbach (1972) and Rivory (1977), but the evidence is weak because of the large uncertainties involved. Similarly, the trend of effective mass on addition of copper to gold seems to be downwards, but the sample-to-sample variation is of the same order or greater than the alloying effect.

### 7.5.2 Drude-like Relaxation time

It is well-known (eg. Mott and Jones 1936) that, for perfect crystals, alloying tends to reduce the electronic relaxation time compared with the pure metal values, due to impurity scattering. The effect is observable optically provided well-annealed samples are used (Rivory 1970). No such effect has been found in the present study. There are a variety of possible reasons for this, the most significant probably being the quantity of structural defects introduced by mechanical polishing. Scattering from defects acts to reduce the relaxation time, masking the effect of impurities. The effect of using pseudo-optical constants for the relaxation time calculation has also been investigated; the presence of likely contamination films would be to increase the computed value ( $\sim 0.6 \times 10^{-15}$  sec nm<sup>-1</sup>). Using Rivory's (1977) data it has been shown that values are in accord with those in the literature only for energies of less than 1eV, at higher energies shorter relaxation times are found. This anomalous behaviour is extremely variable, some samples even giving negative relaxation times. Such behaviour invariably disappeared when the sample was repolished. Hunderi (1973) offers a model which may go some way to explain these results. Work performed on silver samples with a micro-crystalline structure indicated strong absorption ( $\epsilon_2 \sim 20$ ) at energies below the interband threshold, which Hunderi interpreted as due to the stimulation of plasma oscillations in grain boundaries, which formed a large proportion of the volume of his

samples. It has frequently been suggested that mechanical polishing produces a defective, microcrystalline surface, as shown by electron diffraction studies. Only a small amount of plasmon absorption at energies of about 1 - 2eV would be sufficient to explain the present results. Interestingly, Stahl et al (1969) show an absorption spectrum for a sputtered Au-Cu alloy which has a non-Drude-like tail in this energy range.

#### 7.6 Heterogeneous Alloys

The most striking feature of the spectral curves for the two-phase Ag-Cu alloys is that they are not (considered one composition at a time) qualitatively different from those for the various homogeneous alloys studied. This is so despite the fact that all the optical and electronic theory used to derive these functions was derived for homogeneous media. Most pertinently, the question that arises is, "Do these 'effective medium' calculations offer genuine insight into the behaviour and properties of the metals?" In particular, does use of an effective dielectric function give a worthwhile approximation to the reflectance in typical viewing conditions? If not, the CIE colour coordinates derived in Chapter 6 do not represent the colour variation with composition in this system.

Micrographic examination of the alloys revealed the expected mixture of eutectic and  $\alpha$ - or  $\beta$  primary phases. Homogenisation of the samples by mechanical working resulted in an extremely fine mixture of the phases such that even at the limit of resolution of optical microscopy the finest

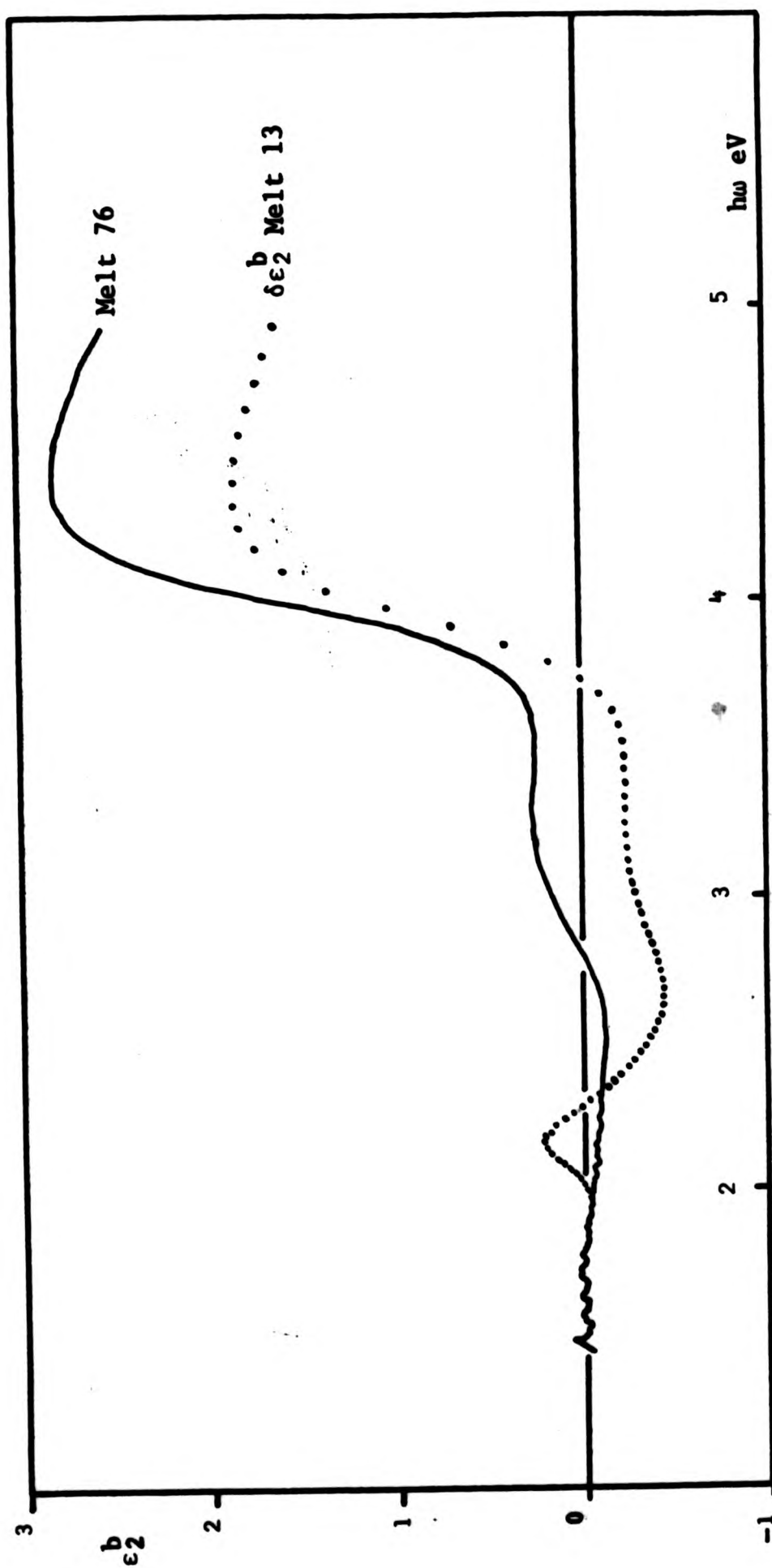


**Figure 7.6** The full curve shows the interband absorption of a saturated  $\alpha$ -phase Ag-Cu alloy. The experimental absorption of sample Melt 13 has had a term equal to 0.202 times the absorption of a saturated  $\beta$ -phase alloy subtracted, yielding a function  $\delta\epsilon_2^b$ . Note the peak in  $\delta\epsilon_2^b$  near to 2.2eV.

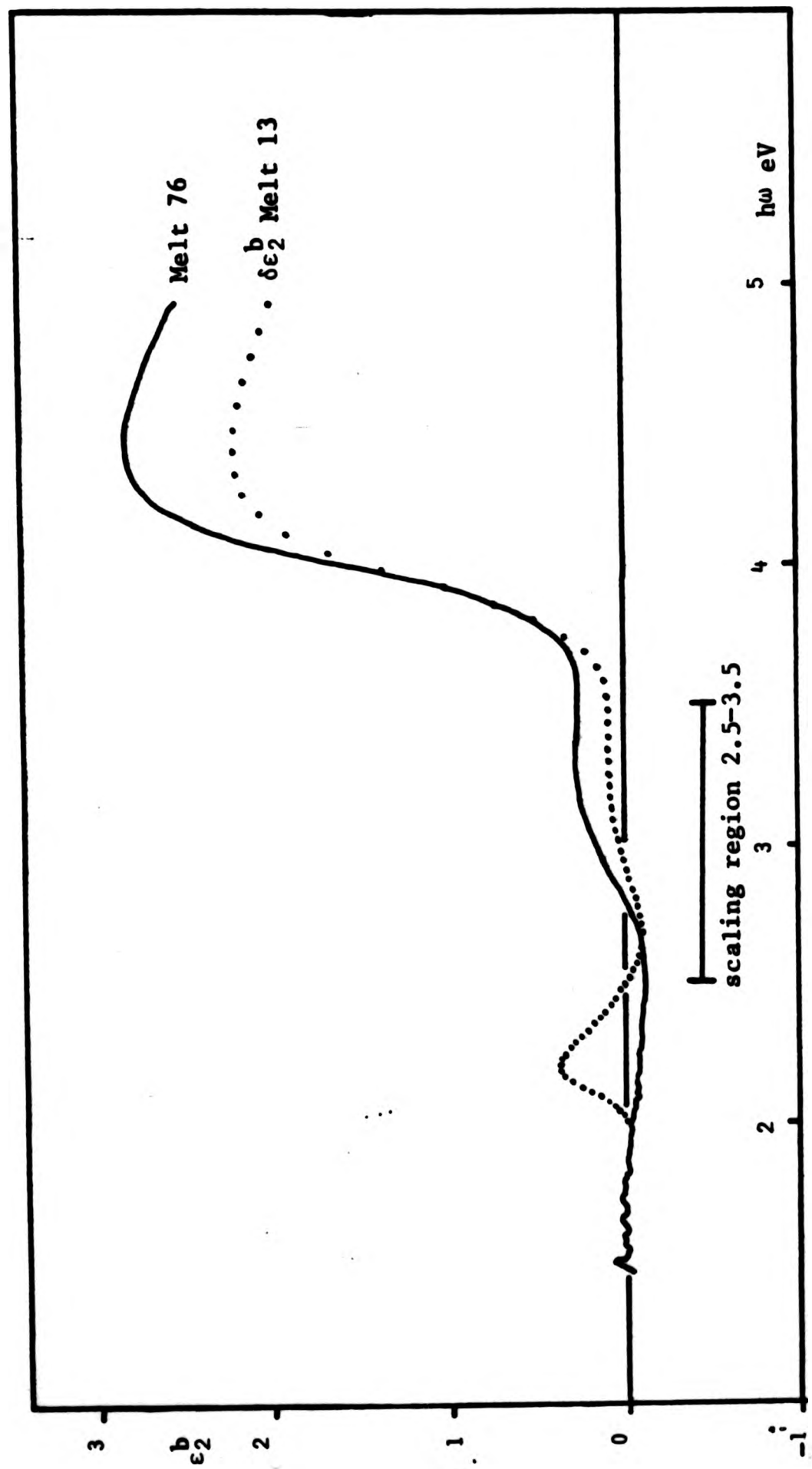


Figure 7.7. This is similar to Figure 7.6 except that the value of 0.202 for the volume fraction of  $\beta$ -phase has been replaced by the empirical value of 0.114, which gives the best agreement between the functions shown near to 3eV.

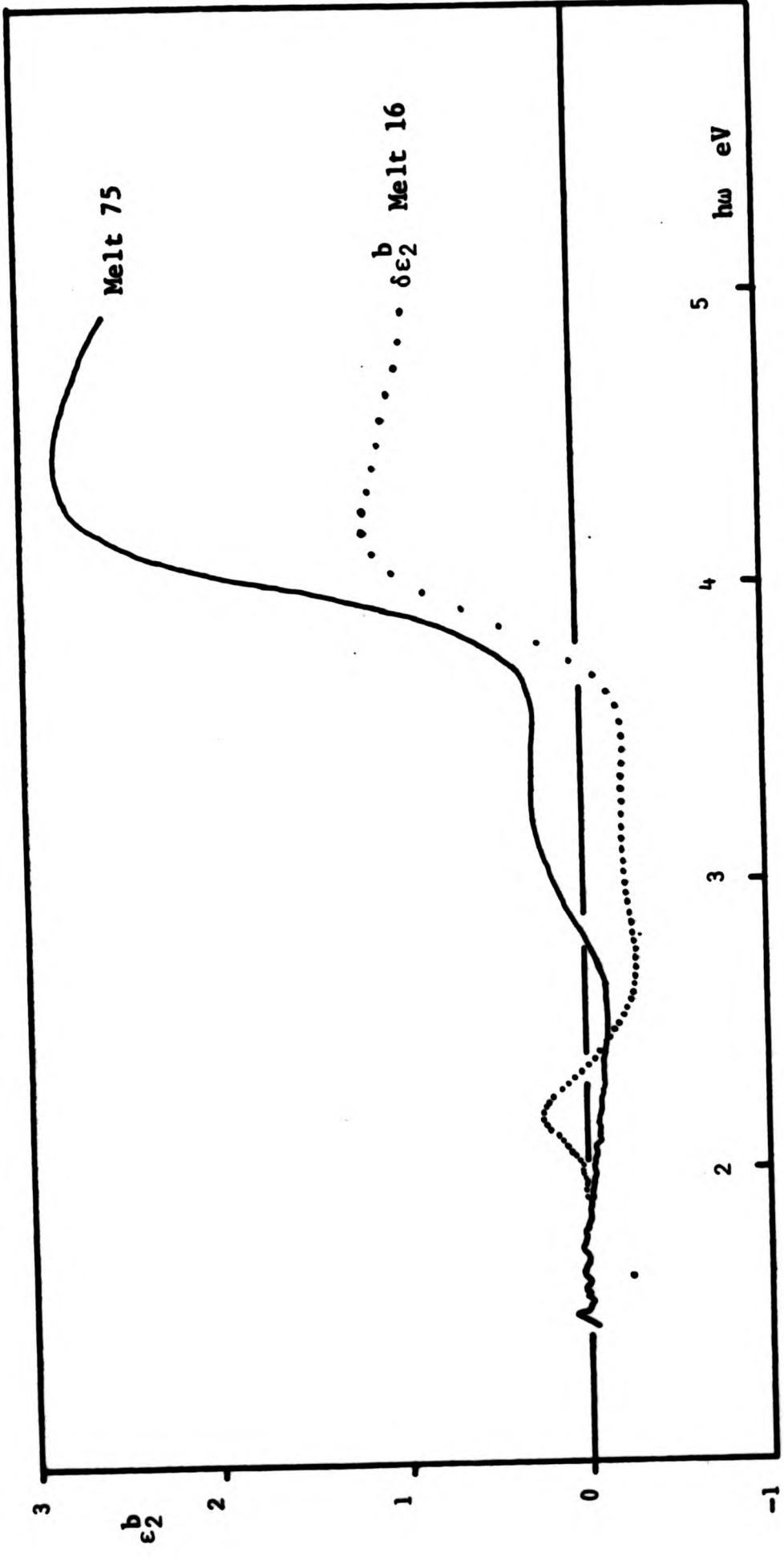


Figure 7.8. Interband absorption of Melt 16, after subtraction of the  $\beta$ -phase contribution. Proportion of  $\beta$ -phase used in the calculation = 0.531.

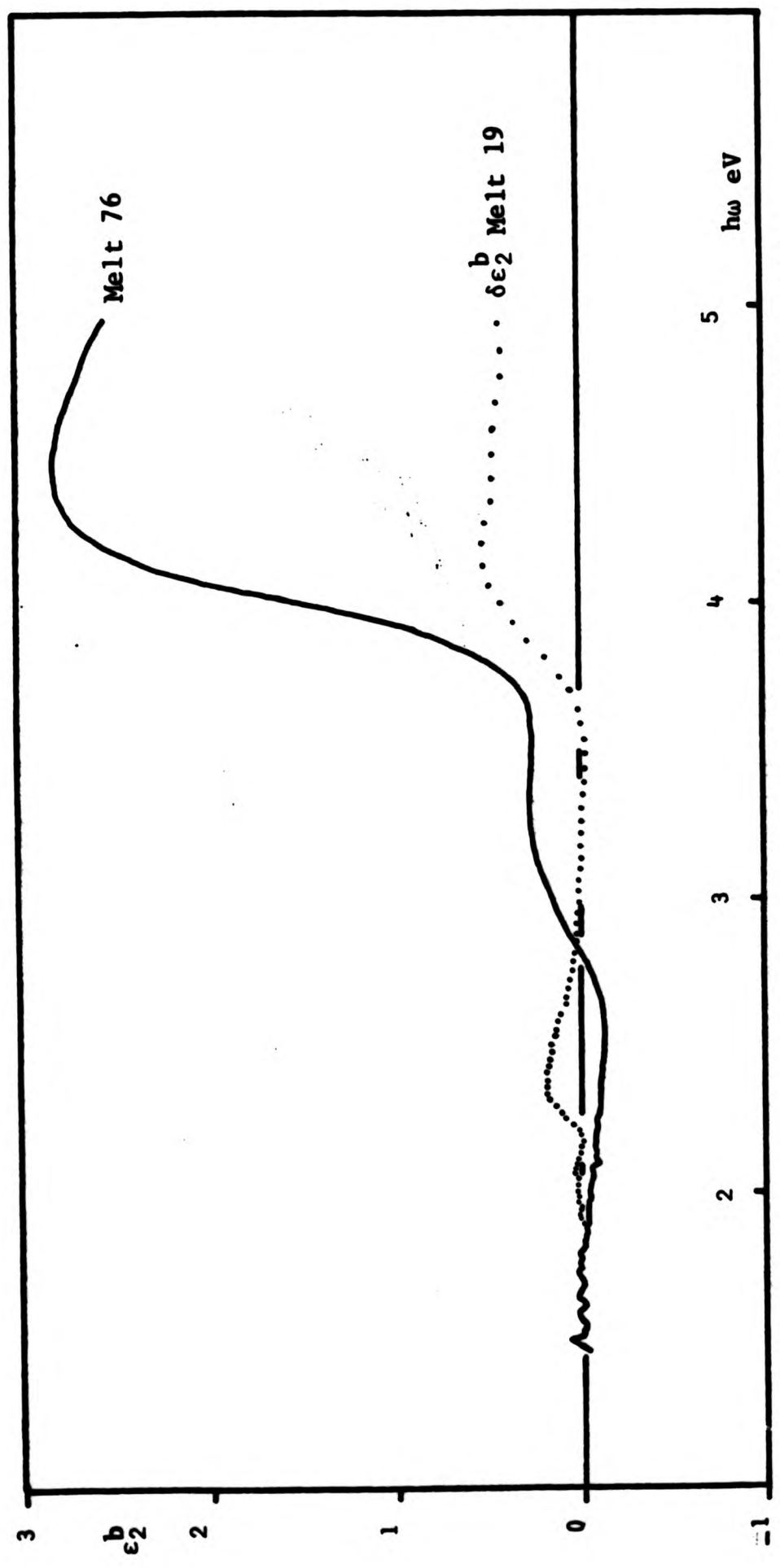
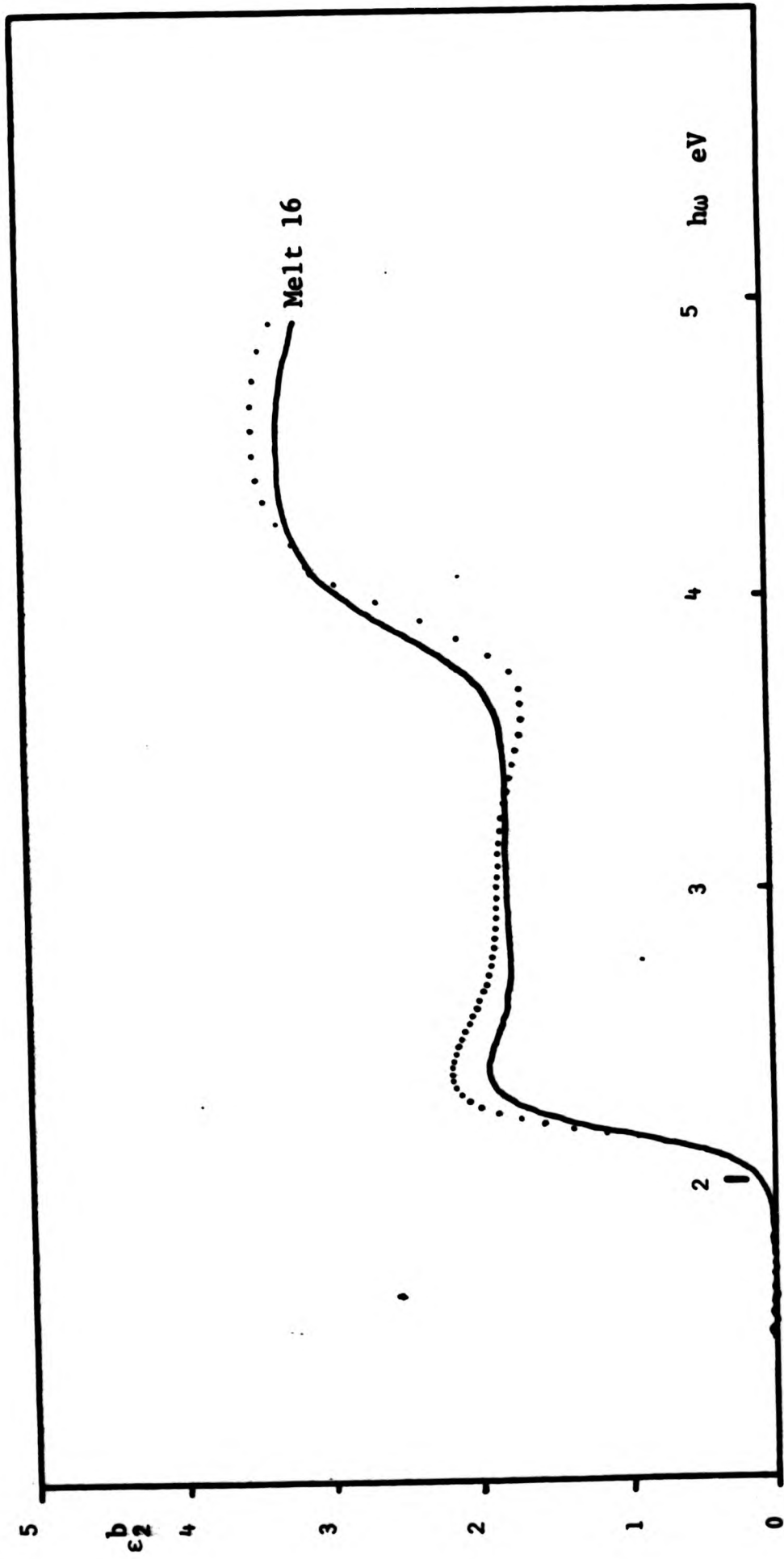


Figure 7.9. Interband absorption of sample Melt 19, after subtraction of the  $\beta$ -phase contribution. The proportion of  $\beta$ -phase used in the calculation was 0.843.



**Figure 7.10.** Interband absorption of the heterogeneous sample Melt 16, (bold line) compared with a calculated function using data from the limiting solutions and a volume fraction calculated from the phase diagram (dotted line).

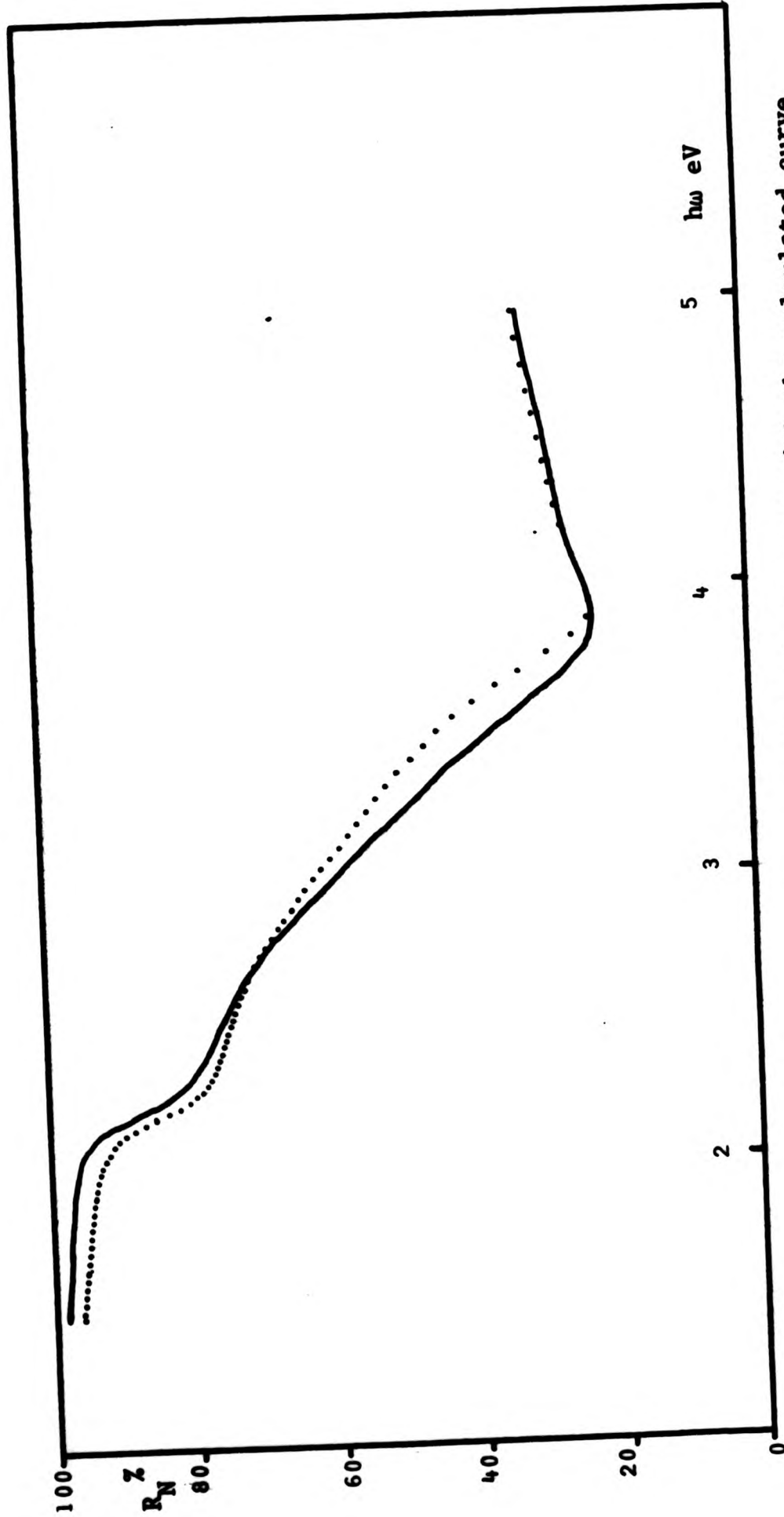


Figure 7.11. Normal reflectance of sample Melt 16, compared with the calculated curve using data from the limiting solid solutions and the volume fraction calculated from the phase diagram.

precipitates could not be resolved. Frequent and prolonged annealing resulted in spherodisation of the precipitates, preventing optical anisotropy. It was not possible to carry out micro-ellipsometric or micro-reflectance measurements on each of the precipitates in any of the two-phase alloys, and so samples were prepared of the appropriate compositions for the  $600^{\circ}\text{C}$   $\alpha$ - and  $\beta$ -phase boundary compositions. These were quenched from  $750^{\circ}\text{C}$  to ensure a single phase structure, since the small amount of additional structural disorder introduced by the higher temperature was considered less significant than the effect of phase separation. The small amount of silver in the  $\beta$ -phase sample (Melt 75; 6.6 at.%) affect the colour in manner similar to the effect of moderate roughening. An attempt has been made to derive the experimental results for the series of two-phase samples, from data obtained on the limiting concentration single-phase alloys above, combined with the volume fraction derived from the phase diagram.

Figures 7.6 - 7.7 compare the interband absorption of the  $\alpha$ -phase alloy (Melt 75) with the absorption strength remaining in various two-phase alloys when a quantity (proportional to the volume fraction) due to the  $\beta$ -phase has been subtracted. A notable feature of these curves is the peak near to 2.2eV; this can be interpreted as a shift of the absorption edge to lower energies in the heterogeneous alloys. This is borne out by the derivative calculations of Table 6.15; a small, but systematic,

change is evident. When the optical interference theory (Section 4.4) is used to derive the effective dielectric function of the two-phase alloys a similar shift with volume fraction is observed. It is probable, therefore, that the d-band energies are governed only by the local composition and are independent of the morphology of the alloy.

In the energy range 2.5 - 3.5eV the computed absorption is too large for the interference theory, as it is for simple additive behaviour, compared with the experimental function. This could be explained if the volume fraction of  $\beta$ -phase were larger than expected for the 600°C isothermal, as might happen if the quenching rate of the samples were inadequate, and the phase structure of the alloys corresponded to a lower temperature. Interestingly, a higher equilibrium temperature would increase the concentration of copper in the  $\alpha$ -phase, which would increase the absorption in this energy range by virtual bound states. It would be necessary to study a range of equilibrium temperatures in order to clarify this point.

Reflectance curves calculated from ellipsometric data on these alloys differ by up to 5% from the values derived using the interference theory. Since this difference is certainly visually perceptible, the modelling of the reflection process cannot be considered adequate.

8. CONCLUSIONS AND SUGGESTIONS FOR FURTHER WORK

It has been shown that spectral ellipsometry is capable of yielding a quantitative description of the colours of the Ag-Au-Cu alloy system, and of providing enough information to permit interpretation of these colours in terms of the underlying physical processes. Repeatability of the experiments is such that compositional changes of the order of 5% (atomic) or greater are detectable, suggesting that sources of error in sample preparation and experiment are less significant than this. Sources of instrumental error that have not been examined closely are modulator core birefringence; compensator transmission and retardation error; compensator azimuth error; sample alignment; polariser ellipticity and monochromator accuracy. Improvements in these areas should enable colorimetry of simple specular surfaces to exceed the discrimination of the human eye. Few changes in the optical components would be necessary, as calibration and correction for these errors would be straightforward, especially as in the present instrument none of these imperfections are large. Simple two-zone averaging would significantly reduce many of the errors, but more desirable would be the modification of the computational procedures to permit correction of single-zone data. The same sources of error also limit interpretation in terms of electronic properties. Here, however, improvement in the theoretical model is also required. For instance, interpretation of the conduction electron adsorption in terms of a single relaxation time has not been very successful, and the possibility of interband absorption

below the main absorption edge requires quantitative study. Theoretical work of this nature could be performed within the framework of the Coherent Potential Approximation (Elliott 1974) and the Random Phase Approximation (Mueller 1967). Further experimental work in the wavelength range  $1\mu$  to  $25\mu$  would also be necessary to clarify the reasons for the departure from simple theory in the wavelength range 650-850nm.

Reinterpretation of the present results using Kramers-Kronig inversion of the calculated  $\epsilon_2^b(\omega)$  would also be possible; by explicit computation of  $\epsilon_1^b(\omega)$  the assumption of constant  $\epsilon_1^b$  at long wavelengths could be discarded, so that more accurate results for the optical effective masses could be obtained. Understanding of the colours of heterogeneous alloys would be improved if a joint ellipsometry and reflectance study could be carried out. This would test the applicability of the simple theory of Chapter 4 and fuel further theoretical work.

In the context of the electronic properties of solids, the most informative optical techniques are piezoreflectance and differential reflectance (ie. directly measuring the difference between alloys of similar composition), combined with Kramers-Kronig inversion. Both these methods are in essence modulation techniques. It is difficult to conceive of an arrangement by which difference measurements on alloys could be performed ellipsometrically, because of the sensitivity of ellipsometry to angle of incidence and therefore sample wobble.

However, certain types of piezo-measurement would be quite possible, for instance using a piezo-ceramic substrate with a thick film sample on it. Alternatively, the optical bandwidth could be reduced (possibly by the use of a cooled photomultiplier and increased electronic integration time) and a more accurate monochromator could be used. This would enable high order numerical derivatives to be calculated, which are comparable to electroreflectance spectra but rather simpler to interpret. The only other source of error which is difficult to compensate for is multiple reflections in the optical components, the air-gap polarising prisms being particularly troublesome.

The results in terms of alloy colours can be summarised as follows:

- (1) The colour change yellow + green + white found as silver is alloyed with gold is due to an increase in width of the d-FS gap near L from 2.5 to 4eV. Transitions to the first empty conduction band, such as contribute to the absorption of silver above 4eV, do not significantly affect the colour. Broadening of the absorption edge upon alloying also takes place, presumably because of substitutional disorder, and increases the bleaching effect for silver additions of about 50 weight per cent. This broadening does not affect the brightness of the alloys, which increases monotonically from gold to silver.

(2) The colour change yellow  $\rightarrow$  red found as copper is alloyed with gold is due mainly to a reduction of the width of the  $d \rightarrow FS$  gap near L from 2.5 to 2.2eV. The change in saturation for the copper-rich alloys is due to an increase in the reflectance below the absorption edge as copper is added. This is due to either an increase in oxide thickness (of about  $30\text{\AA}$ ) from 50Au-50Cu to pure copper, or to a modification of the weak interband absorption below the edge, or to both these effects.

(3) The colour change white  $\rightarrow$  red found as copper is alloyed with silver is due mainly to the resulting change in the proportions of the white  $\alpha$  phase and the red  $\beta$  phase. The  $\alpha$  phase is slightly yellower than fine silver because of the presence of an impurity absorption band, itself due to the large difference in the d-band energies of silver and copper. In the heterogeneous alloys the morphology of the  $\alpha$  phase is likely to lead to surface plasmon absorption, producing a further slight yellow shift.

REFERENCES

- Abeles, F (1965) in "Optical Properties and Electronic Structure of Metals and Alloys", ed. F Abeles, Publ. North-Holland.
- Abeles, F (1969) in "Optical Properties of Solids" ed. F Abeles, Publ. North-Holland.
- Antonangeli, F., Colavita, E, Rosei, R and Salusti, S E (1974) *Il Nuovo Cimento* 24B(1), 121.
- Atkins, P W and Wilson, A D (1970), *Surf. Sci.*, 22, 433-458.
- Aspnes, D (1976a) in "Optical Properties of Solids: New Developments" ed. B Seraphin, North-Holland.
- Aspnes, D (1976b) *Surf. Sci.* 56, 322-33.
- Bartell, L S and Churchill, D (1961), *J. Phys. Chem.* 65, 2242.
- Bassett, M and Beaglehole, D (1976) *J. Phys. F* 6(6), 1211.
- Beaglehole, D (1965) *Proc. Phys. Soc., Lond.* 85, 1007-20.
- Beaglehole, D (1966) *Proc. Phys. Soc., Lond.* 87, 401.
- Beaglehole, D and Erlbach, E (1972) *Phys. Rev. B* 6(4), 1209.
- Beaglehole, D and Hendrickson, T J (1969) *Phys. Rev. Lett.* 22(4), 133.
- Beaglehole, D and Hunderi, O (1970) *Phys. Rev. B* 2(2), 309.
- Beaglehole, D and Wihl (1972) *J. Phys. F* 2, 43.
- Beattie, J R and Conn, G K T (1955) *Phil. Mag.* 46, 989.
- Beeferman, L W and Ehrenreich, H (1970) *Phys. Rev. B* 2(2), 364.
- Bennett and Bennett (1966) in "Optical Properties and Electronic Structure of Metals and Alloys", ed. F Abeles, publ. North-Holland.
- Bennett, H E and Porteus, J O (1969) *J. Opt. Soc. Am.* 51, 123.
- Billmeyer, F W, Beasley, J K and Sheldon, J A (1961) *J. Opt. Soc. Am.* 65(7), 834.
- Booma (1971) "Physical Aspects of Colour", publ. Macmillan.
- Brauwiers, M and Brouers, F (1970) *Phys. Stat. Sol. b* 75, 519.
- Bronsveld, P M and Radelaar, S (1975) *J. Phys. Soc. Jap.* 38(5), 1336.
- Burge, D R and Bennett, H E, (1964) *J. Opt. Soc. Am.* 54(12), 1428.
- Cahan, B D (1976) *Surf. Sci.* 56, 354-372.
- Chan, E C, Marton, J P and Brown, J D (1976), *J. Vac. Sc. Technol.* 13(4), 981.

Cheyssac, P, Garrigos, R, Kofman, R, Penavaire, L, Richard, J and Saissy, A (1972) *Thin Solid Films* 13, 275-9.

Chopra, K L (1969) "Thin Film Phenomena" McGraw Hill.

Chopra, K L, Thakoor, A P, Barthwal, S K and North, P (1977) *Phys. Stat. Sol. A* 40, 247.

Christensen, N E (1972) *Phys. Stat. Sol. B* 54, 551.

Christensen, N E and Seraphin B O (1971) *Phys. Rev. B* 4(10), 3321-44.

Connolly, J W D and Johnson K H (1970) Progress Report: Solid State and Molecular Theory Group, MIT No. 72.

Colavita E, Modesti, S and Rosei, R (1975) *Solid State Commun.* 17,931-34.

Cooper, H, Ehrenreich and Phillipp (1965) *Phys. Rev.* 138A, 494-507.

Crowell, J and Ritchie R H (1970) *J. Opt. Soc. Am.* 60, 794.

Cyrot, M (1976) *Solid State Commun.* 20, 467-71.

Daude, A, Savary, A and Robin, S (1972) *Thin Solid Films* 13, 255-259.

Davies, H (1953) *Proc. IEEE* 101, 209.

Desjonqueres, M C and Cyrot-Lackmann F (1977) *J. Phys. F* 7(1), 61.

Donovan, T M, Ashley, E J and Bennett, H E (1963) *J. Opt. Soc. Am.* 53(12), 1403-9.

Doremus, R H and Turkalo, A M (1976) *J. Mat. Sci.* 11(2), 638.

Dresselhaus, G (1969) *Solid State Commun.* 7, 419-429.

Drude, P (1890) *Ann. D. Physik*, 39, 514.

Dujardin, M and Theye, M (1971) *J. Phys. Chem. Sol.* 32, 2033.

Dy, K S and Shi-Yu Wu (1971) *Phys. Rev. B* 3(4), 1173.

Ehrenreich, H (1966) in "Optical Properties and Electronic Structure of Metals and Alloys" Ed. F Abeles, publ. North-Holland.

Ehrenreich, H and Phillipp, H R (1962) *Phys. Rev.* 128, 1622.

Elliott, R J, Krumhansl, J A and Leath, P L (1974) *Rev. Mod. Phys.* 46, 465-543.

Fano, U (1941) *J. Opt. Soc. Am.* 31, 213.

Feldkamp, L A, Davis, L C and Stearns, M B (1977) *Phys. Rev. B* 15(12), 5535.

Fenstermaker, C H and McCrackin, F L (1969) *Surf. Sci.* 16, 85.

Flaten, C J and Stern, E A (1975) *Phys. Rev. B* 11(2), 638.

Forsterling, K and Freedericksz, V (1913) *Ann. d. Physik.* 40, 201.

French, R C (1932) *Nature* 129, 169.

- Friedel, J (1969) in "Optical Properties of Solids" ed. F Abeles, publ. North-Holland.
- Fromhold, A T (1963) *Il Nuovo Cimento* 28, 1127-45.
- Fukutani, H (1971) *J. Phys. Soc. Jap.* 30(2), 399.
- Fukutani H and Sueoka, O (1966) in "Optical Properties and Electronic Structure of Metals and Alloys" ed. F Abeles, publ. North-Holland.
- Gardam, G E (1966) *Trans. Inst. Metal Finishing* 44, 186-8.
- Garfinkel, M, Tieman, J J and Engeler, W F (1966) *Phys. Rev.* 148, 695.
- Gasvik, K (1977) *Opt. Commun.* 22(1), 61.
- Gelatt and Ehrenreich, H (1974) *Phys. Rev. B* 10, 398
- Gerhardt, U (1968) *Phys. Rev.* 172, 651.
- Gerhardt, U, Beaglehole, D and Sandrock, R (1967) *Phys. Rev. Lett.* 19,309.
- Givens, M P (1958) *Solid State Physics* 6, 343.
- Golovashkin, A I, Kopeliovich, A I and Motulevich, G P (1968) *Soviet Physics JETP* 26(6), 1161.
- Gottesfeld, S, Babai, M and Reichman, B (1976) *Surf. Sci.* 56, 373-93.
- Green, E I and Muldrew, L (1970) *Phys. Rev. B* 2(2), 330.
- Grebennik, I P, Podus, G N and Semin'ko, I V (1975) *Fiz. Metal. Metalloved* 39(6), 1198-1204.
- Haas, G and Thomas, R E (1976) *J. Appl. Phys.* 48(1), 86.
- Ham, F S and Segall, B (1961) *Phys. Rev.* 124(6), 1786.
- Heavens, O S (1955) "Optical Properties of Thin Solid Films", Butterworth.
- Heavens, O S (1960) *Rep. Prog. Phys. (GB)* 23, 2-65.
- Hodgson, J N (1955) *Proc. Phys. Soc. B* 68, 593.
- Hodgson (1968) *J. Phys. Chem. Sol.* 29, 2175-81.
- Hunderi, O (1973) *Phys. Rev. B* 1, 3418.
- Hunderi, O (1976A) *Thin Solid Films* 37, 275-280.
- Hunderi, O (1976B) *Surf. Sci.* 61, 515-520.
- Hunderi, O and Beaglehole, D (1969) *Physics Lett.* 29A(6), 335.
- Hunderi, O and Beaglehole D (1970) *Phys. Rev. B* 2(2), 321.
- Hunderi, O and Myers, H P (1973) *J. Phys. F* 3, 683.
- Irani, G B, Huan, T and Wooten, F W (1971) *Phys. Rev. B* 2, 330.

- Janak, J F, Williams, A R and Moruzzi, V L (1975) Phys. Rev. B 11,1522.
- Jette, E R and Foote, F (1935) J. Chem. Phys. 3, 605-16.
- Johnson, J A and Bashara, N M (1971) J. Opt. Soc. Am. 61(4), 457.
- Johnson, P B and Christy, R W (1972) Phys. Rev. B 6(12), 4370-9.
- Johnson, P B and Christy, R W (1975) Phys. Rev. B 11(4), 1315.
- Jungk, G (1971) Phys.Stat. Sol. b44, 239.
- Jungk, G (1973) Phys. Stat. Sol.b55, 579.
- Knittl (1976) "Optics of Thin Films" publ. Wiley.
- Koike, H, Yamaguchi, S and Hanya, T (1975) J. Phys. Soc. Jap. 38(5),1370.
- Koster, W and Stahl, R (1967) Z. Metallkde. 58(11), 768.
- Kreibig, U (1974) J. Phys. F: Metal Physics 4, 999.
- Krolikowski, W F and Spicer, W E (1970) Phys. Rev. B 1(2), 478.
- Lenham (1967) J. Opt. Soc. Am. 57, 473-6.
- Levin and Ehrenreich, H (1971) Phys. Rev. B 3, 4172.
- Lewis, P E and Lee, P M (1968) Phys. Rev. 175(3), 795.
- Lifshits, V A and Starchenko, I. P (1973) Sb. Tr., Vseo. Nauch-Issled. Proekt-Konstr. Inst. Yuvelirnoi Prom. 2, 104-21.
- Lowery (1936) Phil. Mag. 22, 769.
- Malin, M and Vedam, K (1976) Surf. Sci. 56, 49-63.
- Margenau, H (1929) Phys. Rev. 33, 1033
- Mathewson, A G (1970) J. Phys. C 3, 341.
- McAlister, A J, Stern, E.A and McGroddy, J C (1965) Phys. Rev. 140(6A),2105.
- McIntyre, J D E and Aspnes, D E (1971) Surf. Sci. 24, 417.
- Metcalfe, E and Leake, J A (1975) Acta Mat. 23, 1135.
- Minor (1903) Ann. d. Physik. 10, 581.
- Modesti, S, Rosei, R and Colavita, E (1977) Il Nuovo Cimento 39B(2), 442.
- Morris, C E and Lynch, D W (1969) Phys. Rev. 182, 719.
- Mott, N F and Jones, H (1936) "The Theory of the Properties of Metals and Alloys", publ. Dover, New York.
- Mueller, F M and Phillips, J C (1967) Phys. Rev. 157(3), 600.
- Myers, H P (1976) J. Phys. F 6(1), 141.

- Myers, H P, Wallden, L and Karlsson, A (1968) *Phil. Mag.* 18, 725.
- Naegele, K and Plieth, W J (1976) *Surf. Sci.* 61, 504-14.
- Nathanson, J B (1938) *J. Opt. Soc. Am.* 28, 300.
- Neal, W E J, Fane, R W and Grimes, N W (1970) *Phil. Mag.* 21, 167.
- Nilsson, P O (1970) *Phys. Kondens. Mater.* 11, 1.
- Nilsson, P O and Forsell (1974) *J. Phys. (Paris)* 35, C4-57.
- Nilsson, P O, Lindau, I and Hagstrom, S B M (1970) *Phys. Rev. B* 1(2), 498.
- Nilsson, P O and Norris (1969) *Phys. Lett. A* 29, 22.
- Nilsson, P O, Persson A and Hagstrom, S (1968) *Solid State Commun.* 6, 297.
- Nilsson, P O and Sandell, B (1970) *Solid State Commun.* 8, 721.
- Novak M., Reddy, AKN and Wroblava, H (1970) *J. Electrochem. Soc: Electrochem. Sci.* 117(6), 733.
- O'Handley (1974) *Surf. Sci.* 46, 24-42.
- O'Handley, R C (1975) *Surf. Sci.* 50, 407-33.
- O'Handley, R C and Burge, D K (1975) *Surf. Sci.* 48, 214-228.
- Ohlidal, I and Lukes, F (1972) *Opt. Acta* 19, 817.
- Ohlidal, M, Ohlidal, I and Lukes, F (1976) *Surf. Sci.* 55, 467-76.
- Ohta, N and Wysecki, G (1975) *J. Opt. Soc. Am.* 65(7), 834.
- Oldham, W G (1969) *Surf. Sci.* 16, 97-103.
- Owen (1972) N A S A Report TR R-393.
- Paik and Bockris cited by Yamaguchi (1972)
- Pant, M M and Joshi, S K (1970) *Phys. Rev. B* 1(2), 506.
- Pauli, H (1976) *J. Opt. Soc. Am.* 66(8), 866.
- Pells, G P and Shiga, M (1969) *J. Phys. C* 2(2), 1835.
- Peterson, C W and Knight, B W (1973) *J. Opt. Soc. Am.* 63(10), 1238.
- Phillips, J C (1968) *J. Appl. Phys.* 39(2), 755.
- Porteus, J O (1973) *J. Opt. Soc. Am.* 53, 1394.
- Raub, C (1975) *Gold Bulletin* 8(3), 70.
- Ramachandrarao, P, Banerjee, D and Anantharaman T.R. (1970) *Metallurgical Transactions* 1, 2655.
- Rich, R M and Billmeyer, F W (1975) *J. Opt. Soc. Am.* 65(8), 956.

- Rivory, J (1969) *Opt. Commun.* 1(2), 53.
- Rivory, J (1976) *Thin Solid Films* 37, 345-50.
- Rivory, J (1977) *Phys. Rev. B* 15(6), 3119.
- Rivory, J and Theye, M L (1975) *Journal de Physique Lett.* 36, 129.
- Roberts, E F I (1973) *Gold Bulletin* 6(2), 42.
- Roberts, S (1959) *Phys. Rev.* 118(6), 1509.
- Robertson, A R (1972) *Appl. Opt.* 11, 1936.
- Roth, J, Rao, B and Dignam, M J (1975) *J. Chem. Soc. Farad. Trans.* 2 Vol. 71, 86.
- Rouard, P (1965) *Appl. Opt.* 4, 947.
- Schlosser, H (1970) *Phys. Rev. B* 1(2), 491.
- Schueler, D (1969) *Surf. Sci.* 16, 104-11.
- Schultz, L G (1957) *Adv. in Phys.* 6, 102-144.
- Scott and Muldrew (1974) *Phys. Rev. B* 9, 1115.
- Shevchik, N J and Goldmann, A (1974) *V. Electron Spectrosc. & Related Phenom. (Netherlands)* 5, 631-40.
- Shewchun, J and Rowe, E C (1970) *J. Appl. Phys.* 41(10), 4128-38.
- Sivukhin (1956) *Soviet Physics JETP* 3, 269.
- Slechta, J (1976) *J. Phys. F* 6(11), 2081.
- Smith, T (1976) *Surf. Sci.* 56, 252-271.
- Soven, P (1967) *Phys. Rev.* 156(3), 809.
- Spencer, W T and Givens, M P (1964) *J. Opt. Soc. Am.* 54(11), 1337.
- Stanford, J L and Bennett, H E (1969) *Appl. Opt.* 8, 2556.
- Stahl, R, Spranger, H J and Aubauer, H P (1969) *Z. Metallkde.* 60(12), 933.
- Steel, M R (1972) *J. Phys. F: Metal Physics* 2, 605.
- Steel, M R and Trehearne D.M. (1972) *J. Phys. F: Metal Physics* 2, 199.
- Stern, E A (1966) *Phys. Rev.* 144, 545.
- Stern, E A (1967) *Phys. Rev.* 162, 565-74.
- Stern, F (1963) *Solid State Physics* 15, eds. F Seitz and D Turnbull, publ. Academic Press.
- Stoering, R and Conrad, H (1969) *Acta Met.* 17, 933.
- Theye, M (1970) *Phys. Rev. B* 2(8), 3060-78.
- Timashiev, S F and Krykin, M A (1976) *Phys. Stat. Sol. b* 76, 67.

- Tool (1910) Phys. Rev. 31, 1.
- Truong, V V and Scott, G D (1976) J. Opt. Soc. Am. 67(4), 502.
- Veal, B W and Paulikas, A P (1974) Phys. Rev. B 10(4), 1280.
- Velicky, B, Kirkpatrick, S and Ehrenreich, H (1968) Phys. Rev. 175(3), 747.
- Velicky, B and Levin, K (1970) Phys. Rev. B 2(4), 936.
- Verleur (1968) J. Opt. Soc. Am. 58, 1356.
- Verses, J A and Louis, E (1977) Solid State Commun. 22, 636-666.
- Wallden, L and Gustavsson, T (1972) Phys. Scripta. 6, 73.
- Ward (1969) Brit. J. Appl. Phys. (J. Appl. Phys. D) 2(2), 123.
- Weast, R C (1971) "Handbook of Chemistry and Physics", The Chemical Rubber Co., U S A.
- Weiss, D E and Muldrew, L (1974) Phys. Rev. B 10(6), 2254.
- Wessel, P R (1963) Phys. Rev. 132, 2062.
- Wieder, H and Czernanda, A W (1966) J. Appl. Phys. 37, 184.
- Winterbottom (1955) Kgl. Norske Videnskab. Selskabs Fosh. Skrifte 1, 95.
- Winterbottom (1961) Norges tekniske hogskole, Trondheim.
- Winsemius (1973) Rijks Universiteit te Leiden, Leiden, Netherlands, Ph.D. thesis.
- Winsemius, van Kampen, Lengkeek and van Went (1976) J. Phys. F 6(8), 1583.
- Wooten, F (1972) "Optical Properties of Solids", publ. Academic Press.
- Yamaguchi, T, Yoshida, S and Kinbara, A (1972) J. Opt. Soc. Am. 62(5), 634-8.
- Young, F W and Cathcart, J V (1956) Acta Metallurgica 41, 145.
- Young, F W and Gwathmey, A T (1951) Rev. d. Metallurgie 48, 232.
- Zhuravleva, L I and Noskov, M M (1959) Fiz. metal. Metalloved. 7(3), 475-476.
- Ziman, J (1972) "Principles of the Theory of Solids", publ. Cambridge Univ. Press.

## The effects of surface damage and oxide films on the optical properties of cuprite

P. RASTALL, K. MC. CLARKE, AND E. F. I. ROBERTS

Department of Metallurgy and Materials, City of London Polytechnic, Whitechapel High Street, London E1 7PF

**SUMMARY.** Spectral ellipsometry in the range 240 nm to 540 nm has been used to investigate the influence of surface damage induced by mechanical polishing and surface films of CuO on the optical properties of pure synthetic cuprite. Comparison is made between bulk CuO and thin film CuO produced by low-temperature oxidation of cuprite. The effects of strain and disorder are discussed in relation to the suppression of excitonic transitions. Recently developed techniques have been used to simplify the analysis and take full advantage of the spectral data.

It has long been known that structural defects in crystal lattices, whether point, line, or plane, have a marked effect on absorption phenomena and electronic transitions. Semi-conductors are particularly sensitive as their electrical properties are strongly affected by those defects. Cuprous oxide is a typical 'deficit' semi-conductor with a band gap of approximately 2.4 eV (Roberts and Rastall, 1978) and much investigation has been carried out into the excitonic transitions in its absorption spectrum.

Excitons are electron hole pairs in orbit produced by photon absorption in various parts of the spectrum, and their nature and properties have been discussed at length (e.g. Gross, 1962). Various workers have studied the dependence of the excitonic structure on lattice perfection. Agekyan *et al.* (1975) have shown that the method of production of Cu<sub>2</sub>O crystals strongly affects the sharpness of the exciton peaks, hydrothermally grown crystals exhibiting sharper transitions than less perfect material prepared from Cu metal by oxidation. The defect structure and stoichiometry of Cu<sub>2</sub>O is markedly affected by annealing, and Spyrideles *et al.* (1977) have indicated that vacancy aggregation in bulk samples, controlled by oxygen partial pressure in the annealing process, is responsible for suppression or enhancement of the exciton peaks. Work carried out by Hayfield (1961) on thin-film Cu<sub>2</sub>O obtained by low-temperature oxidation of copper again suggests a relationship between lattice defects and optical absorption.

Experiments involving reflected light such as the ellipsometric measurements in this study are not only sensitive to bulk structural defects but are also affected by the state of the crystal surface. Surface conditions which affect the ellipsometric parameters are: (1) Surface roughness: degree of polish, presence of etch pits, grain boundaries, and scratches, etc. (2) Polish damage: disordering, increased density of the surface layers. (3) Surface film presence: incidental atmospheric contamination or controlled oxidation.

The purpose of this present study is to evaluate the effects of (2) and (3), above, on the optical properties of synthetic cuprite, and to investigate anomalously high values of the absorption index obtained in our previous study (Roberts and Rastall, 1978), which we suggested might be due to the presence of a thin absorbing surface film of CuO.

*Surface condition and etching procedure.* Specimens of pure, polycrystalline cuprite were prepared by a similar method to that described previously. After oxidation, however, the samples were not cooled slowly in a partial vacuum, but were given a separate annealing treatment of 700 °C and 10<sup>-1</sup> torr for 24 hours.

Spectral scans were carried out on an automatic following ellipsometer, the details of which are described by Roberts and Meadows (1964). The system has since been modified by the replacement of silica and glass Faraday-cell cores by water cores to reduce systematic errors and facilitate experimental procedure (Hunt, 1979).

To remove the polish-damaged layer before further measurement, samples were etched by immersing them in a mixture of concentrated nitric (20%), phosphoric (40%), and acetic (40%) acids (v/v) for 20 seconds, at room temperature. All the specimens were washed in soap solution, ultrasonically cleaned in distilled water, and dried in pure ethanol and warm air.

*Oxidation of Cu<sub>2</sub>O.* Oxidation studies, both batch and *in situ*, were carried out on polished and etched

material. Batch samples were heated in air at temperatures of 225 °C and 250 °C for various times before spectral measurements were made.

For *in situ* measurements, specimens were attached by clips to a heating element with a variable resistance control. Chromel-alumel thermocouple leads were spot-welded to the element on either side of the specimen and the apparatus was temperature-calibrated. A spectral scan was carried out before the oxidation process was started. To follow the oxidation process, the monochromator was set at 525 nm and the temperature at 250 °C. Values of the analyser and polarizer angles were recorded, ever few seconds during the initial period of rapid change and every 5 to 10 minutes thereafter, until no further changes were observed.

**Results and discussion.** Figs. 1 and 2 show the normal reflectance ( $R$ ) and  $n$ ,  $k$ , spectra for both polished and etched cuprite. The region 250 nm to 540 nm is one of high absorption with an edge at the long-wavelength end and peaks corresponding to direct allowed transitions from the  $\text{Cu}(3d)$  levels to the conduction band (Gross, 1962). It can be seen that etching has several effects on the spectra. There is a general decrease in  $k$  except in the region of excitonic transition (445 to 520 nm) and a corresponding increase in the values of  $n$  and  $R$ . The most marked effects are the sharpening of the  $R$  peaks at 290 nm and 360 nm and a resolution of the blue and blue-green exciton series whose maxima occur at 465 nm and 480 nm respectively. There is a slight shift to shorter wavelength of the peak at 290 nm.

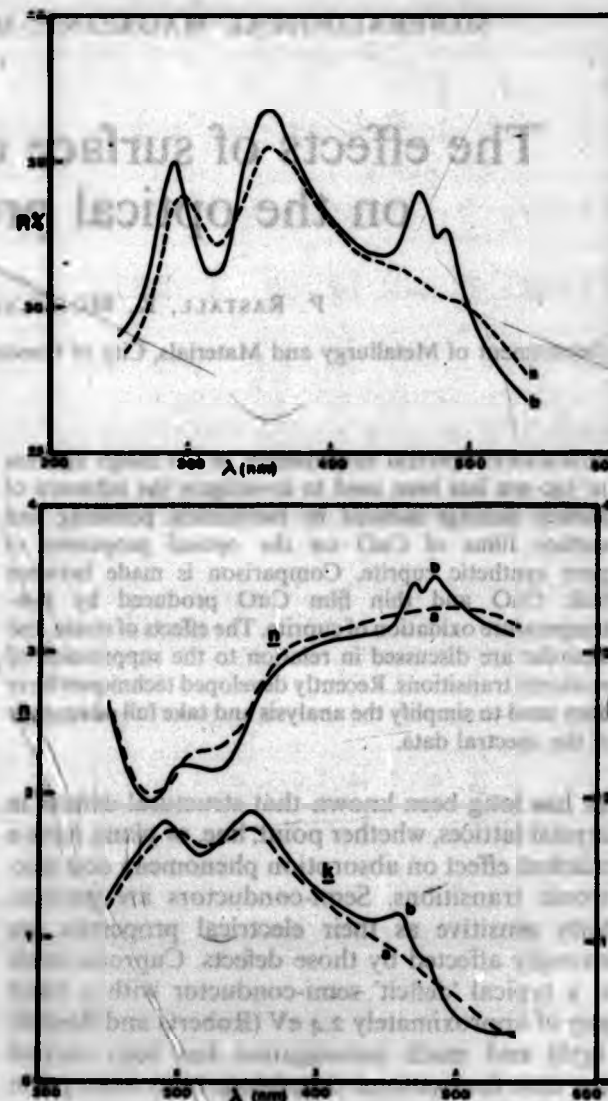
We postulate that the smearing out of the maxima is a consequence of disorder in the lattice created by abrasion of the surface layers. This is particularly apparent in the case of the exciton which can only exist in lattices displaying long-range order (some have radii of about 20 nm). At room temperature the resolution of individual members of the exciton series is not possible due to thermal broadening and the peak heights correspond to the first member of the series.

According to Gross, the radius of an exciton may be expressed as:

$$r_{\text{exc}} = \frac{\epsilon_0 h^2 n^2}{4\pi^2 \mu e^2} \times 10^{10} (\text{\AA})$$

If  $\epsilon_0$  (dielectric permittivity of  $\text{Cu}_2\text{O}$  at 465 nm) =  $11 (\times 8.8 \times 10^{-12}) \text{ Fm}^{-1}$ ,  $\mu$  (effective reduced mass of the electron) =  $0.025 m_0$  ( $m_0 = 9.1 \times 10^{-31} \text{ kg}$ ),  $n$  (quantum number of the exciton) = 1,  $e$  (electron charge) =  $1.6 \times 10^{-19} \text{ C}$ ,  $h$  (Planck's constant) =  $6.63 \times 10^{-34} \text{ Js}$ , then a value of  $c. 18 \text{ \AA}$  is obtained from the first exciton member of the blue series.

Excitons are annihilated when they interact with



FIGS. 1 and 2. FIG. 1 (top). Spectral reflectance of polycrystalline cuprite. (a) Mechanically polished. (b) Mechanically polished and etched. FIG. 2 (bottom). Spectral dispersion of  $n$  and  $k$  for cuprite. (a) Mechanically polished. (b) Mechanically polished and etched.

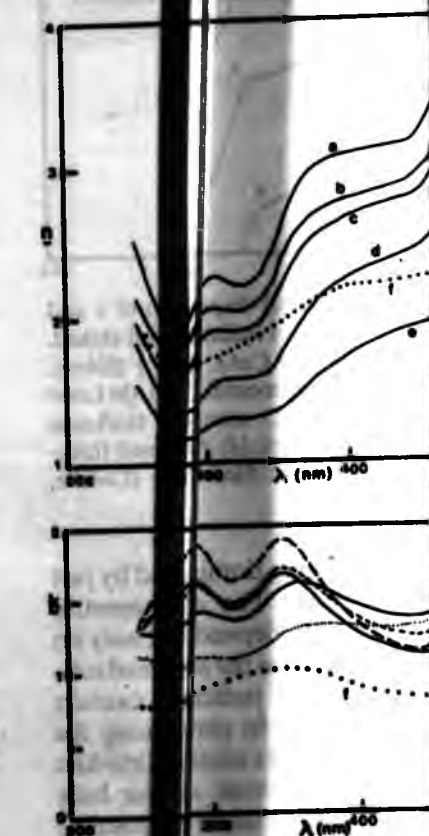
defects and the implication of these results is that the disorder induced by polishing must be extensive, the mean free path of the exciton being drastically reduced.

Other consequences of the polishing process have been investigated by several authors. Vedam and Mahin (1974), who have made ellipsometric measurements on polish-damaged vitreous silica, suggest that an increased density of the surface layers occurs with a consequent increase in the value of  $n$ ; though in the case of crystalline  $\text{Cu}_2\text{O}$ , this mechanism is not possible and the change in  $n$  and  $k$  obtained here is due to disorder and an increased dislocation density in the surface which, in turn, causes a decrease in the density.

Reflectance measurements made by Donovan *et al.* (1963) suggest general disorder accompanying melting, the surface subjected to inelastic scattering, which, they postulate, causes a decrease in the energies of the surface peaks at the material.

The depth of the disordered layer is accurately deduced from film-fitting as the optical properties of the layer are similar to those of ordered cuprite surface. It is reasonable to assume that it extends to a depth corresponding to the size of the disordered region used in the final polishing stage (20 nm), it is likely that the sharp interface exists between the damaged layer and the rest of the material.

Figs. 3 and 4 show the  $n$  and  $k$  spectra for a specimen of cuprite polished and oxidized in air at various times. The spectrum of Cu<sub>2</sub>O is compared with a gradual broadening is evident with each successive oxidation.



FIGS. 3 and 4. FIG. 3 (top). Spectral dispersion of  $n$  for cuprite and  $\text{CuO}$ . (a) Mechanically polished. (b) Oxidized, 225 °C, in air, 12 hours. (c) Oxidized, 225 °C, in air, 16 hours. (d) Oxidized, 225 °C, in air, 16 hours. FIG. 4 (bottom). Spectral dispersion of  $k$  for cuprite and  $\text{CuO}$  under the same conditions.

## The effects of surface damage and oxide films on the optical properties of cuprite

P. RASTALL, K. MC. CLARKE, AND E. F. I. ROBERTS

Department of Metallurgy and Materials, City of London Polytechnic, Whitechapel High Street, London E1 7PF

**SUMMARY.** Spectral ellipsometry in the range 240 nm to 540 nm has been used to investigate the influence of surface damage induced by mechanical polishing and surface films of CuO on the optical properties of pure synthetic cuprite. Comparison is made between bulk CuO and thin film CuO produced by low-temperature oxidation of cuprite. The effects of strain and disorder are discussed in relation to the suppression of excitonic transitions. Recently developed techniques have been used to simplify the analysis and take full advantage of the spectral data.

It has long been known that structural defects in crystal lattices, whether point, line, or plane, have a marked effect on absorption phenomena and electronic transitions. Semi-conductors are particularly sensitive as their electrical properties are strongly affected by those defects. Cuprous oxide is a typical 'deficit' semi-conductor with a band gap of approximately 2.4 eV (Roberts and Rastall, 1978) and much investigation has been carried out into the excitonic transitions in its absorption spectrum.

Excitons are electron hole pairs in orbit produced by photon absorption in various parts of the spectrum, and their nature and properties have been discussed at length (e.g. Gross, 1962). Various workers have studied the dependence of the excitonic structure on lattice perfection. Agekyan *et al.* (1975) have shown that the method of production of Cu<sub>2</sub>O crystals strongly affects the sharpness of the exciton peaks, hydrothermally grown crystals exhibiting sharper transitions than less perfect material prepared from Cu metal by oxidation. The defect structure and stoichiometry of Cu<sub>2</sub>O is markedly affected by annealing, and Spyrideles *et al.* (1977) have indicated that vacancy aggregation in bulk samples, controlled by oxygen partial pressure in the annealing process, is responsible for suppression or enhancement of the exciton peaks. Work carried out by Hayfield (1961) on thin-film Cu<sub>2</sub>O obtained by low-temperature oxidation of copper again suggests a relationship between lattice defects and optical absorption.

Experiments involving reflected light such as the ellipsometric measurements in this study are not only sensitive to bulk structural defects but are also affected by the state of the crystal surface. Surface conditions which affect the ellipsometric parameters are: (1) Surface roughness: degree of polish, presence of etch pits, grain boundaries, and scratches, etc. (2) Polish damage: disordering, increased density of the surface layers. (3) Surface film presence: incidental atmospheric contamination or controlled oxidation.

The purpose of this present study is to evaluate the effects of (2) and (3), above, on the optical properties of synthetic cuprite, and to investigate anomalously high values of the absorption index obtained in our previous study (Roberts and Rastall, 1978), which we suggested might be due to the presence of a thin absorbing surface film of CuO.

*Surface condition and etching procedure.* Specimens of pure, polycrystalline cuprite were prepared by a similar method to that described previously. After oxidation, however, the samples were not cooled slowly in a partial vacuum, but were given a separate annealing treatment of 700 °C and 10<sup>-1</sup> torr for 24 hours.

Spectral scans were carried out on an automatic following ellipsometer, the details of which are described by Roberts and Meadows (1964). The system has since been modified by the replacement of silica and glass Faraday-cell cores by water cores to reduce systematic errors and facilitate experimental procedure (Hunt, 1979).

To remove the polish-damaged layer before further measurement, samples were etched by immersing them in a mixture of concentrated nitric (20%), phosphoric (40%), and acetic (40%) acids (v/v) for 20 seconds, at room temperature. All the specimens were washed in soap solution, ultrasonically cleaned in distilled water, and dried in pure ethanol and warm air.

*Oxidation of Cu<sub>2</sub>O.* Oxidation studies, both batch and *in situ*, were carried out on polished and etched

material. Batch samples were heated in air at temperatures of 225 °C and 250 °C for various times before spectral measurements were made.

For *in situ* measurements, specimens were attached by clips to a heating element with a variable resistance control. Chromel-alumel thermocouple leads were spot-welded to the element on either side of the specimen and the apparatus was temperature-calibrated. A spectral scan was carried out before the oxidation process was started. To follow the oxidation process, the monochromator was set at 525 nm and the temperature at 250 °C. Values of the analyser and polarizer angles were recorded, ever few seconds during the initial period of rapid change and every 5 to 10 minutes thereafter, until no further changes were observed.

**Results and discussion.** Figs. 1 and 2 show the normal reflectance ( $R$ ) and  $n$ ,  $k$ , spectra for both polished and etched cuprite. The region 250 nm to 540 nm is one of high absorption with an edge at the long-wavelength end and peaks corresponding to direct allowed transitions from the  $\text{Cu}(3d)$  levels to the conduction band (Gross, 1962). It can be seen that etching has several effects on the spectra. There is a general decrease in  $k$  except in the region of excitonic transition (445 to 520 nm) and a corresponding increase in the values of  $n$  and  $R$ . The most marked effects are the sharpening of the  $R$  peaks at 290 nm and 360 nm and a resolution of the blue and blue-green exciton series whose maxima occur at 465 nm and 480 nm respectively. There is a slight shift to shorter wavelength of the peak at 290 nm.

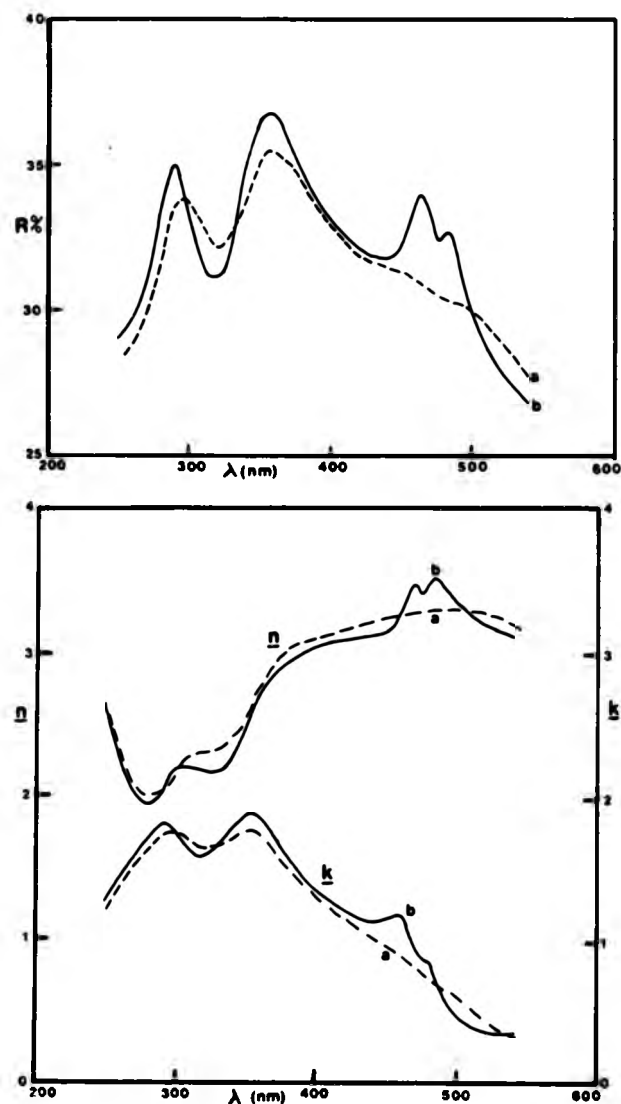
We postulate that the smearing out of the maxima is a consequence of disorder in the lattice created by abrasion of the surface layers. This is particularly apparent in the case of the exciton which can only exist in lattices displaying long-range order (some have radii of about 20 nm). At room temperature the resolution of individual members of the exciton series is not possible due to thermal broadening and the peak heights correspond to the first member of the series.

According to Gross, the radius of an exciton may be expressed as:

$$r_{\text{exc}} = \frac{\epsilon_0 h^2 n^2}{4\pi^2 \mu e^2} \times 10^{10} (\text{\AA})$$

If  $\epsilon_0$  (dielectric permittivity of  $\text{Cu}_2\text{O}$  at 465 nm) =  $11 (\times 8.8 \times 10^{-12}) \text{ Fm}^{-1}$ ,  $\mu$  (effective reduced mass of the electron) =  $0.025 m_e$  ( $m_e = 9.1 \times 10^{-31} \text{ kg}$ ),  $n$  (quantum number of the exciton) = 1,  $e$  (electron charge) =  $1.6 \times 10^{-19} \text{ C}$ ,  $h$  (Planck's constant) =  $6.63 \times 10^{-34} \text{ Js}$ , then a value of  $c. 18 \text{ \AA}$  is obtained from the first exciton member of the blue series.

Excitons are annihilated when they interact with

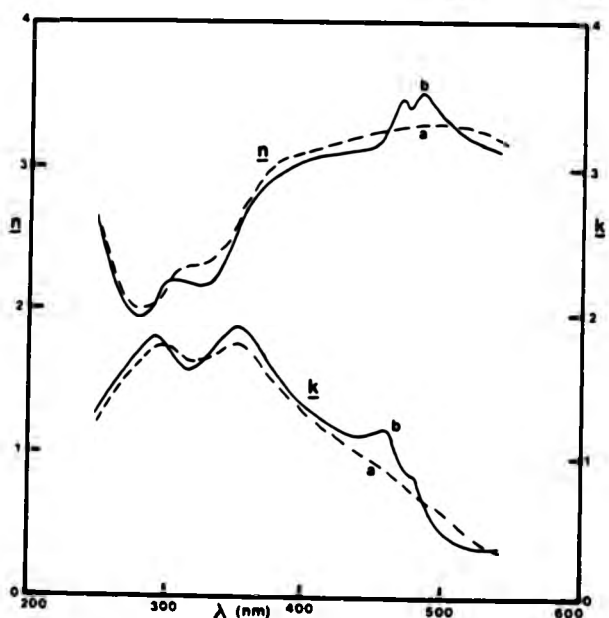
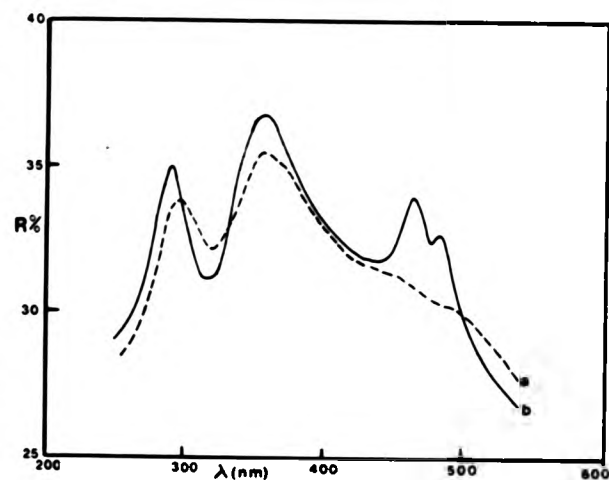


FIGS. 1 and 2. FIG. 1 (top). Spectral reflectance of polycrystalline cuprite. (a) Mechanically polished. (b) Mechanically polished and etched. FIG. 2 (bottom). Spectral dispersion of  $n$  and  $k$  for cuprite. (a) Mechanically polished. (b) Mechanically polished and etched.

defects and the implication of these results is that the disorder induced by polishing must be extensive, the mean free path of the exciton being drastically reduced.

Other consequences of the polishing process have been investigated by several authors. Vedam and Malin (1974), who have made ellipsometric measurements on polish-damaged vitreous silica, suggest that an increased density of the surface layers occurs with a consequent increase in the value of  $n$ ; though in the case of crystalline  $\text{Cu}_2\text{O}$ , this mechanism is not possible and the change in  $n$  and  $k$  obtained here is due to disorder and an increased dislocation density in the surface which, in turn, causes a decrease in the density.

ated in air at  
C for various  
s were made.  
specimens were  
element with a  
Chromel-alumel  
ded to the elec-  
specimen and the  
ated. A spectral  
oxidation process  
on process, the  
n and the tem-  
e analyser and  
er few seconds  
ange and every  
further changes



FIGS. 1 and 2. FIG. 1 (top). Spectral reflectance of polycrystalline cuprite. (a) Mechanically polished. (b) Mechanically polished and etched. FIG. 2 (bottom). Spectral dispersion of  $n$  and  $k$  for cuprite. (a) Mechanically polished. (b) Mechanically polished and etched.

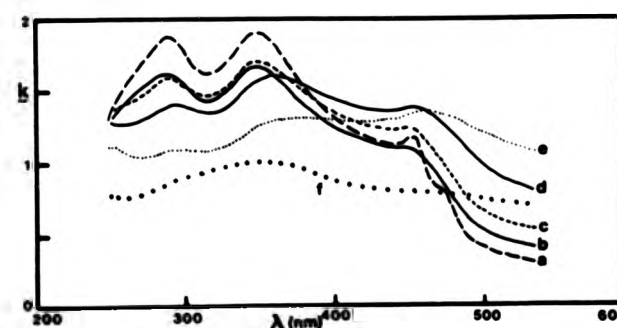
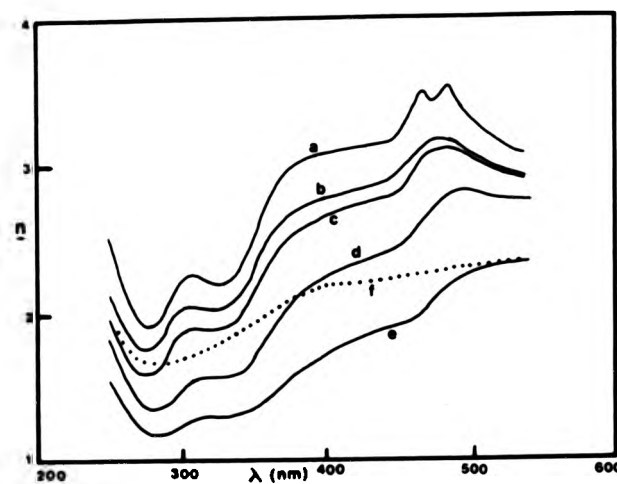
defects and the implication of these results is that the disorder induced by polishing must be extensive, the mean free path of the exciton being drastically reduced.

Other consequences of the polishing process have been investigated by several authors. Vedam and Malin (1974), who have made ellipsometric measurements on polish-damaged vitreous silica, suggest that an increased density of the surface layers occurs with a consequent increase in the value of  $n$ ; though in the case of crystalline  $\text{Cu}_2\text{O}$ , this mechanism is not possible and the change in  $n$  and  $k$  obtained here is due to disorder and an increased dislocation density in the surface which, in turn, causes a decrease in the density.

Reflectance measurements made on germanium by Donovan *et al.* (1963) suggest that apart from general disorder accompanying mechanical polishing, the surface is subjected to inelastic tensile stress which, they postulate, causes a shift to lower energies of reflectance peaks at 600 nm in this material.

The depth of the disordered layer cannot be accurately deduced from film-fitting calculations, as the optical properties of the layer appear very similar to the ordered cuprite substrate, but it is reasonable to assume that it extends to a depth corresponding to the size of the diamond particles used in the final polishing stage (250 nm). It is also likely that no sharp interface exists between the damaged layer and the rest of the crystal.

Figs. 3 and 4 show the  $n$  and  $k$  spectra for a bulk specimen of cuprite, polished and etched in the usual manner and oxidized in air at 225 °C for various times. The spectrum of  $\text{CuO}$  is shown for comparison. A gradual broadening of all the peaks is evident with each successive oxidation and the



FIGS. 3 and 4. FIG. 3 (top). Spectral dispersion of  $n$  for cuprite and  $\text{CuO}$ . (a) Mechanically polished and etched. (b) Oxidized, 225 °C, in air, 4 hours. (c) Oxidized, 225 °C, in air, 12 hours. (d) Oxidized, 225 °C, in air, 16 hours. (e) Oxidized, 225 °C, in air, 20 hours. (f)  $\text{CuO}$ . FIG. 4 (bottom). Spectral dispersion of  $k$  for cuprite and  $\text{CuO}$  under the same conditions.

value of  $k$  increases at long wavelength, with the increasing thickness of the  $\text{CuO}$  layer. As the bulk specimen of  $\text{CuO}$  was produced by a similar, though more intense oxidation process, it is expected that the continuation of the low-temperature process will produce a  $\text{CuO}$  layer thick enough completely to obscure the influence of the substrate.

Batch experiments such as the above are subject to errors in ellipsometric alignment because the films produced do not always display uniform thickness, and it is very difficult to replace the specimen in exactly the same position each time. Initial surface contamination also causes difficulty in accurate determination of the oxidation-rate law, though by repeating the first measurements at the blue end of the spectrum after completion of the scan, we have found that negligible room-temperature oxidation occurs during the experiments. Alignment errors can be eliminated by *in situ* measurements and these also facilitate monitoring of the initial stages of oxidation. The results of such an experiment at 250 °C are shown in figs. 5 and 6. Fig. 5 shows the change in the ellipsometric parameters at 525 nm as the oxidation proceeds and it is compared with the theoretical curve calculated assuming a clean substrate of cuprite ( $n' = 3.91$ ,  $k' = 0.36$ ) and films of  $\text{CuO}$  ( $n' = 2.35$ ,  $k' = 0.70$ ) of increasing thickness. The experimental curve may be divided into three parts. Part (A)

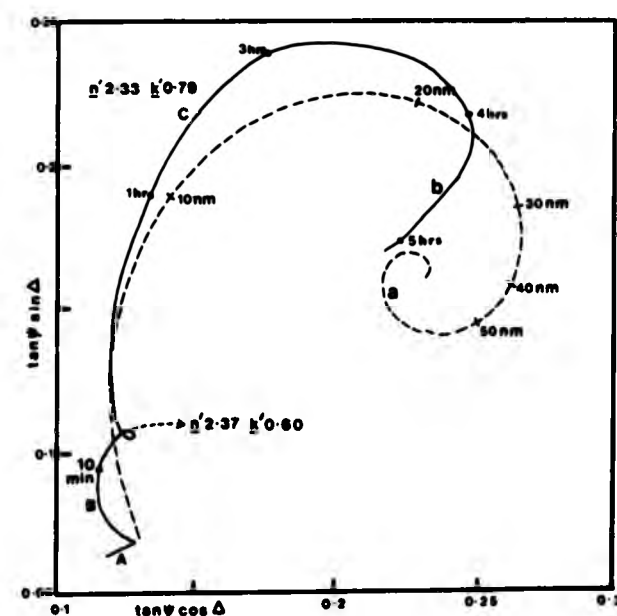


FIG. 5. Ellipsometric parameters for *in situ* oxidation of cuprite at 250 °C. Wavelength 525 nm, angle of incidence 75°. (a) Theoretical:  $\text{Cu}_2\text{O}$  substrate ( $n = 3.91$ ,  $k = 0.36$ ).  $\text{CuO}$  film ( $n = 2.35$ ,  $k = 0.70$ ). (b) Experimental: (A) desorption; (B)  $n = 2.37$ ,  $k = 0.60$ ; (C)  $n = 2.33$ ,  $k = 0.79$ . [See note p. 637.]

seems to indicate an initial desorption process, or a change in the surface state of the crystal prior to any oxide growth. The rest of the experimental locus corresponds to film growth. The film appears to undergo a change when it reaches a thickness of approximately 6 nm; taking the curve as two separate loci, labelled (B) and (C), it is possible to calculate the film  $n'$  and  $k'$  for each part

$$B = n' 2.37, k' 0.60 \text{ (dashed with arrow)}$$

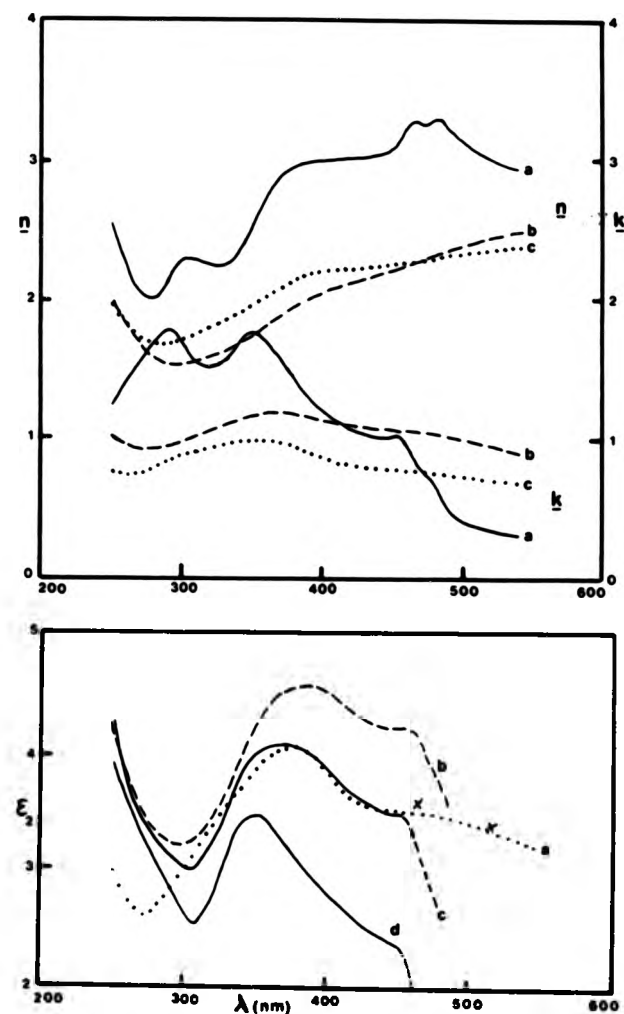
$$C = n' 2.23, k' 0.79.$$

Both these values are close to those used for the theoretical curve, though film (C) appears to be slightly more absorbing than either film (B) or the bulk CuO. Whether this change is due to re-ordering of the lattice on increasing thickness or other factors, possibly to do with surface contamination, is not known though further work in controlled atmosphere is planned.

It can be seen from fig. 6 that the spectrum of the oxidized system obtained from the *in situ* experiment at 250 °C is much closer to that of CuO than the one obtained from the batch oxidation at 225 °C but, before comparison can be made between bulk and thin film spectra, some explanation of the analytical technique is relevant.

The optical properties ( $n$ ,  $k$ ,  $\epsilon_1$ ,  $\epsilon_2$ ) of bulk specimens were derived assuming these were isotropic, homogeneous, plane, and free from surface contamination. These assumptions enable film-fitting computations to be used without serious error. The calculation of the complex refractive index ( $n-ik$ ) of a surface film from ellipsometric data must be done by iteration, as analytical methods cannot be used. If an independent measure of thickness is available,  $n-ik$  may be obtained directly from a knowledge of  $\Psi$  and  $\Delta$ . Conversely, if  $n-ik$  is known for the film, a unique value of its thickness may be determined. Without an independent thickness measurement additional ellipsometric data are necessary. One approach is to make spectral measurements and choose the refractive index, absorption coefficient, and thickness which give calculated values of  $\Psi$  and  $\Delta$  which most closely match the experimental data. Least-squares analysis is then used to perform the matching automatically, fitting the film  $n$  and  $k$  for various trial thicknesses. This is done by minimizing a function of the difference between calculated and experimental parameters (Clarke, 1979). The shape of the spectra and the magnitude of the absorption vary with the assumed thickness. The results of this operation are shown in fig. 7, the computed film spectra giving a probable value of 27 nm for the CuO film, grown *in situ* at low temperature.

It is clear that a good match between the spectra is possible only over a limited region (300 to



FIGS. 6 and 7. FIG. 6 (top). Spectral dispersion of  $n$  and  $k$  for *in situ* oxidation of cuprite. (a) Polished and etched. (b) Oxidized *in situ* at 250 °C. (c) CuO. FIG. 7 (below). Spectral dispersion of  $\epsilon_2$ . (a) Experimental CuO. (b) Least squares analysis thin film of CuO assumed thickness 35 nm. (c) Assumed thickness 27 nm. (d) Assumed thickness 20 nm. Crosses are for thick-film CuO (Ladelfe, *et al.*, 1972).

450 nm); this region in fact being dominated by just one  $\text{Cu}_2\text{O}$  absorption peak. The ellipsometric results for CuO films, however, depend not only on the assumed thickness but also on the assumed substrate ( $\text{Cu}_2\text{O}$ ) spectrum which indicates caution when interpreting these results. In performing the film-fitting operation we have also assumed the film properties to be identical to those of the bulk material; no account has been taken of possible differences of structure between them. Structural analysis of CuO films by other methods would be of use, but apart from measurements made by Ladelfe *et al.* (1972) at 450 nm and 500 nm (fig. 7), we have been unable to find any previous work on the optical properties of CuO in this wavelength region (fig. 7).

on process, or a crystal prior to experimental film appears a thickness of curve as two is possible to part

h arrow) used for the appears to be film (B) or the s due to re- thickness or surface con- rther work in

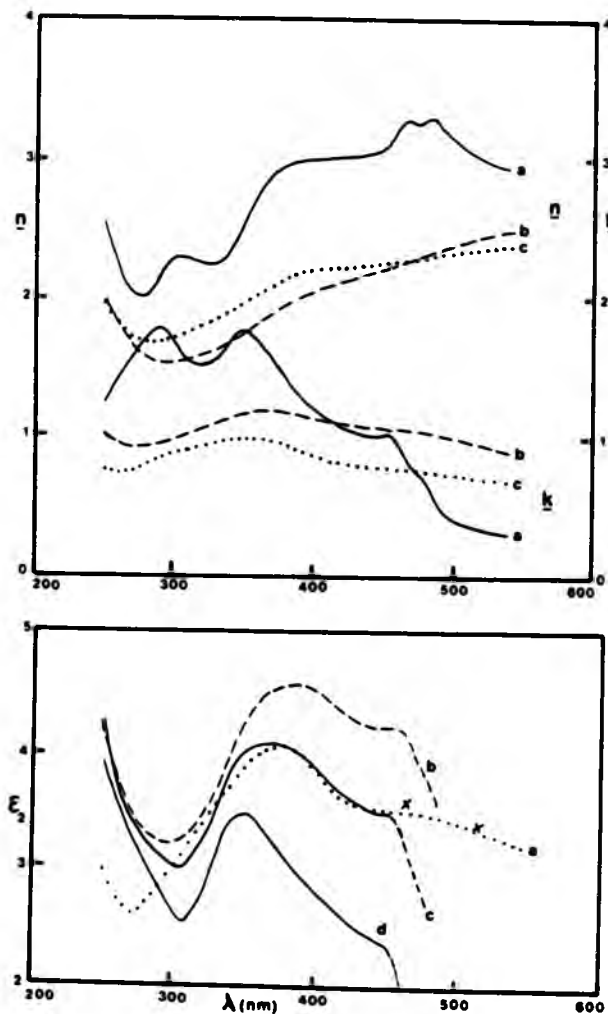
the spectrum of the *in situ* er to that of batch oxida- can be made some explana- evant.

of bulk speci- ere isotropic, surface con- e film-fitting us error. The index ( $n-ik$ ) of must be done

not be used. is available, a knowledge own for the ay be deter- erness measure- re necessary. easurements

orption col- alated values n the experi- then used to gting the film This is done nce between ers (Clarke, e magnitude d thickness. wn in fig. 7, bable value *in situ* at low

the spectra on (300 to



FIGS. 6 and 7. FIG. 6 (top). Spectral dispersion of  $n$  and  $k$  for *in situ* oxidation of cuprite. (a) Polished and etched. (b) Oxidized *in situ* at 250 °C. (c) CuO. FIG. 7 (below). Spectral dispersion of  $\epsilon_2$ . (a) Experimental CuO. (b) Least squares analysis thin film of CuO assumed thickness 35 nm. (c) Assumed thickness 27 nm. (d) Assumed thickness 20 nm. Crosses are for thick-film CuO (Ladelfe, *et al.*, 1972).

450 nm); this region in fact being dominated by just one  $\text{Cu}_2\text{O}$  absorption peak. The ellipsometric results for CuO films, however, depend not only on the assumed thickness but also on the assumed substrate ( $\text{Cu}_2\text{O}$ ) spectrum which indicates caution when interpreting these results. In performing the film-fitting operation we have also assumed the film properties to be identical to those of the bulk material; no account has been taken of possible differences of structure between them. Structural analysis of CuO films by other methods would be of use, but apart from measurements made by Ladelfe *et al.* (1972) at 450 nm and 500 nm (fig. 7), we have been unable to find any previous work on the optical properties of CuO in this wavelength region (fig. 7).

In the light of these results it is possible to offer an explanation for the anomalously high absorption index ( $k$ ) obtained in previous work. Air-formed films of CuO on  $\text{Cu}_2\text{O}$  require temperatures somewhat above ambient to reach a thickness accurately determinable by the methods employed here; however, when experiments are carried out at atmospheric pressure, some adsorption of oxygen into the surface layers is inevitable. Fig. 5 demonstrates the complex nature of the initial stages of the oxidation process.

We have also demonstrated that the surface is easily disordered and strained by preparative treatments and that this disordered layer displays abnormally high absorption at long wavelengths.

## REFERENCES

- Agekyan (V. T.), Kuz'mina (I. P.), Lobachev (A. N.), Predtchenski (B. S.), Starostina (L. S.), and Kaidukov (N. M.), 1975. *J. Appl. Spectrosc.* **22**, 582. (trans. of *Zh. Prikl. Spekt.*)
- Clarke (K. Mc.), 1979. C.N.A.A. Ph.D. Thesis. City of London Polytechnic.
- Donovan (T. M.), Ashley (E. J.), and Bennet (H. E.), 1963. *J. Opt. Soc. Am.* **53**, 1403.
- Gross (E. F.), 1962. *Sov. Phys. Uspekhi*, **5**, 195. (trans. of *Uspekhi fiz. Nauk.*)
- Hayfield (P. C. S.), 1961. 1st Int. Cong. Metallic Corrosion, April, p. 670.
- Hunt (R.). Private communication, to be published in C.N.A.A. Ph.D. Thesis. City of London Polytechnic.
- Ladelfe (P. C.), Czanderna (A. W.), and Biegen (J. R.), 1972. *Thin Solid Film*, **10**, 403.
- Roberts (E. F. I.) and Meadows (A.), 1964. *J. phys. E.* **7**, 379.
- and Rastall (P.), 1978. *Mineral. Mag.* **42**, 505.
- Spyrideles (J.), Stoimenos (J.), and Economov (N.), 1977. *Phys. Stat. Solidi*, **20**, 623.
- Vedam (K.) and Malin (M.), 1974. *Mat. Res. Bull.* **9**, 1503.

[Note added in proof. FIG. 5. The film thickness values on the experimental curve should be doubled. i.e. for 10 nm read 20 nm, etc.]

[Manuscript received 19 June 1979; revised 24 September 1979]

## Optical Properties of Alloys\*

E. F. I. ROBERTS, K. MC. CLARKE and R. HUNT

Department of Metallurgy and Materials, City of London Polytechnic, Whitechapel, London E1 (Gt. Britain)

### SUMMARY

Results are reported of studies using an automatic nulling spectroellipsometer on binary and ternary alloys of single- and two-phase composition. The significance of these results is discussed in relation to the electronic structure and appearance of such alloys.

### 1. INTRODUCTION

Historically the optical properties of metals have been central to studies of the electronic structure [1 - 3]. The term "metallic lustre" is common recognition of the particular properties of opacity and high reflectance which have made possible the application and development of reflection optical microscopy. Considerable effort has been expended among mineralogists in classifying and measuring the optical characteristics of opaque minerals and not a little success can be reported for the optical discrimination of minerals by reflective photometry [4 - 6]. More recently colour characterization, standardization and quality control have featured in several metallurgical industries, e.g. the gold jewellery industry for aesthetic surface coatings [7 - 10]. Ellipsometric studies of thin film growth kinetics during the corrosion of metallic substrates can almost without exception be considered to involve composition alterations of the substrate [11]. This is particularly so in more practical studies of alloys where de-alloying and surface enrichment have been commonly observed. Consequently the systematic application of ellipsometry to the corrosion

of alloys demands an understanding of the optical characteristics of alloy substrates. The conventional ellipsometric models rely upon a perfectly plane homogeneous isotropic substrate [12, 13] and metallurgists will recognize the limitations of such ideal assumptions. The present programme was aimed at measuring the effects of alloying on ellipsometric measurements when both complete solid solutions and limited-range solid solutions occurred. Furthermore, the optical constants  $n$  and  $k$  of the alloys were related to their colour characteristics and a comparison was made with reflectance measurements.

### 2. EXPERIMENTAL STUDIES

Extensive optical studies of the Group Ib metals copper, silver and gold have contributed to the electron theory of metals [14 - 17]. The ternary system Au-Ag-Cu was chosen for study partly because of the theoretical framework and partly because gold jewellery alloys are based upon this system. The Au-Ag-Cu system also includes two series of solid solutions (Ag-Au and Cu-Au) and a eutectic (Ag-Cu) which extend into the ternary system. Additionally, the Cu-Au binary system possesses a series of order-disorder reactions and these also appear in the ternary system [18]. The nobility of the alloys promotes relative inertness from atmospheric attack and, apart from the copper-rich alloys, corrosion problems do not intrude.

All alloys were prepared from fine gold, fine silver and spec. pure copper. Samples were made at 10 wt.% intervals throughout the ternary diagram. Alloys were induction melted in carbon crucibles under a reducing atmosphere and bottom-cast into a polished steel dish containing oil. The cast bead was

\*Presented at the International Chalmers Symposium on Surface Problems in Materials Science and Technology, Göteborg, Sweden, June 11 - 13, 1979.

worked into a plaquette by cold working and annealing. The final specimen was water quenched from a 16 h anneal at 600 °C. After mounting, the specimens were carefully polished metallographically down to a 0.25  $\mu\text{m}$  diamond paste. No organic solvents were used after the final rinsing with distilled water. Within minutes of polishing the specimens were mounted on an automatic self-nulling high precision spectroellipsometer and measurements of the relative phase shift  $\Delta$  and the relative amplitude change  $\tan \psi$  were made at wavelength intervals of 5 nm from 250 to 800 nm [19]. The data collected were then processed on a DEC10 computer system to generate dispersions of the complex refractive index  $\tilde{n}(\lambda) = n(\lambda) - ik(\lambda)$ , the complex dielectric function  $\tilde{\epsilon}(\lambda) = \epsilon_1(\lambda) + i\epsilon_2(\lambda)$  and the normal reflectance  $R_n(\lambda)$ . It was also possible to determine standard CIE colour coordinates for each of the alloys (CIE 1970) and to analyse the dispersion curves by multiple differentiation, normalization, difference calculations etc. Some of these results will be demonstrated in the discussion.

### 3. RESULTS

#### 3.1. Solid solutions

Both the gold-based binary systems Au-Ag and Au-Cu form solid solutions (although in the latter case ordering may occur at temperatures below the final annealing temperature). Microscope and X-ray examinations of these alloys indicated that they were all single phase. The ternary diagram isothermal section for 600 °C displays an extensive two-phase region based upon the limited solid solubility regions formed in the Cu-Ag binary and its eutectic. Ternary alloys that are gold rich or contain relatively small quantities of the third component are also solid solutions. Figures 1 and 2 show the reflectance curves determined for the binary solid solution alloys Au-Ag and Au-Cu, and Fig. 3 shows similar curves for a gold-rich series of ternary alloys exhibiting only solid solutions.

#### 3.2. Duplex alloys

The two-phase alloys are based upon the binary Cu-Ag limited-miscibility eutectic system. Two-phase ternary alloys occupy an

extensive range in the isothermal section studied here and the tie-lines for this range have been determined to lie almost parallel to the Ag-Cu composition line. Figure 4 shows the variation of reflectance for Ag-Cu and Figs. 5 and 6 show similar curves for ternary alloys with constant gold contents of 30 and 50 wt.%.

An analytical examination of the quantities computed from  $\epsilon_1$  and  $\epsilon_2$  is presented in the discussion.

### 4. DISCUSSION

#### 4.1. Optical properties of solids

The reflectance of a metal at a given wavelength  $\lambda$  is determined by its refractive index  $\tilde{n}(\lambda)$  and by the surface topography. The relation is simple for an ideal plane film-free surface. Furthermore, the refractive index is equal to  $\{\tilde{\epsilon}(\lambda)\}^{1/2}$  where  $\tilde{\epsilon}(\lambda)$  is the dielectric function [1]. The refractive index and dielectric functions are in general complex quantities since they describe the attenuation and phase change of light incident upon the metal. The dielectric function can be understood in terms of the polarization of the metal by an electromagnetic wave. For metals at optical frequencies only polarization of the electrons is significant. A causal chain exists between fundamental electronic properties and the visual appearance of a metal. Optical measurements are made at some point in the chain such that fundamental information (e.g. the electronic structure) or gross visual properties may be usefully collected and quantified. The complex dielectric function may be expressed in real and imaginary terms:

$$\tilde{\epsilon}(\lambda) = \epsilon_1(\lambda) + i\epsilon_2(\lambda)$$

The dielectric function of a material wherein the electrons are classically bound to the atoms is described by a lorentzian function. Such electrons may undergo forced vibrations at a resonant frequency  $\omega_0$ ; this resonance corresponds to a peak in  $\epsilon_2$ . For conduction electrons the natural frequency is zero — this gives rise to special lorentzian absorption known as Drude absorption. For a lorentzian oscillator the reflectance rises at low energies (long wavelengths) as  $\epsilon_2$  begins to rise but remains large until  $\epsilon_1$  approaches zero. Therefore the highly reflecting region of

nsive range in the isothermal section  
ied here and the tie-lines for this range  
been determined to lie almost parallel to  
Ag-Cu composition line. Figure 4 shows  
variation of reflectance for Ag-Cu and  
5 and 6 show similar curves for ternary  
ys with constant gold contents of 30 and  
7t.%.

n analytical examination of the quantities  
puted from  $\epsilon_1$  and  $\epsilon_2$  is presented in the  
ussion.

#### DISCUSSION

##### Optical properties of solids

he reflectance of a metal at a given wave-  
th  $\lambda$  is determined by its refractive index  
and by the surface topography. The  
ion is simple for an ideal plane film-free  
ce. Furthermore, the refractive index is  
l to  $\{\hat{\epsilon}(\lambda)\}^{1/2}$  where  $\hat{\epsilon}(\lambda)$  is the dielectric  
tion [1]. The refractive index and  
lectric functions are in general complex  
tities since they describe the attenuation  
phase change of light incident upon the  
l. The dielectric function can be under-  
d in terms of the polarization of the  
l by an electromagnetic wave. For metals  
optical frequencies only polarization of the  
rons is significant. A causal chain exists  
een fundamental electronic properties  
the visual appearance of a metal. Optical  
urements are made at some point in the  
n such that fundamental information  
the electronic structure) or gross visual  
erties may be usefully collected and  
tified. The complex dielectric function  
be expressed in real and imaginary terms:

$$\hat{\epsilon}(\lambda) = \epsilon_1(\lambda) + i\epsilon_2(\lambda)$$

he dielectric function of a material  
rein the electrons are classically bound to  
atoms is described by a lorentzian  
tion. Such electrons may undergo forced  
tions at a resonant frequency  $\omega_0$ ; this  
ance corresponds to a peak in  $\epsilon_2$ . For  
uction electrons the natural frequency  
o — this gives rise to special lorentzian  
rption known as Drude absorption. For  
entzian oscillator the reflectance rises at  
energies (long wavelengths) as  $\epsilon_2$  begins  
e but remains large until  $\epsilon_1$  approaches  
Therefore the highly reflecting region of

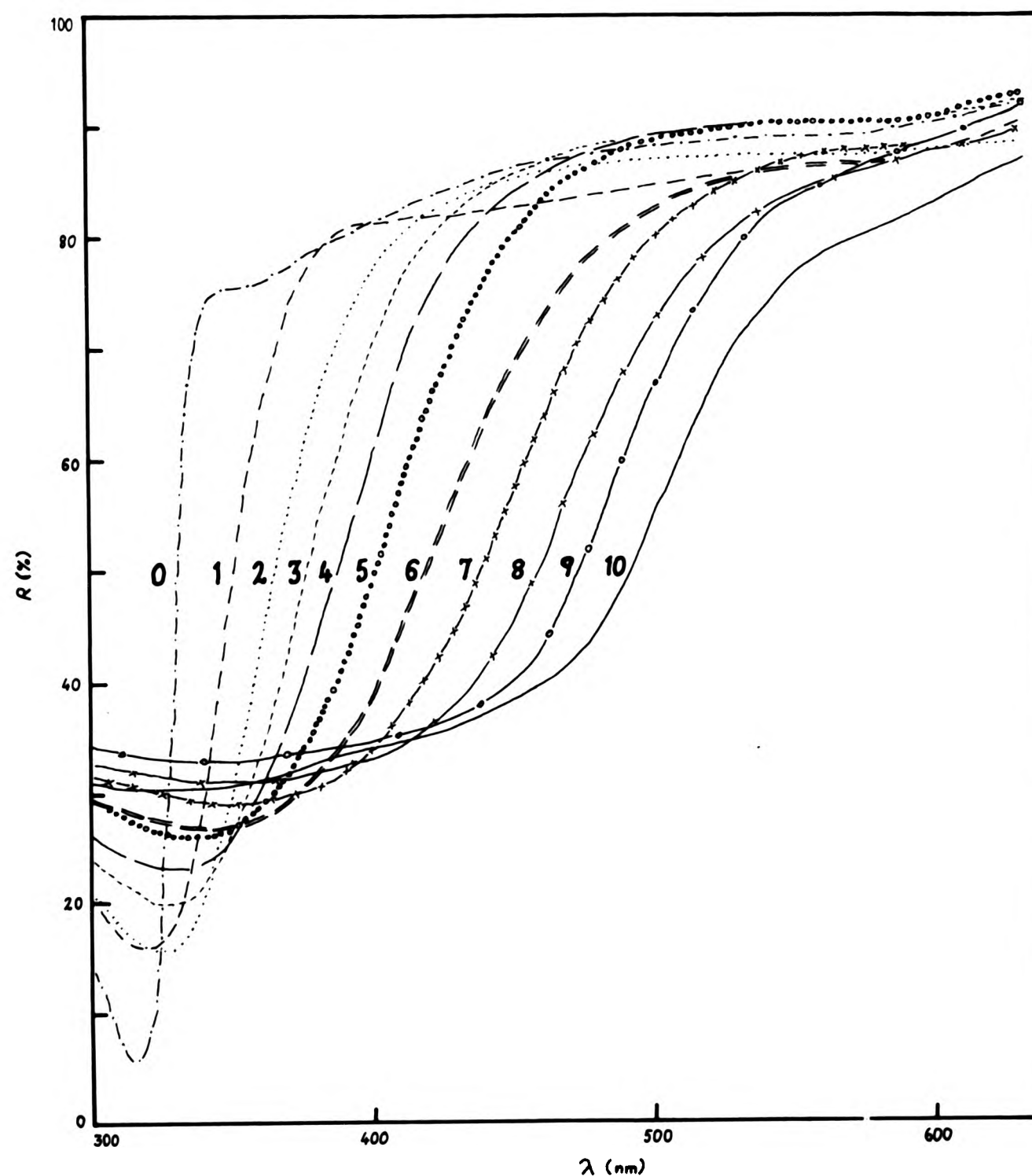


Fig. 1. Reflectance curves for Au-Ag single-phase binary alloys obtained by ellipsometry. The figures on the curves correspond to the nominal gold content (%) of the alloys.

a solid is on the high energy (short wavelength) side of the resonance frequency  $\omega_0$ . For metals with  $\omega_0 = 0$  we have high reflectance at long wavelengths.

In addition to the Drude absorption that characterizes free-electron metals we have to consider interband transitions. If the range of such transition(s) is narrow the values of  $\epsilon_2$ ,  $\epsilon_1$  and  $R$  will be similar to those of a single lorentzian oscillator. The additional absorp-

tion due to interband transitions reduces the reflectance. The high energy reflecting region may be completely suppressed by a succession of oscillators but structural features of the electronic bands will remain.

Metals are regarded as having free electrons. Partially filled bands or overlapping bands provide a continuum of unoccupied states adjacent to a continuum of occupied states which permits transitions at arbitrarily small

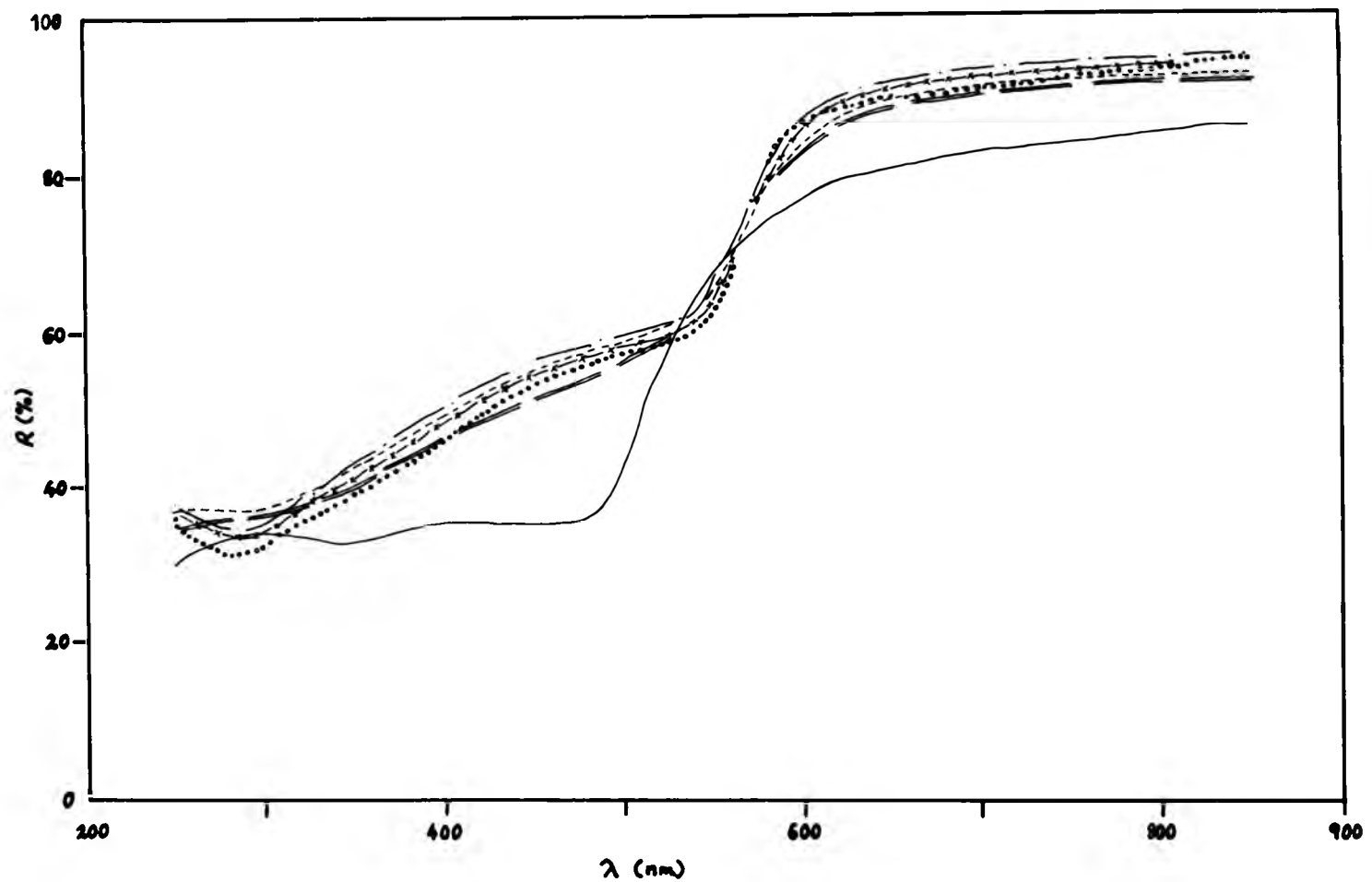


Fig. 2. Reflectance curves for Au-Cu single-phase binary alloys obtained by ellipsometry: —, 100Au; = =, 80Au-20Cu; ····, 60Au-40Cu; - · - ·, 40Au-60Cu; -x-, 20Au-80Cu; °°°°, 100Cu.

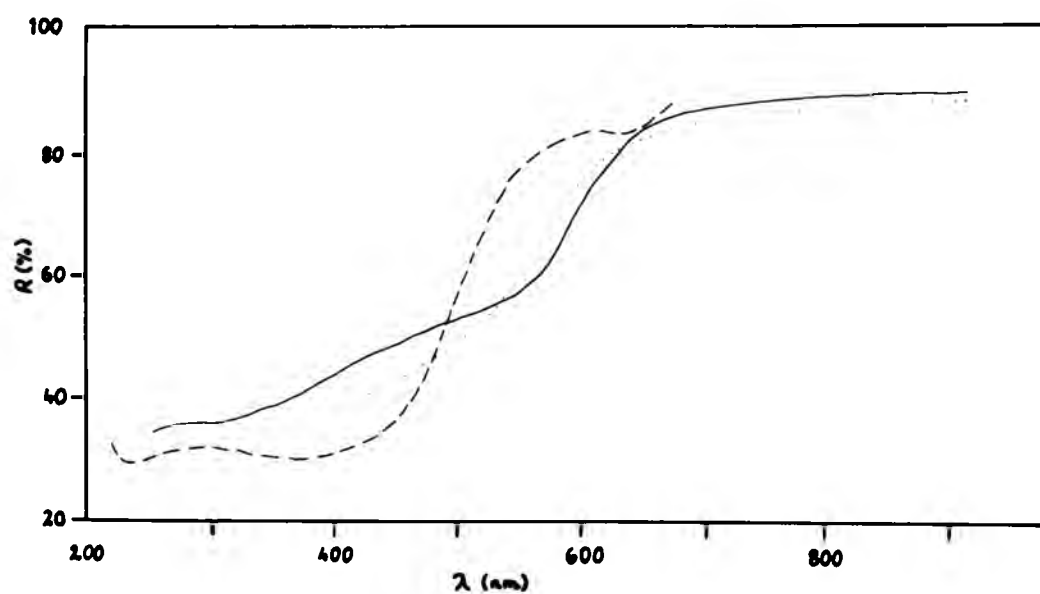
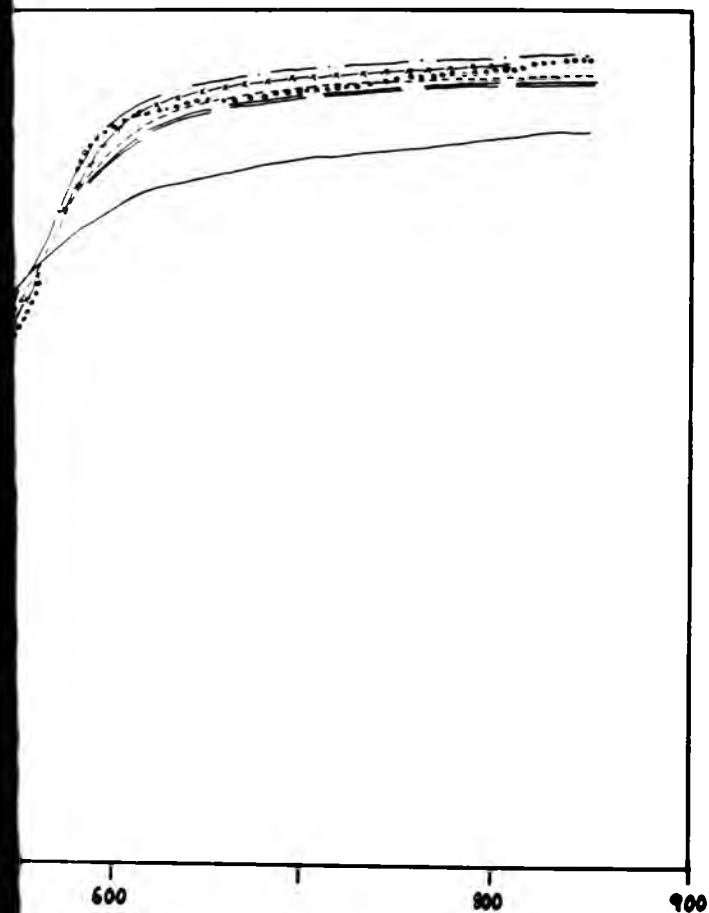


Fig. 3. Reflectance curves for 80Au-*n*Ag-*m*Cu single-phase ternary alloys obtained by ellipsometry: —, 80Au-20Cu; ····, 80Au-10Ag-10Cu; - - -, 80Au-20Ag.

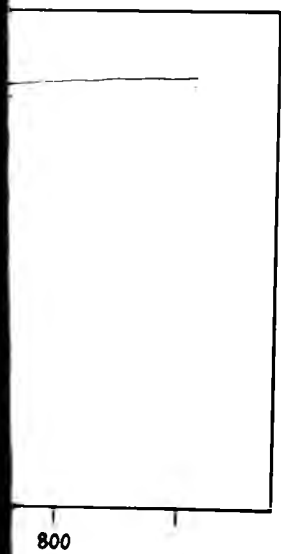
photon energies. This explains the high reflectance at low energies. The onset of interband transitions causes the reflectance to fall. The intraband characteristics are determined primarily by the relaxation time  $\tau$ , the density  $N$  of the conduction electrons and the effective mass  $m^*$ .

#### 4.2. Effect of alloying

The reflectance curves for Au-Ag (Fig. 1) (calculated from ellipsometric data) show good correlation with curves determined spectrophotometrically for similar alloys by Wessel [20] and Fukutani and Sueoka [21]. There is also good agreement with the results



Alloys obtained by ellipsometry: —, 100Au; = =, Au-80Cu; ○○○, 100Cu.



Binary alloys obtained by ellipsometry: —, 80Au-

## 2. Effect of alloying

The reflectance curves for Au-Ag (Fig. 1) calculated from ellipsometric data) show good correlation with curves determined spectrophotometrically for similar alloys by Messel [20] and Fukutani and Sueoka [21]. There is also good agreement with the results

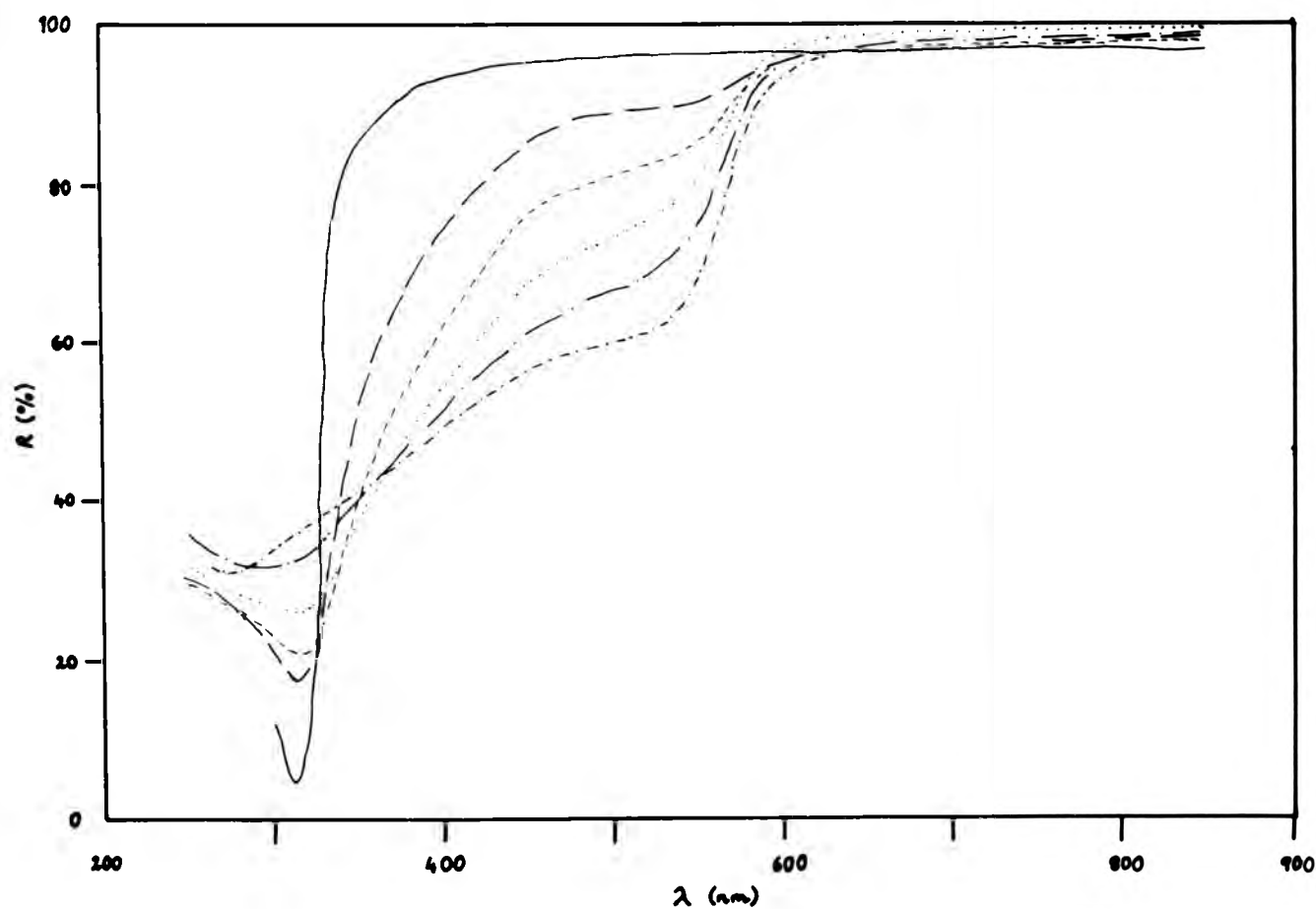


Fig. 4. Reflectance curves for Ag-Cu two-phase binary alloys obtained by ellipsometry: —, 100Ag; — —, 80Ag-20Cu; ····, 60Ag-40Cu; ····, 40Ag-60Cu; — — —, 20Ag-80Cu; ····, 100Cu.

obtained by Rivory [22] who made reflectance and transmittance measurements on thin vapour-deposited Au-Cu films. A number of workers, *e.g.* Friedel [23], have shown that dilute solid solutions of metals with similar electronic structures and weakly perturbed lattices form composite energy bands. Thus in some solid solutions alloying produces a smooth transformation of the energy bands and the dispersion curves of the optical constants or dielectric function will then also vary smoothly with composition throughout the solid solution range. The Au-Ag and Au-Cu disordered alloys obtained at 600 °C demonstrate this very well (Figs. 2 and 7).

Calculations of  $\tau$  and  $m^*$  using these results do not reveal a marked dependence upon composition and any variations can be considered to arise as random elements, probably from surface preparation and the concomitantly induced damage. For the Au-Ag system (Fig. 7) the shift in the fundamental absorption edge is so large (1.5 eV) that no serious error arises from neglecting the intraband contribution to  $\epsilon_2(\omega)$  in the region of

the absorption edge. (This is not the case for the Au-Cu system.) No significant shift of the absorption peak at 3.8 eV occurs in the gold-rich alloys upon addition of silver. At this energy two different components of similar magnitude operate, namely the d band  $\rightarrow$  Fermi surface (FS) and the FS  $\rightarrow$  conduction band transitions. To identify the influence of these we must decompose the dielectric function into bound- and free-electron terms; it may be possible to determine the line shape and energy of the d  $\rightarrow$  FS transition from thermomodulation optical experiments [24]. The present samples have smaller values of  $\epsilon_2^b(\omega)$  than those of Rivory but evidently the conduction electron transition  $L'_2 \rightarrow L_1$  is weakened more than the d band transition. However, alloying silver with gold does not spread the conduction electron transition into the visible region and this obviates the necessity to include conduction band effects when discussing the visual appearance of Au-Ag alloys. The onset of interband transitions in both copper and gold is due to d  $\rightarrow$  FS transitions over extended regions of the Brillouin zone. The variation of the onset

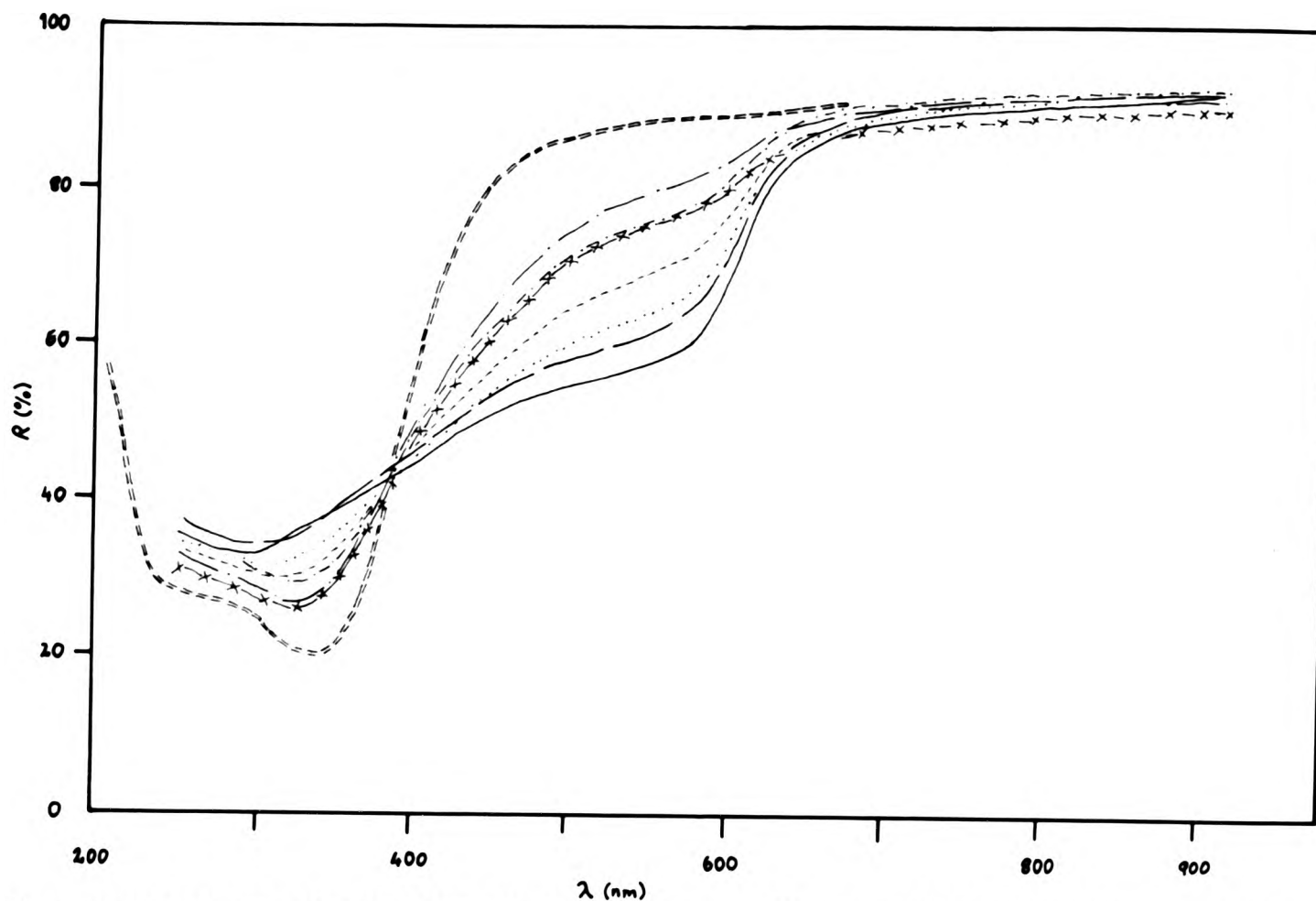


Fig. 5. Reflectance curves for  $1\text{Au}-30\text{Ag}-m\text{Cu}$  two-phase ternary alloys obtained by ellipsometry: —, 30Ag-70Cu; — —, 10Au-30Ag-60Cu; ····, 20Au-30Ag-50Cu; - - - -, 30Au-30Ag-40Cu; - · - ·, 40Au-30Ag-30Cu; - - - -, 50Au-30Ag-20Cu; - x - x, 60Au-30Ag-10Cu; = = =, 70Au-30Ag.

energy with composition has been determined for Au-Cu alloys (Fig. 8), no significant change being found for compositions containing up to 50 at.% Au. Beyond this composition the interband onset energy increases rapidly and monotonically to a final value of 2.5 eV for gold. This behaviour is similar to that of Au-Ag alloys but the deviation from linearity is much more marked. Piezo-reflectance measurements of the change of band gap with lattice spacing could be applied to Au-Cu alloys and corrections could be made to the above data leaving only variations due to the ionic potential of the alloying. The addition of copper to gold moves the peak in  $\epsilon_2^b(\omega)$  near 3.8 eV to higher energies, and the lower maximum (or rather point of inflection) at 3.3 eV moves to lower energies upon addition of copper. The higher energy peak also moves more rapidly for copper-rich alloys. These results are in agreement with those of Rivory [22] but not with those of Beaglehole and Erlbach [25]. This rapid change with the copper-rich alloys is

consistent, however, with the observation of Beaglehole and Erlbach that the ionic potential effect on alloying gold and copper (which opposes the lattice effect in this system) is much weaker for copper-rich alloys than for gold-rich ones.

Several experiments were conducted on single-phase Ag-Cu terminal solid solutions. A silver-rich alloy (containing 6.6 at.% Cu) and a copper-rich alloy (1.25 at.% Ag) showed optical spectra remarkably similar to their respective solvents. The absorption edge was broadened slightly, however, by approximately 0.02 eV and apparently an impurity band centred at  $\hbar\omega = 3$  eV occurred. Interestingly for small amounts of copper added to silver the changes were almost indistinguishable from roughness-induced surface plasmon absorption. The impurity band has been postulated as arising from virtual bound state absorption [22].

The heterogeneous alloys of the Ag-Cu binary eutectic system were also examined (Fig. 9). "Effective medium" calculations

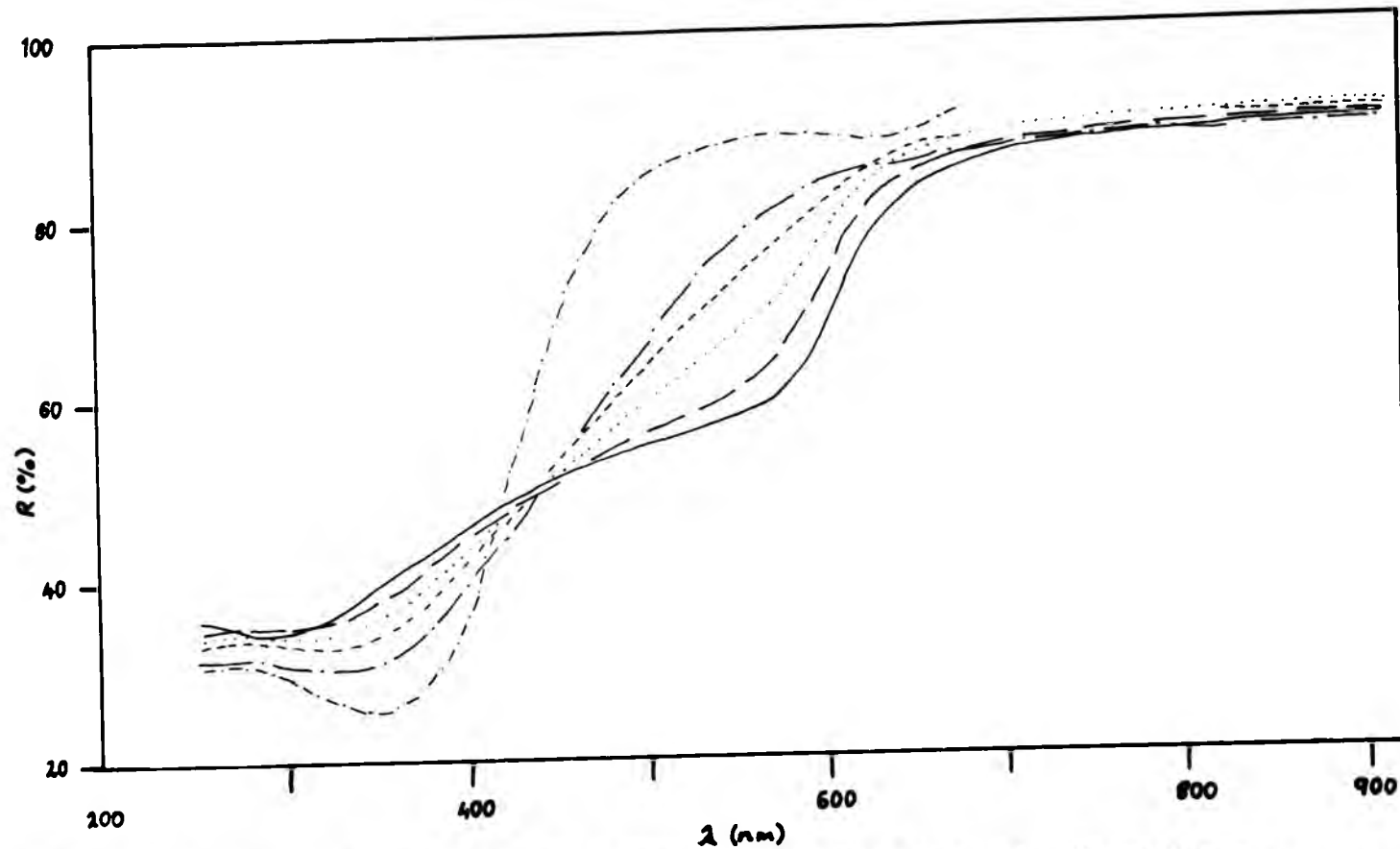
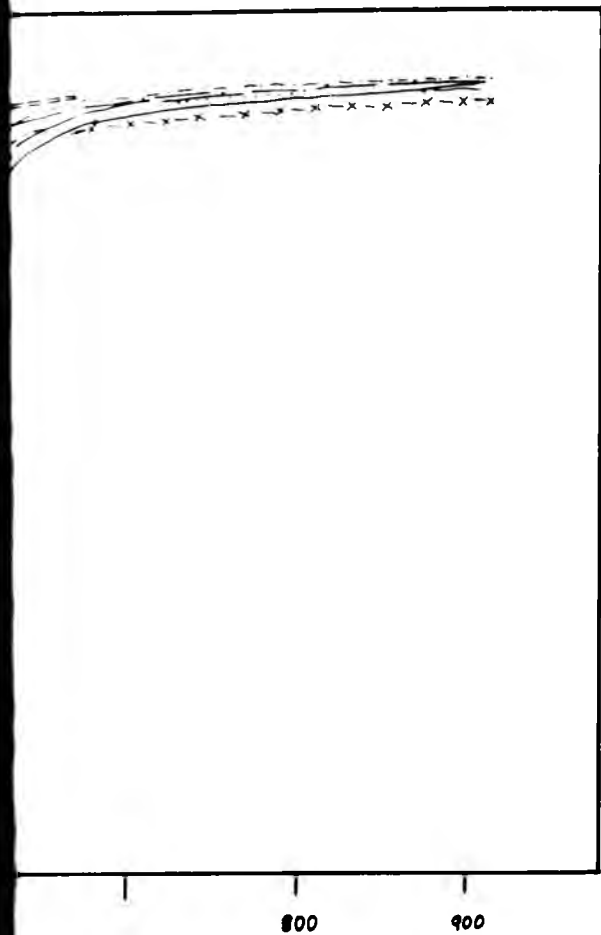


Fig. 6. Reflectance curves for 50Au-*n*Ag-*m*Cu two-phase ternary alloys obtained by ellipsometry: —, 50Au-50Cu; ---, 50Au-10Ag-40Cu; ····, 50Au-20Ag-30Cu; - - - - , 50Au-30Ag-20Cu; - · - · , 50Au-40Ag-10Cu; · - · - · , 50Au-50Ag.

Alloys obtained by ellipsometry: —, 30Ag-70Au-30Ag-40Cu; - - - - , 40Au-30Ag-30Cu; ····, 50Au-50Ag.

istent, however, with the observation of Ehole and Erlbach that the ionic potential effect on alloying gold and copper which opposes the lattice effect in this system is much weaker for copper-rich alloys than for gold-rich ones. Several experiments were conducted on two-phase Ag-Cu terminal solid solutions. A copper-rich alloy (containing 6.6 at.% Cu) showed spectra remarkably similar to their respective solvents. The absorption edge was shifted slightly, however, by approximately 0.02 eV and apparently an impurity band centred at  $\hbar\omega = 3$  eV occurred. Interest for small amounts of copper added to the changes were almost indistinguishable from roughness-induced surface plasmon absorption. The impurity band has been related as arising from virtual bound state absorption [22]. The heterogeneous alloys of the Ag-Cu eutectic system were also examined (9). "Effective medium" calculations

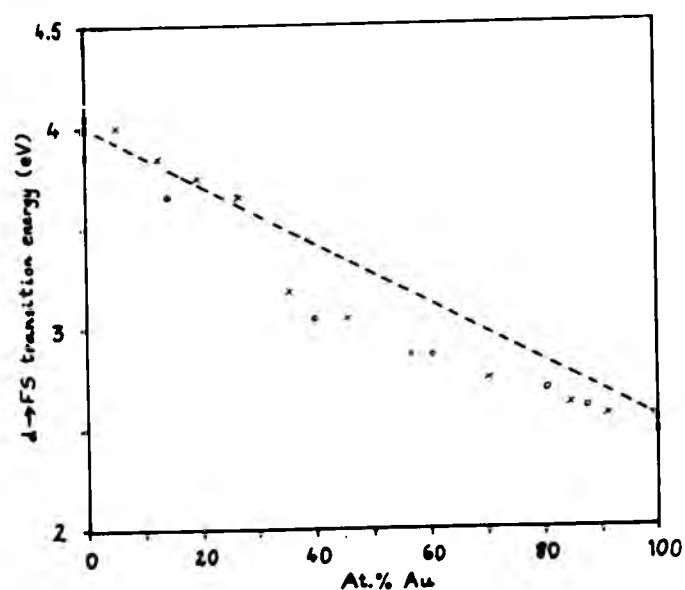


Fig. 7. The position of the low energy absorption edge for Au-Ag alloys: x, the energy for  $d^2\epsilon_2/d\omega^2$  (this work); o, from ref. 22.

were used, neglecting the inhomogeneity of the material. The justification for this is presented below (the nulling ellipsometer established a clear null for these alloys no matter how the null was approached). The optical spectra for these alloys are qualitatively similar to the spectra of homogeneous alloys. The alloys show various amounts of

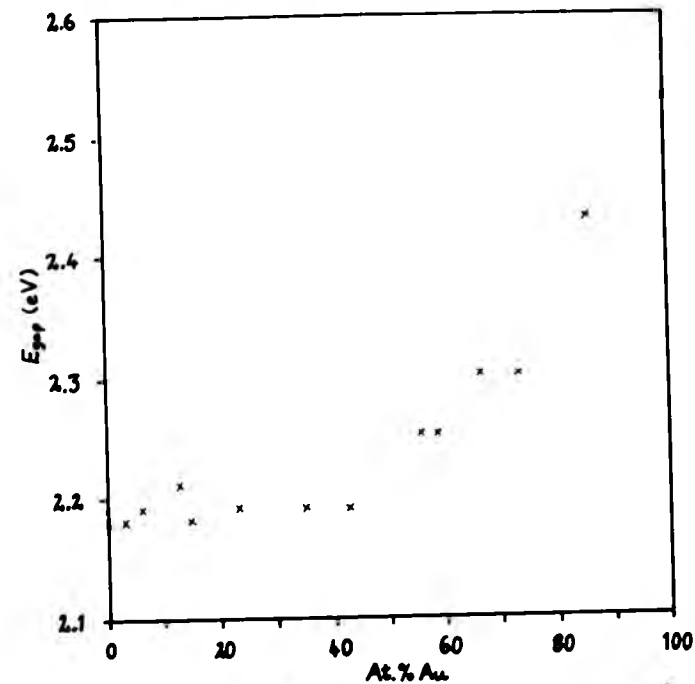


Fig. 8. The energy  $E_{gap}$  of the absorption edge in  $\epsilon_2^b$  for Au-Cu alloys.

primary phase ( $\alpha$  or  $\beta$ ) and eutectic ( $\alpha + \beta$ ). The optical constants of bulk  $\alpha$  and  $\beta$  were determined from separate specimens; for any of the binary alloys the respective  $\alpha$  and  $\beta$  phases have a constant composition and thus invariant optical constants. The optical

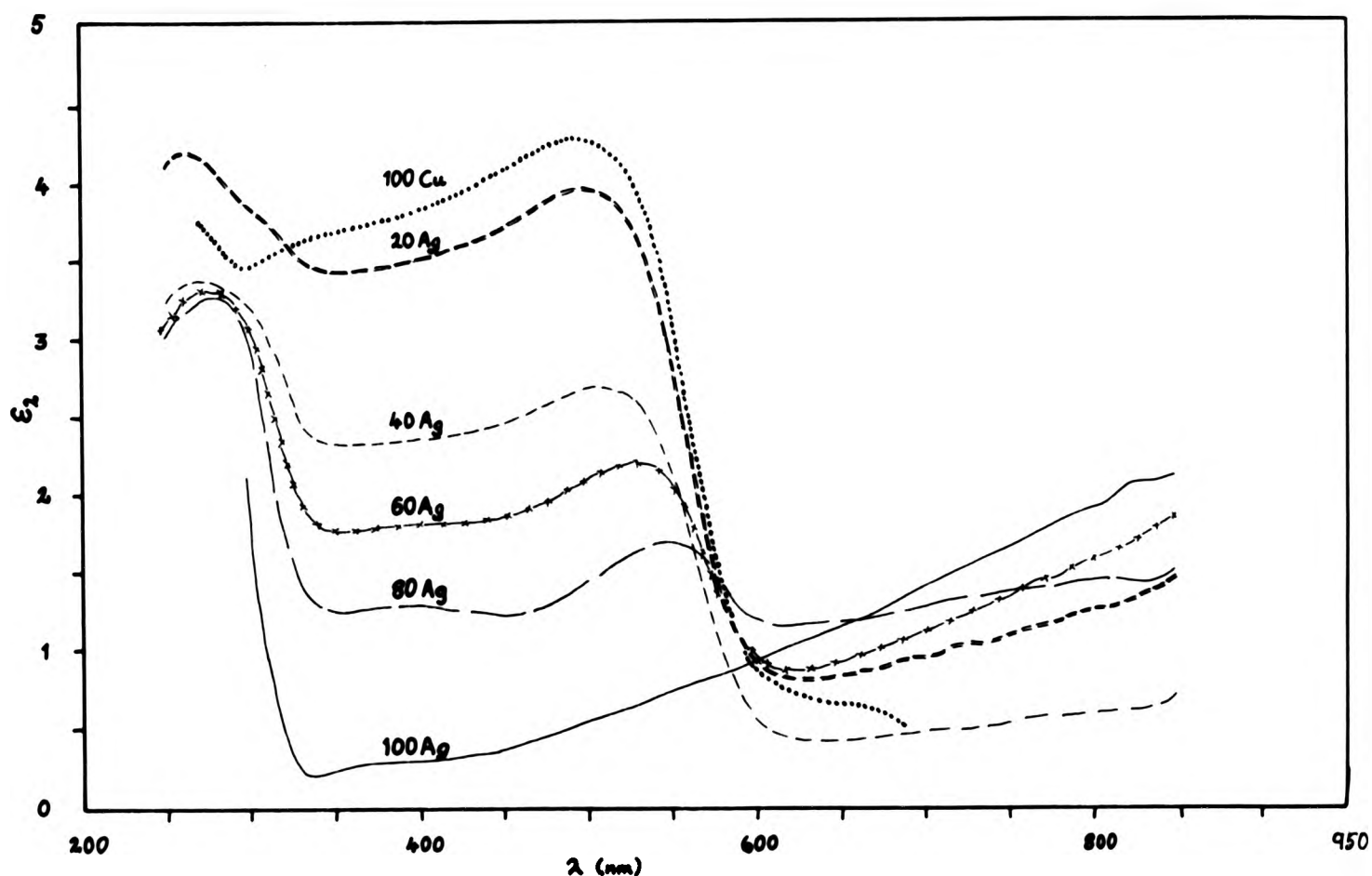


Fig. 9. The imaginary part  $\epsilon_2$  of the dielectric function for Ag-Cu alloys.

properties of the bulk alloy can thus be expected to be determined by the volume fractions and optical constants of each of the phases in the mixture. Since the  $\alpha$  and  $\beta$  phases are almost pure silver and copper it is necessary to examine the influence of mixing on the spectral characteristics of these components. Firstly the sharp interband absorption of silver at 3.8 eV does not appear to be either shifted or broadened, although in the copper-rich alloys the detail tends to be obscured by the influence of the copper. While reflectivity for copper is high for energies greater than 1.9 eV the interband transition analogous to the 3.8 eV transition for silver occurs at 2.2 eV; upon mixing this copper edge appears to be neither shifted nor broadened. However, the plateau between 2.9 and 2.3 eV in copper rises steadily with the addition of silver until it completely disappears in the presence of pure silver. Furthermore, the slope between 2.9 and 3.8 eV increases steadily from pure copper to pure silver. Thus the two fundamental absorption edges in Ag-Cu do not move and only their relative strength alters with composition.

This suggests that apart from a slight terminal solubility the two components silver and copper retain their electronic and optical characteristics independently and that they will contribute to the final alloy behaviour in proportion to the volume fraction of the  $\alpha$  and  $\beta$  phases.

The relative phase and amplitude changes occurring in incoherently reflected light at an inhomogeneous plane surface may be determined by comparing the sum of the two Stokes vectors arising from reflection at the two types of reflecting surfaces in the inhomogeneous alloy with the column vector of a single homogeneous phase surface. This appears to be legitimate since the nulling ellipsometer provides a well-defined unambiguous null as long as the sampling beam width is large compared with the dimension of the inhomogeneity. The resulting equations for the relative phase change  $\Delta$  and the relative amplitude change  $\tan \psi$  are

$$\Delta = \tan^{-1} \left\{ \frac{q |\rho_{s\alpha}| |\rho_{p\alpha}| \sin \Delta_\alpha + (1-q) |\rho_{s\beta}| |\rho_{p\beta}| \sin \Delta_\beta}{q |\rho_{s\alpha}| |\rho_{p\alpha}| \cos \Delta_\alpha + (1-q) |\rho_{s\beta}| |\rho_{p\beta}| \cos \Delta_\beta} \right\}$$

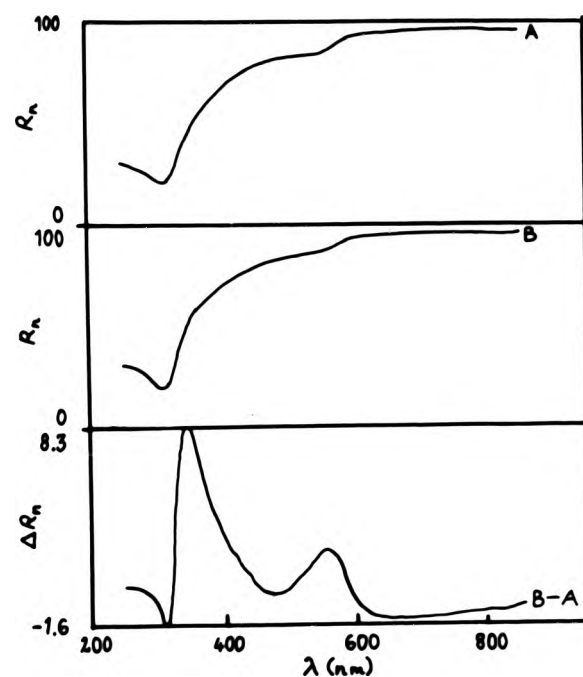


Fig. 10. Experimental (curve A, 70Ag-30Cu) and theoretical (curve B, volume fraction  $q = 0.676$ ) reflectance curves for two-phase alloys with nominally the same volume fraction.

$$\tan \psi = \left\{ \frac{q |\rho_{p\alpha}|^2 + (1-q) |\rho_{p\beta}|^2}{q |\rho_{s\alpha}|^2 + (1-q) |\rho_{s\beta}|^2} \right\}^{1/2}$$

where  $\rho_s$  and  $\rho_p$  are the Fresnel reflection coefficients in the s and p directions,  $q$  is the volume fraction of  $\alpha$ ,  $1 - q$  is the volume fraction of  $\beta$ ,  $\Delta$  is the relative phase change for phases  $\alpha$  and  $\beta$  and the subscript indicates the phase.

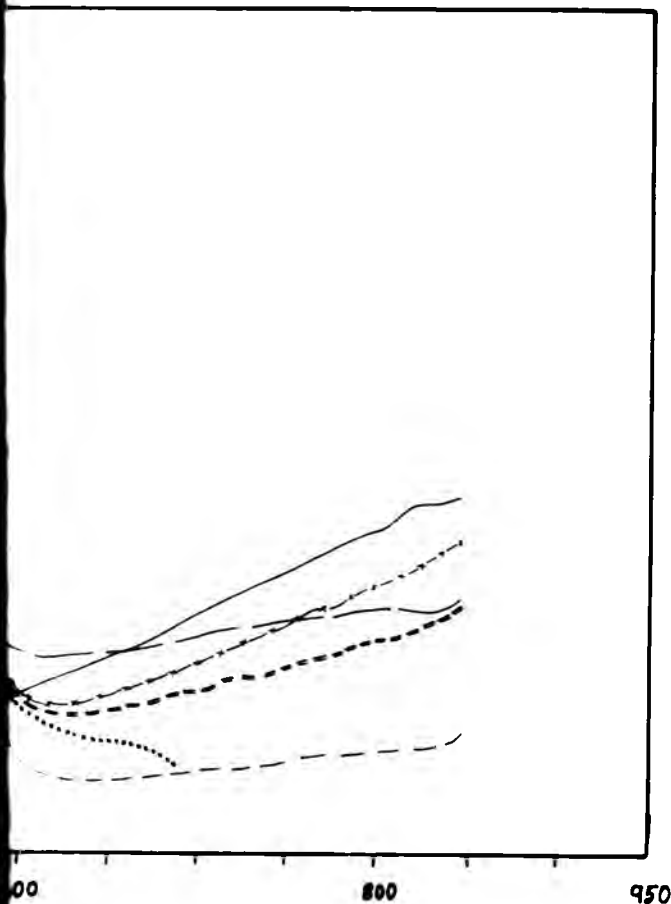
Figure 10 shows a normal reflectance curve for a theoretical two-phase alloy with the same volume fractions of  $\alpha$  (silver-rich terminal solid solution) and  $\beta$  (copper-rich terminal solid solution) as for the 70Ag-30Cu alloy used to obtain the experimental normal reflectance curve. If the optical spectra of two (or more) duplex alloys are available an inversion of the equations permits the determination of the optical properties of the terminal solid solutions. Furthermore this modelling explains special features of the colour identification of such duplex alloys when the identification is made from ellipsometrically derived normal reflectance and compared with normal spectrometry. It is easy to determine the CIE [26] chromaticity coordinates for each of the specimens using the normal reflectance determined by either spectrometry or spectroellipsometry. Colour theory predicts that the series of colours derived from a

mixture of two colours, e.g. white and red, will lie on a straight line in the chromaticity diagram. Such behaviour is *a priori* expected from the  $\alpha + \beta$  alloy mixtures. However, the colour coordinates of such alloy mixtures determined ellipsometrically lie on a curve. Spectral reflectance (and hence the colour of metal alloys) will also vary with the angle of incidence of the probe beam. Care must therefore be exercised in comparing reflectance values, particularly those of polyphase alloys. The optical constants  $n$  and  $k$  and the dielectric functions do not suffer from this and therefore techniques to establish primarily these quantities are to be preferred for optical measurements of metals.

## 5. CONCLUSION

Spectroellipsometry has become accepted as a method of determining the optical characteristics of metals and alloys. Despite the extreme sensitivity of ellipsometry to surface films and surface preparation the application of environmental control, sample annealing and cleaning must promote the application of the technique to studies of reactive metals and alloys.

The optical behaviour of solid solutions is consistent with the model of extensive band mixing as the composition alters. The dielectric function in particular has a single band whose strength and peak alters progressively with composition. The behaviour of alloys which exhibit a solution limit and a separation into two (or more) phases differs in that the terminal phases retain their composition but alter their proportion (*i.e.* volume fraction). This effect is observed in the dispersion curves, particularly of the interband component of the dielectric function, as a separation of the constituent spectra which in turn vary in strength with volume fraction. The optical appearance and in particular the colour of the alloys can be determined objectively by computing the normal reflectivity  $R_n$  from the optical constants and calculating the CIE chromaticity coordinates. Variations in chromaticity coordinates correlate well with changes in alloying but care has to be taken in using the data for polyphase alloys. A model is introduced that permits the evalua-



Cu alloys.

This suggests that apart from a slight terminal instability the two components silver and copper retain their electronic and optical characteristics independently and that they all contribute to the final alloy behaviour in proportion to the volume fraction of the  $\alpha$  and  $\beta$  phases.

The relative phase and amplitude changes occurring in incoherently reflected light at an inhomogeneous plane surface may be determined by comparing the sum of the two Stokes vectors arising from reflection at the two types of reflecting surfaces in the inhomogeneous alloy with the column vector of a single homogeneous phase surface. This appears to be legitimate since the nulling ellipsometer provides a well-defined unambiguous null as long as the sampling beam width is large compared with the dimension of the inhomogeneity. The resulting equations for the relative phase change  $\Delta$  and the relative amplitude change  $\tan \psi$  are

$$\tan^{-1} \left\{ \frac{q |\rho_{s\alpha}| |\rho_{p\alpha}| \sin \Delta_\alpha + (1-q) |\rho_{s\beta}| |\rho_{p\beta}| \sin \Delta_\beta}{q |\rho_{s\alpha}| |\rho_{p\alpha}| \cos \Delta_\alpha + (1-q) |\rho_{s\beta}| |\rho_{p\beta}| \cos \Delta_\beta} \right\}$$

tion of the optical characteristics of polyphase alloys. The inversion of this model also permits the quantification of volume fractions of polyphase alloys or the determination of the chromaticity of constituent phases.

#### ACKNOWLEDGMENTS

The authors wish to thank Dr. L. L. Shreir for providing facilities within the Department of Metallurgy and Materials, the ILEA and The International Gold Corporation for funding the work reported here, and Mr. R. Cohen and Mrs. M. Evans who prepared the materials essential for the study.

#### REFERENCES

- 1 F. Wooten, *Optical Properties of Solids*, Academic Press, New York, 1972.
- 2 D. L. Greenaway and G. Harbeke, *Optical Properties and Band Structure of Semiconductors*, Pergamon, Oxford, 1968.
- 3 N. W. Ashcroft and N. D. Mermin, *Solid State Physics*, Holt, Rinehart and Winston, New York, 1976.
- 4 B. D. Cervell, C. Levy, N. F. M. Henry and T. N. Shadlun, *Bull. Mineral.*, 101 (1978) 234.
- 5 R. G. J. Strens and R. Freer, *Mineral. Mag.*, 42 (1978) 19.
- 6 R. G. Burns and D. J. Vaughan, *Am. Mineral.*, 55 (1970) 1576.
- 7 E. F. I. Roberts and K. Mc. Clarke, *Gold Bull.*, 12 (1979) 9.
- 8 G. E. Gardam, *Trans. Inst. Met. Finish.*, 41 (1964) 190.
- 9 G. E. Gardam, *Trans. Inst. Met. Finish.*, 44 (1966) 196.
- 10 R. S. Hunter, *The Measurement of Appearance*, Interscience, London, 1975.
- 11 D. Ross, *Ph.D. Thesis*, University of London, 1978.
- 12 P. Drude, *Ann. Phys. (Leipzig)*, 39 (1890) 514.
- 13 R. M. A. Azzam and N. M. Bashara, *Ellipsometry and Polarized Light*, North-Holland, Amsterdam, 1977.
- 14 L. G. Shultz, *Adv. Phys.*, 6 (1957) 102.
- 15 M. P. Givens, *Solid State Phys.*, 6 (1958) 343.
- 16 H. Ehrenreich and H. R. Philips, *Phys. Rev.*, 128 (1962) 1622.
- 17 P. O. Nilsson, *Solid State Phys.*, 29 (1974) 139.
- 18 W. S. Rapson and T. Groenewald, *Gold Usage*, Academic Press, New York, 1978.
- 19 E. F. I. Roberts and A. Meadows, *J. Phys. E*, 7 (1974) 379.
- 20 P. R. Wessel, *Phys. Rev.*, 132 (1963) 2062.
- 21 H. Fukutani and O. Sueoka, in F. Abelès (ed.), *Optical Properties and Electronic Structure of Metals and Alloys*, North-Holland, Amsterdam, 1965.
- 22 J. Rivory, *Phys. Rev., Sect. B*, 15 (1977) 3119.
- 23 J. Friedel, *Adv. Phys.*, 3 (1954) 446.
- 24 F. Antonangeli, E. Colarita, R. Rosei and S. E. Saluski, *Nuovo Cimento B*, 24 (1974) 121.
- 25 D. Beaglehole and E. Erlbach, *Phys. Rev., Sect. B*, 6 (1972) 1209.
- 26 *CIE International Lighting Vocabulary*, CIE, Paris, 3rd edn., 1970, p. 9.

Attention is drawn to the fact that the copyright of this thesis rests with its author.

This copy of the thesis has been supplied on condition that anyone who consults it is understood to recognise that its copyright rests with its author and that no quotation from the thesis and no information derived from it may be published without the author's prior written consent.

III

**D37677 '81**

**END**

Attention is drawn to the fact that the copyright of this thesis rests with its author.

This copy of the thesis has been supplied on condition that anyone who consults it is understood to recognise that its copyright rests with its author and that no quotation from the thesis and no information derived from it may be published without the author's prior written consent.

I